The Electroweak Phase Transition: Corralling the Higgs with Colliders & Cosmology

by

Andrew J. Long

A dissertation submitted in partial fulfillment of
the requirements for the degree of

Doctor of Philosophy
(Physics)

at the
University of Wisconsin – Madison
2012

Defended on July 24, 2012

Dissertation approved by the following members of the Final Oral Committee:

Daniel Chung · Associate Professor of Physics

Vernon Barger · Vilas Professor and Van Vleck Professor of Physics

Akikazu Hashimoto · Associate Professor of Physics

Peter Timbie · Professor of Physics

Ellen Zweibel · William L. Kraushaar Professor of Astronomy & Physics

Abstract

Through this thesis, I investigate the way in which the electroweak phase transition, and therefore the Higgs boson, bridges high energy particle physics and early universe cosmology; moreover, I argue that it is particularly interesting to explore this bridge today as experiments such as the Large Hadron Collider begin to uncover the nature of physics at the electroweak scale. I will discuss how measurements of the properties of the Higgs boson at the Large Hadron Collider allow one to determine the nature of the phase transition that was responsible for electroweak symmetry breaking in the early universe. That information in turn will allow one to assess whether the asymmetry between the abundances of matter and anti-matter in the universe may have been generated during the electroweak phase transition. Additionally, I will discuss the impact of the electroweak phase transition on another cosmological relic: namely, the dark matter. Precise measurements of the mass and abundance of dark matter today yield further information about the nature of the electroweak phase transition, in some scenarios. This information may be used to test the hypothesis that the cosmological constant, assumed to be a good model of dark energy, is finely tuned. In this way, I hope to demonstrate the importance of the electroweak phase transition as a bridge between terrestrial tests of high energy physics and cosmological tests of the physics of the early universe.

Acknowledgements

I am most grateful to many people who taught me, supported me, challenged me, and comforted me during my Ph.D. work.

First, I thank my thesis advisor – Daniel Chung – for insisting upon excellence, for teaching me to think deeply, and for correcting me when I was wrong. I feel immensely fortunate to have had the opportunity to study with Dan. He tackled my every question with an inspiring tenacity (which I only very slightly resented when our meetings entered their fourth or fifth hour) that ensured that every question received a satisfactory answer.

I thank my research collaborators – Vernon Barger and Lian-Tao Wang – for their indispensable contributions to our work together.

I thank my thesis committee – Professors Barger, Chung, Hashimoto, Timbie, and Zweibel – for their critical evaluations of my research. I also thank Professor Sebastian Heinz for attending my thesis defense on short notice.

I thank the physics faculty at UW-Madison – Professors Balantekin, Chubukov, Chung, Dasu, Halzen, Han, Joynt, Ramsey-Musolf, and Shiu – whose classes have taught me, among other things, that "physics is a lifestyle."

I thank the faculty whose assistance was invaluable in my job search this spring – Professors Barger and Everett – and for going out of their way to be supportive and encouraging.

I thank my friends in theoretical HEP – Mike Glatzmaier, Matthew Gonderinger, Valerie Plaus, Alex Stuart, Hojin Yoo, Peng Zhou, and particularly Paul McGuirk and Hiren Patel – for sharing their expertise with me through very stimulating discussions.

I thank my friends – Adam Dally, Laura Gladstone, David Hover, Elliot Kaplan, Jeff & Karen Klukas, the KIVA, Mike McFarlane, Naomi Lipke, Mark Stockett, Zilin

Zhu – for being there to explore Wisconsin with me.

I thank my mother and sister, for their love, for their support, and for the many gift packages of steak and candy.

Finally, I thank my fiancé, Minh-Dan Tran, for her infinite love and patience during my six years of exile in Wisconsin. The happiest part of completing my degree – without a doubt – is that I'll be with you once again.

Contents

Chapter 1

Introduction

I can't imagine a more exciting time to be a high energy physicist. As I am writing this document, the Higgs boson has just been discovered at the Large Hadron Collider facility in Geneva, Switzerland. The Higgs represents the final piece of the puzzle in the Standard Model of particle physics, and put more broadly, its discovery can be counted as one of science's greatest successes of all time. Over the next few years, studies of the properties of the Higgs boson will open wide the window on a new and unexplored realm of physics. We have some suspicions about what beasts that realm may contain. In the field of cosmology, high-precision measurements of the cosmic microwave background over the past decade have revolutionized our understanding of the universe and its makeup. We live in a universe brimming with a mysterious dark matter and an enigmatic dark energy, both of which pose challenges to our understanding of high energy physics. Moreover, the observed abundance of matter over anti-matter can only be explained if Nature is more complex and dynamic than the Standard Model would have us believe. In the coming years, the Planck satellite will probe the temperature fluctuations of the cosmic microwave background with unprecedented precision, dark matter detection experiments will increase their

sensitivity and may yield a discovery of dark matter, and galaxy surveys will extend their breadth and depth to test the nature of dark energy. The Higgs boson may have been the first great discovery of the 21$^{\text{st}}$ century, but it will not be the last.

These exciting topics in high energy physics–the Higgs boson, the matter / anti-matter asymmetry, dark matter, and dark energy–may seem to be entirely distinct fields of research. However, as I will discuss throughout this manuscript, they are linked together by the electroweak phase transition. This event, which is hypothesized to have taken place in the first femtoseconds after the Big Bang when the universe was very hot and dense, is responsible for inducing electroweak symmetry breaking, which allows the Higgs to provide mass to the Standard Model fields. Thus, on one hand the electroweak phase transition has direct connections to the physics of the Higgs boson: the temperature at which the phase transition took place and its thermodynamic "order" are controlled by the mass of the Higgs boson and the coupling of the Higgs boson to new particles. On the other hand, the electroweak phase transition, by virtue of taking place in the very early universe, has connections with the physics of dark matter and dark energy: the phase transition can indirectly affect the abundance of dark matter in the universe today and may act as a probe of dark energy in the early universe. In this way, the electroweak phase transition bridges two otherwise separate fields of physics – cosmology and high energy particle physics. It is the subject of this manuscript to study this connection further.

We begin in Chapter 2 by discussing the Higgs boson, the essential role that it plays in the Standard Model, the history of searches for the Higgs particle, and its connection to the baryon asymmetry of the universe via electroweak baryogenesis and the electroweak phase transition. In Chapter 3, we discuss the physics of the electroweak phase transition, and introduce a quantity, called the thermal effective potential, which will be an invaluable tool in the following phase transition analyses.

In Chapters 4, 5, and 6, we employ these concepts to investigate the connection between the Higgs boson and baryogenesis in various scenarios. In Chapter 7, we discuss the physics of dark matter and dark energy and evidence for their existence in our universe. In Chapters 8 and 9, we investigate the impact of the electroweak phase transition on the dark matter relic abundance, and we propose a way of testing the hypothesis of the fine-tuning of the cosmological constant.

Throughout this manuscript, we will be using "physicist's units" in which $\hbar = c = 1$. Consequently, mass, energy, inverse time, and inverse length are measured with the same unit. We will primarily use the GeV, which is approximately equal to the mass of the proton.

Part I

The Higgs Boson and Electroweak Baryogenesis

Chapter 2

The Two Faces of the Higgs

In the introduction, we discussed that the Higgs boson is especially suited to the task of bridging high energy particle physics at colliders with the high energy cosmology of the early universe. In this part of the manuscript, we will make this terrestrial-cosmological connection more concrete. We begin this chapter in Sec. 2.1 by discussing the physics of the Higgs boson: the critical role it plays in the SM, its participation in spontaneous symmetry breaking and the Higgs mechanism, and constraints on Higgs physics from collider experiments. In Sec. 2.2 we will turn our attention to the role that the Higgs plays in creating the cosmic baryon asymmetry in the early universe through electroweak baryogenesis. We will see the success of electroweak baryogenesis hinges upon the nature of the electroweak phase transition. Finally, we will establish the connection between the terrestrial and cosmological sides of the Higgs by using the baryogenesis success criterion to derive a bound on the mass of the Higgs boson in the Standard Model and to motivate the search for physics beyond the Standard Model.

2.1 The Terrestrial Higgs: Weak Boson Masses

In the Standard Model (SM) of particle physics, the Higgs boson is charged with the critical task of providing mass to the matter fields and weak gauge bosons ($W^{\pm}$ and Z). Without the Higgs, for example, electrons would be massless particles and would not bind with nuclei into atoms. Consequently our universe would be devoid of molecules, planets, and life as we know it. However, as we will see, the truly indispensable job of the Higgs is providing mass to the weak gauge bosons. If we lived in a universe lacking a weak nuclear force, but instead only the strong nuclear force and electromagnetic forces were present, then the Higgs would not be required to generate mass for the matter fields. In this regard, the Higgs is essential.

The SM is a *Yang-Mills theory* (1) built upon the symmetry group $\mathrm{SU}(3)_C \times \mathrm{SU}(2)_L \times \mathrm{U}(1)_Y$. Each of the symmetry groups is associated with one of the fundamental forces (with the exception of the gravitational force, which stands apart). The $\mathrm{SU}(3)_C$ group is the foundation of *quantum chromodynamics* (QCD) (2; 3), the theory which describes the strong force that is responsible for binding quarks together into nucleons. Since our primary subject of interest – the Higgs boson – does not participate in the strong interaction, we will speak no further of QCD. The $\mathrm{SU}(2)_L \times \mathrm{U}(1)_Y$ group (4) is the basis of the Glashow-Weinberg-Salam Model (GWS) (5–7) of the unified electromagnetic and weak nuclear forces. Studies of the electromagnetic force were pioneered in the 19^{th} century by Michael Faraday, James Maxwell Clerk, and others. Today, the models which describe the electromagnetic force are arguably the most well tested in all of science[1]. The weak nuclear force is most familiar for its role in mediating the radioactive decay of heavy nuclei, a phenomenon first observed by Becquerel and the Curie's at the end of the 19^{th} century. Subsequently, the theory of

[1]E.g., recent measurements of the magnetic moment of the electron agree with the predictions of quantum electrodynamics at the order of 0.1 parts per billion (8).

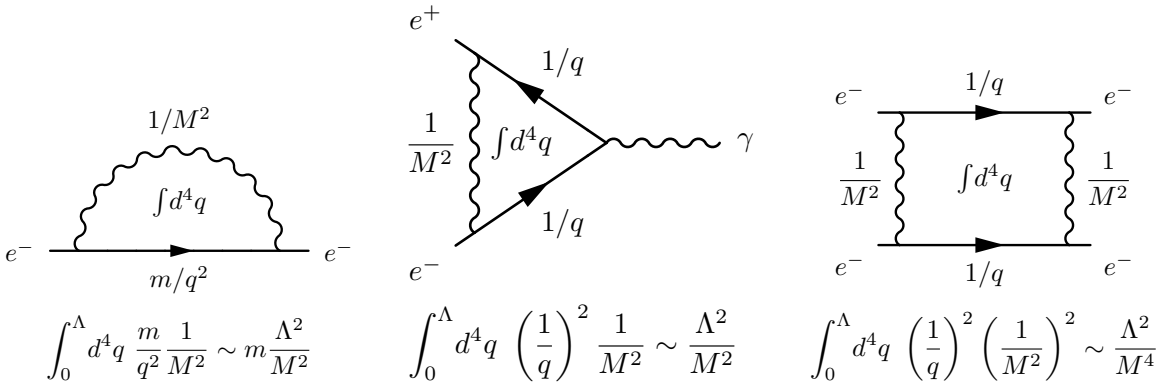

Figure 2.1: Feynman graphs showing interactions between electrons (straight lines) and a massive photon (wiggly lines). I am grateful to Hiren Patel for assistance in creating this figure.

the weak interaction underwent a number of revisions, beginning with Fermi's four-fermion model in 1933 (9; 10), the inclusion of parity violation in the 1950's (11; 12), and finally culminating with the GWS model in the 1960's. As we will discuss further below, the Higgs plays a staring role in the GWS model.

The Trouble with Vector Boson Masses

It is well known that unlike electromagnetism, the weak force is a *short range force* (see, e.g., the textbook (13)). However, in analogy with electromagnetism, one can model such an interaction with an intermediate vector (spin equal to one) boson provided that this boson is allowed to be massive. If the boson has a mass M then the range of the interaction is given approximately by $r \sim M^{-1}$. Indeed, in the case of the weak interactions this boson must be quite heavy, since it was not produced in either nuclear or muonic decays. This picture was confirmed in 1983 when the $W^{\pm}$ and Z bosons were discovered at the Super Proton Source (SPS) accelerator with masses 80.4 GeV and 91.2 GeV, respectively (14).

The weak force is the only known fundamental force that is mediated by mas-

sive vector bosons. It turns out to be very difficult to develop a theory of massive spin-1 fields that is theoretically consistent and predictive. In fact, it wasn't until 1971 that 't Hooft and Veltman (15; 16) demonstrated that this task may be accomplished by employing a Higgs field. In order to illustrate the difficulty that arises – and thereby demonstrate the importance of the Higgs boson – let us consider the hypothetical interaction of electrons with a massive photon. Suppose that we are interested in calculating perturbative corrections to the mass of the electron and to its electromagnetic coupling with the photon. This calculation may be performed by evaluating various one-loop Feynman graphs, some of which are shown in Figure 2.1. As a consequence of quantum mechanics, the *virtual particles* in the loops are allowed to have an arbitrarily large momentum q, and we anticipate that this may cause divergences to arise in our calculation. Focusing our attention on estimating the degree of divergence, we can calculate the graphs using the following "Feynman rules"

$$\begin{aligned} \text{each loop}: &\qquad \lim_{\Lambda\to\infty}\int_0^\Lambda d^4q \\ \text{electron line}: &\qquad \frac{1}{\not{q}-m} \xrightarrow{q\gg m} \frac{1}{q}+\frac{m}{q^2} \\ \text{photon line}: &\qquad \frac{-g_{\mu\nu}+\frac{q_\mu q_\nu}{M^2}}{q^2-M^2} \xrightarrow{q\gg M} \frac{q_\mu q_\nu}{q^2M^2} \sim \frac{1}{M^2} \end{aligned} \tag{2.1}$$

where m and M are the electron and photon masses, respectively. Here, we have written the upper bound on the momentum integration as Λ, anticipating that the integral will be divergent. Applying these rules to the first graph in Figure 2.1, corresponding to corrections to the electron's mass, we estimate the amplitude as[2]

$$\lim_{\Lambda\to\infty}\int_0^\Lambda d^4q\left(\frac{1}{q}+\frac{m}{q^2}\right)\frac{1}{M^2} \sim \lim_{\Lambda\to\infty} m\frac{\Lambda^2}{M^2}\,, \tag{2.2}$$

which diverges like Λ^2/M^2. Divergences like this are not uncommon in quantum field theory, and can be removed by the procedure known as *renormalization*. That is, after

[2]The term which would be $O\left(\Lambda^3\right)$ vanishes as a consequence of Lorentz invariance.

measuring the electron's mass, we can add a *counterterm* to the theory which will cancel the divergence and leave behind only the physical mass. The second graph is also divergent, and can be renormalized by using a measurement of electron scattering to determine the electromagnetic coupling constant. However, the persistence of the divergence in the third graph, and similar higher order graphs, is ruinous. Ultimately in order to cancel the divergences to all orders we would need an infinite number of measurements to specify the infinite number of counterterms. In this way, the theory looses its predictive power and is said to be *non-renormalizable*. Note that this problem does not arise for a massless photon, since in that case each photon line comes in with a factor of $1/q^2$ and renders the higher-order integrals convergent.

The Incredible Edible Higgs

The purpose of the Higgs in the GWS model of the electroweak interactions is to provide a mass to the weak gauge bosons in a way that allows the theory to remain renormalizable. The GWS model is formulated as follows. The gauge group is

$$G_{\rm EW} = {\rm SU}(2)_L \times {\rm U}(1)_Y \tag{2.3}$$

with associated gauge fields W^a_μ (for $a = 1, 2, 3$) and B_μ and coupling constants g and g'. The Higgs field transforms as a doublet under the ${\rm SU}(2)_L$ and carries a charge $Y_H = 1$ under the ${\rm U}(1)_Y$. Therefore it can be written as $H = (H^+\,,\, H^0)^T$. The matter fields (quarks and leptons) are also incorporated into the theory, but they are not pertinent to this discussion and will be neglected. The interactions between the Higgs and the electroweak gauge bosons are specified by the Lagrangian

$$\mathcal{L} = \left| \partial_\mu H - i\, g \frac{\sigma^a}{2} W^a_\mu H - i\, g' \frac{Y_H}{2} B_\mu H \right|^2 \tag{2.4}$$

where σ^a are the Pauli matrices. It is straightforward to show that the Lagrangian Eq. (2.4) remains invariant under the action of the gauge group

$$\begin{aligned} H &\to \exp\big[i\frac{\sigma^a}{2}\theta_L^a + i\frac{Y_H}{2}\theta_Y\big]H \\ W_\mu^a &\to W_\mu^a + \frac{1}{g}\partial_\mu\theta_L^a - \epsilon^{abc}\theta_L^b W_\mu^c \\ B_\mu &\to B_\mu + \frac{1}{g'}\partial_\mu\theta_Y \end{aligned} \tag{2.5}$$

where $\theta_L^a(x)$ and $\theta_Y(x)$ are smooth functions of the spacetime coordinate x. It is also important to note the theory Eq. (2.4) is renormalizable.

It is immensely useful to build a theory upon a symmetry group. The symmetry controls the allowed interactions and determines the conserved quantities. However, in this situation, the symmetry Eq. (2.3) is quite limiting. To correctly model the weak interactions, we need the weak gauge bosons acquire a mass, but the mass terms $M_W^2 W_\mu^a W^{\mu\,a}$ and $M_B^2 B_\mu B^\mu$ cannot be added to the Lagrangian without breaking the symmetry (i.e., they are not invariant under Eq. (2.5)). The way in which we get around this restriction is to suppose that the symmetry is broken not at the level of the Lagrangian, but instead broken by the vacuum state of the theory. In such a situation we say that *spontaneous symmetry breaking* has occurred. In 1962 Goldstone, Salam, and Weinberg (17) proved that in such a situation the spectrum should contain a massless scalar field – known as a *Goldstone boson* (18; 19) – for every spontaneously broken (continuous, global) symmetry. The Goldstone boson seems undesirable (and unphenomenological), however it is just what is needed to generate masses for the gauge bosons. The *Higgs mechanism*, proposed in 1964 by Peter Higgs (20–22), Englert & Brout (23), and Guralnik, Hagen, & Kibble (24), allows the scalar Goldstone boson to be "eaten" by the longitudinal polarization component of the vector boson and thereby endow it with a mass. The Higgs mechanism is operative provided the symmetry group being broken is a gauge group, which is the

case in the GWS model.

The following calculation illustrates how the symmetry $\mathrm{SU}(2)_L \times \mathrm{U}(1)_Y$ is broken so as to give the weak gauge bosons masses and maintain the massless photon. Spontaneous symmetry breaking is manifest in the fact that the Higgs acquires a nonzero vacuum expectation value (VEV)

$$\langle 0 | H | 0 \rangle = \begin{pmatrix} 0 \\ \frac{v}{\sqrt{2}} \end{pmatrix} . \tag{2.6}$$

Making this replacement in Eq. (2.4) we obtain (suppressing the μ subscripts)

$$\mathcal{L} = \frac{1}{8} \left| \begin{pmatrix} gW^3 + g'B & g(W^1 - iW^2) \\ g(W^1 + iW^2) & -gW^3 + g'B \end{pmatrix} \begin{pmatrix} 0 \\ \frac{v}{\sqrt{2}} \end{pmatrix} \right|^2 . \tag{2.7}$$

Now defining

$$W^{\pm} = W^1 \mp W^2 \quad , \quad A = \frac{g'W^3 + gB}{\sqrt{g^2 + g'^2}} \quad , \quad Z = \frac{gW^3 - g'B}{\sqrt{g^2 + g'^2}} \tag{2.8}$$

we can write Eq. (2.7) as

$$\mathcal{L} = \frac{1}{2} M_W^2 W^+ W^- + \frac{1}{2} M_Z^2 Z^2 + \frac{1}{2} M_A^2 A^2 \tag{2.9}$$

where

$$M_W = \frac{1}{2} v g \quad , \quad M_Z = \frac{1}{2} v \sqrt{g^2 + g'^2} \quad , \quad M_A = 0 . \tag{2.10}$$

In this way we see that the GWS model predicts masses for the weak gauge bosons and a massless photon. This model of Glashow, Weinberg, and Salam didn't receive much attention until 1971 when 't Hooft and Veltman (15; 16) showed that the the renormalizability of the original Lagrangian Eq. (2.4) is maintained through the process of spontaneous symmetry breaking. Thus, the Higgs managed to deliver the long sought after renormalizable theory of massive weak bosons. Measurements of the

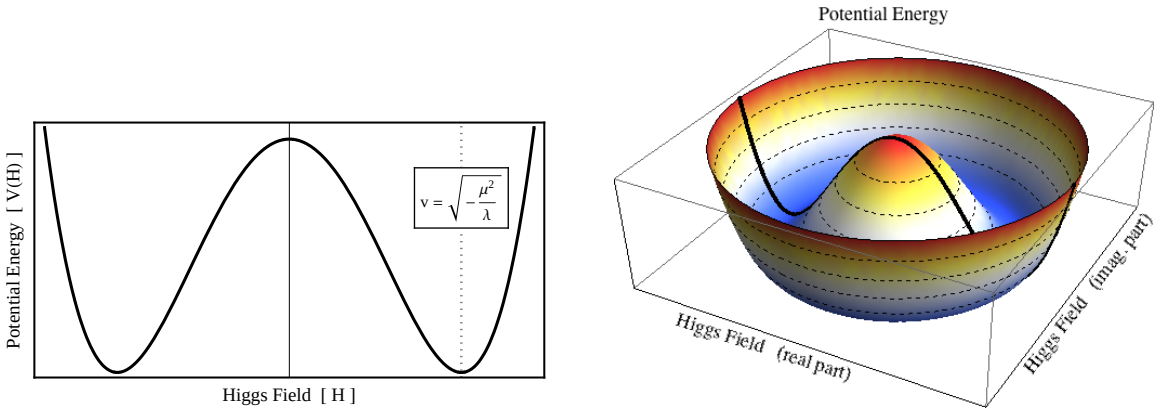

Figure 2.2: The Higgs potential illustrating spontaneous symmetry breaking.

weak neutral current merited Glashow, Weinberg, and Salam the 1979 Nobel Prize, and 't Hooft and Veltman received their prizes in 1999.

The crux of the GWS models is that the Higgs acquires a VEV and thereby breaks the $\mathrm{SU}(2)_L \times \mathrm{U}(1)_Y$ symmetry spontaneously. Spontaneous symmetry breaking is accomplished by introducing a potential energy (density) function for the Higgs field which renders $H = (0\,,\,0)^T$ unstable. The potential may be written as

$$V(H) = \mu^2 H^\dagger H + \lambda (H^\dagger H)^2\,. \tag{2.11}$$

Provided that $\mu^2 < 0$, the origin is an unstable maximum and spontaneous symmetry breaking occurs. A potential of this form is illustrated in Figure 2.2. The true vacuum state is found by minimizing $V(H)$ to obtain

$$v = \sqrt{\frac{-\mu}{\lambda}} \tag{2.12}$$

where we have used Eq. (2.6). The GWS model predicts a relationship between the coupling constant G_F of Fermi's four-fermion theory and the VEV of the Higgs: $G_F = \sqrt{2}\, g^2/8m_W^2 = (\sqrt{2}v^2)^{-1}$. Thus, a measurement of $G_F \approx 1.166 \times 10^{-5}$ GeV^{-2} (14) allows one to determine $v \approx 246$ GeV. Higgs boson particles corresponds to fluctuations of the Higgs field on top of this nontrivial background. To study their

mass and interactions, we can perform an expansion $H = \left(0\,,\,(v+h)/\sqrt{2}\right)$ and write Eq. (2.11) as

$$\hat{V}(h) = \frac{1}{2}(2\lambda v^2)h^2 + \frac{1}{3}(3\lambda v^2)h^3 + \frac{\lambda}{4}h^4\,. \tag{2.13}$$

From this expression, we see that the mass of the Higgs boson is related to its self-coupling λ by

$$M_H = v\sqrt{2\lambda}\,. \tag{2.14}$$

Since λ is a free parameter, the Higgs mass is all together unconstrained in the GWS model.

The Great Higgs Hunt

Predictions of the GWS model were very quickly confirmed. The predicted weak neutral current (mediated by the Z boson) was first observed in 1973 at CERN's Gargamelle bubble chamber through the processes $e^-\nu_e \rightarrow e^-\nu_e$ (25) and $\nu N \rightarrow \nu + \text{hadrons}$ (26). On-shell production and discovery of the weak bosons, however, had to wait another decade. The $W^\pm$ boson was the first to be discovered in 1983 at the UA1 detector at SPS (27). The Z boson discovery came a few months later (28). The only missing piece of the puzzle was the Higgs boson itself. For nearly the past half century, the search for the Higgs boson has been the driving force behind high energy particle physics (see e.g., (29) for a historical overview). Here, I review the progress (and success!) that has been made in the great Higgs hunt.

Pre-Collider Constraints

As the GWS model began to receive attention in the early 1970's, many physicists were hoping for the Higgs boson to turn up. As it so happened, in 1971 measurements

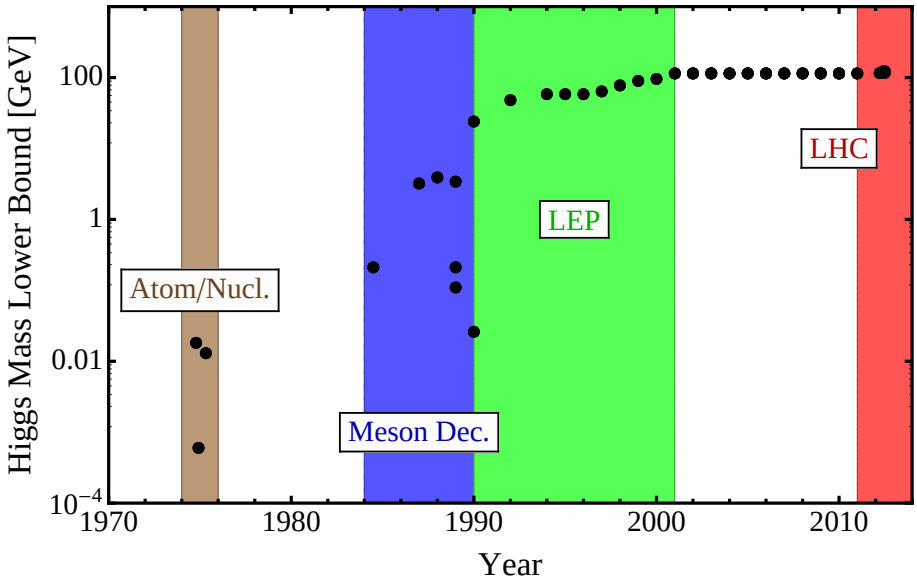

Figure 2.3: Constraints on the Higgs mass by various searches. The figure was compiled using references in the text and the Particle Data Group archives (30).

of muonic x-rays, i.e. the x-ray emission by atomic transitions in muonic atoms, revealed a discrepancy between the predicted and measured spectra (31; 32). In 1972, the seminal paper *Is There a Light Scalar Boson?* (33) investigated the possibility that a light scalar Higgs particle may be able to account for the anomaly. They determined that the discrepancy could indeed be explained by the Higgs and placed an *upper* bound on its mass $M_H < 8.5$ MeV. Moreover, they proposed that the existence of a light Higgs could be confirmed if one were to measure the $0^+ \to 0^+ + H$ nuclear transition and search for a e^+e^- pair emitted upon decay of the Higgs boson. Two years later (34), this search[3] was performed in the decay of excited ^{16}O(6.05 MeV) and ^{4}He(20.2 MeV) nuclei. The results were null and provided one of the earliest bounds on the Higgs mass, 1.030 MeV $< M_H <$ 18.2 MeV, where the lower limit is constrained by $2m_e$ and the upper limit by the scale of the nuclei observed. Later that year, another group (35) recognized that a light scalar boson would mediate a

[3]To my knowledge, this was the first dedicated "Higgs search." Regrettably, the paper has a mere forty-two citations listed on Inspire-HEP.

long-range force, and they sought out the Higgs by looking for anomalous behavior in the neutron-electron and deuteron-electorn elastic scattering processes. This allowed them to exclude the entire range $M_H < 0.6$ MeV. Similarly, the following year low energy neutron-nucleus scattering experiments yielded an exclusion of $m_H < 13$ MeV (36). In 1975, Sato & Sato (37) ruled out the 0.1 eV $< M <$ 100 eV mass range by considerations of the impact of out of equilibrium Higgs diphoton decays on the cosmic microwave background. A few months later, the same group (38) considered stellar cooling by Higgs particle emission and excluded $M_H < 350$ keV. The low mass Higgs was quickly becoming ruled out.

In 1975, Ellis, Gaillard, and Nanopolous (39) released the groundbreaking paper *A Phenomenological Profile of the Higgs Boson.* They discussed possible detection of the Higgs particle at a high energy collider experiment, and calculated the branching ratios for Higgs decays over a mass range of 1 MeV to 100 GeV. At the end of their paper, the authors offer an apology to their experimentalist colleagues for not being able to pin down the mass or couplings of the Higgs boson. They conclude by saying, *"For these reasons we do not want to encourage big experimental searches for the Higgs boson, but we do feel that people performing experiments vulnerable to the Higgs boson should know how it may turn up."* Despite their cautious attitude, their paper heralded the era of high energy Higgs searches.

Meson Decay Searches

The next leap forward in the hunt for the Higgs occurred in the 1980's at which point various facilities were studying mesons. If the Higgs were sufficiently light, it may have been produced in the decay of these mesons and then decayed to a detectable pair of charged leptons. This allowed the mass ranges up to $2m_\mu \approx 211$ MeV and $2m_\tau \approx 3.4$ MeV to be probed. In 1984, an experiment at KEK looked for the decay

$K^{\pm} \to \pi^{\pm} H$ decay and excluded the mass range 50 MeV $< M_H < 2m_\mu$ (40). A few years later, a group at BNL excluded $M_H < 26$ MeV by the non-observation of $K^{\pm} \to \pi^{\pm} +$ nothing, since a light Higgs would be longer lived and escape the detector (41). In 1987, the CUSB collaboration failed to observe the decay $\Upsilon \to \gamma H$ and excluded 600 MeV $< M <$ 3.2 GeV (42; 43). In 1989, SPS looked for the decay $K_L^0 \to \pi^0 H$ with $H \to e^+e^-$ and was able to exclude 15 MeV $< M < 2m_\mu$ (44). Furthermore, the SINDRUM collaboration searched for the decay $\pi^+ \to e^+ \nu_e H$ with $H \to e^+e^-$ and finding no anomalous behavior, they excluded the range 10 MeV $< M <$ 110 MeV (45). In the same year, CLEO excluded 211 MeV $< M <$ 3.4 GeV by the non-observation of the $B \to KH$ decay with subsequent $H \to (\mu^+\mu^-)(\pi^+\pi^-)(K^+K^-)$ (46). These constraints from meson decays pushed the Higgs mass bound across the GeV threshold and thereby extended the exclusion region by two orders of magnitude more than earlier nuclear experiments. However, the hadronic physics involved in these processes was not well understood and these bounds came along with large theory uncertainties.

LEP – ALEPH, DELPHI, OPAL, & L3

In 1989, the Large Electron-Positron Collider (LEP) began operation at CERN. Running in the first phase (LEP1) until 1995, the center-of-mass energy was fixed at $\sqrt{s} \approx M_Z$ so as to produce on-shell Z bosons. This allowed for the Higgs to be searched for via the Bjorken process in which the on-shell Z decays to a Higgs and an off-shell Z, which subsequently decays to fermions ($Z \to HZ^* \to Hf\bar{f}$). If the Higgs mass were in this energy range, the Higgs would then decay dominantly to $b\bar{b}$ with a small fraction to $\tau^+\tau^-$. By 1996, the non-observation of a Higgs signal placed the bound $M_H > 65.2$ at 95% CL (47). In its second phase (LEP2), the center-of-mass energy was increased up to 209 GeV. This allowed for a Higgs search via the

Higgs-strahlung production process in which an off-shell Z boson was created and subsequently decayed to a Higgs and an on-shell Z ($Z^* \rightarrow ZH$). The nonobservation of a Higgs signal placed a lower bound on the Higgs mass $M_H > 114.4$ GeV at 95% CL (48). The collider was decommissioned in 2000, and construction on the LHC was already undeway.

Tevatron – D0 & CDF

Meanwhile, the Tevatron began operation at Fermilab in 1983. The Tevatron collided protons and antiprotons at energies up to 1.96 TeV. At a hadron collider, a sub-TeV Higgs is most likely to be produced by the *gluon fusion* process in which the protons radiate a pair of gluons which annihilate into a Higgs by way of a top quark loop. The machine shut down in the fall of 2011, but data analysis continued. In the March of 2012, the Tevatron collaborations announced that they had found the hint of a Higgs boson in the 125 GeV mass range. In particular, the CDF and D0 detectors uncovered a statistical excess (2.7σ local, 2.2σ global over $115 - 135$ GeV) of Higgs-like events in combined channels, although dominantly $b\bar{b}$ decays (49). After increased analysis, the collaborations announced in July of that year that the statistical significance had risen (3.0σ local, 2.5σ global over $115 - 140$ GeV) (50; 51), however discovery was still beyond their reach.

LHC – ATLAS & CMS

The Large Hadron Collider (LHC) began operations at CERN in 2009 with the goal of discovering the Higgs boson and (/or) uncovering the nature of electroweak symmetry breaking. Like the Tevatron, the LHC is a hadron collider, however it operates a higher energy – approximately 7 TeV per beam – and thus has a higher event rate. This allows the LHC's detectors, ATLAS and CMS, to search for rare, "clean" decay

channels which were too infrequent to be useful at the Tevatron. In particular, the *golden channel* for the discovery of a light Higgs is the gluon fusion and diphoton decay channel ($gg \to H \to \gamma\gamma$). In this decay, the photons are easily identified by their recognizable clusters in the electron calorimeter, and their energy may be measured precisely. Moreover, this channel is considered clean, because although the background processes (jets faking photons) are large, they are also reducible. The second best channel for Higgs detection is $H \to ZZ \to \ell^+\ell^-\ell^+\ell^-$. Although this process is rare, the background is very low.

In December of 2011, the Atlas and CMS experiments hinted at a Higgs signal in the $H \to \gamma\gamma$ channel at $M_H \approx 126$ GeV. The official results were released in the early spring. In the diphoton channel, CMS saw an excess (3.1σ local, 1.8σ global over $110 - 150$ GeV) at $m_H \approx 124$ GeV (52; 53). In the $ZZ \to 4\ell$ channel, they saw excesses at $m_H \approx 126$ GeV (1.5σ local) and at $m_H \approx 119$ GeV (2.7σ local) (52; 54). At the same time, ATLAS uncovered and excess (2.8σ local, 1.5σ global over $110 - 150$ GeV) in the diphoton channel at $m_H \approx 126.5$ GeV (55; 56) as well as in the $ZZ \to 4\ell$ channel at $m_H \approx 125$ GeV (2.1σ local) (56; 57). Finally on July 4, 2012 – forty years after the hunt for the Higgs had began – the collaborations announced the discovery of a new scalar particle that fit the profile of the SM Higgs. Success!

2.2 The Cosmological Higgs: Electroweak Baryogenesis

As we saw in the previous section, a critical assumption of the SM is that the electroweak symmetry is broken today by the nonzero VEV of the Higgs field. This fact may have surprising consequences for early universe cosmology. In 1972 Kirzhnits

and Linde (58; 59) were the first to predict that the electroweak symmetry is restored in the high temperature conditions of the early universe. Their argument is motivated by an analogy with the Meissner effect in a superconductor, and relies on the intuition that the free energy $F = U - TS$ is minimized at high temperature by a disordered state in which the entropy is maximized. Their results were confirmed two years later by Weinberg (60) and Dolan & Jackiw (61) who reevaluated the problem using thermal effective potential techniques. The phenomenon of thermal symmetry restoration suggests that as the universe cooled, spontaneous symmetry breaking could have been accomplished through an electroweak phase transition (EWPT).

Remarkably, the electroweak phase transition may have set the stage for the generation of the *baryon asymmetry of the universe* (BAU), i.e., the abundance of matter over antimatter. In 1985 Kuzmin, Rubakov, & Shaposhnikov (62) conjectured that during the EWPT, the BAU may have been produced by recently discovered baryon-number violating processes known as electroweak sphalerons. Their investigation revealed that, nominally, the SM contains all of the requisite ingredients for baryogenesis, but that the EWPT must satisfy certain conditions[4] in order for the BAU to be generated successfully. These results were confirmed by Cohen, Kaplan, & Nelson in 1990 (63; 64) who further developed the mechanism now known as *electroweak baryogenesis* (EWBG).

Of course empirically, absolutely nothing is known about the nature of the electroweak symmetry breaking, since the Higgs boson has only recently been discovered, and its properties and couplings to new physics are still undetermined. However, the success of electroweak baryogenesis is predicated on certain conditions being met at the electroweak phase transition. Thus, if one insists that electroweak baryogenesis is to be responsible for creating the BAU, one can derive constraints on properties of

[4]In the SM, these conditions translate into an upper bound on the Higgs mass $m_H \lesssim 60$ GeV, as we will see below.

Higgs boson, such as its mass, its participation in CP-violation, and its coupling to exotic particles. In this way, EWBG augments Higgs searches at colliders with an additional constraint on models of the EW sector. This connection to terrestrial Higgs physics makes electroweak baryogenesis arguably the most compelling and testable baryogenesis mechanism.

The Baryon Asymmetry of the Universe

The abundance of matter over antimatter is one of the most apparent yet mysterious properties of our universe. The only antimatter that exists on the Earth are produced fleetingly through high energy particle collisions in accelerator facilities or in the upper atmosphere during cosmic ray showers. There is evidence that a small fraction of the cosmic rays are, themselves, antiprotons – approximately one in ten-thousand (65) – however, this tiny abundance is consistent with secondary production in astrophysical accelerators, and does not suggest a primordial antimatter abundance. On larger scales, one might guess that antimatter may be found sequestered in distant galaxies or galaxy clusters. However, if this were the case gamma rays would nevertheless be produced at the interface of the matter / antimatter domains. The non-observation of this diffuse gamma ray background puts a lower bound on the sequestration scale which exceeds the size of the visible universe (66; 67). It seems that for all intents and purposes, we live in a universe of matter.

The BAU can be quantified using the *baryon-to-photon* ratio. This parameter is defined as

$$\eta \equiv \frac{n_B}{n_\gamma} \tag{2.15}$$

where n_b ($n_{\bar{b}}$) is the number density of baryons (antibaryons), $n_\gamma \simeq 2\zeta(3)T^3/\pi^2$ is the number density of photons at temperature T, and $n_B = n_b - n_{\bar{b}}$ is the number

density of baryon number (B). Although both n_B and n_γ are functions of time, when defined in this way η remains constant at late times.

The baryon-to-photon ratio was famously measured by comparing the abundances of light elements with the predictions of Big Bang Nucleosynthesis (BBN) (68). Assuming that BBN takes places after the BAU is generated, η represents the relative number of nucleons (p and n) to photons. Larger η would therefore bias the production of ^{4}He, produced through the nuclear reactions[5] $p(n,\gamma)\mathrm{D}(\mathrm{D},n)^3\mathrm{He}(\mathrm{D},p)^4\mathrm{He}$, and cause a reduction in the abundances of ^{3}He and D. The abundances of light elements can be measured in metal-poor astrophysical systems where the effects of stellar processing are thought to be minimized. Extrapolating to zero metallicity, the primordial abundances may be inferred and, comparing with the predictions of BBN, used to constrain the baryon-to-photon ratio to be (69)

$$\mathrm{BBN}: \qquad (5.1\times10^{-10}) < \eta < (6.5\times10^{-10}) \qquad \text{at } 95\%\ \mathrm{CL}\,. \tag{2.16}$$

This measurement indicates that our universe contains approximately 60 protons for every billion photons.

Measurements of the power spectrum of the *cosmic microwave background radiation* (CMB) provide an independent and yet more precise determination of η. The CMB was formed when the universe was approximately 300,000 years old and it had cooled to a temperature of a few eV. At this point, electrons and hydrogen nuclei were able to recombine without becoming immediately dissociated once again by hot photons. Subsequently, it became possible for photons to *free stream* through the optically thin, neutral hydrogen gas. On reaching us today, these photons fill the sky with a diffuse, thermal radiation in the microwave band. The distribution of temperature fluctuations over the sky bears the imprint of density fluctuations at the time

[5]The notation $A(B,C)D$ refers to the two processes $A+B\to C+D$ and $A+C\to B+D$ by which A is converted into D.

of recombination. The pattern of peaks and dips in the CMB power spectrum owe their origin to the *baryon acoustic oscillations* (BAO) which preceded recombination.

Prior to recombination, baryons[6] and photons were kept tightly coupled by Compton scattering. At the temperature of recombination, the baryons were non-relativistic and pressureless ($p_b = 0$) whereas the photons were ultrarelativistic ($p_\gamma = \rho_\gamma/3$). Together they formed a *baryon-photon fluid* (BPF) with a sound speed

$$c_s = \frac{1}{\sqrt{3(1+R)}} \tag{2.17}$$

where

$$R \equiv \frac{p_b + \rho_b}{p_\gamma + \rho_\gamma} \approx \frac{45}{2\pi^4}\zeta(3)\frac{m_b}{T}\eta\,. \tag{2.18}$$

In the second equality we have neglected the electron mass and used $\rho_b = m_p n_b$ and $\rho_\gamma = \pi^4 T n_\gamma/30\zeta(3)$. Since $T \approx$ eV at the time of recombination and $m_p \approx 1$ GeV, we can estimate $R \approx 0.17 \times \eta/(6 \times 10^{-10})$. Since $R \sim 1$, we expect c_s to depend sensitively on η. We can use c_s to get a handle on the behavior of the BPF. For larger η, we find that c_s decreases implying that the BPF behaves more like a pressureless gas of baryons; whereas for smaller η we find that c_s increases toward $1/\sqrt{3}$ implying that the BPF behaves like a relativistic gas of photons.

The propagation of sound waves played an important role in the formation of the BAO. Before recombination, density fluctuations of the BPF evolved in the gravitational potential sourced by the distribution of dark matter. We can understand this system by considering an isolated overdensity of dark matter and a homogenous background of BPF. Initially, the BPF begins to collapse onto the dark matter, but as its own density grows there comes a point where its repulsive pressure overcomes the gravitational attraction, the infall turns around, and the BPF begins to recede. This initiates an oscillatory process which goes on until recombination reduces the pressure

[6]Conventionally, the term "baryons" is used here to refer to protons as well as electrons.

of the BPF to zero. As a result, the CMB power spectrum displays a harmonic progression of peaks and dips corresponding to the points of maximal compression and rarefaction. Varying η affects the power spectrum primarily by varying the relative heights of the even and odd peaks. For instance, increasing η decreases c_s and makes the BPF behave more like a pressureless baryonic gas. As a result of this *baryon loading*, the compression stages of the oscillation have a greater "inertia," since there is not as great a pressure to retard the collapse, and the density fluctuations are able to grow larger (70). In this way, measuring the height of the first (compression) peak of the CMB allows for an excellent determination of the baryon-to-photon ratio (71)

$$\text{CMB}: \qquad \eta = (6.19 \pm 0.15) \times 10^{-10} \qquad (68\%\,\text{CL})\,. \tag{2.19}$$

Comparing Eq. (2.16) and Eq. (2.19), we are encouraged by their remarkable agreement despite the fact that they independently probe η at totally different epochs in the cosmic history.

Baryogenesis at the Electroweak Phase Transition

As we have discussed above, on cosmic scales the baryon asymmetry may be quantified as $\eta = n_B/n_\gamma \approx 6 \times 10^{-10}$. In order to put this number into perspective, we can ask what the baryon asymmetry would be today if the universe had began in an initially baryon symmetric state ($\eta = 0$) and if no baryogenesis had taken place. In this scenario, the universe today would contain a gas of relic protons and antiprotons which is so diffuse that annihilations are extremely rare and effectively impossible. Consequently, the universe today would have a *global* baryon asymmetry of zero, but it could have a nonzero *local* baryon asymmetry if p and $\bar{p}$ had somehow become sequestered on scales larger than the size of the visible universe. It is straightforward to estimate the proton relic abundance. In the early universe, protons remained ther-

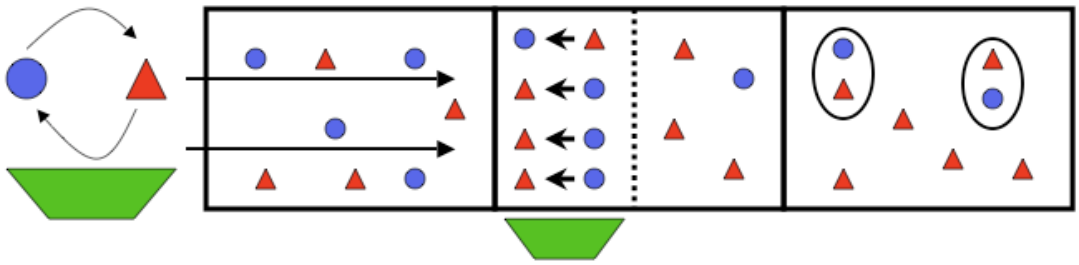

Figure 2.4: A cartoon illustrating hypothetical "electron-genesis" in analogy with EWBG. a) An L-violating process inter-converts electrons and positrons. b) The presence of a background electric field violates CP and biases a spatial separation of L. c) The L-violating process is only active in the region containing the positron excess. d) The L-violating process goes out of thermal equilibrium and is rendered inactive, residual electrons and positrons annihilate, and the L-asymmetry is generated.

malized and $\eta \approx n_p/n_\gamma \approx (m_p/T)^{3/2}\exp\left[-m_p/T\right]$. *Freeze out* occurred when the $p\bar{p}$ annihilation rate dropped below the Hubble expansion rate, roughly at a temperature of $T_{fo} \approx 20$ MeV (see e.g., (72)). Subsequently, η remained approximately constant, and thus its value today should be given by $\eta_{fo} \approx 10^{-20}$, which is much too small. Alternatively, one may admit the unnatural solution that $\eta \sim 10^{-10}$ is merely an initial condition of the "Big Bang." However, the concordance model of cosmology incorporates an inflationary phase which would have diluted any initial B-asymmetry to zero. We are left with only one possibility: that the B-asymmetry was created during a baryogenesis event in the course of the cosmic history, and more specifically, prior to BBN.

In 1976 Sakharov (73) proved that any baryogenesis mechanism must satisfy three criteria: B-violation, both C- and CP-violation, and a departure from thermal equilibrium[7]. These can be thought of as the ingredients that must be combined to yield a BAU, and compared to other baryogenesis mechanism, EWBG mixes these components in an interesting and unique way. Schematically, EWBG works in the following way, which is also illustrated in Figure 2.4 in the fictitious case of "electron-genesis."

[7]In general, the out of equilibrium condition may be replaced by CPT-violation.

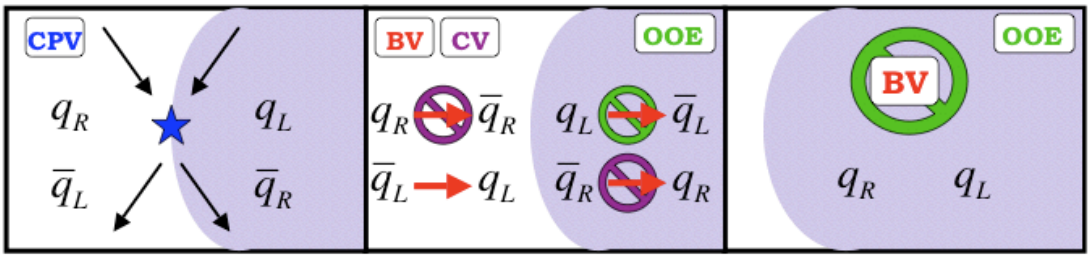

Figure 2.5: The mechanism of electroweak baryogenesis, as discussed in the text.

The existence of a B-violating process allows one to convert an antibaryon $\bar{b}$ into a baryon b. However, if such a process were simply applied to a thermal distribution of b and $\bar{b}$, no net B would be generated since CPT ensures that b is converted back to $\bar{b}$ at the same rate. The way in which EWBG gets around this impediment is to separate the b and $\bar{b}$ into different regions of space, and ensure that the B-violating process is only active in the region containing $\bar{b}$. The spatial separation of b and $\bar{b}$ relies on the fact that these antiparticle partners carry opposite charges, and thus they behave oppositely under C- and CP-violating interactions. After the $\bar{b} \to b$ conversion is complete, the B-violating processes is rendered inactive provided that it is not in thermal equilibrium, and the BAU has been generated.

Although the discussion of the previous paragraph captures the primary features of EWBG, the actual mechanism is a bit more involved. For example, the "L-violating" process discussed in Figure 2.4 also violates the conservation of electric charge, and therefore creates a cosmic charge asymmetry as well, which is not present in our universe. Let us now review in more detail the EWBG mechanism (63; 64), which is also represented in Figure 2.5. As the universe cools below $T \sim M_{\rm EW} \approx 100$ GeV, it is necessary that electroweak symmetry breaking proceeds through a first order phase transition. This subject will be discussed further in Chapter 3. For the present, we need only note that at a first order EWPT, bubbles of EW-broken phase ($\langle H \rangle \neq 0$) form within a background of EW-symmetric phase ($\langle H \rangle = 0$). These bubbles

provide the spatial boundary at which the B-asymmetry will be generated and satisfy Sakharov's out of equilibrium condition.

In the first step of EWBG, CP-violating interactions between the Higgs field and the particles in the plasma will bias the transmission and reflection of quarks and antiquarks from the bubble wall. For instance, if a left-handed quark q_L is incident on the bubble wall, it has a different probability to be transmitted as a q_L than to be reflected as a right-handed quark q_R. Consequently, q_R and $\bar{q}_L$ build up outside of the bubble wall while q_L and $\bar{q}_R$ build up within. In the second step, B-violating process, known as the EW-sphaleron, acts on the $\bar{q}_L$ outside of the bubble and converts it to q_L and charged leptons, such that electric charge is conserved. More will be said about the EW-sphaleron transition in Sec. 2.2, but for the moment two points should be emphsized. First, the EW-sphaleron only acts on field that carry a charge under the SM SU(2) gauge group. This ensures that the q_R outside of the bubble are not converted back into $\bar{q}_R$. Moreover, in this way, C is violated. Second, it is critical that the EW-sphalerons are inactive inside of the bubble. If this is not the case, then the q_L will be converted into $\bar{q}_L$, and there will be no global production of B-asymmetry. In the third and final step, the bubble wall expands to overtake the B-asymmetry where it is protected from further processing by EW-sphalerons, and EWBG terminates.

"Baryopreservation" and the Washout Criterion

In light of the discussion in the preceding section, we see that the EWBG mechanism relies upon baryon number generation at the bubble wall and baryon number preservation within the bubbles. It is essential that the latter "baryopreservation" stage is successful. If this stage fails, then the issue of whether or not a baryon asymmetry was generated at the wall in the first place is moot. Moreover, as we will see, the requirement of baryopreservation imposes direct constraints on the scale of the

electroweak phase transition and thereby, it places a model-dependent lower bound on the Higgs mass. Therefore, a measurement of merely the Higgs mass at colliders yields powerful constraints on EWBG models. For this reason, the question of viable baryopreservation will be the focus of the remainder of our discussion.

In EWBG, the B-violation is accomplished through thermal EW-sphaleron transitions. However, B-violation is forbidden at the classical level since the EW interactions respect a $U(1)_B$ symmetry and B is a conserved quantity. In order to achieve a violation of B, the symmetry associated with B conservation must be anomalous. The so-called *Adler-Bell-Jackiw anomaly* was first identified in 1969 (74; 75), but its connection to B-violation wasn't recognized until 1976 by 't Hooft (76; 77). 't Hooft discovered that B may be violated[8] by the non-perturbative processes known as *instantons*, which had been constructed in the previous year by Belavin, et. al. (78). 't Hooft noted that the rate of B-violation by instanton processes is proportional to a factor of $\exp\left[-4\pi/(\alpha_W\hbar)\right]$. The presence of $\hbar$ in the denominator indicates that the rate vanishes as we take $\hbar$ to zero. This allows us to interpret the instanton as the process associated with quantum mechanical tunneling through a barrier (79; 80) Using $\alpha_W = g^2/4\pi \approx 1/30$ for the weak coupling constant the suppression factor is approximately equal to 10^{-163}, and consequently B-violation by instanton processes is unobservable and insufficient for baryogenesis.

In 1985 Kuzmin, Rubakov, and Shaposhnikov (62; 81; 82) recognized that in the hot conditions of the early universe B-violation may proceed by "hopping over" the barrier instead of tunneling through it[9]. They employed a different non-perturbative process called the *sphaleron*, which had been discovered two years earlier (83; 84).

[8]Strictly speaking the anomaly mediates B+L violation where L is the lepton number. Since the combination B - L remains exactly conserved, B+L-violation allows B-violation accompanied by an equal amount of L-violation.

[9]Here I follow the standard language used in contrasting instantons and sphalerons. However, it is worth clarifying that the instanton is a scale invariant solution, and therefore its tunneling is associated with a barrier the action and not the potential energy, as in the case of the sphaleron.

The sphaleron, which takes its name from the Latin for "ready to fall," represents the static field configuration at the top of the potential energy barrier separating two topologically distinct states which differ by $\Delta(B+L) = 3$. The energy of the sphaleron represents the height of the barrier and is given by $E_{\rm sph} = B \times 4\pi v/g \approx 9$ TeV where $B \approx 2$ is a slowly varying function of m_H^2/m_W^2. At finite temperature, the height of the barrier grows smaller as the expectation value of the Higgs field $v(T)$ begins to decrease, leading to the scaling behavior (85)

$$E_{\rm sph}(T) \approx E_{\rm sph}\frac{v(T)}{v}\,. \tag{2.20}$$

We can estimate the rate per unit volume of B-violation as $T^4 \exp\big[-E_{\rm sph}(T)/T\big]$ where the Boltzman factor appears because the sphaleron is a thermal process and the T^4 is added on dimensional grounds. A more rigorous calculation yields (86; 87)

$$\frac{\Gamma_{\rm sph}}{V} \approx (2.8\times 10^5)\,T^4\left(\frac{\alpha_W}{4\pi}\right)^4 \kappa \left(\frac{E_{\rm sph}(T)}{BT}\right)^7 \exp\big[-E_{\rm sph}(T)/T\big] \tag{2.21}$$

where $10^{-4} < \kappa < 10^{-1}$ is a dimensionless prefactor that must be calculated numerically. It is also worth noting that outside of the bubbles the sphaleron processes, which are responsible for creating the B-asymmetry in the first place, are unsuppressed and proceed at a rate

$$\frac{\Gamma_{\rm sph}}{V} \approx k\,(\alpha_W T)^4 \tag{2.22}$$

where $0.1 < k < 1$.

We have stressed that baryopreservation requires the EW-sphaleron processes to be inactive within the bubbles. If these processes are not inactive, they any baryon asymmetry inside of the bubbles will be washed out by a factor of

$$\exp\big[-\int_{t_c}^{\infty}\Gamma_{\rm sph}dt\big] \tag{2.23}$$

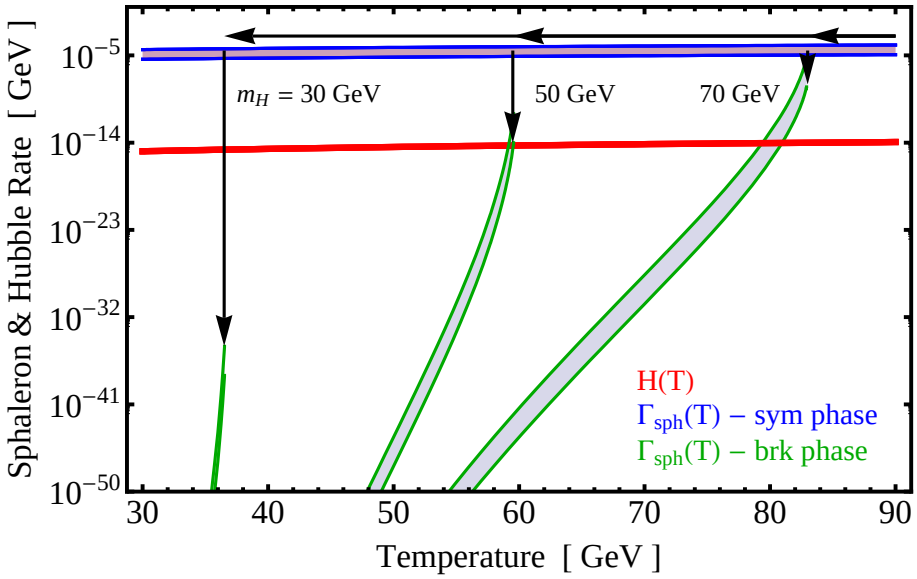

Figure 2.6: The rate of B-violation by sphaleron processes $\Gamma_{\rm sph}$ in the broken phase must fall below the Hubble expansion rate $H(T)$ at the time of the phase transition in order for the B-asymmety to be preserved. In the SM, this is the case for $m_H \lesssim 50$ GeV. The error bands correspond to uncertainty in κ and k.

where t_c is the time at which the phase transition occurred. This condition can be stated by saying that the rate Eq. (2.21) must be much smaller than the Hubble expansion rate at the time of the phase transition (62). At the time of the phase transition, the universe is radiation-dominated and the Hubble rate is given by $H(T) \sim (\pi/3)\sqrt{g_*/10}(T^2/M_p)$ where $g_* \simeq 106$ is the number of relativistic degrees of freedom and $M_p \simeq 10^{18}$ GeV is the Planck mass. Numerically, this competition is represented in Figure 2.6 where $H(T)$ is plotted along with the sphaleron rate in the broken phase Eq. (2.21) and in the symmetric phase Eq. (2.22). Analytically, requiring $H(T)$ to exceed the EW-sphaleron rate Eq. (2.21) averaged over a volume of T^{-3} we find a lower bound (88)

$$\frac{E_{\rm sph}(T)}{T} > 37 - 45 \tag{2.24}$$

where the variation arises from the uncertainty in κ. This bound must be satisfied at all times after the EWPT has occurred. Since both $E_{\rm sph}$ and $1/T$ are growing

functions of time (decreasing temperature), it is sufficient to impose the bound at the temperature T_c just after the EWPT. Furthermore, using the scaling relation Eq. (2.20), we can rewrite the bound Eq. (2.24) as

$$\frac{v(T_c)}{T_c} \gtrsim 1.0 - 1.3\,. \tag{2.25}$$

This bound is known as the *washout criterion*; if it fails to be satisfies, the baryon asymmetry will be erased by EW-sphaleron processes, and EWBG will have failed; if it is satisfied, we say that the EWPT is *strongly first order* (SFOPT). As we will see in the next chapter, both $v(T)$ and T_c depend upon the properties of the Higgs such as its mass and coupling to BSM physics. Therefore the bound Eq. (2.25) imposes a direct constraint on properties of the Higgs boson.

Baryogenesis in the Standard Model and Beyond

It is interesting to note that electroweak baryogenesis is the only baryogenesis mechanism that has the potential to generate the BAU using only ingredients drawn from the SM (88). Unfortunately, the SM falls short of the necessary requirements of EWBG in two ways. First, the only source of CP violation in the SM is the phase angle in the quark mixing matrix, and this tiny angle is insufficient to generate the BAU. Second, the SM fails to satisfy the requirement of a strongly first order elecroweak phase transition, which is expressed in Eq. (2.25). In fact, the phase transition is not even a phase transition at all; it is a continuous crossover without any departure from thermal equilibrium. It was known in the earliest discussions of EWBG that the SFOPT requirement imposed an upper bound on the Higgs mass (82). This bound, which is derived in the following chapter (see Eq. (3.43)) is given by

$$m_H < (m_H)_{\max} = \sqrt{\frac{2m_W^3 + m_Z^3}{\pi v}} \approx 48 \text{ GeV}\,. \tag{2.26}$$

This bound is also seen in the numerical calculation of the sphaleron rate shown in Figure 2.6. Lattice simulations of the phase transition later confirmed that for a Higgs mass above $(m_H)_{\max} \approx 66.5$ GeV, electroweak symmetry breaking proceeds through a continuous crossover (89; 90). As we discussed in the previous chapter, such a light Higgs was excluded in the late 1990s (see Figure 2.3). The Standard Model is incapable of generating a cosmic baryon asymmetry.

The failure of EWBG in the Standard Model is a disappointment, but at the same time it is an incentive. Many extensions of the SM are able to accommodate EWBG. The minimal supersymmetric generalization of the SM, known as the MSSM, allows for additional CP violation through the so-called μ term. Additionally, the EWPT may be rendered strongly first order by the presence of stops – new, colored scalar particles which couple strongly to the Higgs. However, searches for the Higgs and for the superpartners of the SM fields sharply constrain EWBG in the MSSM (91). The only remaining viable corner of parameter space is the limit in which stops are light (92) and the strength of the phase transition is enhanced by two-loop effects (93). In extensions of the MSSM, such as the nMSSM (94), the NMSSM (95; 96), and the $\mu\nu$SSM (97), electroweak baryogenesis is easier to accommodate. Electroweak baryogenesis may also be achieved in non-supersymmetric extensions of the SM. In particular, many models have been studied (98–119) which add a singlet scalar field to the SM in order to render the phase transition strongly first order. Whatever one's preference may be, the baryon asymmetry of the universe makes it *necessary* to venture beyond the Standard Model. Although electroweak baryogenesis may not provide the roadmap, it certainly points the way.

Chapter 3

The Phase Transition Calculation

In Sec. 2.2 we saw that electroweak baryogenesis may be able to account for the baryon asymmetry of the universe provided that the bound $v(T_c)/T_c > 1$ is satisfied. Since this bound – and the electroweak phase transition, more generally – will play a central role in the succeeding chapters, we will spend this chapter introducing the concepts and the techniques used in the phase transition calculation. At the conclusion of this chapter, we would like calculate the ratio $v(T_c)/T_c$ for the Standard Model electroweak phase transition. To reach this point, we will require a tool, known as the thermal effective potential, which facilitates the calculation of quantities like T_c and $v(T)$. A formal derivation of this function is beyond the scope of our discussion. Instead, we will define the effective potential as a free energy that depends upon an order parameter and temperature. Since these may not be familiar concepts, we will begin our discussion with a heuristic introduction to the phase transition analysis in two simple systems where we may underline the important concepts without the distraction of technical details.

3.1 Heuristic Introduction

Phase transitions are among the most interesting, complex, and yet familiar physical phenomena. Examples include the solid-liquid-gas transitions in many materials, the ionization and recombination of a hot plasma, the demagnetization of a heated ferromagnet, superconductivity in various cooled materials, and superfluidity in liquid helium. Although these systems are very distinct, they nevertheless share a number of common features. In systems like the ferromagnet and liquid helium, the microscopic dynamics respect a symmetry that is *spontaneously broken* at low temperature but restored above some *critical temperature* T_c. *Symmetry restoration* follows from the fact that a system in thermal equilibrium will evolve to a minimum of the free energy $F = E - T\,S$, which corresponds to a state of minimal energy at low temperature and to a state of maximal entropy at high temperature. Thus, it is often useful to identify an *order parameter* which quantifies the degree of symmetry breaking. As we will see, the temperature dependence of the order parameter provides useful information about the nature of the phase transition.

Ferromagnetic Transition

Consider the Ising Model in the absence of any external magnetic field. The system consists of N atoms arranged on a regular d-dimensional lattice of volume V, such that each lattice site has n neighbors. Each atom has spin 1/2 (due to an unpaired electron), which is aligned with the z-axis and can either point up or down. We will let N_u be the number of upward spins and $N_d = N - N_u$ be the number of downward spins. A particular spin configuration is illustrated in Figure 3.1. To model a ferromagnet, we suppose that the Hamiltonian of the system is such that misaligned spins are energetically disfavored. To be concrete, we can let ε be the

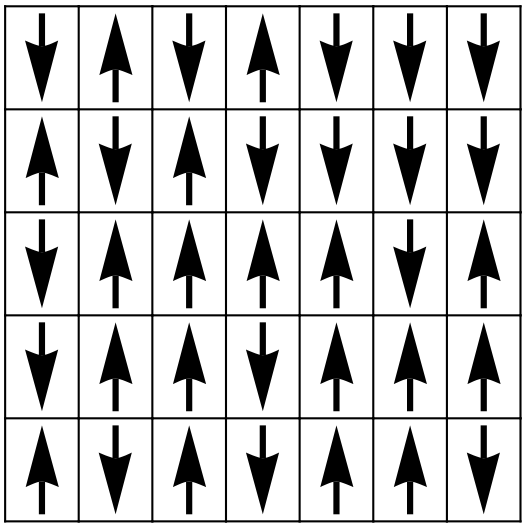

Figure 3.1: An illustration of the system of spins discussed in the text, where we have let $d = 2$ and $n = 4$.

energy cost of having a pair of adjacent, misaligned spins and let $-\varepsilon$ be the energy liberated by having a pair of adjacent, aligned spin. Thus, the maximal energy state is the one in which for every atom, the spins on all adjacent lattice sites are misaligned. The energy of this configuration is $E_{\max} = Nn\varepsilon/2$, where the factor of $1/2$ eliminates double counting. Conversely, the ground state of the system is the one in which all spins are aligned (either all up or all down) and the energy is $E_0 = -Nn\varepsilon/2$.

We may now investigate the behavior of this system at finite temperature through the following thought experiment. Suppose that the system is prepared by allowing it to relax to its ground state in which all of the spins are up, $N_u = N$ and $E = E_0$. We immerse the system into a heat bath at temperature T. As the system exchanges energy with the heat bath, some of the spins will flip downward at random. An energy of approximately $2n\varepsilon$ is required to flip the spin of an atom. This is illustrated in Figure 3.2. Thus, if an energy on the order of Nk_BT is absorbed from the heat bath, the number of flipped spins will be approximately $N_d = Nk_BT/(2n\varepsilon)$. As the temperature is raised, N_d cannot grow without bound since there are only a finite

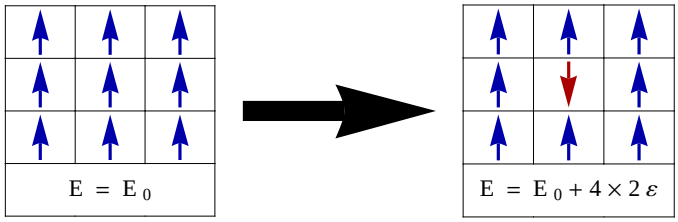

Figure 3.2: An isolated flipped spin increases the energy of the configuration by $n \times 2\varepsilon$.

number of spins on the lattice. Symmetry arguments, which we will discuss further below, demonstrate that N_d maxes out at $N/2$. This occurs at a temperature given approximately by $T_c = n\varepsilon/k_B$. At temperatures greater than T_c, the fraction of upward and downward spins each remain approximately equal to $N_u \approx N_d \approx 1/2$.

The temperature T_c demarcates an important threshold across which the macroscopic properties of the system vary dramatically. This can be seen by looking at the magnetization. For a given configuration, the average magnetization M (coarse grained over V) can be calculated as $M = \mu_B(N_u - N_d)/V$ where μ_B is the Bohr magneton. In the ground state with all spins aligned upward, the magnetization is simply $M_0 = \mu_B N/V$. When the system is immersed in the heat bath, the number of flipped spins increases like $N_d \sim T$ and the magnetization begins to decrease like $M = M_0(1-T/T_c)$. As the temperature approaches T_c, the magnetization approaches zero, and for all temperatures above T_c the magnetization remains approximately fixed at zero since $N_d \approx N_u$. We can see that the temperature T_c demarcates the boundary between the low-temperature magnetized phase and the high-temperature demagnetized phase. It may be identified as the phase transition temperature, also called the Curie temperature in this particular system.

A second way of identifying that a phase transition occurs at T_c it so look at the analyticity of the free energy. The free energy is calculated as $F = U - TS$ where U is the average energy and S is the entropy. In the ground state at $T = 0$ we have $U = E_0$.

At the temperature T_c and above, it is reasonable to suppose that $U = 0$. This guess is motivated by our earlier observation that at temperatures above T_c, there are an equal number of upward spins and downward spins. We may also expect that there are an equal number of aligned and misaligned spin pairs. Since aligned spin pairs provide a positive contribution to U while misaligned spins contribute negatively, it follows that on average U vanishes above T_c. The entropy S scales like the logarithm of the number of states (spin configurations) that are accessible provided an "energy budget" of Nk_BT. Thus, the entropy vanishes at $T = 0$ where the configuration of uniformly aligned spins is the only allowed state. Above T_c, we have just argued that the system is equally likely to be found in any of the states. Since the number of spin configurations scales exponentially with the number of atoms N on the lattice, we find that the entropy reaches a constant of approximately Nk_B above T_c. Combining these two contributions to F, we find that as the temperature is raised from zero to T_c, the two terms which enter into F compete: U increases while $-TS$ decreases. The latter terms wins out and F decreases from E_0 to approximately $-Nk_BT_c$ at T_c. At temperatures above T_c, the average energy is fixed at zero and F decreases further, linearly with T. The temperature dependence of M and F are shown together in Figure 3.3. The key observation here is that the behavior of F is non-analytic as the temperature crosses the threshold T_c. This non-analyticity in some thermodynamic quantity is a characteristic feature of a phase transition.

Finally, it is important to recognize that the magnetization acts as the order parameter of the symmetry of this system. The Hamiltonian makes no distinction between up spins and down spins, but instead only depends upon the alignment or misalignment of adjacent spins. Thus, the system possesses a symmetry relating any given spin configuration and the one in which all spins are flipped. The invariance of the Hamiltonian under this symmetry transformation ensures that the two conjugate

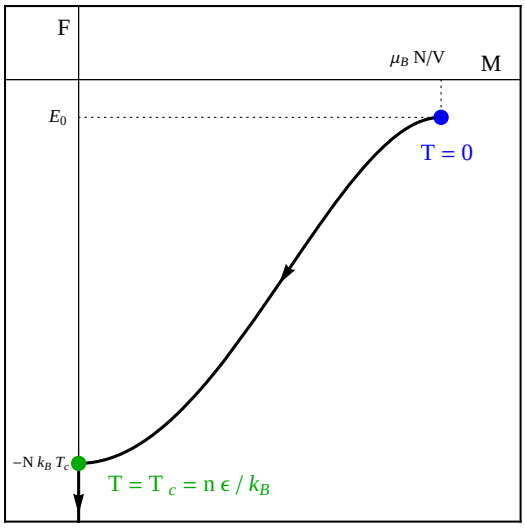

Figure 3.3: A sketch free of the energy F and magnetization M of the ferromagnetic system discussed in the text as the system is heated and the phase transition takes place.

configurations are degenerate. However under this transformation, the magnetization changes sign. Thus we can identify M as the order parameter of the spin flip symmetry.

The key features of the ferromagnetic phase transition which will be relevant in the remainder of this section are the following. A phase transition is (frequently) associated with symmetry breaking or restoration. As the temperature is increased, the system passes from the symmetry broken (ordered) to symmetry restored (disordered) phase, because the maximization of entropy becomes more important than the minimization of energy. This change occurs abruptly at a temperature threshold called the critical temperature T_c. One can identify the presence of a phase transition using an order parameter, appropriately defined to be nonzero in the symmetry broken phase and to vanish in the symmetry restored phase. One can also study the phase transition by investigating the non-analytic behavior of the free energy.

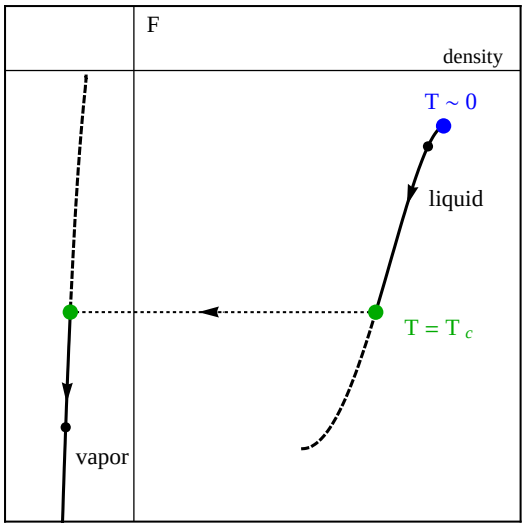

Figure 3.4: A schematic representation of the phase transition from vapor to liquid.

Water Vapor Condensation

The ferromagnetic phase transition, which was discussed above, is known as a second order phase transition. In such a phase transition, the order parameter and free energy vary continuously across the temperature threshold $T = T_c$, but the second derivative of the free energy varies discontinuously. In our investigation of the electroweak phase transition, we will be more interested in first order phase transitions. These transitions are characterized by a discontinuity in the order parameter at T_c and an associated coexistence of phases in the form of bubbles. A familiar example of a first order phase transition is the condensation of water vapor into liquid water at a temperature of approximately 100° C. In this system there is no spontaneously broken symmetry, but we can still identify an order parameter as the density of the material. The temperature dependence of the free energy and order parameter are shown schematically in Figure 3.4. The primary distinction with the ferrogmagnetic system is that now there exists a range of temperature at which the system could be found in either the liquid or gaseous phase. Above the critical temperature T_c, the

system has a smaller free energy in the gaseous phase, and below this temperature the free energy is smaller in the liquid phase. The phase transition occurs as the vapor is cooled to the temperature $T_c \approx 100^\circ$ C, at which point the free energy in the two phases are equal. Bubbles of condensed liquid begin to form, and the phases coexist at a temperature T_c until all of the vapor is converted into liquid. It is important to note that the order parameter, the density of the material, varies discontinuously as a function of temperature at the phase transition. This will be the hallmark feature of first order phase transitions in our study of the electroweak phase transition.

3.2 The Thermal Effective Potential

In the study of phase transitions, the thermal effective potential is an invaluable tool. As we saw in the examples of Sec. 3.1, the phase transition may be studied by calculating an order parameter and free energy as functions of temperature. However, it would be very useful to employ a thermodynamic potential, in analogy with a potential energy function of classical mechanics, which represents the free energy of the system at a given temperature as a function of *all possible values of the order parameter*. One may obtain the physical value of the order parameter and free energy at a given temperature by minimizing the thermodynamic potential. Figure 3.5 illustrates the application of such a thermodynamic potential for the systems discussed above. This thermodynamic potential is precisely the thermal effective potential we seek to define and calculate in this remainder of this section.

The non-thermal effective potential was first introduced by Heisenberg & Euler in 1936 (120) and by Schwinger in 1951 (121; 122). This formalism was applied to studies of spontaneous symmetry breaking by Goldstone, Salam, and Weinberg in 1962 (17), Jona-Lasinio in 1964 (123), and throughout the early 1970s by various authors (124–

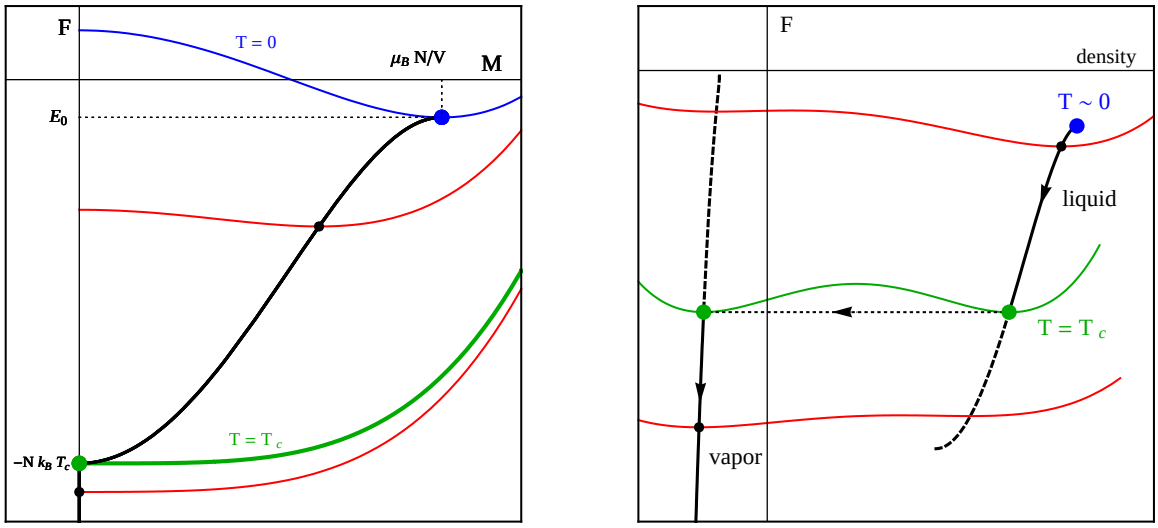

Figure 3.5: Schematic representations of the utility of a thermodynamic potential as applied to the study of phase transitions.

127). Meanwhile, thermal field theory was developed throughout the 1950s and 1960s (128–133). The thermal effective potential was introduced and applied to the issues of symmetry restoration and phase transitions by Weinberg (60) and Dolan & Jackiw (61) in 1974. I will follow the presentation of Guth (134), and sidestep the tricky issues of Green's functions at finite temperature by immediately restricting the discussion to a homogenous, static scalar field condensate.

Formal Definition

In this section we calculate the *thermal effective potential* $V_{\rm eff}(\phi_c, T)$ for a system at temperature T in which the scalar field condensate takes the value ϕ_c. The condensate may represent the order parameter of a symmetry breaking phase transition. In order to treat ϕ_c as a independent variable, as opposed to a function of T, we employ a subtle trick. We will take the Hamiltonian of the theory and add to it a source term for the scalar field such that the desired value of the scalar field condensate may be obtained by choosing the source appropriately. After calculating the free

energy density the explicit dependence on the source term is removed by a Legendre transformation. The result is the desired function $V_{\text{eff}}(\phi_c, T)$ which is independent of the source.

Consider the system in which the degrees of freedom consist of a real scalar field $\hat{\Phi}(\mathbf{x})$[1] and potentially other fields $\hat{\Psi}_i$ of arbitrary spin. The dynamics of this system are described by the Hamiltonian density $\hat{\mathcal{H}}(\hat{\Pi}, \hat{\Phi})$ where $\hat{\Pi}(\mathbf{x})$ is the momentum conjugate to $\hat{\Phi}$, and the dependence on $\hat{\Psi}_i$ and their conjugate momenta have been suppressed for clarity. Since we will be interested in the homogenous scalar field condensate, it will be convenient to define the spatially averaged field operator

$$\hat{\bar{\Phi}}(\Omega) = \frac{1}{\Omega} \int_{\Omega} d^3x \, \hat{\Phi}(\mathbf{x}) \tag{3.1}$$

which is coarse grained over a spatial volume Ω that we will eventually take to infinity. As discussed above, we are actually interested in the sourced Hamiltonian

$$\hat{H}(j, \Omega) = \int_{\Omega} d^3x \left(\hat{\mathcal{H}}(\hat{\Pi}, \hat{\Phi}) - j \, \hat{\bar{\Phi}} \right) \tag{3.2}$$

where j is the classical source field, assumed to be homogenous and static. At finite temperature the system is described by a *mixed state* – a statistical ensemble of *pure states* (e.g., eigenstates of the Hamiltonian). Eigenvalues of the *density matrix* $\hat{\rho}$ give the probability of finding the system in the associated (pure state) eigenstate. In thermal equilibrium at temperature T, and in the absence of any conserved charges (i.e., chemical potentials vanish), the density matrix is given by the Boltzmann distribution

$$\hat{\rho}(j, \Omega, T) = \frac{1}{Z(j, \Omega, T)} \exp\left[-\hat{H}(j, \Omega)/T \right] \tag{3.3}$$

where the *partition function*

$$Z(j, \Omega, T) = \text{Tr}\left(\exp\left[-\hat{H}(j, \Omega)/T \right] \right) \tag{3.4}$$

[1] Working in the Schrödinger picture, the operators are time-independent. Operators are denoted by a hat.

ensures that the density matrix is properly normalized $\mathrm{Tr}\big(\hat{\rho}\big) = 1$. We can calculate the *expectation value* of some operator $\hat{\mathcal{O}}$ using the density matrix as

$$\big\langle \hat{\mathcal{O}} \big\rangle_{j,\Omega,T} = \mathrm{Tr}\big(\hat{\rho}(j,\Omega,T)\,\hat{\mathcal{O}}\big)\,. \tag{3.5}$$

This expectation value is an ensemble (or thermodynamic) average, and it is not to be confused with a vacuum expectation value.

Equipped with the density matrix and partition function we can proceed to calculate thermodynamic quantities. The *von Neumann entropy* is calculated as

$$S(j,\Omega,T) = -\left\langle \ln \hat{\rho}(j,\Omega,T) \right\rangle_{j,\Omega,T}\,. \tag{3.6}$$

We define the free energy as

$$F(j,\Omega,T) = \big\langle \hat{H}(j,\Omega) \big\rangle_{j,\Omega,T} - T\,S(j,\Omega,T) = -T \ln Z(j,\Omega,T) \tag{3.7}$$

where the second equality follows from taking the logarithm of Eq. (3.3). We can eliminate the explicit dependence on the source by performing a Legendre transformation. We will take the new independent variable to be the *scalar field condensate*

$$\phi_c = -\frac{1}{\Omega}\frac{\partial F}{\partial j} = \big\langle \hat{\bar{\Phi}} \big\rangle_{j,\Omega,T}\,, \tag{3.8}$$

which is the expectation value of the coarse grained field calculated at a temperature T *in the sourced theory.* The Legendre transformation yields the function

$$A(\phi_c,\Omega,T) = F(j,\Omega,T) + \int_\Omega d^3x\, j\,\phi_c\,, \tag{3.9}$$

which is independent of the source provided that

$$j = \frac{1}{\Omega}\frac{\partial A}{\partial \phi_c}\,. \tag{3.10}$$

The effective potential is obtained by calculating the free energy density in the infinite volume limit. Thus,

$$V_{\text{eff}}(\phi_c,T) = \lim_{\Omega\to\infty}\frac{1}{\Omega}A(\phi_c,\Omega,T) = \lim_{\Omega\to\infty} -\frac{T}{\Omega}\ln Z(j,\Omega,T) + j\phi_c\,. \tag{3.11}$$

Combining Eq. (3.11) with Eq. (3.4), one obtains the formal expression for the effective potential:

$$V_{\text{eff}}(\phi_c, T) = \lim_{\Omega\to\infty} -\frac{T}{\Omega} \ln \text{Tr}\left(e^{-(1/T)\int_\Omega d^3x\left(\hat{\mathcal{H}} - j\left(\hat{\tilde{\Phi}} - \phi_c\right)\right)}\right), \tag{3.12}$$

where j is to be eliminated using Eq. (3.8).

One-Loop Expansion

The effective potential can only be calculated exactly in very limited cases. For practical applications, the effective potential may be calculated perturbatively as an expansion in coupling constants. In the diagrammatic formalism, the leading order corrections may be calculated by summing the set of Feynman diagrams with a single loop and no external lines. Some of these vacuum bubble graphs are illustrated in Figure 3.6. The resulting expression for V_{eff} is known as the *one-loop thermal effective potential* $V_{1-\text{loop}}$. Reproducing the rigorous calculation of $V_{1-\text{loop}}$ is beyond the scope of this paper. Instead, we will present a limited derivation that captures the primary features of the approximation, and simply write down the full expression afterward.

For simplicity, assume that the system contains only one species of particle, which may be either a boson or fermion. Since we are interested in studying a thermal bath of particles, when we calculate the partition function, we will include only states in the Fock space and neglect, for example, non-perturbative field configurations. For this set of states, the spectrum of the Hamiltonain Eq. (3.2) will depend upon the additional source term in two ways. First, the explicit presence of the term $-\int d^3x j\hat{\tilde{\Phi}}$ will change the energy of the ground state by an amount $-\Omega j\phi_c$. Second, the implicit effect of this term is to source the homogenous scalar field and shift all of the states of the theory in a way that depends on j. Thus, the "shifted" spectrum

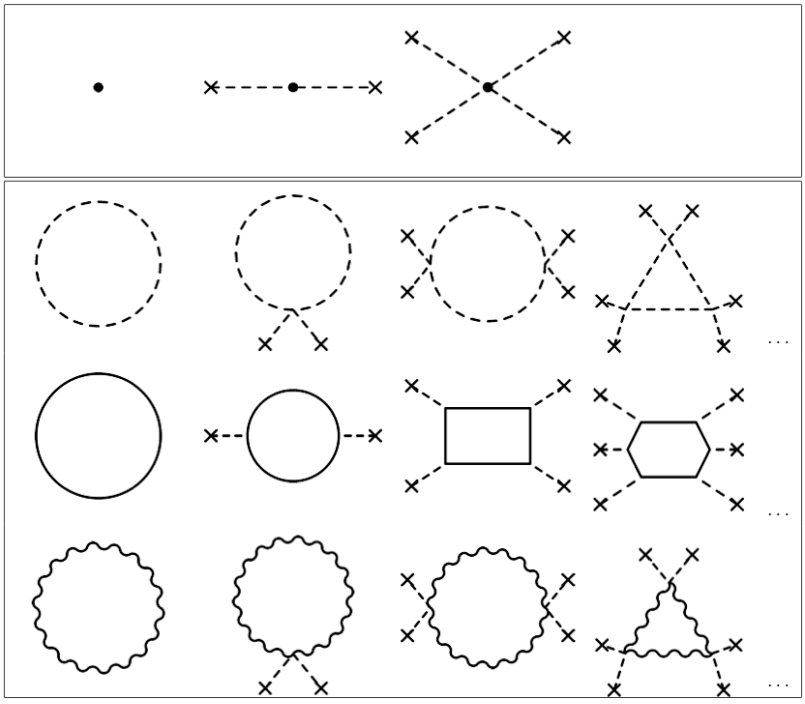

Figure 3.6: A typical set of tree-level and 1PI vacuum bubble graphs which are summed when calculating the thermal effective potential perturbatively. The **X**'s represent insertions of the condensate ϕ_c.

of the Hamiltonian $\hat{H}(j)$[2] consists of the vacuum $\big|0\big\rangle_j$ with energy ${}_j\big\langle 0\big|\hat{H}(j)\big|0\big\rangle_j = E_0(j) - \Omega j\phi_c$, one-particle states $\big|\mathbf{p}\big\rangle_j$ with energy ${}_j\big\langle \mathbf{p}\big|\hat{H}(j)\big|\mathbf{p}\big\rangle_j = E(\mathbf{p};j)$, and multi-particle states $\big|\mathbf{p_1},\mathbf{p_2},\ldots\big\rangle_j$ with energies $E(\mathbf{p_1},\mathbf{p_2},\ldots;j)$. The partition function is calculated by performing the trace in Eq. (3.4) to obtain

$$Z(j,T) = {}_j\big\langle 0\big|e^{-(E_0(j)-\Omega j\phi_c)/T}\big|0\big\rangle_j + \text{“}\sum_{|\mathbf{p}\rangle_j}\text{”}\,{}_j\big\langle \mathbf{p}\big|e^{-E(\mathbf{p};j)/T}\big|\mathbf{p}\big\rangle_j + \text{“}\sum_{|\mathbf{p_1},\mathbf{p_2}\rangle_j}\text{”}\,{}_j\big\langle \mathbf{p_1},\mathbf{p_2}\big|e^{-E(\mathbf{p_1},\mathbf{p_2};j)/T}\big|\mathbf{p_1},\mathbf{p_2}\big\rangle_j + \ldots . \tag{3.13}$$

For simplicity, we have written the sum over states schematically.

We make the “one-loop approximation," by neglecting interactions between particles. This allows us to write the multi-particle states as tensor products of one-particle

[2]We suppress the argument Ω hereafter for simplicity.

states with the appropriate (anti-)symmetrization for (fermions) bosons. For example

$$\left|\mathbf{p_1}, \mathbf{p_2}\right\rangle = \frac{1}{\sqrt{2}} \begin{cases} \left|\mathbf{p_1}\right\rangle \otimes \left|\mathbf{p_2}\right\rangle + \left|\mathbf{p_2}\right\rangle \otimes \left|\mathbf{p_1}\right\rangle & \text{bosons} \\ \left|\mathbf{p_1}\right\rangle \otimes \left|\mathbf{p_2}\right\rangle - \left|\mathbf{p_2}\right\rangle \otimes \left|\mathbf{p_1}\right\rangle & \text{fermions} \end{cases} . \tag{3.14}$$

Consequently, the energy of a general multi-particle state reduces to

$$E(\mathbf{p_1}, \mathbf{p_2}, \ldots; j) = E(\mathbf{p_1}; j) + E(\mathbf{p_2}; j) + \ldots . \tag{3.15}$$

With these replacements, we can reorganize the sum over states in Eq. (3.13) in terms of a product over one particle states and a sum over their occupancies. Extracting the ground state from this product and defining $E_{\mathbf{p}} \equiv E(\mathbf{p}; j) - E_0 + \Omega j \phi_c$, Eq. (3.13) becomes

$$Z(j,T) = e^{-\frac{E_0(j)}{T} + \frac{\Omega}{T} j \phi_c} \text{“}\prod_{\mathbf{p}}\text{”} \sum_{n_{\mathbf{p}}=0}^{n_{\max}} e^{-E_{\mathbf{p}}(j) n_{\mathbf{p}}/T} \quad \begin{cases} n_{\max} = \infty & \text{bosons} \\ n_{\max} = 1 & \text{fermions} \end{cases} . \tag{3.16}$$

Performing the sum over the mode occupancies, we obtain

$$Z(j,T) = e^{-\frac{E_0(j)}{T} + \frac{\Omega}{T} j \phi_c} \times \text{“}\prod_{\mathbf{p}}\text{”} \begin{cases} \frac{1}{1 - e^{-E_{\mathbf{p}}(j)/T}} & \text{bosons} \\ \left(1 + e^{-E_{\mathbf{p}}(j)/T}\right) & \text{fermions} \end{cases} . \tag{3.17}$$

Finally we can calculate the effective potential using Eq. (3.11). As we mentioned at the outset, the spectrum contains both explicit an implicit dependence on the source j. The Legendre transformation ensures that the explicit dependence on j cancels between Eq. (3.11) and Eq. (3.17), and that the implicit dependence on j can be expressed as a dependence on ϕ_c instead. Evaluating Eq. (3.11) with the partition function Eq. (3.17), we find

$$V_{1-\text{loop}}(\phi_c, T) = \frac{E_0(\phi_c)}{\Omega} + \begin{cases} +\frac{T}{\Omega} \text{“}\sum_{\mathbf{p}}\text{”} \ln\left(1 - e^{-E_{\mathbf{p}}(\phi_c)/T}\right) & \text{bosons} \\ -\frac{T}{\Omega} \text{“}\sum_{\mathbf{p}}\text{”} \ln\left(1 + e^{-E_{\mathbf{p}}(\phi_c)/T}\right) & \text{fermions} \end{cases} \tag{3.18}$$

where we have used $\ln \text{“}\Pi_{\mathbf{p}}\text{”} = \text{“}\sum_{\mathbf{p}}\text{”} \ln$. This expression provides an intuitive understanding of the effective potential. At low temperature $T \ll E_{\mathbf{p}}$, the effective potential reduces to the *vacuum energy density* E_0/Ω which consists of classical and quantum contributions to the energy of the ground state. We are unable to evaluate E_0/Ω as a function of ϕ_c without going into a more rigorous calculation of the effective potential. The temperature dependent pieces, not surprisingly, resemble the Bose-Einstein and Fermi-Dirac distribution functions, as a consequence of the spin statistics of Eq. (3.14). We can evaluate these expressions further by noting that the energy of a one-particle state of mass m can be expressed as $E = \sqrt{\mathbf{p}^2 + m^2}$. Thus, to leading order the presence of the condensate ϕ_c simply modifies the dispersion relation by replacing $m^2 \to \tilde{m}^2(\phi_c)$.

Having deriving the effective potential for a gas of free particles in Eq. (3.18), we will bypass the full calculation and simply proceed to write down the general one-loop effective potential. However, it is important to note that in the course of the calculation, one encounters UV divergent loop integrals (corresponding to the E_0 term of Eq. (3.18)) which must be regulated and renormalized. We will restrict ourselves to dimensional regularization and the $\overline{\text{MS}}$ regularization scheme with renormalization scale μ. This calculation yields (61)

$$V_{1-\text{loop}}(\phi_c, T) = V_{\text{ren}}(\phi_c) + \Delta V_1^0(\phi_c) + \Delta V_1^T(\phi_c, T) \tag{3.19}$$

where V_{ren} is the renormalized scalar potential. The non-thermal correction term ΔV_1^0, known as the *Coleman-Weinberg potential* (124), may be expressed as

$$\Delta V_1^0(\phi_c) = \sum_i n_i (-1)^{2s_i} \frac{\left(\tilde{m}_i^2(\phi_c)\right)^2}{64\pi^2} \left[\ln\left(\frac{\tilde{m}_i(\phi_c)^2}{Q^2}\right) - C_i\right]. \tag{3.20}$$

In this expression, the sum runs over fields labeled by i: n_i is the number of dynamical degrees of field i, s_i is the spin of field i, and C_i is a constant that depends on the

renormalization scheme; it equals 3/2 for a scalar or fermion field and 5/6 for a vector boson. The thermal correction term is given by

$$\Delta V_1^T(\phi_c, T) = \frac{T^4}{2\pi^2}\sum_i n_i \begin{cases} J_B\left(\frac{\tilde{m}_i^2(\phi_c)}{T^2}\right) & s_i = 0, 1 \\ -J_F\left(\frac{\tilde{m}_i^2(\phi_c)}{T^2}\right) & s_i = 1/2 \end{cases} \tag{3.21}$$

where the thermal loop functions are given by

$$J_{B,F}(y) \equiv \int_0^\infty dx\ x^2\ \log\left[1 \mp e^{-\sqrt{x^2+y}}\right]. \tag{3.22}$$

We have already seen the emergence of this term in Eq. (3.18) through our simple derivation.

It is useful and important to note that the functions $J_{B,F}$ admit a polynomial expansion in the so-called *high temperature limit* where $\tilde{m}_i^2 \ll T^2$. These expansions are (61)

$$J_B(y) \xrightarrow{y\ll 1} -\frac{\pi^4}{45} + \frac{\pi^2}{12}y - \frac{\pi}{6}(y)^{3/2} - \frac{1}{32}y^2\ln\frac{y}{a_b} + O\left(y^3\right) \tag{3.23a}$$

$$J_F(y) \xrightarrow{y\ll 1} +\frac{7\pi^4}{360} - \frac{\pi^2}{24}y - \frac{1}{32}y^2\ln\frac{y}{a_f} + O\left(y^3\right) \tag{3.23b}$$

where $a_b = 16a_f = 16\pi^2\exp\left[3/2 - 2\gamma_E\right]$. The most significant distinction between J_B and J_F in this limit is the presence of the non-analytic term $(y)^{3/2}$ in the expansion of J_B. This term is associated with the non-analyticity of the Bose-Einstein distribution function $(1-\exp\left[E/T\right])^{-1}$ at $E = 0$. This term will play an important role in helping to render the electroweak phase transition strongly first order.

3.3 The Standard Model Electroweak Phase Transition

To illustrate how the effective potential may be used to analyze the physics of a phase transition, we will consider the electroweak phase transition in the Standard

Model. The scalar potential is given by the non-derivative terms in the renormalized Lagrangian,

$$-\mathcal{L}_{\rm ren} \ni \mu^2 H^\dagger H + \lambda \left(H^\dagger H\right)^2 . \tag{3.24}$$

where $H = (\phi^+ , \phi^0)^T$ is the Higgs doublet scalar field. By choosing $\mu^2 = -\lambda v^2$, the Higgs will develop a vacuum expectation value $\left\langle 0\middle|H\middle|0\right\rangle = \left(0 , v/\sqrt{2}\right)$. Thus, we will calculate the effective potential as a function of the condensate $h = \sqrt{2}\,\langle \mathrm{Re}[\phi^0]\rangle$. Here, we have departed from our earlier notation of using ϕ_c to represent the condensate in favor of a more intuitive notation.

The leading contribution to the one-loop effective potential Eq. (3.19) is the renormalized scalar potential

$$V_{\rm ren}(h) = -\frac{\lambda v^2}{2} h^2 + \frac{\lambda}{4} h^4 . \tag{3.25}$$

To obtain the quantum and thermal corrections, we must identify the field-dependent masses $\tilde{m}_i^2(h)$ of the particles in the plasma. The dominant contributions come from those species which couple most strongly to the Higgs field. Namely, we need only include the top quark, weak gauge bosons, and Higgs particles, and we can neglect the light quarks, leptons, photon, and gluon. The field dependent Higgs mass is obtained from Eq. (3.25) by differentiating $\tilde{m}_H^2(h) = V''_{\rm ren} = \lambda(3h^2 - v^2)$. Defining the physical Higgs mass as $m_H^2 = \tilde{m}_H^2(v)$ we can make the replacement $\lambda = m_H^2/2v^2$. The other field-dependent particle masses may be obtained from relevant terms in the full SM Lagrangian. For these particles we have

$$\begin{aligned}
\tilde{m}_t^2(h) &= \frac{m_t^2}{v^2} h^2 & n_t &= 12 & s_t &= 1/2 & C_t &= 3/2 \\
\tilde{m}_W^2(h) &= \frac{m_W^2}{v^2} h^2 & n_W &= 6 & s_W &= 1 & C_W &= 5/6 \\
\tilde{m}_Z^2(h) &= \frac{m_Z^2}{v^2} h^2 & n_Z &= 3 & s_Z &= 1 & C_Z &= 5/6 \\
\tilde{m}_H^2(h) &= \frac{m_H^2}{2v^2}(3h^2 - v^2) & n_H &= 1 & s_H &= 0 & C_H &= 3/2 ,
\end{aligned} \tag{3.26}$$

where m_t, m_W, and m_Z are the pole masses of the top quark, W-boson, and Z-boson. The degrees of freedom are counted as $n_t = 3 \times 4$ for color and spin, $n_W = 3 \times 2$ for polarization and charge, and so on. Using Eq. (3.26) we can evaluate the remaining contributions to the one-loop effective potential given by Eq. (3.20) and Eq. (3.21). The result is the one-loop thermal effective potential for the SM,

$$\begin{aligned} V_{1-\text{loop}}^{(\text{SM})}(h,T) = &-\frac{m_H^2}{4}h^2 + \frac{\lambda}{4}h^4 \\ &+ \frac{1}{16\pi^2}\Big(F_t(h) + F_W(h) + F_Z(h) + F_H(h)\Big) \\ &+ \frac{T^4}{2\pi^2}\left(-12\, J_F\left(\frac{m_t^2 h^2}{v^2T^2}\right) + 6\, J_B\left(\frac{m_W^2 h^2}{v^2T^2}\right)\right. \\ &\left. + 3\, J_B\left(\frac{m_Z^2 h^2}{v^2T^2}\right) + J_B\left(\frac{m_H^2(3h^2 - v^2)}{2v^2T^2}\right)\right), \end{aligned} \tag{3.27}$$

where

$$\begin{aligned} F_t(h) &\equiv -\frac{3m_t^4\, h^4}{v^4}\ \ln\left(\frac{m_t^2 h^2}{v^2Q^2e^{3/2}}\right) \\ F_W(h) &\equiv \frac{3m_W^4\, h^4}{2v^4}\ \ln\left(\frac{m_W^2 h^2}{v^2Q^2e^{5/6}}\right) \\ F_Z(h) &\equiv \frac{3m_Z^4\, h^4}{4v^4}\ \ln\left(\frac{m_Z^2 h^2}{v^2Q^2e^{5/6}}\right) \\ F_H(h) &\equiv \frac{m_H^4(3h^2 - v^2)^2}{16v^4}\ \ln\left(\frac{m_H^2(3h^2 - v^2)}{2v^2Q^2e^{3/2}}\right). \end{aligned} \tag{3.28}$$

The expression Eq. (3.27) is a bit unwieldy. To obtain a more intuitive expression, we can employ the high temperature approximation Eq. (3.23). Provided that $h^2 \ll v^2T^2/m_t^2$ we can approximate,

$$V_{1-\text{loop}}^{(\text{SM})}(h,T) \approx \frac{1}{2}c\,(T^2 - T_0^2)h^2 - \frac{e\,T}{12\pi}(h^2)^{3/2} + \frac{\lambda}{4}h^4 \tag{3.29}$$

where the effective parameters are given by

$$T_0^2 = \frac{m_H^2}{2c} \tag{3.30}$$

$$c = \frac{4m_t^2 + 4m_W^2 + 2m_Z^2 + m_H^2}{8v^2} \tag{3.31}$$

$$e = \frac{6m_W^3 + 3m_Z^3}{v^3}\,. \tag{3.32}$$

In calculating Eq. (3.29) from Eq. (3.27), we have left out the residual terms $\delta V = \Omega + (\sigma/2)h^2 + (\tau/4)h^4$ where

$$\Omega(h,T) = -\frac{427\pi^2}{360}T^4 - \frac{m_H^4}{256\pi^2}\ln\left(\frac{m_H^2(3h^2-v^2)}{2v^2T^2a_b}\right) + \frac{m_H^3T\sqrt{2}\sqrt{3h^2-v^2}}{48\pi v} \tag{3.33}$$

$$\sigma(h,T) = \frac{3m_H^4}{64\pi^2v^2}\ln\left(\frac{m_H^2(3h^2-v^2)}{2v^2T^2a_b}\right) - \frac{m_H^3T\sqrt{2}\sqrt{3h^2-v^2}}{8\pi v^3} \tag{3.34}$$

$$\begin{aligned}\tau(h,T) = \frac{1}{16\pi^2}\Bigg[&12\frac{m_t^4}{v^4}\ln\left(\frac{m_t^2h^2}{v^2T^2a_f}\right) - 6\frac{m_W^4}{v^4}\ln\left(\frac{m_W^2h^2}{v^2T^2a_b}\right) \\ &- 3\frac{m_Z^4}{v^4}\ln\left(\frac{m_Z^2h^2}{v^2T^2a_b}\right) - \frac{9m_H^4}{4v^4}\ln\left(\frac{m_H^2(3h^2-v^2)}{2v^2T^2a_b}\right)\Bigg]\,.\end{aligned} \tag{3.35}$$

The correction δV is a small, slowly varying function of h when the temperature is on the order of the electroweak scale, and it may be neglected for the purposes of an approximate analytic analysis.

The approximate expression Eq. (3.29) illuminates the consequence of interactions between the condensate and the plasma. The dominant thermal contribution induces an effective mass $m_{\rm eff}^2(T) = c\,(-T_0^2 + T^2)$ for the Higgs field. Since spontaneous symmetry breaking is driven by the tachyonic mass $m_{\rm eff}^2(0) = -cT_0^2$, we expect that the broken symmetry will be restored above a temperature $T \approx T_0$ where the tachyonic instability becomes lifted. Equation (3.30) reveals that this temperature scale is set by the Higgs mass and also depends upon the dimensionless thermal mass parameter c. Qualitatively, c represents the tightness of the coupling between the condensate and the plasma. For large c, thermal interactions are very effective at stabilizing

the symmetric phase, and symmetry restoration occurs at a lower temperature. The non-analytic term $(h^2)^{3/2}$ arises from interactions with weak gauge bosons. This term plays an important role rendering the phase transition first order by allowing. Near the phase transition temperature, we expect the three terms in Eq. (3.29) to be comparable in magnitude.

With Eq. (3.29) at hand, we are equipped to study the SM electroweak phase transition. We obtain the physical value of the Higgs condensate $v(T)$ at a given temperature by minimizing the effective potential. The equation

$$\left.\frac{\partial V^{(\mathrm{SM})}_{1-\mathrm{loop}}(h,T)}{\partial h}\right|_{h=v(T)} = 0 \tag{3.36}$$

has two solutions. The first, $v_{\mathrm{sym}}(T) = 0$, represents the Higgs condensate in the symmetric phase, and the second,

$$v_{\mathrm{brk}}(T) = \frac{e}{8\pi\lambda}T + \sqrt{\left(\frac{e}{8\pi\lambda}\right)^2 T^2 + \frac{c}{\lambda}(T_0^2 - T^2)}\,, \tag{3.37}$$

represents the broken phase condensate. Note that the broken phase condensate does not exist for temperatures above

$$T_{\mathrm{max}} = \frac{T_0}{\sqrt{1-\alpha^2}} \tag{3.38}$$

where $\alpha \equiv e/(8\pi\sqrt{\lambda c})$. The free energy density in the broken phase is given by the value of the effective potential at this minimum,

$$\begin{aligned}\mathcal{F}_{\mathrm{brk}}(T) = V^{(\mathrm{SM})}_{1-\mathrm{loop}}(v_{\mathrm{brk}}(T),T) = \\ -\frac{c^2}{4\lambda}T_0^4 - \frac{2c^2}{3\lambda}T_0^2\alpha\sqrt{T_0^2 - T^2(1-\alpha^2)}\,T + \frac{c^2}{2\lambda}T_0^2\left(1-2\alpha^2\right)T^2 \\ + \frac{2c^2}{3\lambda}\alpha\left(1-\alpha^2\right)\sqrt{T_0^2 - T^2(1-\alpha^2)}\,T^3 - \frac{c^2}{4\lambda}\left(1 - 4\alpha^2 + \frac{8}{3}\alpha^4\right)T^4\,.\end{aligned} \tag{3.39}$$

At $T = 0$, the free energy density is just equal to the negative classical potential energy of the ground state, i.e., $(-1)(c^2T_0^4/4\lambda) = -\lambda v^4/4$. At $T = T_{\mathrm{max}}$, the free energy is

positive and equal to $(c^2T_0^4/4\lambda)(\alpha^4/[3(1-\alpha^2)^2])$. In the symmetric phase, the free energy density remains fixed at $\mathcal{F}_{\rm sym}(T)=0$, since we have dropped the T^4 pieces from the effective potential. Thus, the broken phase is energetically favored at low temperature, and the symmetric phase is energetically favored at high temperature, as we would expect. The equality occurs at a temperature T_c defined by

$$\mathcal{F}_{\rm sym}(T_c)=\mathcal{F}_{\rm brk}(T_c) \tag{3.40}$$

which resolves to

$$T_c=\frac{T_0}{\sqrt{1-\frac{8}{9}\alpha^2}}\,. \tag{3.41}$$

Finally, using Eq. (3.37) and Eq. (9.70) we can estimate the order parameter of the electroweak phase transition to be

$$\frac{v(T_c)}{T_c}=\frac{e}{6\pi\lambda}=\frac{2m_W^3+m_Z^3}{\pi m_H^2 v}\,. \tag{3.42}$$

Then by imposing the washout condition $v(T_c)/T_c>1$, we obtain an upper bound on the Higgs mass

$$(m_H)_{\rm max}=\sqrt{\frac{2m_W^3+m_Z^3}{\pi v}}\approx 48\ {\rm GeV}\,. \tag{3.43}$$

In Figure 3.7 we have illustrated the temperature dependence of the effective potential for a scenario with the Higgs mass just at the threshold value Eq. (3.43). If the Higgs were lighter, the phase transition would be more strongly first order. However, in light of the Higgs search bound $m_H\gtrsim 115$ GeV (48), we conclude that the SM electroweak phase transition is not strongly first order.

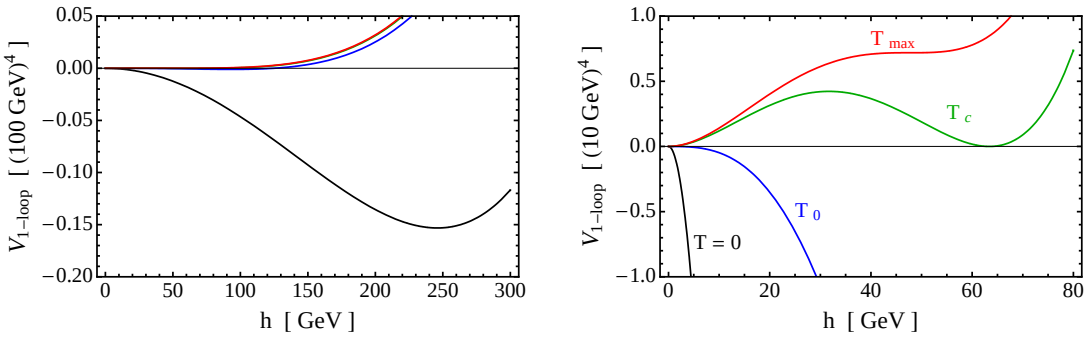

Figure 3.7: The SM thermal effective potential for a 45 GeV Higgs. The phase transition occurs at a temperature of $T_c \approx 56$ GeV at which point $v_{\rm brk}(T_c) \approx 65$ GeV, and since $v_{\rm brk}(T_c)/T_c > 1$, the electroweak phase transition is strongly first order phase transition.

Chapter 4

Electroweak Phase Transition in the $\mu\nu$SSM

An extension of the MSSM called the $\mu\nu$SSM does not allow a conventional thermal leptogenesis scenario because of the low scale seesaw that it utilizes. Hence, we investigate the possibility of electroweak baryogenesis. Specifically, we identify a parameter region for which the electroweak phase transition is sufficiently strongly first order to realize electroweak baryogenesis. In addition to transitions that are similar to those in the NMSSM, we find a novel class of phase transitions in which there is a rotation in the singlet vector space.

This work was performed in collaboration with Daniel Chung. It was published in Physical Review **D** in June of 2010 (97).

4.1 Introduction to the Chapter

An extension of the MSSM called the $\mu\nu$SSM (135) is a model similar to the NMSSM (136) (with the usual $\mathbb{Z}_3$ charge assignment) except that the singlet whose vacuum

expectation value (VEV) gives rise to the μ term also serves the role of a right handed neutrino, thereby violating R-parity. Because the VEV generates the μ-term and the right handed neutrino mass, the right handed neutrino masses are of order TeV, leading to a low scale type I seesaw. Given the absence of high scale seesaw, thermal leptogenesis is difficult in the $\mu\nu$SSM. Hence, it is interesting to consider whether or not electroweak baryogenesis (EWBG) (62) can occur in this class of models. One of the most stringent constraints of EWBG on the $\mu\nu$SSM is the requirement of a sufficiently strongly first order phase transition (SFOPT) such that the created baryons are not washed out (137).

Because the $\mu\nu$SSM contains 3 singlet chiral superfields (right handed neutrinos), mainly motivated by generality, standard model generation replication pattern, and phenomenological convenience (135; 138), there is a "larger" SFOPT parameter space for EWBG when compared to the NMSSM. More precisely, there can be SFOPT where the singlet VEVs rotate in the singlet vector space during the electroweak phase transition. The price paid for this is a more complicated global minimum analysis at both finite and zero temperatures. The aim of this paper is not to uncover the most general parameter space consistent with EWBG, but is to simply give a couple of parametric regions to show the existence of possibilities.

Depending on the path of the phase transition, the exact $\mu\nu$SSM parametric dependence of the phase transition strength $v(T_c)/T_c$ is complicated. Nonetheless, we find that it is typically true that to achieve SFOPT, the parameters are close to satisfying the following condition:

$$\frac{E_{\text{eff}}}{\lambda_{\text{eff}} v(0)} \approx \frac{1}{2} \tag{4.1}$$

where E_{eff} is the effective cubic coupling, λ_{eff} is the effective quartic coupling, and $v(0)$ is the magnitude of the scalar field space VEV (including both the Higgs and

singlets) at zero temperature. Physically, this corresponds to the parametric region where the critical temperature T_c is small compared to $v(0)$ during the electroweak phase transition. In the examples provided in this paper, whether or not the SFOPT proceeds from the origin, the leading nonvanishing value of E_{eff} in the $\mu\nu$SSM arises from the soft terms

$$\sum_i^3 \left[-a_\lambda H_1 H_2 \tilde{\nu}_i^c + \frac{1}{3} a_\kappa \left(\tilde{\nu}_i^c\right)^3 + \text{h.c.} \right] \tag{4.2}$$

where $\tilde{\nu}_i^c$ are singlet fields. The dimensionful coupling a_λ is distinguished from a_κ in that a_λ also enhances the mixing between the Higgs sector and the singlet sector. The leading contribution to λ_{eff} comes from the superpotential and D-terms.

Beyond these general results, we find a somewhat interesting feature because we focus on the parametric region analyzed by (138). In this parametric region, an approximate $\mathbb{S}_3$ symmetry (permutation symmetry) arises due to the right handed neutrino generation independence of the non-Yukawa couplings and the smallness of the neutrino Yukawa couplings. Hence, to avoid any extra complications associated with domain wall formations, one might naively try to avoid $\mathbb{S}_3$ symmetry breaking phase transitions by considering parameters which yield zero temperature vacua preserving $\mathbb{S}_3$. Hence, this is the boundary condition that we impose in this paper. Interestingly, we find that despite this boundary condition, $\mathbb{S}_3$ is typically spontaneously broken multiply at finite temperatures in a way that is sensitive to quantum radiative corrections. As the temperature is lowered from high temperatures, this leads to multi-step phase transitions starting from the trivially $\mathbb{S}_3$ symmetric vacuum in which all VEVs vanish. The electroweak symmetry breaking phase transition occurs with $\mathbb{S}_3$ symmetry *restoration* to a vacuum in which all sneutrino VEVs are identical and nonvanishing. We also find one step SFOPTs in which the scalar fields (including the singlet fields) make a transition from the origin to the electroweak

symmetry breaking minimum. The numerical values of the parametric regions uncovered in this paper is in the paragraph containing Eq. (4.46) and regions IIIa and IIIb depicted in Fig. 4.5.

Since this work is most closely related to previous work on SFOPT in the NMSSM, we give here a little preview of some of the differences between our work and previous works, in addition to the multi-dimensional aspect stressed above. In Ref. (96), SFOPT in the context of the NMSSM is first analyzed and the author points out that the tree level cubic term coming from the soft SUSY breaking sector is important. Note that Ref. (96) uses the definition of critical temperature in which scalar mass squared matrix develops a vanishing eigenvalue. We take a more robust definition of T_c being the temperature at which a new coexistence phase occurs even though this definition is harder to implement in practice.

The authors of Ref. (139) also analyze the NMSSM, but they include a μ-term on the basis that it is more general and its nonzero value eliminates the $\mathbb{Z}_3$ symmetry which can be cosmologically dangerous with respect to the problem of domain wall formation (140). The non-zero μ-term leads to false vacuum not being at the origin. In this case the critical temperature criterion used by Ref. (96) is invalid. Therefore, the authors of Ref. (139) take the coexistence phase definition of critical temperature as we do in this paper. They also include a bilinear soft term in the Higgs which break the $\mathbb{Z}_3$ symmetry. Although we do not include such $\mathbb{Z}_3$ breaking terms directly, we will assume that non-renormalizable terms can be included to obtain acceptable phenomenology with respect to any possible domain wall formation. However, it is to be noted that $\mathbb{Z}_3$ breaking can often lead to UV instabilities in the singlet tadpoles, making the UV stability of these theories (including the one considered in this paper) a model building challenge as noted by (140).

The analysis (95) considers the generalized NMSSM similar to (139). They run 9

parameters with a popular choice of "universal" boundary conditions from the GUT scale down to the electroweak scale to generate their model. They do not reject metastable vacua based on the intuition that longevity of the false vacuum on the horizon scale today is not difficult to attain. To be conservative and to avoid potentially complicated discussions of metastability, we accept only stable vacua in this paper.

A model related to the NMSSM and the $\mu\nu$SSM is the nMSSM in which the discrete charge assignment is modified as to eliminate the singlet cubic term in the superpotential. This model was analyzed by (94) for SFOPT. For a significant portion of the parameter space in which SFOPT occurs, a linear tadpole term in the superpotential plays a significant role in contrast to our scenario.

The analysis of (111) considers the EWPT in an extension of the SM which adds a real singlet S. These authors find a large region of the parameter space of their model that is consistent with SFOPT and LEP Higgs search bounds. They argue that the strength of the phase transition can be enhanced by 1) choosing a large negative value for the SH^2 coupling, 2) choosing a negative value for the S^2H^2 coupling, or 3) allowing the singlet to have a non-zero VEV before the electroweak symmetry is broken. In the language of this paper, the first two points correspond to increasing E_{eff} and decreasing λ_{eff}, respectively.

Before we begin the main body of the work, let's list here all the caveats to our analysis. We do not take into account explicitly the high energy Landau pole constraint (i.e. perturbativity up to the GUT scale) because we will take the attitude that the $\mu\nu$SSM is well motivated mainly by its ability to have all fields participate at low energy and thereby have potential measurability. Nonetheless, the parametric region that we uncover lies at the border of perturbativity up to the GUT scale (inferring from the work of Refs. (138; 141)), which means that the UV cutoff for our

theory can be taken to be far above the TeV scale. We do not take into account explicit $\mathbb{Z}_3$ breaking effects because small amount of breaking can address most cosmological domain wall problems, as we later demonstrate. We do not take into account explicit CP violation effects in the phase transitions as this will typically lead to less than order 10% effects since CP violating phases compatible with phenomenology are typically order 0.1 or smaller. For robustness, we accept in this paper as phenomenological possibility only absolutely stable global zero temperature vacua instead of analyzing the phenomenological possibilities of metastable vacua. Finally, all of our numerical work is kept in control to only order 10% accuracy.

The order of presentation is as follows. In the next section, we present the Lagrangian including its discrete symmetry properties and radiative/thermal corrections. The section concludes by highlighting the $\mu\nu$SSM differences from the NMSSM scenario. In Sec. 4.3, we describe the parametric region relevant for SFOPT in terms of one-dimensional field space slice parameterization. There we also qualitatively describe how the multidimensional paths of the phase transition and discrete symmetries play a role. Next, in Sec. 4.4, we explicitly show that singlets do not play a significant role in terms of numerical value of the sphaleron action controlling the $B+L$ violating rate in the broken phase. The main numerical results are presented in Sec. 4.5 where explicit existence of SFOPT parameter region is demonstrated. Details of the transition paths organized in terms of discrete symmetries, phenomenological bounds placed, and explicit mass spectra for a sample parametric point are given. In Sec. 4.6, we demonstrate that cosmological domain wall problem is easily evaded with an inclusion of a weak $\mathbb{Z}_3$ symmetry breaking operator in our scenario. We then conclude with a summary of the results. Several appendices then follow giving useful technical details. In Appendix 4.A, we list the field dependent mass matrices used for computing the effective potential. In the next appendix, we give details

regarding the approximate thermal masses used in the paper. In Appendix 4.C, we describe analytically the boundaries of in Figure 4.5 which is one of our main results. Finally, in Appendix 4.D, we show that it is generically possible to construct a non-renormalizable $\mathbb{Z}_3$ superpotential to obtain a CP conserving global minimum in the absence of any explicit CP violating parameters.

4.2 The Thermal Potential Differences Between the NMSSM and the $\mu\nu$SSM

The $\mu\nu$SSM that we consider in this paper is specified by the following superpotential and soft terms

$$\begin{aligned} W = \sum_i^3 \Big\{ & Y_u^i \hat{Q}_i \cdot \hat{H}_2 \hat{u}_i^c + Y_d^i \hat{H}_1 \cdot \hat{Q}_i \hat{d}_i^c + Y_e^i \hat{H}_1 \cdot \hat{L}_i \hat{e}_i^c \\ & + Y_\nu^i \hat{L}_i \cdot \hat{H}_2 \hat{\nu}_i^c - \lambda \hat{H}_1 \cdot \hat{H}_2 \hat{\nu}_i^c + \frac{1}{3} \kappa \left(\hat{\nu}_i^c\right)^3 \Big\} \end{aligned} \tag{4.3}$$

$$\begin{aligned} -\mathcal{L}_{\text{soft}} = & \sum_i^3 \Big\{ m_{\tilde{Q}}^2 |\tilde{Q}_i|^2 + m_{\tilde{u}^c}^2 |\tilde{u}_i^c|^2 + m_{\tilde{d}^c}^2 |\tilde{d}_i^c|^2 + m_{\tilde{L}}^2 |\tilde{L}_i|^2 + m_{\tilde{e}^c}^2 |\tilde{e}_i^c|^2 + m_{\tilde{\nu}^c}^2 |\tilde{\nu}_i^c|^2 \Big\} \\ & + \sum_i^3 \Big\{ a_u \tilde{Q}_i \cdot H_2 \tilde{u}_i^c + a_d H_1 \cdot \tilde{Q}_i \tilde{d}_i^c + a_e H_1 \cdot \tilde{L}_i \tilde{e}_i^c + a_\nu \tilde{L}_i \cdot H_2 \tilde{\nu}_i^c + \text{h.c.} \Big\} \\ & + \sum_i^2 m_{H_i}^2 |H_i|^2 - \frac{1}{2} \left(\sum_i^3 M_i \tilde{\lambda}_i \tilde{\lambda}_i + \text{h.c.} \right) \\ & + \sum_i^3 \Big[-a_\lambda H_1 \cdot H_2 \tilde{\nu}_i^c + \frac{1}{3} a_\kappa \left(\tilde{\nu}_i^c\right)^3 + \text{h.c.} \Big] . \end{aligned} \tag{4.4}$$

Where indicated by a dot, the SU(2) indices are contracted with the antisymmetric tensor and $\epsilon_{12} = 1$. First, note in addition to the usual $\mathbb{Z}_3$ symmetry used to forbid an explicit μ term, there is an exact CP symmetry due to the reality of the coupling constants. We ignore the CKM phases since these will only give corrections smaller

than the $\mathcal{O}(10\%)$ accuracy that we are aiming for in this paper. The CP transformation in the scalar effective potential can be effectively taken to be each scalar field transforming to its conjugate. Next, note that the couplings of the $\tilde{\nu}_i^c$ sector to the SM were taken to be generation independent, except for the Yukawa couplings, and that the singlets do not couple to one another directly in the superpotential. This choice is motivated by trying partially to match the work of (138). Hence, we see there is an enhanced $\mathbb{S}_3$ symmetry (permutation symmetry) in the $\tilde{\nu}_i^c$ sector if we neglect the Yukawa couplings. This approximate symmetry $\mathbb{S}_3$ is nearly exact because of the smallness of the symmetry breaking Yukawa couplings $Y_{e,\nu}^i$. As discussed in the introduction, the exact global $\mathbb{Z}_3$ symmetry itself is plausibly assumed to be broken by non-renormalizable operators such that cosmological domain wall problem does not arise.

At tree level there is an additional global symmetry in the phase in which the electroweak symmetry is unbroken such that $H_i = 0$ and all electromagnetically charged scalars vanish. Hence, in the high temperature phase in which the non-singlet fields are assumed to be frozen at their classical potential minimum, we have an enhanced symmetry in the effective potential as a function of the singlets only. The enhanced tree level symmetry is $\mathbb{Z}_3 \otimes \mathbb{Z}_3 \otimes \mathbb{Z}_3$, where each singlet can be phase rotated independently:

$$\tilde{\nu}_j^c \longrightarrow e^{in_j 2\pi/3} \tilde{\nu}_j^c. \tag{4.5}$$

This symmetry appears because we have tuned the superpotential $\tilde{\nu}_1^c \tilde{\nu}_2^c \tilde{\nu}_3^c$ coupling to vanish. Unlike the approximate $\mathbb{S}_3$ symmetry, this high temperature phase classical symmetry has significant breaking at 1-loop from perturbative interactions even about the electroweak symmetry preserving minima. Nonetheless, it will be useful in understanding the SFOPT in which there is a rotation in the singlet sector space

during the phase transition.[1]

In addition to the Yukawa and gauge couplings, there are 19 adjustable parameters in this model which are $\{\lambda, \kappa, m^2_{\tilde{Q},\tilde{u}^c,\tilde{d}^c,\tilde{L},\tilde{e}^c,\tilde{\nu}^c}, m^2_{H_{1,2}}, M_i, a_{u,d,e,\nu,\lambda,\kappa}\}$. These are taken to be defined at the renormalization scale of 100 GeV in the $\overline{\text{DR}}$ scheme. Because the neutrino Yukawa couplings control the neutrino Dirac mass via the up-type Higgs VEV, these Yukawas are small for reasonable values of $\tan\beta$,

$$Y_\nu \approx 6 \times 10^{-7} \left(\frac{\sin[\beta]}{\sin[\arctan 2.6]} \right)^{-1}, \tag{4.6}$$

and will play a negligible dynamical role. The neutral scalar field vector space belonging to the fields $\{H_1, H_2, \tilde{L}_i, \tilde{\nu}^c_i\}$ is parameterized as follows:

$$\begin{aligned} H^0_i &= v_i(T) + \frac{\phi_i + i a_i}{\sqrt{2}} && i \in \{1,2\} \\ \tilde{\nu}^{(c)}_j &= v_{\tilde{\nu}^{(c)}_j}(T) + \frac{\phi_{\tilde{\nu}^{(c)}_j} + i a_{\tilde{\nu}^{(c)}_j}}{\sqrt{2}} && j \in \{1,2,3\} \end{aligned} \tag{4.7}$$

where the VEVs at finite temperature are denoted by $\{v_i(T), v_{\tilde{\nu}_i}(T), v_{\tilde{\nu}^c_i}(T)\}$. To maintain the $\mathbb{S}_3$ symmetry in the electroweak symmetry breaking vacuum at zero temperature and to avoid unnecessary complexities in the $SU(2)_L$ charged sector, we choose the sneutrino VEVs to be independent of generation, such that

$$\{v_i(0) = \text{real}, v_{\tilde{\nu}_i}(0) = v_{\tilde{\nu}}(0) = \text{real}, v_{\tilde{\nu}^c_i}(0) = v_{\tilde{\nu}^c}(0) = \text{real}\}. \tag{4.8}$$

To fix the VEVs in this way, we solve the potential minimization condition for the four parameters $\{m^2_{H_1}, m^2_{H_2}, m^2_L, m^2_{\tilde{\nu}^c}\}$. In addition to the desire to simplify the phase transition history, one of our main motivation in choosing $v_{\tilde{\nu}^c_i}(0) = v_{\tilde{\nu}^c}(0)$ is to preserve the $\mathbb{S}_3$ symmetry manifest in Eqs. (4.3) and (4.4). Interestingly enough, as we will see, this $\mathbb{S}_3$ symmetry spontaneously breaks at finite temperature. The left-handed

[1] One may also wonder whether omitting the $\tilde{\nu}^c_1\tilde{\nu}^c_2\tilde{\nu}^c_3$ term is radiatively stable. It turns out that this term is generated at 2-loop order, which means that as far as one loop analysis of this paper is concerned, this term can be omitted self-consistently. However, this must be viewed as fine tuning motivated by staying consistent with Ref. (138).

sneutrino VEV is small, as we argue below, and the Higgs VEVs satisfy $v_1^2(0)+v_2^2(0)+3v_{\tilde{\nu}}^2(0) \approx v_1^2(0)+v_2^2(0) = v^2(0) = (174\ \text{GeV})^2$. The rest of the parameter specification will be discussed in Sec. 4.5.

To study the electroweak phase transition we need to calculate the thermal effective potential V_{eff}^T as a function of temperature and the field directions which participate in the phase transition. There are no charged scalars with VEVs at zero temperature and we assume that there are no charge or color breaking minima to appear at finite temperature. In general, the left-handed sneutrinos receive VEVs $v_{\tilde{\nu}}(0)$ and participate in electroweak symmetry breaking, but these VEVs must be much less than the electroweak scale to avoid excessive stellar energy loss (142) by $\tilde{\nu}$ emission. Hence, we can neglect $O\left(v_{\tilde{\nu}}\right)$ contributions and reduce the relevant degrees of freedom to the five dimensional complex field space $\{H_1^0, H_2^0, \tilde{\nu}_i^c\}$. Although a part of the complex phase degrees of freedom in the Higgs sector is a gauge degree of freedom, for simplicity we will use the notation $\{H_1^0, H_2^0, \tilde{\nu}_i^c\}$ and keep in mind that there are nine real degrees of freedom.

We compute the zero temperature effective potential as a loop expansion over the field space $\{H_1^0, H_2^0, \tilde{\nu}_i^c\}$. The leading order term is the tree-level potential given by

$$\begin{aligned} V_0 = & m_{H_1}^2 \left|H_1^0\right|^2 + m_{H_2}^2 \left|H_2^0\right|^2 + m_{\tilde{\nu}^c}^2 \sum_i \left|\tilde{\nu}_i^c\right|^2 + \frac{g_1^2+g_2^2}{8}\left(\left|H_1^0\right|^2 - \left|H_2^0\right|^2\right)^2 \\ & + \sum_i \left[-a_\lambda H_1^0 H_2^0 \tilde{\nu}_i^c + \frac{1}{3} a_\kappa \left(\tilde{\nu}_i^c\right)^3 - \kappa\lambda \left(H_1^0 H_2^0\right)^\star \left(\tilde{\nu}_i^c\right)^2 + \text{h.c.}\right] \\ & + 3\lambda^2 \left|H_1^0\right|^2 \left|H_2^0\right|^2 + \left|H_2^0\right|^2 \sum_i \left(Y_\nu^i\right)^2 \left|\tilde{\nu}_i^c\right|^2 \\ & + \lambda^2 \left(\left|H_1^0\right|^2 + \left|H_2^0\right|^2\right) \left|\sum_i \tilde{\nu}_i^c\right|^2 + \kappa^2 \sum_i \left|\tilde{\nu}_i^c\right|^4 . \end{aligned} \tag{4.9}$$

We exchange the three parameters $\left\{m_{H_1}^2, m_{H_2}^2, m_{\tilde{\nu}^c}^2\right\}$ for the real VEVs $\{v_1(0), v_2(0), v_{\tilde{\nu}^c}(0)\}$

by solving the five minimization equations

$$\begin{aligned}
\left.\frac{\partial V_0}{\partial H_1^0}\right|_{\text{VEV}} = 0 = m_{H_1}^2 v_1 + \frac{g_1^2+g_2^2}{4}\left(v_1^2 - v_2^2\right)v_1 + 3\left[-a_\lambda v_2 v_{\tilde{\nu}^c} - \kappa\lambda v_2 v_{\tilde{\nu}^c}^2\right] \\
+ 3\lambda^2 v_1 v_2^2 + 9\lambda^2 v_1 v_{\tilde{\nu}^c}^2 \\
\left.\frac{\partial V_0}{\partial H_2^0}\right|_{\text{VEV}} = 0 = m_{H_2}^2 v_2 - \frac{g_1^2+g_2^2}{4}\left(v_1^2 - v_2^2\right)v_2 + 3\left[-a_\lambda v_1 v_{\tilde{\nu}^c} - \kappa\lambda v_1 v_{\tilde{\nu}^c}^2\right] \\
+ 3\lambda^2 v_2 v_1^2 + 9\lambda^2 v_2 v_{\tilde{\nu}^c}^2 \\
\left.\frac{\partial V_0}{\partial \tilde{\nu}_i^c}\right|_{\text{VEV}} = 0 = m_{\tilde{\nu}^c}^2 v_{\tilde{\nu}^c} + \left[-a_\lambda v_1 v_2 + a_\kappa\left(v_{\tilde{\nu}^c}^2\right) - 2\kappa\lambda v_1 v_2 v_{\tilde{\nu}^c}\right] \\
+ 3\lambda^2\left(v_1^2 + v_2^2\right)v_{\tilde{\nu}^c} + 2\kappa^2 v_{\tilde{\nu}^c} v_{\tilde{\nu}^c}^2
\end{aligned} \tag{4.10}$$

where "VEV" represents evaluating the fields at the zero-temperature vacuum $\{H_1^0, H_2^0, \tilde{\nu}_i^c\} = \{v_1(0), v_2(0), v_{\tilde{\nu}^c}(0)\}$. Terms proportional to Y_ν^i and $v_{\tilde{\nu}}$ are negligible and have been omitted. Because of the $\mathbb{S}_3$ permutation symmetry of our potential, the three equations associated with the sneutrino field directions are identical.

The one-loop radiative correction to the effective potential is given by the Coleman-Weinberg potential (124) as a function of the field-dependent mass matrices M_i^2 calculated in the Landau gauge ($\xi = 0$). The mass matrices which we use are included in Appendix 4.A along with n_i, the degrees of freedom associated with each matrix that correspond to suppressed indices (negative for fermions). Regulating UV divergences in $d = 4 - 2\epsilon$ dimensions, the Coleman-Weinberg potential becomes

$$\Delta V_1^0 = \frac{1}{64\pi^2}\sum_i n_i \text{Tr}\ M_i^4\left(\log\frac{M_i^2}{\mu^2} - \frac{3}{2} - C_{\text{UV}}\right) \tag{4.11}$$

where $C_{\text{UV}} = \frac{1}{\epsilon} - \gamma_E + \ln 4\pi$ and μ is the t'Hooft scale. We impose a mixed renormalization scheme in which the counterterms for the parameters $\left\{m_{H_1}^2, m_{H_2}^2, m_{\tilde{\nu}^c}^2\right\}$ are chosen such that the zero-temperature vacuum is unshifted by the radiative correc-

tions. This condition is equivalent to requiring tadpole graphs to vanish and imposes

$$\begin{aligned}
\delta m_{H_1}^2 &= -\frac{1}{v_1}\left.\frac{\partial \Delta V_1^0}{\partial \left(H_1^0\right)^*}\right|_{\text{VEV}} \\
\delta m_{H_2}^2 &= -\frac{1}{v_2}\left.\frac{\partial \Delta V_1^0}{\partial \left(H_2^0\right)^*}\right|_{\text{VEV}} \\
\delta m_{\tilde{\nu}^c}^2 &= -\frac{1}{v_{\tilde{\nu}^c}}\left.\frac{\partial \Delta V_1^0}{\partial \left(\tilde{\nu}_i^c\right)^*}\right|_{\text{VEV}} .
\end{aligned} \tag{4.12}$$

The remaining parameters are determined by the $\overline{DR}$ scheme and all parameters are specified at a renormalization scale of $\mu = 100$ GeV. We make no assumptions about dominant contributions to the one-loop corrections but instead calculate Eq. (4.11) by summing all species that couple to the Higgs sector.

At finite temperature, the effective potential receives an additional one-loop correction

$$\Delta V_1^T = \frac{T^4}{2\pi^2}\left[\sum_b n_b \text{Tr}\ J_B\left(M_b^2/T^2\right) + \sum_f n_f \text{Tr}\ J_F\left(M_f^2/T^2\right)\right] \tag{4.13}$$

where the traces run over bosonic (b) and fermionic (f) mass matrices. The thermal functions can be expressed as a a sum of modified Bessel functions of the second kind,

$$\begin{aligned}
J_B(y) &= \int_0^\infty dx\, x^2 \log\left(1 - e^{-\sqrt{x^2+y}}\right) = -\sum_{n=1}^\infty \frac{1}{n^2} y K_2\left(n\sqrt{y}\right) \\
J_F(y) &= \int_0^\infty dx\, x^2 \log\left(1 + e^{-\sqrt{x^2+y}}\right) = -\sum_{n=1}^\infty \frac{(-1)^n}{n^2} y K_2\left(n\sqrt{y}\right).
\end{aligned} \tag{4.14}$$

Because these integrals are computationally taxing, we use the Bessel function representation and truncate the sum at five terms. This is a very good approximation and introduces less than one percent of error.

At high temperatures, the perturbative expansion fails unless higher order "daisy" graphs which diverge quadratically with temperature are resummed. This procedure effectively replaces the bosonic field dependent mass matrix M_b^2 with $M_b^2 + \Pi_b$ where

$\Pi_b \propto T^2$ and amounts to including a term into the potential given by

$$\Delta V_{\text{daisy}} = -\frac{T}{12\pi}\sum_b n_b \text{Tr}\left[\left(M_b^2 + \Pi_b\right)^{3/2} - \left(M_b^2\right)^{3/2}\right]. \tag{4.15}$$

The thermal mass corrections Π_b are included in Appendix 4.B. Combining all of the radiative and finite temperature terms, the one-loop finite-temperature effective potential plus daisy resummation becomes

$$V_{\text{eff}}^T(T) = V_0 + \Delta V_1^0 + \Delta V_1^T(T) + \Delta V_{\text{daisy}}(T). \tag{4.16}$$

The main difference between the NMSSM and the $\mu\nu$SSM relevant for strongly first order EWPT can be summarized as follows:

1. Because of the multidimensionality of the singlet field space $\{v_{\tilde{\nu}_i^c}(T)\}$, there can be electroweak phase transitions accompanied by rotations within the singlet field space. This opens up a new class of phase transitions that are unlike any of the NMSSM transitions since for example the phase transition can take place with the singlet VEV hopping from one nonzero value to another:

$$\{v_{\tilde{\nu}_i^c}(T_c) = x_i \neq 0, \langle H_j\rangle = 0\} \longrightarrow \{v_{\tilde{\nu}_i^c}(T_c) = y_i \nparallel x_i, \langle H_j\rangle \neq 0\}. \tag{4.17}$$

   The terms in Eqs. (4.3) and (4.4) that will play a particularly important role for this rotational hopping are the soft terms $-a_\lambda H_1 \cdot H_2 \tilde{\nu}_i^c + \frac{1}{3}a_\kappa \left(\tilde{\nu}_i^c\right)^3$ (which control the cubic and lower dimension tree level couplings which in turn control radiative corrections) and the superpotential terms $-\lambda \hat{H}_1 \cdot \hat{H}_2 \hat{\nu}_i^c + \frac{1}{3}\kappa \left(\hat{\nu}_i^c\right)^3$ (which control the quartic and lower dimension tree level couplings).[2]

2. There is a soft term coupling the singlet to the Higgs H_2

$$\Delta V_{\text{soft}} \sim a_\nu v_{\tilde{\nu}} v_2 v_{\tilde{\nu}^c}. \tag{4.18}$$

[2]As we will see later, the shift of the field origin will generically generate lower dimension couplings from higher dimensional couplings.

which potentially provides a cubic coupling for the Higgs sector. Unfortunately, this term does not play an important role in the analysis because $v_{\tilde{\nu}} \ll \mathcal{O}(\text{GeV})$.

3. Superpotential has a Yukawa coupling of the singlet to the left handed lepton and Higgs, leading to the following additional F-terms:

$$\Delta V_F = 2Y_\nu v_{\tilde{\nu}} \left[\kappa v_2 v_{\tilde{\nu}^c}^2 - v_1 \lambda (v_2^2 + 3 v_{\tilde{\nu}^c}^2)\right] + Y_\nu^2 (v_2^2 v_{\tilde{\nu}}^2 + v_2^2 v_{\tilde{\nu}^c}^2 + 3 v_{\tilde{\nu}}^2 v_{\tilde{\nu}^c}^2) \tag{4.19}$$

Given the smallness of the Yukawa couplings $Y_\nu \sim \mathcal{O}(10^{-7})$, these terms are not particularly important for the phase transition when the transition occurs with VEVs of order 10^7 GeV or less. Note that all of these terms are quartic in nature owing to the absence of dimensionful parameters in the superpotential. Also, since the origin of R-parity violation is the leptonic Yukawa coupling which is also the source of ΔV_F , we see that these do not play a significant role.

Hence, a generic feature of the $\mu\nu$SSM SFOPT not reproducible by the NMSSM is the feature due to point 1 above. This will be emphasized in the numerical exploration below. We will also find one step transitions, which are qualitatively similar to the NMSSM transitions.

4.3 Qualitative Description of The Desired Parametric Region

A novel feature of the $\mu\nu$SSM compared to the NMSSM is the transition depicted in Eq. (4.17). In such cases one can shift the origin of the field such that the phase transition of interest occurs from the origin. With such shifted coordinates in mind, we define the field ϕ to be the radial magnitude

$$\phi \equiv \sqrt{(\vec{v})^2 + (\Delta\vec{v}_{\tilde{\nu}})^2 + (\Delta\vec{v}_{\tilde{\nu}^c})^2} \tag{4.20}$$

for a phase transition controlled by the potential $V_T(\phi)$ in which the vector of CP even Higgs scalars attains an order parameter change of $\vec{v}$. Explicitly, the strength of the phase transition is approximately characterized by the $SU(2)_L$ breaking $|\vec{v}|/T_c$ and not ϕ_c/T_c where the critical temperature T_c is defined by the condition $V_{T_c}(0) \approx V_{T_c}(\phi_c)$.

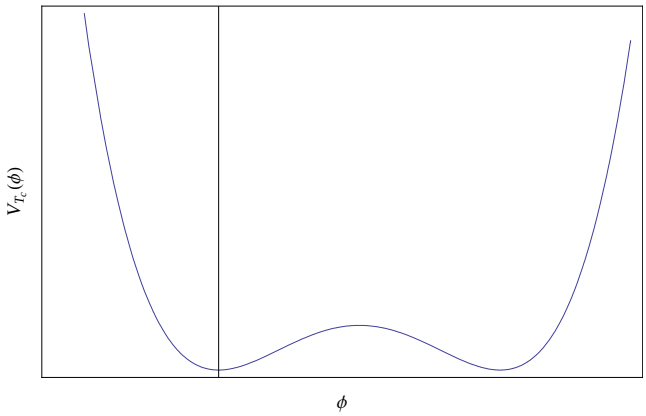

Figure 4.1: A schematic plot of the finite temperature effective potential at the critical temperature of Eq. (4.22). The vertical line represents $\phi = 0$ and helps to visualize the effect of $\phi \to -\phi$ symmetry breaking effect of the cubic term which is responsible for the bump at $\phi > 0$ for $\{E > 0, F_{\rm na} = 0\}$ in Eq. (4.21).

The finite temperature corrected effective potential of a real scalar field ϕ near the critical temperature will behave approximately as

$$V_T(\phi) \approx (\frac{1}{2}M^2 + c_1 T^2)\phi^2 - E_{\rm eff}\phi^3 + F_{\rm na}(\phi, T) + \frac{\lambda_{\rm eff}}{4}\phi^4 \tag{4.21}$$

up to additional temperature dependences. The $c_1 \sim \mathcal{O}(1)$ constant is proportional to coupling constants responsible for the leading mass correction, and $F_{\rm na}$ is the non-analytic thermal correction contribution that can lead to an effective cubic contribution to the potential. Although in the MSSM $F_{\rm na}$ plays a significant role, with a singlet involved such as in the $\mu\nu$SSM, $F_{\rm na}$ need not play a crucial role. Hence, we will set $F_{\rm na} = 0$. In this section, we neglect "other temperature dependences" in Eq. (4.21). Note that Eq. (4.21) has $M^2 > 0$ even though at $T = 0$, symmetry is broken when $E_{\rm eff} > 0$ and satisfies a condition specified below.

Defining where $v(T_c)$ is the degenerate minimum VEV, we find

$$T_c = \frac{\sqrt{2E_{\text{eff}}^2/\lambda_{\text{eff}} - M^2}}{\sqrt{2c_1}}. \tag{4.22}$$

The potential at the critical temperature is depicted in Fig. 4.1. The unusual sign of $2E_{\text{eff}}^2/\lambda_{\text{eff}} - M^2$ stems from our assumption that the symmetry is broken at zero temperature due to predominantly the E_{eff} term. This situation turns out to be generically beneficial for a SFOPT as we explain soon below. The critical temperature T_c is larger if $E_{\text{eff}} > 0$ because in that case, the negative contribution from the cubic term in Eq. (4.21) is enhanced for $\phi > 0$ which means that the quadratic term which is the leading source of positivity (as ϕ approaches ϕ_c from the left) has to be stronger to cancel the stronger negative contribution. Since there will be no positive mass squared at the origin during the phase transition in the absence of the cubic term, the mass at the origin has to be also larger for increasing $E_{\text{eff}} > 0$. Explicitly, the mass at the origin (which by construction is our starting point of the phase transition) is

$$\partial_\phi^2 V_{T=T_c}(0) = \frac{2E_{\text{eff}}^2}{\lambda_{\text{eff}}}. \tag{4.23}$$

This mass is identical to the mass at $\phi = \phi_c$. We can also understand the VEV

$$\phi_c = \frac{2E_{\text{eff}}}{\lambda_{\text{eff}}} \tag{4.24}$$

which can be heuristically justified by the fact that the broken phase local minimum results from a competition between the cubic and the quartic term (which is the dominant source of positivity as $\phi \to \phi_c^+$) at the time of critical temperature when the mass term is again controlled by Eq. (4.23).

Finally, the strength of the $SU(2)_L$ breaking in the transition is given by

$$\frac{v(T_c)}{T_c} = \frac{v(T_c)\sqrt{2c_1}}{M\sqrt{\frac{2E_{\text{eff}}^2}{\lambda_{\text{eff}}M^2} - 1}} \tag{4.25}$$

where

$$v(T_c) = \phi_c f(\vec{\Omega}) \tag{4.26}$$

and $f(\vec{\Omega})$ is a projection cosine onto the Higgs axis. By definition of the $SU(2)_L$ breaking transition, $\phi_c f(\vec{\Omega}) \lesssim \mathcal{O}(v(0))$. At $T = 0$, $\phi(0) \equiv \langle\phi\rangle_{T=0}$ is related to M through

$$M = \sqrt{\lambda_{\text{eff}}\phi^2(0) - 3E_{\text{eff}}\phi(0)} \tag{4.27}$$

where $\lambda_{\text{eff}}\phi(0) > 3E_{\text{eff}}$. Eq. (4.25) thus can be rewritten in terms of $\phi(0)$ as

$$\frac{v(T_c)}{T_c} = \left(\frac{2E_{\text{eff}}}{\lambda_{\text{eff}}\phi(0)}\right) \frac{\sqrt{2c_1/\lambda_{\text{eff}}}}{\sqrt{\left(1 - \frac{E_{\text{eff}}}{\lambda_{\text{eff}}\phi(0)}\right)\left(1 - \frac{2E_{\text{eff}}}{\lambda_{\text{eff}}\phi(0)}\right)}} f(\vec{\Omega})\,. \tag{4.28}$$

Hence, the strength of the phase transition is controlled mostly by 2 parameters:

$$\left\{\frac{E_{\text{eff}}}{\lambda_{\text{eff}}\phi(0)}, \sqrt{\frac{c_1}{\lambda_{\text{eff}}}}\right\}. \tag{4.29}$$

Note that since $f(\vec{\Omega}) \leq 1$, this angular projection function can only enhance the phase transition in a limited manner. Requiring $\frac{v(T_c)}{T_c}$ be real and requiring $V(\phi(0)) < V(0)$ result in the condition

$$0 \leq \frac{E_{\text{eff}}}{\lambda_{\text{eff}}\phi(0)} \leq \frac{1}{2}. \tag{4.30}$$

Therefore, one should keep in mind that although having a non-vanishing E_{eff} is good for a strong first order phase transition, the enhancement is bounded. Indeed, this bound is approximately satisfied by the numerical analysis, and SFOPT points that we find occur when

$$\frac{E_{\text{eff}}}{\lambda_{\text{eff}}\phi(0)} \approx \frac{1}{2}. \tag{4.31}$$

From the derivation of Eq. (4.28), one can see that Eq. (4.31) corresponds to making T_c as small as possible during the phase transition. When $\frac{E_{\text{eff}}}{\lambda_{\text{eff}}\phi(0)} > \frac{1}{2}$ the origin

becomes the global minimum and the symmetry is unbroken. Note also that because ϕ is defined with respect to the shifted singlet origin in Eq. (4.20), $\phi(0)$ does not correspond to the radial magnitude of the scalar field from the original Lagrangian's field origin.

After this first order phase transition, a second order phase transition might occur when $V''(0) = 0$. However, with $M^2 > 0$, this does not occur for this 1D toy model. Note that (96) assumes that there exists a temperature for which $V'' = 0$ which in fact never occurs for this toy model.

Generically, we are interested in a strong first order phase transition characterized by

$$\sqrt{2}\frac{v(T_c)}{T_c} \gtrsim 1.3 \tag{4.32}$$

(137). If the asymptotic conditions $\frac{E_{\text{eff}}}{\lambda_{\text{eff}}\phi(0)} \to 1/2$ and/or $c_1/\lambda_{\text{eff}} \to \infty$ are met, the phase transition can be arbitrarily strong. However, the following phenomenological constraints prevent/constrain arbitrarily strong transition in Eq. (4.28):

1. Global minima shifts can prevent the saturation of $E_{\text{eff}}/\left[\lambda_{\text{eff}}\phi(0)\right] = 1/2$ for a particular underlying parametric path. For example, as one approaches $E_{\text{eff}}/\left[\lambda_{\text{eff}}\phi(0)\right] = 1/2$ within a particular region of underlying parameter space, [3] the origin of Eq. (4.20) has to be shifted to a new global minimum (where the electroweak symmetry is still not broken, i.e. $\vec{v} = 0$). When this occurs, $\{E_{\text{eff}}, \lambda_{\text{eff}}, c_1\}$ of Eq. (4.21) undergo a discontinuous change as a function of the underlying parameters such as those of Eqs. (4.3) and (4.4).
2. Small λ_{eff} can result in phenomenologically unacceptably light Higgs (or other scalar masses). For example, it is clear from the effective model that

$$m_\phi^2 = 2\lambda_{\text{eff}}\phi^2(0)\left[1 - \frac{3}{2}\frac{E_{\text{eff}}}{\lambda_{\text{eff}}\phi(0)}\right] \tag{4.33}$$

[3] Recall that $E_{\text{eff}}/\left[\lambda_{\text{eff}}\phi(0)\right]$ are effective parameters derivable from underlying Lagrangian parameterized for example as Eqs. (4.3) and (4.4).

where the term in the parenthesis in Eq. (4.33) is positive since $0 \leq E_{\rm eff}/\left(\lambda_{\rm eff}\phi(0)\right) \leq 1/2$. Note that in any models that embed the MSSM, there is a minimal contribution to $\lambda_{\rm eff}$ from the D-terms that also makes it difficult to make it arbitrarily small. Note also that increasing $\frac{E_{\rm eff}}{\lambda_{\rm eff}\phi(0)}$ lowers the ϕ mass as well.

3. When $E_{\rm eff}/(\lambda_{\rm eff}\phi(0)) \to 1/2$, the energy difference ΔV between the false vacuum and true vacuum asymptotically vanishes. Explicitly, we have as $E_{\rm eff} \to E_c \equiv \lambda_{\rm eff}\phi(0)/2$, we find

$$\Delta V \to \frac{2\sqrt{2}\Delta E_{\rm eff} M^3}{\lambda^{3/2}} \to 0 \tag{4.34}$$

$$\frac{v(T_c)}{T_c} \to \left(\frac{2}{\lambda_{\rm eff}}\right)^{1/4} \sqrt{\frac{c_1 M}{\Delta E_{\rm eff}}} \tag{4.35}$$

where $\Delta E_{\rm eff} \equiv E_{\rm eff} - E_c$. Since the validity of this estimate requires $\Delta V > 0$, this region of parameter space becomes very sensitive to radiative corrections.

4. The contributions to c_1 *that maximize* $\sqrt{c_1/\lambda_{\rm eff}}$ typically contribute to $\lambda_{\rm eff}$ as well (with different powers). Hence, particularly in the $\mu\nu$SSM, we are in a region where $\lambda_{\rm eff}$ is on the larger side and not the small side.

The features just discussed qualitatively explain the numerical scan of the parameter space which identifies a particular parametric region in which Eq. (4.32) is satisfied at the same time with some basic phenomenological constraints which we detail in Sec. 4.5. There, more analytic formulae will be given explaining some of the features of the numerical results.

Now, let us consider the general path of the electroweak phase transition. At $T \gg \mathcal{O}(\text{TeV})$, the global minimum will be at

$$\{v_{\tilde{\nu}_i^c}(T) = 0, v_i(T) = 0\}, \tag{4.36}$$

the scalar field origin.[4] As explained previously, the left handed slepton VEVs are undergoing small energy scale transitions which are not particularly relevant to most of the discussion. As the temperature is lowered, non-trivial singlet VEV configuration will realize a global minimum, and the system will consequently make a transition. This transition in the singlets is sometime accompanied by an electroweak symmetry breaking phase transition, and sometimes not. If the first nontrivial singlet transition is accompanied by strongly first order electroweak symmetry breaking, these would be SFOPT from the scalar field origin:

$$\{v_{\tilde{\nu}_i^c}(T_c^+) = 0, v_j(T_c^+) = 0\} \longrightarrow \{v_{\tilde{\nu}_i^c}(T_c^-) \neq 0, v_j(T_c^-) \neq 0\}. \tag{4.37}$$

In this case, the origin of the vector whose magnitude is taken in Eq. (4.20) will be zero.

In addition, there will generically be singlet transitions from the origin at temperature T_O first without an electroweak phase transition, of the form

$$\begin{aligned} &\{v_{\tilde{\nu}_i^c}(T_O^+) = 0, v_j(T_O^+) = 0\} \\ &\qquad \longrightarrow \{v_{\tilde{\nu}_i^c}(T_O^-) = x_i(T_O) \neq 0, v_j(T_O^-) = 0\}\,. \end{aligned} \tag{4.38}$$

Even if this is a first order phase transition, it will typically complete before the subsequent electroweak symmetry breaking, and thus it does not to leading approximation participate in EWBG. However, it can in principle be relevant for gravity waves (see e.g. (112; 115; 116; 143–167)). Afterwards, there is a subsequent electroweak symmetry breaking phase transition

$$\begin{aligned} &\{v_{\tilde{\nu}_i^c}(T_c^+) = x_i(T_c) \neq 0, v_j(T_c^+) = 0\} \\ &\qquad \longrightarrow \{v_{\tilde{\nu}_i^c}(T_c^-) = y_i \neq 0, v_j(T_c^-) \neq 0\} \end{aligned} \tag{4.39}$$

[4]Symmetry restoration typically occurs as long as there are no tadpole contribution proportional to the temperature.

whose strength is important for EWBG. In this case, the origin of the vector whose magnitude is taken in Eq. (4.20) will be $\{v_{\tilde{\nu}_i^c}(T_c^+) = x_i, v_j(T_c^+) = 0\}$. When $x_i \nparallel y_i$, this transition corresponds to a "rotation" of the singlet vector.

Before concluding this section, let's briefly describe how the discrete symmetry discussed below Eq. (4.4) and zero temperature radiative corrections play a role for some of our strong multi-step transitions. Once a phase transition of the form Eq. (4.38) takes place, the set of degenerate global minima will form a coset representation of $\mathbb{Z}_3 \otimes \mathrm{CP} \otimes \mathbb{S}_3$.[5] Because of the approximate $\mathbb{Z}_3 \otimes \mathbb{Z}_3 \otimes \mathbb{Z}_3$ symmetry described in Eq. (4.5), to tree level accuracy, the coset space will be actually bigger: $\mathbb{Z}_3 \otimes \mathbb{Z}_3 \otimes \mathbb{Z}_3 \otimes \mathrm{CP} \otimes \mathbb{S}_3$. Some of the $\mathbb{Z}_3 \otimes \mathbb{Z}_3 \otimes \mathbb{Z}_3$ minima will be split due to the zero temperature radiative corrections, and the global minimum will be at a subset of the $\mathbb{Z}_3 \otimes \mathbb{Z}_3 \otimes \mathbb{Z}_3$ minima (one of which is what we labeled as $\vec{x}(T_O)$ in Eq. (4.38)). Finally, when the temperature drops enough to make one of the EWSB minima degenerate with $\vec{x}(T_c)$, the transition depicted by Eq. (4.39) occurs.

In Sec. 4.5, we will discuss explicit examples of both one-step and multi-step phase transitions.

4.4 Weak Sphaleron and the Singlet

After the baryon asymmetry has been created at a first order electroweak phase transition, it may be washed out by the B-violating sphaleron process (62; 84) in the broken phase. The sphaleron is a non-perturbative field configuration in the Weinberg-Salam theory that interpolates between topologically distinct vacua and violates $B + L$. To avoid washout, one must require that sphaleron transitions are suppressed meaning that the rate of these processes is less than the Hubble parameter

[5] Recall that $\mathbb{S}_3$ is nearly an exact symmetry because of the smallness of the leptonic Yukawa coupling.

at the time of the phase transition. This imposes a lower bound on the sphaleron Euclidean action $E_{\rm sph}(T_c)/T_c \gtrsim 45$ (137) which, in the Standard Model, becomes a lower bound on the Higgs VEV in the broken phase $\sqrt{2}v(T_c)/T_c \gtrsim 1.3$ where $v(0) = 174$ GeV. The six sneutrino fields of the $\mu\nu$SSM which receive VEVs during EWSB could in principle modify this bound. As we will see, the modifications are small because 1) the left-handed sneutrino VEV is much less than the electroweak scale and 2) the singlet sneutrino has a nearly homogenous solution which stays nears the minimum of the potential.

To obtain the sphaleron action at finite temperature, we calculate the zero temperature sphaleron and apply the scaling law (85)

$$E_{\rm sph}(T) = E_{\rm sph}(0)\frac{v(T)}{v(0)} \tag{4.40}$$

which introduces less than a ten percent error. Additionally, we compute the sphaleron solution using the tree level scalar potential V_0 and neglect radiative corrections. To a very good approximation (84) we can also neglect the $\mathrm{U}(1)_Y$ gauge coupling and compute a purely $\mathrm{SU}(2)_L$ sphaleron solution. The sphaleron ansatz is static and possesses an SO(3) rotational symmetry. The ansatz is given by

$$\begin{aligned}
\left\{H_1, H_2, \tilde{L}_i\right\} &= \{v_1 h_1(\xi), v_2 h_2(\xi), v_3 h_3(\xi)\}\, U^\infty \begin{pmatrix} 0 \\ \\ 1 \end{pmatrix} \\
\tilde{\nu}_i^c &= v_4 h_4(\xi) \\
W_i^a \sigma^a dx^i &= -\frac{2i}{g} f\,(\xi)\, dU^\infty (U^\infty)^{-1} \qquad (4.41) \\
U^\infty &= \frac{1}{r}\begin{pmatrix} z & x+iy \\ \\ -x+iy & z \end{pmatrix} \qquad (4.42)
\end{aligned}$$

in terms of the dimensionless radial coordinate $\xi = r/r_0$ rescaled by $r_0 = \left(g\sqrt{2}\sqrt{v_1^2+v_2^2+v_\nu^2}\right)^{-1} \approx \left(g\sqrt{2}v\right)^{-1}$. All VEVs are evaluated at zero temperature and we have introduced

$v_3 = v_{\tilde{\nu}}$ and $v_4 = v_{\tilde{\nu}^c}$ for convenience. We have used the $\mathbb{S}_3$ symmetry to equate the functions that describe the sneutrino fields of different generations, such that the sphaleron solution is given by five functions $h_i(\xi)$ and $f(\xi)$. Using this ansatz and after normalizing the potential to satisfy $V_0(h_i = 1) = 0$ by adding a constant, the field equations become

$$\frac{\xi^2 r_0^2}{v_i^2}\frac{\partial V_0}{\partial h_i} = \begin{cases} \xi^2 h_i'' + 2\xi h_i' - 2(1-f)^2 h_i & i = 1,2 \\ 3\left[\xi^2 h_3'' + 2\xi h_3' - 2(1-f)^2 h_3\right] & i = 3 \\ 3\left[\xi^2 h_4'' + 2\xi h_4'\right] & i = 4 \end{cases}$$

$$\xi^2 f'' - 2f(1-f)(1-2f) = -\frac{1}{4}\xi^2(1-f)g^2 r_0^2 \sum_{i=1}^{3} \theta_i v_i^2 h_i^2 \,. \tag{4.43}$$

where $\theta_i = 1$ for $i = 1,2$ and $\theta_i = 3$ for $i = 3,4$. Note that the term $(1-f)^2 h_i$ is absent for $i = 4$ because the singlet sneutrinos do not couple to the gauge bosons. The sphaleron action is obtained by integrating the sphaleron solution

$$E_{\rm sph}(0) = \frac{4\pi v\sqrt{2}}{g}\int_0^\infty d\xi \left\{ \frac{\xi^2}{2v^2}\sum_{i=1}^{4}\theta_i\left(v_i\frac{dh_i}{d\xi}\right)^2 + \frac{1}{v^2}(1-f)^2\sum_{i=1}^{3}\theta_i v_i^2 h_i^2 \right. \\ \left. + 4\left(\frac{df}{d\xi}\right)^2 + \frac{8}{\xi^2}f^2(1-f)^2 + \xi^2\frac{V_0(h_i)}{g^2 v^4}\right\} \tag{4.44}$$

We can observe immediately that contributions from the left-handed sneutrinos will be negligible because the function h_3 always appears with a prefactor of $v_3 = v_{\tilde{\nu}} \ll v$.

We can study the sphaleron solution by considering the asymptotic limits of Eq. (4.43). In the large ξ limit, all five field profiles must asymptote to unity in order for $E_{\rm sph}$ to be finite. In the small ξ limit, we find that the gauge boson and the three weakly charged scalar functions asymptote to zero, as in the Weinberg-Salam model, but that the singlet function approaches a value which can in general be non-zero:

$$f(\xi) \xrightarrow{\xi\to 0} \alpha\xi^2, \qquad h_i(\xi) \xrightarrow{\xi\to 0} \beta_i\xi \qquad i \in \{1,2,3\}, \qquad h_4 \xrightarrow{\xi\to 0} c + \beta_4\xi^2. \tag{4.45}$$

The singlet function behaves differently in this limit because the gauge coupling term $(1-f)^2 h_4$ in the field equation is absent. The boundary condition on the singlets makes the solution for $h_4(\xi)$ qualitatively different than for the Higgs fields. In particular, the solution $h_4(\xi)$ which minimizes $E_{\rm sph}$ will tend to be homogenous with $h_4 \approx 1$ for all ξ. The solution is homogenous because $E_{\rm sph} \ni (dh_4/d\xi)^2$ is positive semi-definite. Hence, it can be minimized by a constant h_4, and the solution remains near $h_4 = 1$ because this is where V_0 is minimized. As a result, the singlet fields contribute negligibly to the sphaleron action.

The sphaleron solution and energy density for a fiducial parameter set are plotted in Figure 4.2. To obtain the field profiles we solve Eq. (4.43) in the large and small ξ limits analytically, then match the solutions at five radii r_i which are chosen to minimize $E_{\rm sph}$. As discussed above, the singlet solution hovers around $h_4 = 1$ where the potential has a minimum. To display how each terms in Eq. (4.44) contributes to the sphaleron action, we have also plotted the integrand for the gauge kinetic, scalar kinetic, and scalar potential contributions separately. We observe that the sphaleron action is dominated by the kinetic terms. Since the parametric dependence only appears explicitly in the scalar potential, which is negligible, we expect that the sphaleron action is largely independent of our parameter choice. For this parameter set we find $E_{\rm sph}(0) \approx 1.83\frac{4\pi v}{g} \approx 8.7$ TeV which translates into a bound on the Higgs VEV at the critical temperature that is $\sqrt{2}\frac{v(T_c)}{T_c} \gtrsim 1.3$. As such, the Higgs VEV must satisfy the same constraint in the $\mu\nu$SSM as in the SM to avoid washout.

4.5 Parameter Scan and Phenomenological Bounds

We have investigated the $\mu\nu$SSM phase transition by performing a two-dimensional parameter space scan. For the two free parameters we use $m_{\rm ch} = 3\lambda v_{\tilde{\nu}^c}$, which

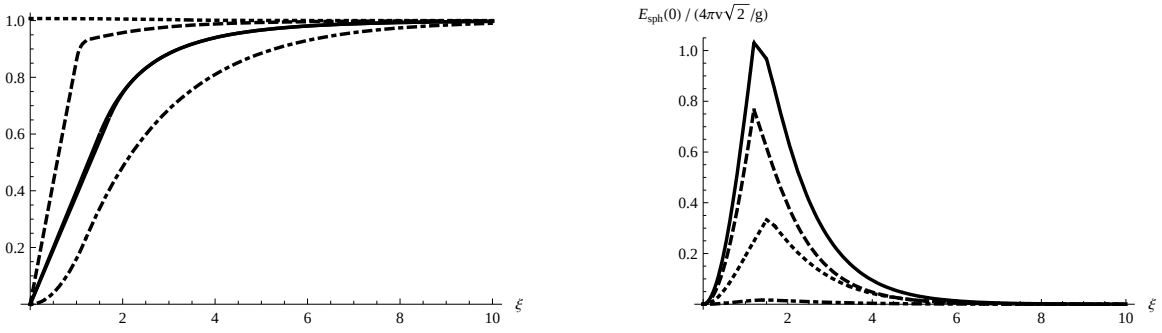

Figure 4.2: On the left, the $\mu\nu$SSM sphaleron solution versus the dimensionless radial coordinate with h_1 and h_2 solid, h_3 dashed, h_4 dotted, and f dot-dashed. The solution $h_{\tilde{\nu}^c}$ for the singlet sneutrinos does not satisfy the same boundary condition at $\xi \to 0$ as the $\mathrm{SU}(2)_L$ charged scalars. Hence, the solution of minimum energy is the one in which $h_{\tilde{\nu}^c} \approx 1$ for all ξ. On the right, the sphaleron energy density, Eq. (4.44), with gauge kinetic terms dashed, scalar kinetic terms dotted, scalar potential terms dot-dashed, and the total energy density solid. This plot illustrates that the sphaleron action is dominated by the kinetic terms and that the contribution from the scalar potential is negligible.

coincides with the charged Higgsino mass in the limit $M_2 \gg m_W, m_{\mathrm{ch}}$, and the dimensionless variable

$$\sigma = 2\left(\frac{a_\lambda}{m_{\mathrm{ch}}\lambda} + \frac{\kappa}{3\lambda}\right). \tag{4.46}$$

These parameters are scanned over the ranges $m_{\mathrm{ch}} : [75\ \mathrm{GeV}, 175\ \mathrm{GeV}]$ and $\sigma : [0, 25]$ by varying $v_{\tilde{\nu}^c}$ and a_λ. The SUSY-breaking parameters are chosen to match the conventions of (138): $\left\{m^2_{\tilde{Q}}, m^2_{\tilde{u}^c}, m^2_{\tilde{d}^c}, m^2_{\tilde{e}^c}\right\}$ are fixed at a fiducial SUSY-breaking scale which is taken to be 1 TeV, gaugino masses are set to $6M_1 = 3M_2 = M_3 = 3$ TeV, and A-terms are scaled by the associated Yukawa couplings as $\{A_{u_i} = a_u/Y_{u_i}, A_{d_i} = a_d/Y_{d_i}, A_{e_i} = a_e/Y_{e_i},$ and fixed at 1 TeV. Note that we have assumed for simplicity common left-handed sneutrino VEVs $v_{\tilde{\nu}_i} = v_{\tilde{\nu}}$ and a diagonal Yukawa matrix $(Y_\nu)_{ij} = Y_\nu \delta_{ij}$. The remaining soft masses $\left\{m^2_{H_1}, m^2_{H_2}, m^2_{\tilde{L}}, m^2_{\tilde{\nu}^c}\right\}$ are exchanged for the VEVs $\{v_1\,(0)\,, v_2\,(0)\,, v_{\tilde{\nu}}\,(0)\,, v_{\tilde{\nu}^c}\,(0)\}$ by solving the minimization equations at zero-temperature. The remaining Higgs sector parameters are chosen to be $\tan\beta = 2.6, \kappa = -0.64, \lambda = 0.18, v_{\tilde{\nu}} = 1.4 \times 10^{-5}$

GeV, and $a_\kappa = -236$ GeV. Given that some of our sparticle masses are far larger than $T_c \sim \mathcal{O}(100)$GeV, we could have integrated out these fields giving rise to a more illuminating effective field theory parameterization within the $\overline{DR}$ scheme.[6] However, to stay similar to the parameterization used in (135; 138), and to give a relatively unrestricted range for possible T_c, we have kept these relatively heavy fields as dynamical.

At each point in the parameter space, we calculate the $\mu\nu$SSM spectrum. In order to get a handle on phenomenological constraints, we impose the MSSM search bounds for the SUSY particles and require the Higgs masses to be $\gtrsim 90$ GeV (14) (later we will show a sample parametric point Higgs spectrum with the lightest Higgs mass of about 110 GeV). Model dependent bounds are of interest, but typically, they are weaker as far as the neutral Higgs is concerned because of singlet mixing effects. A more complete model dependent phenomenological consistency check including the study of charged Higgs mediated $b \to s\gamma$ rates is beyond the scope of this paper. We calculate the spectrum of the charged Higgses ($\phi_i^\pm$), charginos ($\tilde{\chi}_i^\pm$), and neutralinos ($\tilde{\chi}_i^0$) at tree-level and require $\left\{m_{\phi_1^\pm} > 79.3 \text{ GeV}, m_{\tilde{\chi}_1^\pm} > 94 \text{ GeV}, m_{\tilde{\chi}_1^0} > 46 \text{ GeV}\right\}$. The SM-like neutrinos mix with the neutralinos and heavy neutrinos in a seesaw matrix. We are able to reproduce the correct neutrino mass scale but neglected the question of precise neutrino mass pattern since any desired neutrino mass pattern will not be difficult to achieve by adjusting the small Yukawa couplings. Since we have already noted that the smallness of the leptonic Yukawa couplings make their role in the current SFOPT analysis insignificant, this does not present a significant loss of generality.

Because the squark, charged slepton, and left-handed sneutrino masses are supported by their TeV-scale SUSY-breaking mass parameters, they are insensitive to

[6] Recall that in $\overline{DR}$ scheme, decoupling is accomplished "by hand" through computing threshold corrections after integrating out fields.

parameters in the Higgs sector and are not affected by the phenomenological lower bounds. We compute the mass spectrum of Higges and singlet sneutrinos at one-loop order using the effective potential. Since we choose the VEVs for these fields to be real and there is no explicit CP-violation, the CP-even (ϕ_i) and CP-odd (a_i) components do not mix. The mass matrices are given by the curvature of the one-loop effective potential evaluated at the zero-temperature vacuum [7]

$$\left(M_\phi^2\right)_{ij} = \left.\frac{\partial^2 V_{\text{eff}}^0}{\partial(\mathcal{R}\varphi_i)\partial(\mathcal{R}\varphi_j)}\right|_{\text{VEV}} \qquad \left(M_a^2\right)_{ij} = \left.\frac{\partial^2 V_{\text{eff}}^0}{\partial(\mathcal{I}\varphi_i)\partial(\mathcal{I}\varphi_j)}\right|_{\text{VEV}} \tag{4.47}$$

where $\varphi_i \in \left\{H_1^0, H_2^0, \tilde{\nu}_j^c\right\}$. We can separately impose the mass bounds $m_{\phi_1} > 92.8$ GeV and $m_{a_1} > 93.4$ GeV.

At each point in parameter space that satisfies the phenomenological mass bounds, we require the electroweak-breaking vacuum with $v(0) = 174$ GeV to be the global minimum of the one-loop effective potential. This condition imposes particularly strong constraints on the parameter space. To understand these constraints and the nature of our multi-step phase transitions, we must discuss the structure of the $\{H_1^0, H_2^0, \tilde{\nu}_i^c\}$ field space and, in particular, determine the locations of the vacua that could potentially have lower energy than the EWSB vacuum. Recall that in the subspace with $H_1^0 = H_2^0 = 0$ there is a $\mathbb{Z}_3 \otimes \mathbb{Z}_3 \otimes \mathbb{Z}_3$ symmetry at tree level given by Eq. (4.5). To locate the extrema in this field space we solve the three cubic equations

$$\left.\frac{\partial V_0}{\partial \tilde{\nu}_i^c}\right|_{H_1^0 = H_2^0 = 0} = 0 \qquad i \in \{1, 2, 3\} \tag{4.48}$$

for $\tilde{\nu}_i^c$. The solutions of Eq. (4.48) which turn out to be minima (for our choice of the

[7] Since the effective potential is defined as a sum over 1PI diagrams with zero external momentum, this definition of mass differs from the pole in the propagator by the difference of the scalar self-energy evaluated at $p = m_{\text{pole}}$ and $p = 0$.

sign of a_κ) are given by

$$\begin{aligned} \tilde{\nu}_i^c &= \rho_i e^{i n_i \frac{2\pi}{3}} \qquad n_i \in \{0,1,2\} \\ \rho_i &= 0 \quad \text{or} \quad \frac{1}{4\kappa^2}\left(-a_\kappa + \sqrt{a_\kappa^2 - 8 m_{\tilde{\nu}^c}^2 \kappa^2}\right) \approx v_{\tilde{\nu}^c} \end{aligned} \tag{4.49}$$

We will focus on the solutions with $\rho_1 = \rho_2 = \rho_3 \approx v_{\tilde{\nu}^c}$ because these minima are in general deeper than those with $\rho_i = 0$. Then, there are $3^3 = 27$ local minima in the $H_1^0 = H_2^0 = 0$ field space, that we will refer to by $\vec{x}_{n_1 n_2 n_3}$ where the subscript indicates the phases of the three singlets. The $(\mathbb{Z}_3)^3 \otimes \mathbb{S}_3 \otimes \text{CP}$ symmetry ensures the degeneracy of the twenty-seven minima. Moving away from $H_1^0 = H_2^0 = 0$ as illustrated in Figure 4.3, the $(\mathbb{Z}_3)^3$ symmetry is broken to $\mathbb{Z}_3$ by terms in V_0 proportional to a_λ and λ. We will use $\vec{y}_{n_1 n_2 n_3}$ to denote the point in field space near to $\vec{x}_{n_1 n_2 n_3}$ but where $H_1^0/v_1 = H_2^0/v_2 = 1$. For example, in this notation, $\vec{y}_{000}$ corresponds to the EWSB vacuum in which the three singlets have real VEVs.

At one loop order, radiative corrections break the approximate $(\mathbb{Z}_3)^3$ symmetry (described above Eq. (4.5)) and split the degeneracy of the $\vec{x}_{n_1 n_2 n_3}$ minima as represented by Figure 4.4. After including radiative corrections, the preserved symmetry group is $\mathbb{Z}_3 \otimes \mathbb{S}_3 \otimes \text{CP}$. (Here, as an approximation, we are ignoring the fact that the subgroup $\mathbb{S}_3 \otimes \text{CP}$ is explicitly weakly broken in the Lagrangian already while $\mathbb{Z}_3$ must be broken by non-renormalizable operators to evade cosmological inconsistencies caused by domain walls.) The 27-fold degeneracy is split into three classes: a 3-fold degeneracy of the points $\vec{x}_{iii}$, a 6-fold degeneracy of the points $\vec{x}_{ijk}$ for $i \neq j \neq k$, and a 18-fold degeneracy of the points $\vec{x}_{iij}$ plus permutations for $i \neq j$. In order to discuss the phase transition we will choose one representative from each class: $\vec{x}_{000}$, $\vec{x}_{012}$, and $\vec{x}_{001}$. In this notation, if we say a transition occurs from the origin to $\vec{x}_{012}$ we mean that just below the critical temperature the vacuum is localized nearby to one of the six field points in the class that contains $\vec{x}_{012}$.

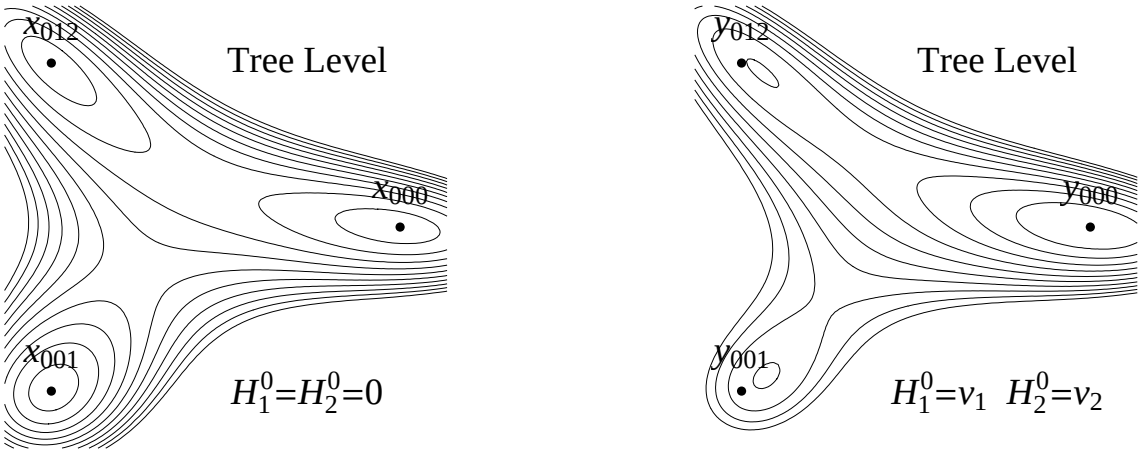

Figure 4.3: The tree level potential plotted over a slice of the $\tilde{\nu}_i^c$ field space with $H_1^0 = H_2^0 = 0$ on the left and $H_1^0/v_1 = H_2^0/v_2 = 1$ on the right. The labeled points are defined in the text, and a stationary point of the potential can be found at or near each of the labeled points. The potential grows farther from the central region. In the EW-preserving subspace, the three minima are degenerate, but the Higgs VEV selects out $\vec{y}_{000}$ as the global minimum.

The radiative corrections will generally split the degeneracy in such a way that some of the EW-preserving vacua will be depressed relative to the EWSB vacuum and may cause the latter to become metastable. This is both good and bad for the parameter space scan and phase transition analysis. It is bad because many points will be excluded because the EWSB vacuum is only metastable. On the other hand, it is good because with appropriate tuning, we can obtain an EW-preserving vacuum that is nearly degenerate with, but slightly higher than, the EWSB vacuum. Along the trajectory connecting these vacua, we can make $E_{\text{eff}}/\left(\lambda_{\text{eff}}\phi(0)\right)$ arbitrarily close to one half and obtain SFOPT. In Appendix 4.C we include analytic bounds which must be satisfied to prevent the EWSB vacuum from becoming metastable.

At each point in parameter space which satisfies the mass and vacuum bounds described above, we calculate the critical temperature T_c and order parameter $v(T_c)$ of the electroweak phase transition. The phase transition is calculated using the

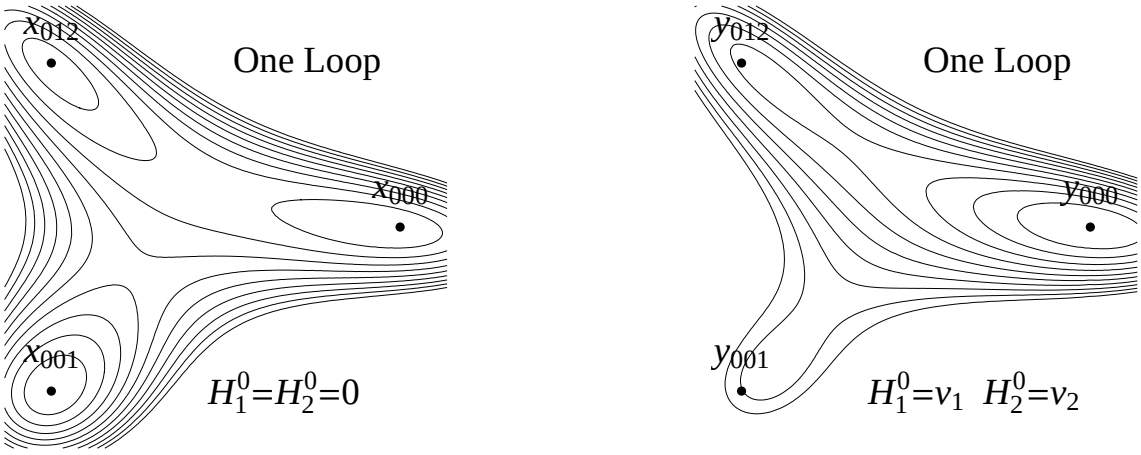

Figure 4.4: Same as Figure 4.3 but the contours represent values of the one loop effective potential at zero temeprature. The degeneracy is broken even in the EW-preserving subspace and induces $V_1^0\left(\vec{x}_{012}\right) < V_1^0\left(\vec{x}_{001}\right) < V_1^0\left(\vec{x}_{000}\right)$.

following procedure: increase the temperature from zero in increments, at each temperature minimize the thermal effective potential to find the EWSB vacuum $\vec{v}_{EWSB}(T) = \left\{v_1(T), v_2(T), v_{\tilde{\nu}_i^c}(T)\right\}$, also find whatever metastable vacua $\vec{v}_{\mathrm{MS},i}$ are near to $\vec{x}_{n_1n_2n_3}$ and $\vec{y}_{n_1n_2n_3}$, as the temperature increases the location and depth of these stationary points will change, converge on the critical temperature T_c at which the EWSB vacuum becomes degenerate with one of the EW-preserving minima $V_{\mathrm{eff}}^{T_c}\left(\vec{v}_{EWSB}(T_c)\right) = V_{\mathrm{eff}}^{T_c}\left(\vec{v}_{\mathrm{MS},i_\star}(T_c)\right)$, compute $v\left(T_c\right) = \sqrt{v_1^2(T_c) + v_2^2(T_c)}$ as the Higgs VEV in the broken phase. Using this procedure, we obtain T_c and $v\left(T_c\right)$ for the lowest temperature phase transition. Generally in this region of parameter space, multiple phase transition steps are required to bring the field configuration from the high-temperature symmetric phase to the zero-temperature broken phase. We must investigate separately earlier steps.

The results of the 2000 point parameter space scan are summarized in Figure 4.5 where regions IIIa and IIIb are the only likely viable regions for SFOPT EWBG. We will describe the different regions here and give an analytic derivation of the

boundaries and their parametric dependence in Appendix 4.C. The points in region I are excluded because the EWSB vacuum, where $v(0) = 174$ GeV, contains a tachyonic direction. The points in region II are excluded because the EWSB vacuum is metastable. For regions IIa,b,c, the actual vacuum can be found at the following points: the origin of field space in region IIa, nearby to x_{012} in region IIb, and nearby to y_{012} in region IIc. That is, in regions IIa and IIb, the electroweak phase transition does not occur. Region IIc does not work for EWBG as well as we will see below. In region III there are no tachyons, no false minima, and all phenomenological mass bounds are satisfied, but as we will see only IIIa and IIIb are likely to give acceptable phase transitions for EWBG.

The phase transition at each point can be classified into one of four types based on the path that the vacuum follows through the $\{H_1^0, H_2^0, \tilde{\nu}_i^c\}$ field space. In the largest region IIIa, the PT makes two steps: from the origin to a $\left\{\mathrm{EW}, \not{\mathbb{Z}}_3, \not{\mathbb{S}}_3, \not{\mathrm{C}}\mathrm{P}\right\}$ phase and then to the $\left\{\not{\mathrm{E}}\mathrm{W}, \not{\mathbb{Z}}_3, \mathbb{S}_3, \mathrm{CP}\right\}$ phase. In region IIIb the EWPT occurs in one step directly from the origin to the EW-broken phase. In region IIIc, the EW symmetry is broken by a second order phase transition in which only H_2^0 gets a VEV; then, a first order phase transition occurs giving the singlets VEVs. Finally in region IIId the phase transitions occur in three or four steps and there are multiple EWSB phases, whose details for a representative point are discussed below. However, as we will see, region IIId is unlikely to give an acceptable of EWBG scenario.

To understand how the $\mu\nu$SSM phase transition differs from the NMSSM scenario, we have taken one representative parameter point from each sector of region III and followed the full phase transition from the origin $\vec{x}_O$ to the zero temperature EWSB vacuum $\vec{y}_{000}$. In the tables, the minima above and below an arrow are degenerate at the temperature indicated. A 0^+ indicates that a second order phase transition occurs along the specified field direction.

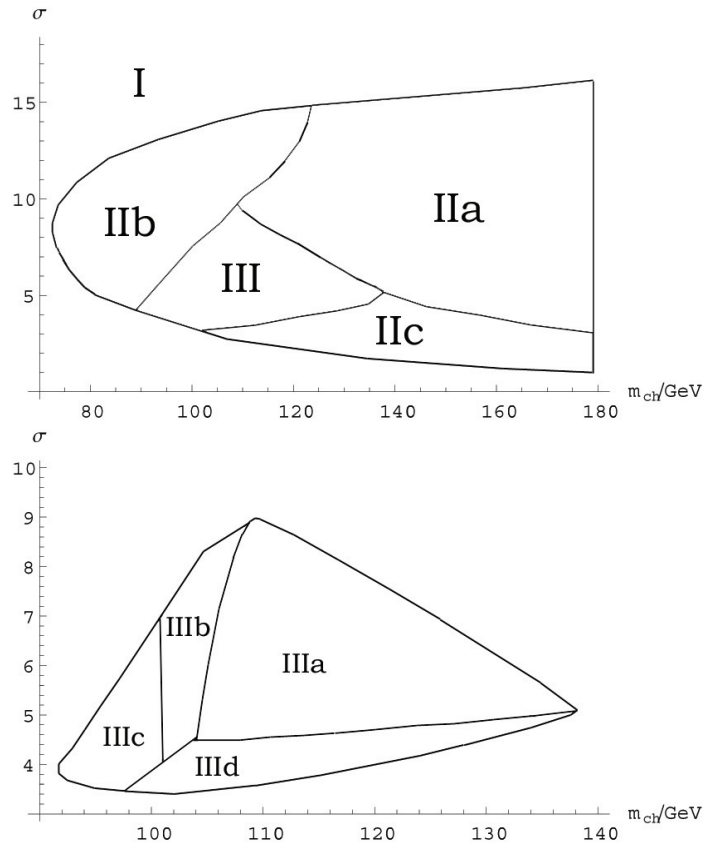

Figure 4.5: A slice of the $\mu\nu$SSM parameter space. Region I suffers from tachyons in the EWSB vacuum. In region II the EWSB vacuum is metastable and we exclude these points. In region III we calculate the electroweak phase transition and find that the path through field space can be classified into one of four types, shown on the right.

IIIa. Two Step Transition via EW-preserving Phase: $\vec{x}_O \xrightarrow{1PT} \vec{x}_{012} \xrightarrow{1PT} \vec{y}_{000}$

Representative point: $\{m_{\rm ch}, \sigma\} = \{108.8 \text{ GeV}, 9.12\}$.

At $T = 75.1$ GeV, a first order phase transition gives the singlets VEVs and breaks $\mathbb{Z}_3, \mathbb{S}_3$, and CP. The EW symmetry is broken by a strongly first order phase transition at 54.6 GeV which also restores $\mathbb{S}_3$ and CP. Baryon number may be generated at the strongly first order EW-breaking PT because spahlerons are suppressed by $\sqrt{2}v(T_c)/T_c = 4.46$ inside the bubble.

T	$\{H_1^0, H_2^0, \tilde{\nu}_i^c\}$ (GeV)	$\sqrt{2}\frac{v(T)}{T}$	Symmetries
$\gg M_w$	$\{0,0,0,0,0\}$	0	$\{\text{EW}, \mathbb{Z}_3, \mathbb{S}_3, \text{CP}\}$
$\xrightarrow{75.1\ \text{GeV}}$	$\{0,0,191.7,191.7e^{i2\pi/3},191.7e^{i4\pi/3}\}$	0	$\{\text{EW}, \not{\mathbb{Z}}_3, \not{\mathbb{S}}_3, \not{\text{C}}\text{P}\}$
	$\{0,0,192.6,192.6e^{i2\pi/3},192.6e^{i4\pi/3}\}$	0	$\{\text{EW}, \not{\mathbb{Z}}_3, \not{\mathbb{S}}_3, \not{\text{C}}\text{P}\}$
$\xrightarrow{54.6\ \text{GeV}}$	$\{61.7,160.7,201.0,201.0,201.0\}$	4.46	$\{\not{\text{E}}\text{W}, \not{\mathbb{Z}}_3, \mathbb{S}_3, \text{CP}\}$
0 GeV	$\{62.5,162.5,201.5,201.5,201.5\}$	N/A	$\{\not{\text{E}}\text{W}, \not{\mathbb{Z}}_3, \mathbb{S}_3, \text{CP}\}$

Table 4.1: Phase transition path for the representative point in region IIIa.

IIIb. One Step: $\vec{x}_O \xrightarrow{1PT} \vec{y}_{000}$

Representative point: $\{m_{\text{ch}}, \sigma\} = \{102.5\ \text{GeV}, 7.22\}$.

T	$\{H_1^0, H_2^0, \tilde{\nu}_i^c\}$	$\sqrt{2}\frac{v(T)}{T}$	Symmetries
$\gg M_w$	$\{0,0,0,0,0\}$	0	$\{\text{EW}, \mathbb{Z}_3, \mathbb{S}_3, \text{CP}\}$
$\xrightarrow{69.6\ \text{GeV}}$	$\{60.3,157.7,188.3,188.3,188.3\}$	3.43	$\{\not{\text{E}}\text{W}, \not{\mathbb{Z}}_3, \mathbb{S}_3, \text{CP}\}$
0 GeV	$\{62.5,162.5,189.8,189.8,189.8\}$	N/A	$\{\not{\text{E}}\text{W}, \not{\mathbb{Z}}_3, \mathbb{S}_3, \text{CP}\}$

Table 4.2: Phase transition path for the representative point in region IIIb.

At $T = 69.6$ GeV, the Higgs and singlets obtain VEVs simultaneously breaking the EW symmetry and $\mathbb{Z}_3$. This one-step phase transition resembles the ones seen in certain parametric regions of the NMSSM and other Higgs-singlet extensions. A baryon number may be generated since $\sqrt{2}v(T_c)/T_c = 3.43$ in the broken phase will suppress washout. For the parameters in region IIIb, we have plotted in Figure 4.6 the order parameter and critical temperature as functions of $E_{\text{eff}}/\left(\lambda_{\text{eff}}\phi(0)\right)$ which we calculate using the tree level potential along the trajectory that joins $\vec{x}_O$ and $\vec{y}_{000}$. The order parameter grows and the critical temperature decreases as $E_{\text{eff}}/\left(\lambda_{\text{eff}}\phi(0)\right)$ approaches 1/2 from below. The data points do not extend all the way to 1/2 because the radiative corrections lift the potential in such a way that parameter sets with $E_{\text{eff}}/\left(\lambda_{\text{eff}}\phi(0)\right) \approx 1/2$ at tree level have a metastable EWSB vacuum at one loop.

IIIc. Two Step via EWSB Phase: $\vec{x}_O \xrightarrow{2PT} \vec{y}_{H_2} \xrightarrow{1PT} \vec{y}_{000}$

Representative point: $\{m_{\rm ch}, \sigma\} = \{95.1 \text{ GeV}, 5.37\}$.

T	$\{H_1^0, H_2^0, \tilde{\nu}_i^c\}$	$\sqrt{2}\frac{v(T)}{T}$	Symmetries
$\gg M_w$	$\{0,0,0,0,0\}$	0	$\{\text{EW}, \mathbb{Z}_3, \mathbb{S}_3, \text{CP}\}$
$\xrightarrow{116.4 \text{ GeV}}$	$\{0,0^+,0,0,0\}$	0^+	$\{\not{\text{EW}}, \mathbb{Z}_3, \mathbb{S}_3, \text{CP}\}$
	$\{0,101,0,0,0\}$	2.5	$\{\not{\text{EW}}, \not{\mathbb{Z}}_3, \mathbb{S}_3, \text{CP}\}$
$\xrightarrow{57.6 \text{ GeV}}$	$\{61.6,160.6,175.4,175.4,175.4\}$	4.25	$\{\not{\text{EW}}, \not{\mathbb{Z}}_3, \mathbb{S}_3, \text{CP}\}$
0 GeV	$\{62.5,162.5,176.2,176.2,176.2\}$	N/A	$\{\not{\text{EW}}, \not{\mathbb{Z}}_3, \not{\mathbb{S}}_3, \text{CP}\}$

Table 4.3: Phase transition path for the representative point in region IIIc.

At a high temperature $T = 116.4$ GeV the EW symmetry is broken by a second order phase transition along the up-type Higgs direction. As the temperature decreases, the global minimum of the effective potential moves along the H_2^0 axis until it becomes degenerate with a minimum localized near to $\vec{y}_{000}$. A first order phase transition occurs with $\sqrt{2}v(T_c)/T_c = 4.25$ inside the bubble and $\sqrt{2}v(T_c)/T_c = 2.5$ outside the bubble. In this scenario, there is no baryon number generation. Because the first transition is of the second order, there is no coexistence of phases. The second transition is first order, but the sphaleron transition rate is suppressed both inside and outside the bubble such that $B + L$ is preserved on both sides.

IIId. Multi-Step: $\vec{x}_O \xrightarrow{1PT} \vec{x}_{012} \xrightarrow{1PT} (\vec{y}_{001} \text{ or } \vec{y}_{002}) \xrightarrow{1PT} \vec{y}_{000}$

Representative point: $\{m_{\rm ch}, \sigma\} = \{121.6 \text{ GeV}, 4.40\}$.

At this parametric point, the phase transition occurs in four steps with the EW symmetry broken in the second step by a second order phase transition. As the temperature drops from 128 GeV to 105 GeV, the sphaleron becomes increasingly suppressed. When the 1PT occurs at 105 GeV, the sphaleron is

T	$\{H_1^0, H_2^0, \tilde{\nu}_i^c\}$	$\sqrt{2}\frac{v(T)}{T}$	Symmetries
$\gg M_w$	$\{0,0,0,0,0\}$	0	$\{\mathrm{EW}, \mathbb{Z}_3, \mathbb{S}_3, \mathrm{CP}\}$
$\xrightarrow{222.3\ \mathrm{GeV}}$	$\{0,0,197,197e^{i2\pi/3},197e^{i4\pi/3}\}$	0	$\{\mathrm{EW}, \not{\mathbb{Z}}_3, \not{\mathbb{S}}_3, \not{\mathrm{C}}\mathrm{P}\}$
	$\{0,0,229,229e^{i2\pi/3},229e^{i4\pi/3}\}$	0	$\{\mathrm{EW}, \not{\mathbb{Z}}_3, \not{\mathbb{S}}_3, \not{\mathrm{C}}\mathrm{P}\}$
$\xrightarrow{128\ \mathrm{GeV}}$	$\{0^+,0^+,229,229e^{i2\pi/3},229e^{i4\pi/3}\}$	0^+	$\{\not{\mathrm{E}}\mathrm{W}, \not{\mathbb{Z}}_3, \not{\mathbb{S}}_3, \not{\mathrm{C}}\mathrm{P}\}$
	$\{0^+,82,232,232e^{i2\pi/3},232e^{i4\pi/3}\}$	1.1	$\{\not{\mathrm{E}}\mathrm{W}, \not{\mathbb{Z}}_3, \not{\mathbb{S}}_3, \not{\mathrm{C}}\mathrm{P}\}$
$\xrightarrow{105\ \mathrm{GeV}}$	$\{29e^{i1.9\pi},117e^{i1.9\pi},229,229,232e^{i2\pi/3}\}$	1.6	$\{\not{\mathrm{E}}\mathrm{W}, \not{\mathbb{Z}}_3, \not{\mathbb{S}}_3, \not{\mathrm{C}}\mathrm{P}\}$
	$\{32.0,128.0,230.3,230.3,232.7e^{i2\pi/3}\}$	2.10	$\{\not{\mathrm{E}}\mathrm{W}, \not{\mathbb{Z}}_3, \not{\mathbb{S}}_3, \not{\mathrm{C}}\mathrm{P}\}$
$\xrightarrow{89.0\ \mathrm{GeV}}$	$\{58.4,152.3,224.4,224.4,224.4\}$	2.59	$\{\not{\mathrm{E}}\mathrm{W}, \not{\mathbb{Z}}_3, \mathbb{S}_3, \mathrm{CP}\}$
0 GeV	$\{62.5,162.5,225.1,225.1,225.1\}$	N/A	$\{\not{\mathrm{E}}\mathrm{W}, \not{\mathbb{Z}}_3, \mathbb{S}_3, \mathrm{CP}\}$

Table 4.4: Phase transition path for the representative point in region IIId.

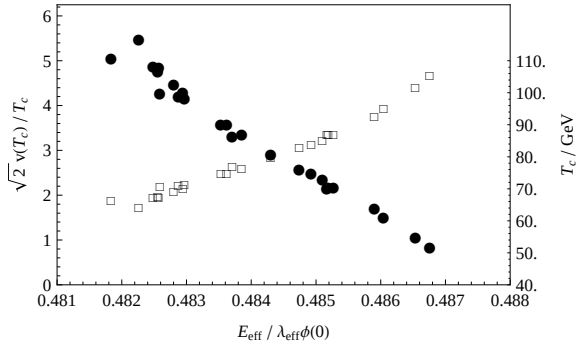

Figure 4.6: The order parameter (squares) and critical temperature (circles) plotted against $E_{\rm eff}/\lambda_{\rm eff}\phi\,(0)$ for the points in parametric region IIIb. We calculate $E_{\rm eff}/\lambda_{\rm eff}\phi\,(0)$ using the tree level potential along the trajectory that connects the origin $\vec{x}_O$ and zero temperature vacuum $\vec{y}_{000}$.

inactive, such that there will be no B-number generation. Not every phase transition in region IIId follows this particular PT path, but the PTs are generally multi-step with at least one EWSB intermediate phase and transitional CP violation.

To give an impression of the particle masses in this region of parameter space, we include here the spectrum for the representative point in region IIIb where $\{m_{\rm ch}, \sigma\} = \{102.5\ \mathrm{GeV}, 7.22\}$. The slepton, squark, gaugino, and left-handed sneutrino masses

are all $O\,(\text{TeV})$ because we have fixed the soft masses in these sectors at a fiducial SUSY-breaking scale. In the case of the $\tilde{\nu}$, we solve for the soft mass using the minimization equations to find $m_{\tilde{L}}^2 \approx -a_\nu v_{\tilde{\nu}^c} v_2 / v_{\tilde{\nu}}$, yet it is still typically TeV scale because $A_\nu = a_\nu / Y_\nu = -1$ TeV. The remaining fermion and charged scalar spectrum is given by

$$\begin{aligned} m_{H^\pm} &= 342 \text{ GeV} \\ m_{\tilde{H}^\pm} &= 96 \text{ GeV} \\ m_{\nu^c} &= 260, 243, 243 \text{ GeV} \\ m_{\tilde{\chi}^0_{1,2}} &= 88.7, 94.5 \text{ GeV}, \text{ mostly Higgsino} \\ m_\nu &= 41, 41, 7.8 \text{ meV} \end{aligned} \tag{4.50}$$

which are calculated at tree-level. The LSP is a Higgsino with mass 88.7 GeV. The degeneracies present in the neutrino sector result from the $\mathbb{S}_3$ symmetry of our Lagrangian. By allowing the left-handed sneutrinos to have different VEVs or choosing different values for the Y_ν Yukawas, we could obtain a correct neutrino hierarcy. We include these masses here to demonstrate that the seesaw matrix produces the correct mass scale for the light neutrinos. The neutral scalar masses are calculated at one-loop using the effective potential. Because there is significant mixing, we have included their mass eigenvalues and field composition in Table 4.5. Once again the degeneracies are a result of our $\mathbb{S}_3$ symmetry in the singlet sector. The lightest Higgs is mostly up-type with a mass of 110 GeV at this parametric point and only varies by 10 GeV over all of region III.

Mass	$\Re H_1^0$	$\Re H_2^0$	$\Re\tilde{\nu}_1^c$	$\Re\tilde{\nu}_2^c$	$\Re\tilde{\nu}_3^c$
395	0.83	0.16	0.00	0.00	0.00
140	0.01	0.21	0.26	0.26	0.26
128	0.00	0.00	0.58	0.01	0.41
128	0.00	0.00	0.09	0.65	0.07
110	0.16	0.63	0.07	0.07	0.07

Mass	$\Im H_1^0$	$\Im H_2^0$	$\Im\tilde{\nu}_1^c$	$\Im\tilde{\nu}_2^c$	$\Im\tilde{\nu}_3^c$
439	0.48	0.07	0.15	0.15	0.15
369	0.00	0.00	0.02	0.39	0.59
369	0.00	0.00	0.65	0.27	0.08
314	0.39	0.06	0.18	0.18	0.18

Table 4.5: CP-even and CP-odd Higgs masses and mixings for a sample parameter point. The masses are in GeV. The field composition is described by the squared eigenvector associated with each eigenvalue.

4.6 Domain Walls

It is well known (140; 168–172) that domain wall formation can be cosmologically problematic when spontaneous breaking of discrete symmetry occurs. In our scenario, we have only one "exact" discrete symmetry $\mathbb{Z}_3$ at the level of explicit parameterization of the Lagrangian. Because of the undesirable cosmological consequences of domain walls, we have implicitly assumed that this symmetry is broken by non-renormalizable operators which are cutoff by a scale [8] larger than many TeV (such as not to disrupt the effective potential analysis). In addition, we have approximate discrete symmetries such as $\mathbb{S}_3 \otimes \mathrm{CP}$ which a priori can cause problems if the symmetry breaking operators are overly suppressed. However, the set of electroweak symmetry breaking vacua of interest in this paper does not break $\mathbb{S}_3 \otimes \mathrm{CP}$ (i.e. our symmetry breaking pattern can naturally select a $\mathbb{S}_3 \otimes \mathrm{CP}$ singlet VEV to be the lowest energy vacuum as partly demonstrated in Appendix 4.D). Hence, we will neglect any transient behavior and focus on $\mathbb{Z}_3$ domain walls even though the analysis is not very specific to the discrete group.[9] Although a full analysis of domain wall histories is

[8] Because we have $\lambda^2+\kappa^2 < 0.5$ in the parametric regime of interest, the couplings should remain perturbative up to close to the GUT scale (141) (see e.g. (138) for explicit plots which suggest that our parametric choice is close to the border of perturbativity up to the GUT scale). Thus we are not severely restricted in the cutoff scale of our effective field theory.

[9] For example, if one wanted to analyze transient domain walls associated with $\mathbb{S}_3$ breaking, one can easily work out from our Lagrangian the leading effective scalar operator breaking $\mathbb{S}_3$ and use the result at the end of this section.

beyond the scope of this paper, here we briefly estimate the effects of the suppressed symmetry breaking operators that will alleviate the cosmological problems associated with domain walls that may form when the discrete symmetries considered in this paper are spontaneously broken. We will follow closely the work of Ref. (140).

In Ref. (140), it is estimated that during the approximate discrete symmetry breaking phase transition, domain walls separating approximately degenerate minima are formed. Then a simplified model of domain wall evolution is considered which approximately accounts for the surface tension of the bubble, the friction coming from bubble wall interaction with the plasma, and the pressure coming from energy density difference between the approximately degenerate minima. This last ingredient (pressure from energy density difference) is what will be coming from the inclusion of suppressed symmetry breaking operators, and we will refer to this simply as "pressure difference." If the pressure difference dominates, one of the approximately degenerate phases will eat away at the higher energy phase regions and eventually dominate in a time scale controlled by the strength of the symmetry breaking operator.

Estimating the friction to be negligible, an approximate sufficient condition for curing the possible domain wall problem from a cosmological perspective is to have the pressure difference dominate before the equilibrium initial condition period of big bang nucleosynthesis: i.e. before the photon temperature reaches about 10 MeV. Explicitly, assuming order unity Lorentz factor γ for the bubble wall speed, one must require

$$\epsilon > \frac{\sigma}{R(t)} \tag{4.51}$$

where ϵ is the energy density difference coming from suppressed symmetry breaking operators, σ is the energy per unit area of the bubble wall, and $R(t)$ is the time dependent radius of a typical bubble. For a dimension $4+u$ non-derivative operator

consisting of scalars only, ϵ can be estimated as

$$\epsilon \sim c_u \frac{v^{4+u}}{\Lambda^u} \tag{4.52}$$

where Λ is the cutoff scale and we have assumed all scalar VEVs to be of common order $v \equiv 174$ GeV (which is appropriate for our scenario). To be able to treat $u = 0$, we will set $\Lambda = 100$ TeV and find a bound on the value of c_u for different values of u. Assuming $R \sim t \sim 1/H$ (where H is the Hubble expansion rate) and $\sigma \sim v^3$, we find

$$c_u > 10^{-24} 500^u \tag{4.53}$$

for $u \geq 0$.[10] Hence, as long as the cutoff is not required to be very large (in contrast with the assumption of Ref. (140)) or the accidental symmetry arising from the UV completion quantum numbers do not make u too large, this bound is very easy to satisfy for the $\mathbb{Z}_3$ domain wall problem. Of course, if the cutoff is taken to be high and/or a UV completion is desired without fine tuning, model building challenges along the lines of Refs. (173; 174) exist.

4.7 Summary of the Chapter

We have uncovered a $\mu\nu$SSM parameteric region giving rise to a first order phase transition sufficiently strong to be useful for the electroweak baryogenesis scenarios involving electroweak symmetry breaking bubbles as the source of out of equilibrium and $SU(2)_L$ $F\tilde{F}$ operators as a source of baryon number violation. The parametric region corresponds to tuning the soft terms in the Lagrangian $a_\lambda H_1 \cdot H_2 \tilde{\nu}_i^c$ and $-m^2_{\tilde{\nu}^c} |\tilde{\nu}_i^c|^2$ to achieve Eq. (4.31). The numerical values of the uncovered parametric region is in the paragraph containing Eq. (4.46) and regions IIIa and IIIb depicted in Fig. 4.5. As expected, the Yukawa coupling of the singlets to the leptonic sector

[10] This result can easily be checked to be consistent with Ref. (140) for $u = 1$.

does not play a role in determining the strength of the phase transitions because of the weakness of the coupling tied to the smallness of the neutrino masses.

The region IIIa transitions are two-step transitions in which the electroweak symmetry breaking is the second transition that starts from a phase in which the singlet scalars of the $\mu\nu$SSM have a non-zero vacuum expectation value (e.g. starts from a vacuum which spontaneously breaks the approximate S_3 symmetry in the singlet sector). These transitions contain a rotation in the singlet field space and do not have an analog in the NMSSM transitions because of the different dimensionality in the singlet complex vector space. The region IIIb transitions are the ones in which electroweak symmetry breaking transition starts from the origin of the scalar field space. All these transitions have useful descriptions in terms of the representations of the approximate discrete symmetries in the system.

Our phenomenological bounds were rather minimal and placed using Ref. (14), but in many parametric regions, the observables are sufficiently far away from the bounds that the plausibility of the phenomenological self-consistency is strong. Follow-up possibilities include a more complete collider related phenomenological investigation in this parameteric regime, studies of domain wall histories due to weak global symmetry breaking operators, and a complete computation of CP asymmetry creation and transport leading to baryon asymmetry.

Given that the $\mu\nu$SSM had to give up the popular thermal leptogenesis scenario due to its low scale implementation of the type I seesaw, this work is of interest as it shows that electroweak baryogenesis may be a promising avenue to create baryon asymmetry in this class of models. Given that the $\mu\nu$SSM is one of the few supersymmetric models in which all dynamical degrees of freedom responsible for the neutrino mass may be accessible at TeV scale colliders, it is encouraging that the model has a good chance at being consistent with the observed baryon asymmetry in the universe.

4.A Appendix A. Field Dependent Mass Matrices

Here we include the tree level, field dependent mass matrices which are required to compute the one loop radiative corrections. We fix the charged scalars at their vanishing VEVs, let the left handed sneutrino VEV $\tilde{\nu}_i = v_{\tilde{\nu}}$ be real, and treat the matrices as functions of the complex fields $\{H_1^0, H_2^0, \tilde{\nu}_i^c\}$.

Neutralinos. Using the basis $(\chi^0)^T = \left\{\tilde{B}, \tilde{W}_3, \tilde{H}_1^0, \tilde{H}_2^0, \nu_1^c, \nu_2^c, \nu_3^c, \nu_1, \nu_2, \nu_3\right\}$, the mass term appears as $\mathcal{L} \ni -\frac{1}{2}(\chi^0)^T M_{\chi^0}(\chi^0) + \text{h.c.}$ with $n_{\chi^0} = -2$ and

$$M_{\chi^0} = \begin{pmatrix} \mathcal{M} & m \\ m^T & 0_{3\times 3} \end{pmatrix} \tag{4.54}$$

$$m^T = \begin{pmatrix} -\frac{g_1}{\sqrt{2}}v_{\tilde{\nu}} & \frac{g_2}{\sqrt{2}}v_{\tilde{\nu}} & 0 & Y_\nu\tilde{\nu}_1^c & Y_\nu H_2^0 & 0 & 0 \\ -\frac{g_1}{\sqrt{2}}v_{\tilde{\nu}} & \frac{g_2}{\sqrt{2}}v_{\tilde{\nu}} & 0 & Y_\nu\tilde{\nu}_2^c & 0 & Y_\nu H_2^0 & 0 \\ -\frac{g_1}{\sqrt{2}}v_{\tilde{\nu}} & \frac{g_2}{\sqrt{2}}v_{\tilde{\nu}} & 0 & Y_\nu\tilde{\nu}_3^c & 0 & 0 & Y_\nu H_2^0 \end{pmatrix} \tag{4.55}$$

and $\mathcal{M}$ is a symmetric, sparse array with elements

$$\mathcal{M}_{\tilde{B}\tilde{B}} = M_1 \tag{4.56}$$

$$\mathcal{M}_{\tilde{B}\tilde{H}_1^0} = -\frac{g_1}{\sqrt{2}}\left(H_1^0\right)^* \tag{4.57}$$

$$\mathcal{M}_{\tilde{B}\tilde{H}_2^0} = \frac{g_1}{\sqrt{2}}\left(H_2^0\right)^* \tag{4.58}$$

$$\mathcal{M}_{\tilde{W}_3\tilde{W}_3} = M_2 \tag{4.59}$$

$$\mathcal{M}_{\tilde{W}_3\tilde{H}_1^0} = \frac{g_2}{\sqrt{2}}\left(H_1^0\right)^* \tag{4.60}$$

$$\mathcal{M}_{\tilde{W}_3\tilde{H}_2^0} = -\frac{g_2}{\sqrt{2}}\left(H_2^0\right)^* \tag{4.61}$$

$$\mathcal{M}_{\tilde{H}_1^0\tilde{H}_2^0} = -\lambda\left(\tilde{\nu}_1^c + \tilde{\nu}_2^c + \tilde{\nu}_3^c\right) \tag{4.62}$$

$$\mathcal{M}_{\tilde{H}_1^0\nu_i^c} = -\lambda H_2^0 \tag{4.63}$$

$$\mathcal{M}_{\tilde{H}_2^0\nu_i^c} = -\lambda H_1^0 + Y_\nu v_{\tilde{\nu}} \tag{4.64}$$

$$\mathcal{M}_{\nu_i^c\nu_j^c} = 2\kappa\tilde{\nu}_i^c\delta_{ij} \quad . \tag{4.65}$$

Charginos. Using the basis $\left(\Psi^+\right)^T = \left\{-i\tilde{\lambda}^+, \tilde{H}_2^+, e_R^+, \mu_R^+, \tau_R^+\right\}$ and $\left(\Psi^-\right)^T = \left\{-i\tilde{\lambda}^-, \tilde{H}_1^-, e_L^-, \mu_L^-, \tau_L^-\right\}$ the mass term appears as $\mathcal{L} \ni -\frac{1}{2}\left(\Psi^+\right)^T M_{\chi^\pm}^T\left(\Psi^-\right) + \text{h.c.}$ with $n_{\chi^\pm} = -2$ and

$$M_{\chi^\pm} = \begin{pmatrix} M_2 & g_2\left(H_2^0\right)^* & 0 & 0 & 0 \\ g_2\left(H_1^0\right)^* & \lambda\left(\tilde{\nu}_1^c + \tilde{\nu}_2^c + \tilde{\nu}_3^c\right) & -Y_e v_{\tilde{\nu}} & -Y_\mu v_{\tilde{\nu}} & -Y_\tau v_{\tilde{\nu}} \\ g_2 v_{\tilde{\nu}} & -Y_\nu\tilde{\nu}_1^c & Y_e H_1^0 & 0 & 0 \\ g_2 v_{\tilde{\nu}} & -Y_\nu\tilde{\nu}_2^c & 0 & Y_\mu H_1^0 & 0 \\ g_2 v_{\tilde{\nu}} & -Y_\nu\tilde{\nu}_3^c & 0 & 0 & Y_\tau H_1^0 \end{pmatrix}. \tag{4.66}$$

Gauge Bosons. The propagators and field dependent masses in the gauge sector have gauge dependence. We work in the Landau gauge ($\xi = 0$), in which the scalar component and ghost propagators have no field dependence. The charged gauge

bosons have field dependent mass

$$M_{W^\pm}^2 = \frac{g_2^2}{2}\left(\left|H_1^0\right|^2 + \left|H_2^0\right|^2 + 3v_{\tilde{\nu}}^2\right) \tag{4.67}$$

and in the basis $\{W_3, B\}$ the neutral gauge bosons have the mass matrix

$$M_{W_3B}^2 = \begin{pmatrix} \frac{g_2^2}{2}\left(|H_1^0|^2 + |H_2^0|^2 + 3v_{\tilde{\nu}}^2\right) & -\frac{g_1 g_2}{2}\left(|H_1^0|^2 + |H_2^0|^2 + 3v_{\tilde{\nu}}^2\right) \\ -\frac{g_1 g_2}{2}\left(|H_1^0|^2 + |H_2^0|^2 + 3v_{\tilde{\nu}}^2\right) & \frac{g_1^2}{2}\left(|H_1^0|^2 + |H_2^0|^2 + 3v_{\tilde{\nu}}^2\right) \end{pmatrix}. \tag{4.68}$$

In order to count the degrees of freedom in the gauge sector, we must distinguish longitudinal and transverse components of the gauge boson fields, $2n_{W_L^\pm} = n_{W_T^\pm} = 4$ and $2n_{W_3B_L} = n_{W_3B_T} = 2$. We do this because only the longitudinal components receive thermal mass corrections in the computation of the daisy correction Eq. (4.15), (175). Note that $v_{\tilde{\nu}}^2$ is numerically negligible in these equations over all parameter regions of interest.

Squarks. Because we assume there is no inter-generational mixing in the squark sector, the squark mass matrix block diagonalizes. The i^{th} generation up- and down-type squarks have mass terms $\mathcal{L} \ni -\frac{1}{2}\tilde{q}_i^\dagger M_{\tilde{q}_i}^2 \tilde{q}_i$ in the basis $\tilde{q}_i = \left\{\tilde{q}_{L_i}, \tilde{q}_{R_i}^*\right\}$ with $n_q = 12$ and

$$\left(M_{\tilde{u}_i}^2\right)_{11} = M_Q^2 + \frac{1}{6}\left(\frac{3g_2^2}{2} - \frac{g_1^2}{2}\right)\left(\left|H_1^0\right|^2 - \left|H_2^0\right|^2 + 3v_{\tilde{\nu}}^2\right) + Y_{u_i}^2\left|H_2^0\right|^2 \tag{4.69}$$

$$\begin{aligned}\left(M_{\tilde{u}_i}^2\right)_{12} = \left(M_{\tilde{u}_i}^2\right)_{21}^* &= a_u\left(H_2^0\right)^* - Y_\nu Y_u v_{\tilde{\nu}}\left(\tilde{\nu}_1^c + \tilde{\nu}_2^c + \tilde{\nu}_3^c\right) \\ &\quad - Y_{u_i}\lambda\left(H_1^0\right)\left(\tilde{\nu}_1^c + \tilde{\nu}_2^c + \tilde{\nu}_3^c\right)\end{aligned} \tag{4.70}$$

$$\left(M_{\tilde{u}_i}^2\right)_{22} = m_{\tilde{u}^c}^2 + \frac{g_1^2}{3}\left(\left|H_1^0\right|^2 - \left|H_2^0\right|^2 + 3v_{\tilde{\nu}}^2\right) + Y_{u_i}^2\left|H_2^0\right|^2 \tag{4.71}$$

$$\left(M_{\tilde{d}_i}^2\right)_{11} = M_Q^2 - \frac{1}{6}\left(\frac{3g_2^2}{2} + \frac{g_1^2}{2}\right)\left(\left|H_1^0\right|^2 - \left|H_2^0\right|^2 + 3v_{\tilde{\nu}}^2\right) + Y_{d_i}^2\left|H_1^0\right|^2 \tag{4.72}$$

$$\left(M_{\tilde{d}_i}^2\right)_{12} = \left(M_{\tilde{d}_i}^2\right)_{21}^* = a_d\left(H_1^0\right) - Y_{d_i}\lambda\left(H_2^0\right)^*\left(\tilde{\nu}_1^c + \tilde{\nu}_2^c + \tilde{\nu}_3^c\right)^* \tag{4.73}$$

$$\left(M_{\tilde{d}_i}^2\right)_{22} = m_{\tilde{d}^c}^2 - \frac{g_1^2}{6}\left(\left|H_1^0\right|^2 - \left|H_2^0\right|^2 + 3v_{\tilde{\nu}}^2\right) + Y_{d_i}^2\left|H_1^0\right|^2 \quad . \tag{4.74}$$

Charged Scalars. The charged Higgs mixes with the charged sleptons. Using the basis $S^+ = \left\{H_1^+, H_2^+, \tilde{e}_L^+, \tilde{e}_R^+, \tilde{\mu}_L^+, \tilde{\mu}_R^+, \tilde{\tau}_L^+, \tilde{\tau}_R^+\right\}$, the mass term is $\mathcal{L} \ni -S^+ M_{H^\pm}^2 S^-$ with $n_{H^\pm} = 2$ and the elements of the Hermetian mass matrix are

$$\begin{aligned}
\left(M_{H^\pm}^2\right)_{H_1H_1} &= m_{H_1}^2 + v_{\tilde{\nu}}^2 \sum_{i=1}^{3} Y_{e_i}^2 + \frac{1}{4}\left(g_1^2 + g_2^2\right)\left|H_1^0\right|^2 \\
&\quad + \frac{1}{4}\left(g_1^2 - g_2^2\right)\left(3v_{\tilde{\nu}}^2 - \left|H_2^0\right|^2\right) + \lambda^2\left|\tilde{\nu}_1^c + \tilde{\nu}_2^c + \tilde{\nu}_3^c\right|^2 \qquad (4.75) \\
\left(M_{H^\pm}^2\right)_{H_1H_2} &= a_\lambda \sum_{i=1}^{3} \tilde{\nu}_i^c + 3v_{\tilde{\nu}} Y_\nu \lambda \left(H_2^0\right)^* + \left(\frac{1}{2}g_2^2 - 3\lambda^2\right)\left(H_1^0 H_2^0\right)^* \\
&\quad + \kappa\lambda \sum_{i=1}^{3} \left(\tilde{\nu}_i^c\right)^{2*} \qquad (4.76) \\
\left(M_{H^\pm}^2\right)_{H_2H_2} &= m_{H_2}^2 + \frac{1}{4}\left(g_1^2 + g_2^2\right)\left|H_2^0\right|^2 - \frac{1}{4}\left(g_1^2 - g_2^2\right)\left(3v_{\tilde{\nu}}^2 + \left|H_1^0\right|^2\right) \\
&\quad + Y_\nu^2 \sum_{i=1}^{3} \left|\tilde{\nu}_i^c\right|^2 + \lambda^2\left|\tilde{\nu}_1^c + \tilde{\nu}_2^c + \tilde{\nu}_3^c\right|^2 \qquad (4.77) \\
\left(M_{H^\pm}^2\right)_{H_1\tilde{\ell}_{L_i}} &= \left(\frac{1}{2}g_2^2 - Y_{e_i}^2\right) v_{\tilde{\nu}} \left(H_1^0\right)^* - Y_\nu \lambda \left(\tilde{\nu}_i^c\right)^* \sum_{i=k}^{3} \tilde{\nu}_k^c \qquad (4.78) \\
\left(M_{H^\pm}^2\right)_{H_1\tilde{\ell}_{R_i}} &= -a_e v_{\tilde{\nu}} - Y_\nu Y_{e_i} \left(H_2^0 \tilde{\nu}_i^c\right)^* \qquad (4.79) \\
\left(M_{H^\pm}^2\right)_{H_2\tilde{\ell}_{L_i}} &= \left(\frac{1}{2}g_2^2 - Y_\nu^2\right) v_{\tilde{\nu}} H_2^0 + \lambda Y_\nu H_1^0 H_2^0 \\
&\quad - Y_\nu \kappa \left(\tilde{\nu}_i^c\right)^2 - a_\nu \left(\tilde{\nu}_i^c\right)^* \qquad (4.80)
\end{aligned}$$

$$\left(M^2_{H^\pm}\right)_{H_2\tilde{\ell}_{R_i}} = -Y_\nu Y_{e_i} H_1^0 \left(\tilde{\nu}_i^c\right)^* - \lambda Y_{e_i} v_{\tilde{\nu}} \sum_{k=1}^{3} \left(\tilde{\nu}_k^c\right)^* \tag{4.81}$$

$$\begin{aligned}\left(M^2_{H^\pm}\right)_{\tilde{\ell}_{L_i}\tilde{\ell}_{L_j}} &= \delta_{ij}\left[m_L^2 + \frac{1}{4}\left(g_1^2 - g_2^2\right)\left(\left|H_1^0\right|^2 - \left|H_2^0\right|^2 + 3v_{\tilde{\nu}}^2\right) + Y_{e_i}^2\left|H_1^0\right|^2\right] \\ &\quad + \frac{1}{2}g_2^2 v_{\tilde{\nu}}^2 + Y_\nu^2 \tilde{\nu}_i^c \left(\tilde{\nu}_j^c\right)^*\end{aligned} \tag{4.82}$$

$$\begin{aligned}\left(M^2_{H^\pm}\right)_{\tilde{\ell}_{R_i}\tilde{\ell}_{R_j}} &= \delta_{ij}\left[m_{e^c}^2 - \frac{1}{2}g_1^2\left(\left|H_1^0\right|^2 - \left|H_2^0\right|^2 + 3v_{\tilde{\nu}}^2\right) + Y_{e_i}^2\left|H_1^0\right|^2\right] \\ &\quad + Y_{e_i}Y_{e_j}v_{\tilde{\nu}}^2\end{aligned} \tag{4.83}$$

$$\left(M^2_{H^\pm}\right)_{\tilde{\ell}_{L_i}\tilde{\ell}_{R_j}} = \delta_{ij}\left[a_{e_i}H_1^0 - \lambda Y_{e_i}\left(H_2^0\right)^* \sum_{k=1}^{3}\left(\tilde{\nu}_k^c\right)^*\right] \quad . \tag{4.84}$$

Neutral Scalars. The neutral Higgses mix with the left- and right-handed sneutrinos in a 16×16 matrix $M^2_{H_0}$. At the EWSB vacuum which respects CP, this matrix block diagonalizes into CP-even and CP-odd sectors. In order to study the phase transition in which there are transitional CP-violating phases, we must retain the off-diagonal blocks. In the basis $\phi^T = \{\Re H_0, \Im H_0\}$ where $H_0 = \{H_1^0, H_2^0, \tilde{\nu}_1^c, \tilde{\nu}_2^c, \tilde{\nu}_3^c, \tilde{\nu}_1, \tilde{\nu}_2, \tilde{\nu}_3\}$ the mass term is given by $\mathcal{L} \ni -\frac{1}{2}\phi^T M^2_{H_0}\phi$ with $n_{H_0} = 1$. One can obtain the mass matrix

$$\left(M^2_{H_0}\right)_{ij} = \begin{pmatrix} M^2_{\Re H_0} & M^2_{\not{C}\not{P}} \\ M^2_{\not{C}\not{P}} & M^2_{\Im H_0}\end{pmatrix}_{ij} = \frac{\partial^2 \bar{V}_0}{\partial\phi_i \partial\phi_j}. \tag{4.85}$$

by differentiating the full scalar potential

$$\begin{aligned}\bar{V}_0 = V_0 &+ m_L^2 \sum_i \left|\tilde{\nu}_i\right|^2 + Y_\nu^2\left(\left|H_2^0\right|^2 \sum_i \left|\tilde{\nu}_i\right|^2 + \left|\sum_i \tilde{\nu}_i\tilde{\nu}_i^c\right|^2\right) \\ &+ \sum_i \left[a_\nu H_2^0 \tilde{\nu}_i \tilde{\nu}_i^c + Y_\nu \kappa \left(H_2^0\tilde{\nu}_i\right)^* \left(\tilde{\nu}_i^c\right)^2 + \text{h.c.}\right] \\ &- \lambda Y_\nu \left[\left|H_2^0\right|^2 H_1^0 \sum_i \tilde{\nu}_i^* + H_1^0\left(\sum_i \tilde{\nu}_i^c\right)\left(\sum_i \tilde{\nu}_i\tilde{\nu}_i^c\right)^* + \text{h.c.}\right] \\ &+ \left[\frac{g_1^2+g_2^2}{8}\left(\left|H_1^0\right|^2 - \left|H_2^0\right|^2 + \sum_i \left|\tilde{\nu}_i\right|^2\right)^2 - \frac{g_1^2+g_2^2}{8}\left(\left|H_1^0\right|^2 - \left|H_2^0\right|^2\right)^2\right]\end{aligned} \tag{4.86}$$

where the dominant contribution V_0 is given by Eq. (4.9).

4.B Appendix B. Bosonic Thermal Masses

In order to calculate the daisy resummation Eq. (4.15) we require the thermal mass corrections Π_b. For the Higgs and singlet fields we compute the thermal mass corrections from the thermal effective potential using the procedure explained in this section. For the left-handed sneutrinos we use

$$\frac{\Pi_{\tilde{\nu}_i}}{T^2} = \frac{g_1^2}{8} + \frac{7g_2^2}{24} + \frac{5Y_{e_i}^2}{24} + \frac{Y_\nu^2}{4} \tag{4.87}$$

which can be calculated by assuming that all species that are summed in ΔV_1^T are light. For the remaining bosonic species, we use the thermal mass functions calculated for the nMSSM by (94) in which the authors assumed that the Higgs, Higgsinos, electroweak gauginos, and SM particles were light.

First, we evaluate the thermal effective potential correction Eq. (4.13) as a function of the eigenvalues of the field dependent mass matrices listed in Appendix 4.A. Let $\tilde{m}_{ij}^2$ be the j^{th} eigenvalue of the i^{th} mass matrix with has n_i associated degrees of freedom. By expanding the traces, Eq. (4.13) can be written as

$$\Delta V_1^T = \frac{T^4}{2\pi^2} \sum_i |n_i| \begin{cases} \sum_j J_B\left(\tilde{m}_{ij}^2/T^2\right) & \text{i bosonic} \\ -\sum_j J_F\left(\tilde{m}_{ij}^2/T^2\right) & \text{i fermionic} \end{cases}. \tag{4.88}$$

In the high-temperature limit, $\tilde{m}_{ij}^2 \ll T^2$ the bosonic and fermionic thermal functions can be expanded as

$$J_B(y) \xrightarrow{y\ll 1} \frac{\pi^2}{12} y + O\left(y^{3/2}\right) \tag{4.89}$$

$$J_F(y) \xrightarrow{y\ll 1} -\frac{\pi^2}{24} y + O\left(y^2\right) \tag{4.90}$$

plus field independent terms. Second, we define the high-temperature thermal poten-

tial correction by imposing a sharp cutoff at $\tilde{m}_{ij}^2 = 2T^2$ to obtain

$$\Delta V_1^{T,\text{high}} = \frac{1}{48} T^2 \sum_i |n_i| \begin{cases} \sum_j 2\tilde{m}_{ij}^2 & \text{i bosonic} \\ \sum_j \tilde{m}_{ij}^2 & \text{i fermionic} \\ 0 & \tilde{m}_{ij}^2 < 2T^2 \end{cases} \tag{4.91}$$

Third, we extract the thermal mass corrections by differentiating with respect to the Higgs and singlet fields,

$$\Pi_{\phi_i} = T^2 \left[\frac{\partial^2}{\partial \phi_i^2} \frac{\Delta V_1^{T,\text{high}}}{T^2} \right]_{H_1^0 = H_2^0 = \tilde{\nu}_j^c = 0, T = 100 \text{ GeV}} \tag{4.92}$$

where $\phi_i \in \{H_1^0, H_2^0, \tilde{\nu}_k^c\}$. The derivatives are evaluated at the origin in field space such that Π_{ϕ_i} is accurate in the high-temperature vacuum. Because the derivative in Eq. (4.92) has only weak field dependence, we expect this expression for Π_{ϕ_i} to be accurate even for our multi-step phase transitions in which the singlets have VEVs before the EWPT. The value of T used in Eq. (4.92) only affects the location of the cutoff in Eq. (4.91). We have chosen the temperature $T = 100$ GeV to be at the appropriate scale for our phase transitions and such that Π_{ϕ_i} does not vary discontinuously in the region of parameter space with first order phase transitions. Using this procedure we obtain $\Pi_{H_1^0} \approx 0.11\ T^2, \Pi_{H_2^0} \approx 0.40\ T^2, \Pi_{\tilde{\nu}_i^c} \approx 0.20\ T^2$ over the region of parameter space with phase transitions.

4.C Appendix C. Analytic Derivation of Parameter Space Boundaries

The boundaries in Figure 4.5 can be understood analytically. In this section, we derive expressions for each of the boundaries and discuss the parametric dependence.

At the interface of regions I and II, the electroweak vacuum develops a tachyonic direction at tree level and $\det M^2_{\Re H_0} = 0$. Since $M^2_{\Re H_0}$ is an 8 by 8 matrix, it would not be useful to write out its determinant. Instead, we observe that the tachyonic direction is directed along $\{H_1^0/v_1, H_2^0/v_2, \tilde{\nu}_i^c/v_{\tilde{\nu}^c} \approx 1, \tilde{\nu}_i = 0\}$.

At the boundary between region IIa and III, the minima at $\vec{x}_{012}$ and $\vec{y}_{000}$ are degenerate at one loop. Note that this degeneracy cannot occur at tree level. To see why, write

$$V_0\left(\vec{x}_{012}\right) - V_0\left(\vec{y}_{000}\right) = \Delta V_0^a + \Delta V_0^b \tag{4.93}$$

with $\Delta V_0^a = V_0\left(\vec{x}_{012}\right) - V_0\left(\vec{x}_{000}\right)$ and $\Delta V_0^b = V_0\left(\vec{x}_{000}\right) - V_0\left(\vec{y}_{000}\right)$. The tree level $\left(\mathbb{Z}_3\right)^3$ symmetry ensures $\Delta V_0^a = 0$. Additionally, the minimization equations Eq. (4.10) require that the potential has a minimum at $\vec{y}_{000}$. Therefore, we have

$$\Delta V_0^b = \frac{1}{8}\left[\left(g_1^2 + g_2^2\right)\cos^2 2\beta + 6\lambda^2 \sin^2 2\beta\right] v^4 > 0. \tag{4.94}$$

At one loop order we calculate the difference in the potential as

$$V_1^0\left(\vec{x}_{012}\right) - V_1^0\left(\vec{y}_{000}\right) = \Delta V_1^a + \Delta V_1^b \tag{4.95}$$

where V_1^0 is the one loop, zero temperature effective potential and $\Delta V_1^{a,b}$ are defined analogously as above. We expect ΔV_1^a to be nonzero and sensitive to the radiative corrections because the $\left(\mathbb{Z}_3\right)^3$ symmetry is broken to $\mathbb{Z}_3$. The terms responsible for this symmetry breaking are the superpotential term $W \ni \lambda \hat{H}_1^0 \hat{H}_2^0 \hat{\nu}_i^c$ and corresponding A-term in the soft SUSY-breaking Lagrangian. We calculate

$$\begin{aligned} 64\pi^2 \Delta V_1^a = {} & 6 m_{\text{ch}}^4 \log \frac{m_{\text{ch}}^2}{e^{3/2}\mu^2} + 4\Bigg[m_{H_1}^4 \log \frac{m_{H_1}^2}{e^{3/2}\mu^2} \\ & + m_{H_2}^4 \log \frac{m_{H_2}^2}{e^{3/2}\mu^2} - \sum_{\pm} m_{\pm}^4 \log \frac{m_{\pm}^2}{e^{3/2}\mu^2} \Bigg] \\ m_{\pm}^2 = {} & m_{\text{ch}}^2 + \frac{m_{H_1}^2 + m_{H_2}^2}{2} \pm \frac{1}{2}\sqrt{\left(m_{H_1}^2 - m_{H_2}^2\right)^2 + \sigma^2 m_{\text{ch}}^4} \end{aligned} \tag{4.96}$$

For the sake of discussion, we can approximate the logarithms in the second term as order one numbers and eliminate the soft masses using Eq. (4.10) to obtain

$$64\pi^2\Delta V_1^a \approx 6m_{\rm ch}^4 \log\frac{m_{\rm ch}^2}{e^{3/2}\mu^2} - 2m_{\rm ch}^4\left(\sigma^2 + 4\sigma\csc 2\beta - 4\right) + 24\lambda^2 v^2 m_{\rm ch}^2 \tag{4.97}$$

Since we are simply trying to estimate the parametric dependence, we can approximate $\Delta V_1^b \approx \Delta V_0^b$. By requiring that the minimum at $\vec{x}_{012}$ is not deeper than the EWSB vacuum, we obtain the bound $\Delta V_1^a + \Delta V_0^b \geq 0$, which is saturated at the interface of regions IIa and III. This bound disfavors large $m_{\rm ch}$ and large σ because of the $-m_{\rm ch}^4\sigma^2$ term in ΔV_1^a.

At the boundary where regions III and IIa meet, the EWSB is degenerate with the origin in field space at one loop. Neglecting the radiative corrections we can approximate the splitting as $V_1^0\left(\vec{x}_O\right) - V_1^0\left(\vec{y}_{000}\right) \approx V_0\left(\vec{x}_O\right) - V_0\left(\vec{y}_{000}\right) \equiv \Delta V_0^c$ with

$$\begin{aligned}\Delta V_0^c = {} & \frac{1}{8}\left[\left(g_1^2 + g_2^2\right)\cos^2 2\beta + 6\lambda^2\sin^2 2\beta\right]v^4 \\ & + m_{\rm ch}^2 v^2\left[1 - \frac{\kappa\sin 2\beta}{6\lambda} - \frac{\sigma\sin 2\beta}{4}\right] + \frac{m_{\rm ch}^4\kappa^2}{27\lambda^4} + \frac{a_\kappa m_{\rm ch}^3}{27\lambda^3}\end{aligned} \tag{4.98}$$

To prevent the origin from becoming the global minimum we require $\Delta V_0^c > 0$ which favors larger $m_{\rm ch}$ and smaller σ.

At the boundary between regions IIc and III, the one loop potential has degenerate minima at $\vec{y}_{012}$ and $\vec{y}_{000}$. We can compute the splitting $\Delta V_0^d \equiv V_0\left(\vec{y}_{012}\right) - V_0\left(\vec{y}_{000}\right)$ by neglecting the radiative corrections to find

$$\Delta V_0^d = \frac{1}{2}m_{\rm ch}^2 v^2\left(\sigma\sin 2\beta - 2\right). \tag{4.99}$$

The condition that the EWSB minimum at $\vec{y}_{000}$ is absolutely stable requires $\Delta V_0^d > 0$ which imposes the lower bound $\sigma \gtrsim 2\csc 2\beta \approx 3$ for $\tan\beta = 2.6$. Figure 4.5 shows that the IIc-III boundary also depends on $m_{\rm ch}$ contrary to Eq. (4.99), but this is a result of the radiative corrections.

4.D Appendix D. Selecting a CP Even Vacuum

In this Appendix, we show formally how a superpotential contribution ΔW that break $\mathbb{Z}_3$ weakly can be constructed to make the CP conserving vacuum to have the lowest energy perturbatively in the absence of any explicit CP violating parameters. Consider the superpotential

$$W = W_0 + \Delta W \tag{4.100}$$

where ΔW represents a irrelevant operator perturbation to renormalizable W_0. We then have

$$\sum_i \left|\frac{\partial W}{\partial \phi_i}\right|^2 = \sum_i \left\{ \left|\frac{\partial W_0}{\partial \phi_i}\right|^2 + 2\Re\left[\left(\frac{\partial \Delta W}{\partial \phi_i}\right)\left(\frac{\partial W_0}{\partial \phi_i}\right)^*\right]\right\} \tag{4.101}$$

$$= V_0 + \sum_i \Delta V_i \tag{4.102}$$

where

$$V_0 \equiv \sum_i \left|\frac{\partial W_0}{\partial \phi_i}\right|^2 \tag{4.103}$$

and

$$\Delta V_i \equiv 2\Re\left[\left(\frac{\partial \Delta W}{\partial \phi_i}\right)\left(\frac{\partial W_0}{\partial \phi_i}\right)^*\right] \tag{4.104}$$

to leading order in ΔW which we will call $\mathcal{O}(\delta)$. As usual, W_0 and ΔW are holomorphic polynomials in fields. Considering $\phi_i \to \phi_i^*$ as a rep of $\mathbb{Z}_2$ which we will call 2, we have

$$\left(\frac{\partial \Delta W}{\partial \phi_i}\right)\left(\frac{\partial W_0}{\partial \phi_i}\right)^* \tag{4.105}$$

being a rep of

$$\oplus \sum_u (2^u \otimes \bar{2}^2) \equiv R. \tag{4.106}$$

If we assume all the coefficients of W and ΔW are real, we can write

$$2\Re\left[\left(\frac{\partial\Delta W}{\partial\phi_i}\right)\left(\frac{\partial W_0}{\partial\phi_i}\right)^*\right] = R \oplus \mathbb{Z}_2(R) \tag{4.107}$$

where $\mathbb{Z}_2(\mathbb{Z}_2(R)) = R$. Hence, we see that ΔV_i is a singlet under $\mathbb{Z}_2$. Given that ΔV_i is a polynomial in $a_j \equiv \Re\phi_j$ and $b_j \equiv \Im\phi_j$ and since under $\mathbb{Z}_2 : \{a_j \to a_j, b_j \to -b_j\}$, we must have

$$\Delta V_i = \sum_k \sum_m c^i_{km} P_k(\{a_j\}) S_m(\{b_j\}) \tag{4.108}$$

where S_m represents a basis of $\mathbb{Z}_2$ singlet polynomial functions composed of b_j and P_k is a basis of polynomial functions composed of a_j. Note that here $c^i_{km} = \mathcal{O}(\delta)$. Hence, given that the part of the effective potential not associated with ΔW had a minimum at $\vec{\phi} = \vec{v}(s)$ where $s \in \{-1, 0, 1\}$ parameterizes the $\mathbb{Z}_3$ fundamental rep elements and $b_j|_{\vec{v}(0)} = 0$ is the singlet element, the energy shift due to ΔW to $\mathcal{O}(\delta)$ is

$$\Delta\rho(s) \equiv \sum_i \Delta V_i|_{\vec{v}(s)} = \sum_i \sum_k \sum_m c^i_{km} P_k(\{v_j \cos\left(\frac{s2\pi}{3}\right)\}) S_m(\{v_j \sin\left(\frac{s2\pi}{3}\right)\}), \tag{4.109}$$

Note that $\Delta\rho(1) = \Delta\rho(-1)$. Hence, we only need to determine whether $\Delta\rho(1) - \Delta\rho(0) > 0$ to see if CP singlet has the lowest energy. Since $c^i_{km} \propto \text{sgn}\Delta W$, we can simply flip the sign of $\Delta\rho(1) - \Delta\rho(0)$ by flipping the sign of ΔW if the original choice of sign gives $\Delta\rho(1) - \Delta\rho(0) < 0$. Of course, all of this is under the assumption that the potential is not destabilized by the non-renormalizable operators such that the smallness of the pertrubation order δ is meaningful. Stability is generic if the nonrenormalizable terms are dominated by the perturbations in the superpotential since the superpotential contribution is positive definite.

Chapter 5

SFOPT Near an Enhanced Discrete Symmetry Point

We propose a group theoretic condition which may be applied to extensions of the Standard Model in order to locate regions of parameter space in which the electroweak phase transition is strongly first order, such that electroweak baryogenesis may be a viable mechanism for generating the baryon asymmetry of the universe. Specifically, we demonstrate that the viable corners of parameter space may be identified by their proximity to an enhanced discrete symmetry point. At this point, the global symmetry group of the theory is extended by a discrete group under which the scalar sector is non-trivially charged, and the discrete symmetry is spontaneously broken such that the discrete symmetry relates degenerate electroweak preserving and breaking vacua. This idea is used to investigate several specific models of the electroweak symmetry breaking sector. The phase transitions identified through this method suggest implications for other relics such as dark matter and gravitational waves.

This work was performed in collaboration with Vernon Barger and Lian-Tao Wang. It was published in the journal Physics Letters **B** in March of 2012 (176).

5.1 Introduction to the Chapter

Standard cosmology of the early universe within the context of a large class of models embedding the Standard Model (SM) of particle physics predicts the existence of an electroweak symmetry breaking (EWSB) phase transition (PT). Collider constraints alone cannot determine the nature of the EWSB PT in a model independent way. However, additional information is available in the form of cosmological relics, which were produced in the early universe and survive as direct probes of the physics of the era during which the temperature was electroweak scale. Relics such as the baryon asymmetry (62), primordial gravitational waves (159; 161; 164; 167), and (modifications to) the dark matter relic abundance (119; 177–179), may have been generated at the electroweak scale PT(s).

Generating the baryon asymmetry through CP violations at electroweak symmetry breaking bubbles (62), requires a strongly first order phase transition (SFOPT) to protect the baryon number in the broken phase. In this context, a SFOPT may be defined as a first order PT in which the (thermal) expectation value of the SM-like Higgs $v(T) = \langle h \rangle$ satisfies $v(T)/T \gtrsim 1$ in the broken phase after the phase transition completes, such that weak sphaleron processes are inactive (62; 84). It is well-known that the SM is unable to accommodate a SFOPT while satisfying the Large Electron-Positron (LEP) Collider bounds on the Higgs mass (90). This is one of the main motivations for considering an extended Higgs sector. Many beyond the Standard Model theories are able to accommodate a SFOPT, including supersymmetry, two Higgs doublet models, and minimal scalar singlet extensions of the SM. However, if the extra scalar fields obtain vacuum expectation values (vevs), one often finds that new patterns of symmetry breaking become accessible. This fact makes the phase transition more difficult to study, because quantities such as $v(T)/T$ are nonanalytic

functions of the parameters of the model. Consequently, many beyond the Standard Model PT analyses rely on an intensive numerical parameter scan to search for SFOPT. Although such scans may be capable of locating SFOPTs, on their own they do not reveal why one particular parametric limit is favored over another.

In this article, we propose a group theoretic guideline which will aid the search for SFOPT in a large parameter space and help to identify why certain parametric limits are favored over others. Our guideline is motivated by the following heuristic argument. In perturbative thermal effective potential computations, the thermal mass is of the order cT^2 where c is a thermal loop factor. Therefore, if all the renormalized coupling constants are of order unity and all mass scales are of the electroweak scale, we expect that the phase transition will occur at a temperature $T \sim v/\sqrt{c}$ such that $v(T)/T \sim \sqrt{c} < 1$, and the PT is typically not strongly first order. Hence, in order to have a SFOPT, the renormalized parameters of the theory must be near a special point in the parameter space. An ideal parametric limit which overcomes the natural thermal loop suppression is the region where $v(T)/T \to \infty$. To achieve this, it would be unnatural to expect $v(T)$ to deviate by many orders of magnitude from the electroweak scale, because of the constraint that $v(0)$ defines the electroweak scale. On the other hand, $v(T)/T$ may be enhanced by taking the $T \to 0$ limit.

The limit of low phase transition temperature and large $v(T)/T$ can be achieved naturally by employing a discrete symmetry. The phase transition begins at the critical temperature T_c, defined as the temperature above which the thermal corrections are sufficiently large as to make the EW symmetric phase energetically favored, and below which the EW broken phase is favored. Hence, at $T = T_c$ the thermal effective potential possesses two degenerate minima corresponding to the EW symmetric and broken phases (see also Appendix 5.A). One may enhance $v(T_c)/T_c$ by taking $T_c \to 0$ provided that there is a mechanism guaranteeing that the theory possesses

such degenerate vacua even in the absence of thermal corrections. One mechanism that yields degenerate vacua is the spontaneous symmetry breaking of a discrete group (see e.g. (180; 181)). After spontaneous symmetry breaking, one finds a set of degenerate vacuum states which fall into a coset representation of the discrete group. Moreover, if the discrete symmetry group does not commute with the electroweak group, then the scenario described above may be achieved: the electroweak symmetry is broken in one vacuum and unbroken in a second degenerate vacuum implying $T_c = 0$ and $v(T_c)/T_c = \infty$.

Of course the existence of degenerate vacua alone does not imply $v(T)/T \gg 1$, since the EW phase transition must take place, and this is not necessarily the case in extensions of the SM with multiple vacua. If the discrete symmetry is exact, then $T_c = 0$ and the phase transition does not proceed because the broken phase never becomes energetically favored. Hence, we will consider models in which the discrete symmetry is generally approximate, but becomes exact at a particular parametric point, referred to as an enhanced discrete symmetry point (EDSP)[1]. Then the heuristic arguments above imply that one can expect to find SFOPT in a parametric neighborhood of an EDSP and connected to it by a continuous "small" deformation which breaks the discrete symmetry. Precisely how "small" a deformation is required depends upon two model-dependent conditions: the condition that the electroweak PT must complete and upon the order unity number that sits at the right of the inequality $v(T)/T > 1$. Hence the takeaway message is that one can make the analysis of and search for SFOPT in a large parameter space more tractable with the aid of an EDSP "lamppost" which signals the parametric neighborhood which is favorable for SFOPT.

The order of presentation is as follows. In Sec. 5.2 we motivate our group theoretic identification of SFOPTs. In Sec. 5.3, we employ our technique to explore three

[1]In general, a model may possess multiple EDSPs each relating the EW broken and symmetric vacua by a different symmetry transformation.

example models. We then finish with some concluding remarks in Sec. 5.4 and an appendix which reviews some relevant basics of phase transitions used in this paper.

5.2 Why Discrete Symmetry?

Suppose that a given theory is exactly invariant under an internal discrete symmetry group G. It is well-known that the spontaneous symmetry breaking of G down to $H \subset G$ leads to the vacua giving a nontrivial coset G/H representation (180; 181). We will first illustrate how this connects to a SFOPT in a perturbative single real scalar field toy model, and then proceed to give a more general discussion.

Quite often in extensions of the SM, other scalar fields along with the Higgs obtain vevs at the electroweak phase transition. One may model such a first order phase transition with the following toy theory in which φ represents the linear combination of the SM Higgs and other scalar fields. Consider the theory of a real scalar field φ with the classical potential

$$U(\varphi) = \frac{1}{2}M^2\varphi^2 - \mathcal{E}\varphi^3 + \frac{\lambda}{4}\varphi^4\,, \tag{5.1}$$

and suppose that φ is coupled to a family of N fermions $\mathcal{L} \supset (m_i + h_i\varphi)\bar{\psi}_i\psi_i$. Note that this theory has no internal symmetries for non-special values of the parameters $\{M^2, \mathcal{E}, \lambda, h_i, m_i\}$. When we turn on temperature, there will be a thermal bath of φ and ψ_i particles. If the fermions are relativistic at the electroweak scale (i.e., $m_i^2 \ll T^2$), then the thermal effective potential can be written to leading order as

$$V_{\text{eff}}(\varphi, T) \approx U(\varphi) + cT^2\varphi^2 \tag{5.2}$$

where $c \approx Nh_i^2/12$ (182). Here, in the so-called high-temperature approximation, we have neglected the subdominant thermal corrections (such as the non-analytic term) and the $\hbar$ radiative corrections.

As long as the supercooling is small (e.g., as measured by the fractional temperature change during the duration of the PT), the PT occurs at the temperature near T_c at which the thermal effective potential V_{eff} displays two degenerate minima (for more details, see Sec. 5.A). Solving this constraint for T_c gives

$$T_c^2 = \frac{\mathcal{E}^2}{\lambda\, c}\left(1 - \frac{\lambda M^2}{2\mathcal{E}^2}\right) . \tag{5.3}$$

In this simple toy model and subject to the approximation Eq. (5.2), there is an enhanced $\mathbb{Z}_2$ symmetry at $T = T_c$. Explicitly, the potential at $T = T_c$ becomes

$$V_{\text{eff}}(\varphi, T_c) = \frac{\lambda\varphi^2}{4}\left(\varphi - \frac{2\mathcal{E}}{\lambda}\right)^2 \tag{5.4}$$

and respects the discrete symmetry

$$\mathbb{Z}_2 \;:\; \left(\varphi - \frac{\mathcal{E}}{\lambda}\right) \to -\left(\varphi - \frac{\mathcal{E}}{\lambda}\right) , \tag{5.5}$$

which was not originally present in Eq. (5.1). This $\mathbb{Z}_2$ exchanges the degenerate vacua at $\varphi = 0$ and $\varphi = v(T_c) = 2\mathcal{E}/\lambda$ across a potential barrier at $\varphi = \mathcal{E}/\lambda$. It is to be noted that Eq. (5.4) is independent of M, and thus this symmetry exists in this toy model for any critical temperature T_c that can be tuned using M.[2]

Although there is no electroweak symmetry in this toy model, there is still a first order phase transition, and we can investigate the parametric dependence of its order parameter $v(T_c)/T_c$. Since $v(T_c) = 2\mathcal{E}/\lambda$ is independent of M^2, the order parameter can be maximized by varying M^2 to minimize T_c. Even though the high-temperature expansion breaks down when T drops below the mass of the fermion, the formal limit $T_c \to 0$ can be taken assuming that the fermions are massless. The formal solution to $T_c = 0$ is[3]

$$\alpha \equiv \lambda M^2/2\mathcal{E}^2 = 1 . \tag{5.6}$$

[2] Although this is an enhanced $\mathbb{Z}_2$ symmetry at $T = T_c$, since the symmetry does not generically exist at other temperatures, it is not the enhanced discrete symmetry point relevant for this paper. See below for further clarification.

[3] The idea of focusing on $T_c \approx 0$ was recently emphasized by (118).

The important observation is that $1-\alpha = 0$ corresponds to an EDSP in the parameter space at which the *zero-temperature* scalar potential Eq. (5.1) is invariant under the symmetry transformation Eq. (5.5). At the EDSP, $1 - \alpha = 0$, the order parameter

$$\frac{v(T_c)}{T_c} = 2\sqrt{\frac{c}{\lambda}}\frac{1}{\sqrt{1-\alpha}} \tag{5.7}$$

formally diverges, and for $1 - \alpha \ll 1$, the phase transition may be made arbitrarily strongly first order.

Hence, our group theoretic guideline leads us to identify the parametric region in the vicinity of the EDSP $1 - \alpha = 0$ as favorable for SFOPT. However, for this region to be truly viable, it must be the case that the rate at which bubbles of the broken phase nucleate is sufficiently large that the phase transition actually completes. This requires the discrete symmetry to be weakly broken, such that the PT occurs at a nonzero T.[4] In the toy model, such breaking can be accomplished explicitly at the classical level through a finite excursion from the EDSP (i.e. $1 - \alpha = \epsilon \neq 0$), or radiatively through the Yukawa coupling. Indeed, in many extensions of the SM where singlets are introduced, the relevant discrete symmetry transforms both the Higgs and the singlet fields. Since the singlets lack SM gauge couplings, radiative corrections necessarily break the discrete symmetry to a degree controlled by the strength of the gauge interactions. If the breaking of the symmetry is so large that the potential does not have the qualitative features of Eq. (5.1) near $\alpha = 1$, then the EDSP method loses its advantage for identifying SFOPT. If the breaking of the symmetry is so small that bubbles will not nucleate fast enough to complete the PT, then any candidate parameter points found with the EDSP method are inherently not viable. Since this non-completion of the PT will be a general feature of the region of parameter space nearby to the EDSP, we must take extra care in choosing the temperature at which to evaluate the EW order parameter $v(T)/T$. Up to this point in the discussion,

[4]Note that the bubble nucleation rate is zero at $T = T_c$.

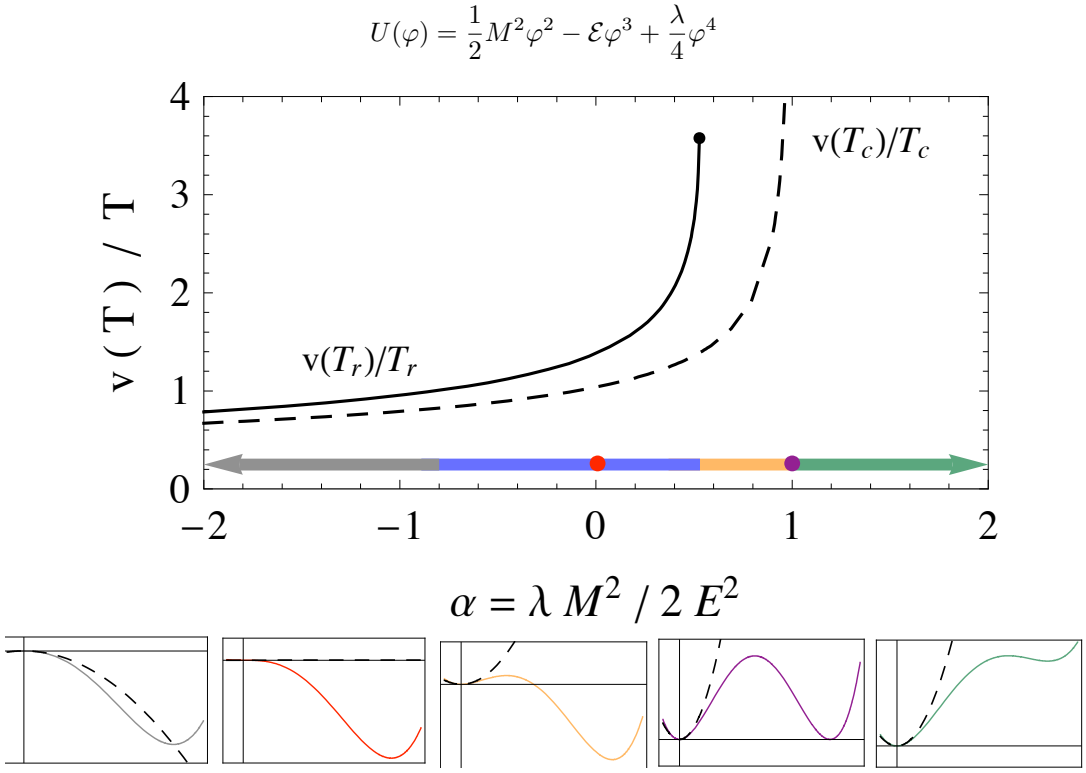

Figure 5.1: The order parameter, calculated as $v(T_c)/T_c$ (dashed) and $v(T_r)/T_r$ (solid), plotted against $\alpha = \lambda M^2/2\mathcal{E}^2$. The insets show $U(\varphi)$ for particular values of α in each of the associated colored regions.

we have evaluated $v(T)/T$ at the degeneracy temperature T_c, which, physically, is the temperature in the symmetric phase at the onset of supercooling. However, a first order phase transition proceeds with the nucleation of bubbles of broken phase which subsequently collide and reheat the plasma to a temperature T_r (see App. 5.A for precise definition). Since the purpose of the SFOPT criterion $v(T)/T \gtrsim 1$ is to ensure suppression of weak sphaleron processes *in the broken phase after the phase transition*, the most physically relevant temperature at which to evaluate $v(T)/T$ is the reheat temperature T_r.

To obtain a numerical intuition for our proposal, consider Fig. 5.1 where we have plotted $v(T_c)/T_c$ (dashed) and $v(T_r)/T_r$ (solid) while varying α and fixing $U'(v) = 0$

at $v = 300$ GeV, $U''(v) = (50\ \text{GeV})^2$, $N = 1$, and $h = 0.3$. In this figure, we also show $U(\varphi)$, such as to make the discrete symmetry evident at the EDSP. As expected, $v(T_c)/T_c$ diverges at the EDSP and is arbitrarily large for arbitrarily small discrete symmetry breaking ($1-\alpha \ll 1$). On the other hand, $v(T_r)/T_r$ cannot be calculated if the discrete symmetry is too weakly broken ($1-\alpha \lesssim 0.5$), because the phase transition does not occur. However, sufficient discrete symmetry breaking ($1-\alpha \gtrsim 0.5$) yields SFOPT which become monotonically weaker as the degree of symmetry breaking grows. We have used the same coloring in Fig. 5.1 as we do in the rest of this article to distinguish the varous regions of parameter space: the phase transition does not occur because the broken phase is not energetically favored (green); the PT does not occur because the bubble nucleation rate is too low (orange); a strongly first order PT occurs (blue); a weakly first order or second order PT occurs (gray); the EDSP (purple dot); and the point at which the barrier disappears (red dot).

Now let us return to a more broad discussion of the connection between discrete symmetry and strongly first order phase transition. In retrospect, we recognize that the existence of an EDSP associated with a discrete symmetry under which the vacua form a coset representation (along with the condition that spontaneous symmetry breaking occurs) is sufficient to obtain $v(T_c)/T_c \to \infty$ since $T_c = 0$ implies a degeneracy at the level of the nonthermal effective potential. Even though the toy model calculation was accomplished using the leading high-temperature T dependence and the classical potential, this statement regarding the EDSP is an exact statement for an exact effective potential. In other words, as far as this exact statement is concerned, it is not particularly important that $T = T_c$ corresponded to an enhanced symmetry point for general T_c as in the case of this simple one dimensional toy model (see Eq. (5.4)), nor is it important that quantum radiative corrections from the Yukawa couplings break the discrete symmetry given by Eq. (5.5). One final ingredient, which

is important for electroweak baryogenesis but is not represented in the toy model is that at least two vacua in the coset space must carry different electroweak quantum numbers. Otherwise, the PT will not be an electroweak symmetry breaking PT. This means that the discrete group must not commute with the electroweak group and one element in the coset representation must be an electroweak singlet. Hence our group theoretic guideline may be summarized as: an arbitrarily strong phase transition (i.e., $v(T_c)/T_c \gg 1$) may be found in the parametric neighborhood of an EDSP if 1) the condition for spontaneous (discrete) symmetry breaking is satisfied (such that there will be degenerate vacua), 2) the discrete group does not commute with the electroweak group, and 3) its coset representation contains an electroweak singlet element (such that the EW symmetry is broken in one vacuum and preserved in another).

5.3 A Few Examples

SM with Low Cutoff

As a first example, we will consider a generic extension of the SM with a low scale cutoff, as studied by (183–185). Provided that the UV physics does not violate the EW symmetry, then upon integrating it out one obtains a classical potential of the form

$$-\mathcal{L} \supset \lambda \left(\left| H^\dagger H \right| - \frac{v^2}{2} \right)^2 + \frac{1}{\Lambda^2} \left(\left| H^\dagger H \right| - \frac{v^2}{2} \right)^3 \tag{5.8}$$

up to terms of order H^8/Λ^4. Writing the Higgs doublet in terms of the fundamental scalar Higgs h as $H = \left(0, h/\sqrt{2}\right)^{\mathrm{T}}$, and using $m_H^2 = 2\lambda v^2$, the potential becomes

$$U(h) = \frac{1}{8\Lambda^2}h^6 - \frac{\lambda}{4}\left(3\frac{v^4}{m_H^2\Lambda^2} - 1\right)h^4 + \frac{\lambda v^2}{4}\left(3\frac{v^4}{m_H^2\Lambda^2} - 2\right)h^2 \tag{5.9}$$

up to constant and higher order terms. There exists an enhanced discrete symmetry point[5] at which a $\mathbb{Z}_2$ symmetry is nonlinearly realized,

$$\text{EDSP}: \quad m_H\Lambda = v^2 \qquad\qquad \mathbb{Z}_2' \;:\; h \to -\frac{h}{2} + \sqrt{v^2 - \frac{3}{4}h^2}\,. \tag{5.10}$$

The $\mathbb{Z}_2'$ symmetry exchanges the minima at $h = 0$ and $h = v$ while leaving the maximum at $h = v/\sqrt{3}$ invariant. We have reproduced an earlier PT analysis (183) in order to illustrate the proximity of SFOPTs to the EDSP. Moreover, we have extended the previous analysis by calculating the more physically relevant order parameter $v(T_r)/T_r$, instead of $v(T_c)/T_c$. Our results are summarized in Fig. 5.2, and are in good agreement with Fig. 2 of (183) which shows the same slice of parameter space. We find that nearby to the EDSP (purple curve), the PT is strongly first order (blue), and that the PT becomes weaker moving away from the EDSP. It is also worth noting that while the barrier persists, the PT most likely does not occur, as evidenced by the lack of blue in the region between the purple and red curves except for a small sliver above $m_H = 200$ GeV.

SM Plus Real Singlet – xSM

Next, we will consider models with multiple scalars in the electroweak sector. Extending the SM by a real scalar singlet s, we obtain a model known as the xSM (108),

[5] It may be more appropriate to use the term "enhanced discrete symmetry plane," as the condition $m_H\Lambda = v^2$ actually specifies a hypersurface in the parameter space, but we will continue using EDSP for simplicity.

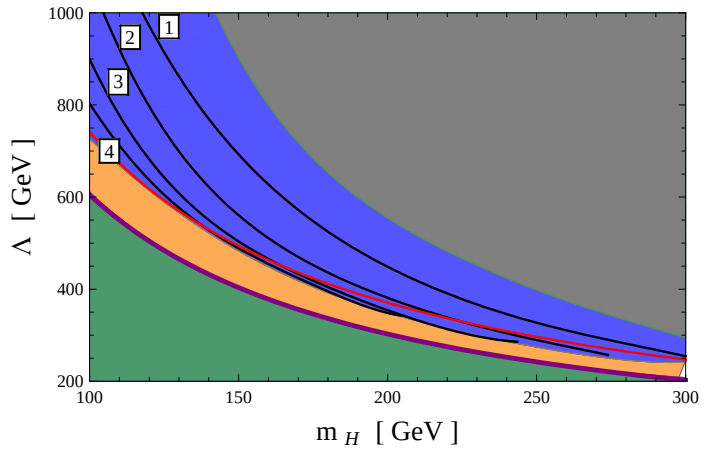

Figure 5.2: The parameter space nearby to the EDSP (purple curve). The coloring is the same as in Fig. 5.1. The PT order parameter $v(T_r)/T_r$ is indicated by the overlaid contours. SFOPTs are found in the blue region and become weaker in the gray region, farther from the EDSP.

which has the classical potential

$$U(h,s) = \frac{\lambda_0}{4}h^4 - \frac{\mu^2}{2}h^2 + \frac{b_4}{4}s^4 + \frac{b_3}{3}s^3 + \frac{b_2}{2}s^2 + \frac{a_2}{4}\,s^2h^2 + \frac{a_1}{4}sh^2\,. \tag{5.11}$$

Since there is no symmetry protecting $s = 0$, generally both h and s will obtain vevs, denoted v and x_0 respectively, and the mass parameters may be written as

$$\mu^2 = \lambda_0 v^2 + \frac{a_2}{2}x_0^2 + \frac{a_1}{2}x_0 \qquad \text{and} \qquad b_2 = -b_4 x_0^2 - b_3 x_0 - \frac{a_2}{2}v^2 - \frac{a_1}{4}\frac{v^2}{x_0}\,. \tag{5.12}$$

Provided that $x_0 \neq 0$, the cubic terms s^3 and sh^2 help to generate a barrier separating the symmetric and broken vacua and make the PT strongly first order. A number of PT analyses (106; 109; 111; 118) have revealed that the xSM can accommodate a strongly first order electroweak PT. They also find that this model displays multiple patterns of symmetry breaking such that, either h and s can obtain vevs at the same temperature, or s can receive a vev prior to electroweak symmetry breaking. If we were to search for SFOPT by randomly choosing order one parameters, there would be no way of anticipating what pattern of symmetry breaking would be realized, or if

the EW symmetry would be spontaneously broken at all. Moreover, since Eq. (5.11) has six free parameters, such a random search could become quite time consuming.

The discrete symmetry technique greatly simplifies the SFOPT search. We are able to specify a desired pattern of symmetry breaking to investigate, identify the corresponding discrete symmetry, compute the associated EDSP, and begin searching by perturbing from the EDSP. Here, we will focus on a particular pattern of symmetry breaking in which both s and h obtain vevs simultaneously, and we will compare our calculation against the "high-T trivial singlet vev" case of (111). The appropriate discrete symmetry is a $\mathbb{Z}_2$ relating the vacua at $\{h, s\} = \{0, 0\}$ and $\{v, x_0\}$. We can identify the associated EDSP by first reducing Eq. (5.11) to Eq. (5.1) and then imposing $\alpha = 1$. This is accomplished by focusing on the one-dimensional linear trajectory $\{h, s\} = \{v, x_0\} \times \varphi/\sqrt{v^2 + x_0^2}$ parametrized by φ, which interpolates between the EW-symmetric and EW-broken vacua. Along this trajectory, the potential can be written in the form of Eq. (5.1) with

$$\begin{aligned} \lambda &= \frac{\lambda_0 v^4 + b_4 x_0^4 + a_2 v^2 x_0^2}{(v^2 + x_0^2)^2} & \mathcal{E} &= -\frac{x_0(3a_1 v^2 + 4b_3 x_0^2)}{12(v^2 + x_0^2)^{3/2}} \\ M^2 &= \sqrt{v^2 + x_0^2}\left(3\mathcal{E} - \lambda\sqrt{v^2 + x_0^2}\right) & \alpha &= \frac{\lambda M^2}{2\mathcal{E}^2}\,. \end{aligned} \tag{5.13}$$

Then, upon resolving the condition $\alpha = 1$ we find the enhanced discrete symmetry point,

$$\begin{aligned} \text{EDSP}: \quad & 0 = 12a_2 v^2 x_0^2 + 3a_1 v^2 x_0 + 4b_3 x_0^3 + 12b_4 x_0^4 + 6\lambda_0 v^4 \\ \mathbb{Z}_2 \ : \ & \left(\varphi - \frac{\mathcal{E}}{\lambda}\right) \to -\left(\varphi - \frac{\mathcal{E}}{\lambda}\right)\,. \end{aligned} \tag{5.14}$$

In general, the PT will not occur along the trajectory parametrized by φ, but nevertheless this linear interpolation is useful for identifying the EDSP.

Once again, we have numerically investigated the strength of first order PTs in the vicinity of the EDSP. We have chosen a parameter set which allows us to reproduce

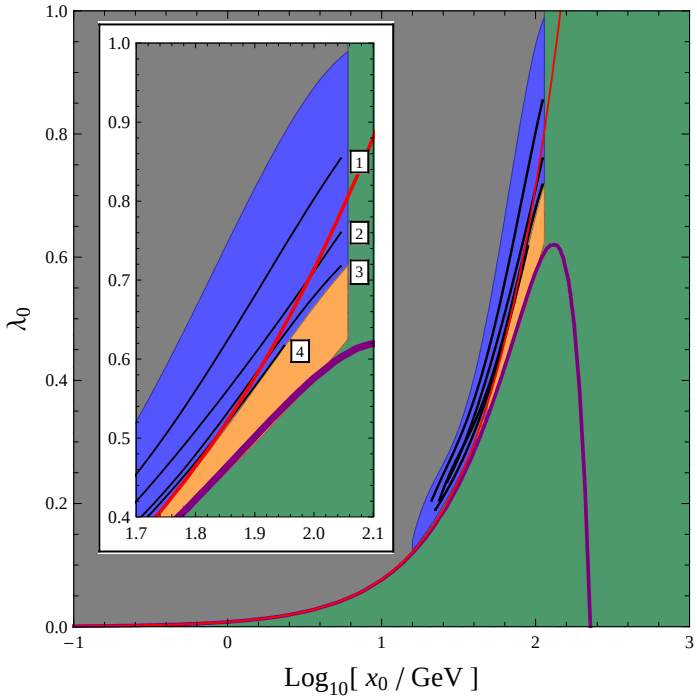

Figure 5.3: A slice of the xSM parameter space showing the proximity of SFOPT (blue region) to the enhanced symmetry axis (purple curve).

Fig. 4 (left panel) of (111) by fixing $a_1 = -933$ GeV, $a_2 = 0.69, b_3 = 356$ GeV, $b_4 = 0.53$ and scanning $\lambda_0 \in [0, 1]$ and $\log_{10} x_0 \in [-1, 3]$. Our results are shown in Fig. 5.3. A few observations may be made. First, as anticipated, the first order PTs are strongest close to the EDSP (purple) curve and become weaker farther away. Second, there is a large region (green) in which the EW remains unbroken. Below the EDSP (purple) curve, the origin remains the global minimum of the effective potential, whereas at large values of $x_0 \gtrsim 10^{2.1}$, the global minimum sits at $s < 0$. Third, in comparing with (111), one must bear in mind that we have fixed the remaining parameters, whereas those authors have scanned the full parameter space and projected onto these coordinates. As such, the region where we find SFOPT is much smaller than what is suggested by Fig. 4 of (111). However, this just goes to show that it is typically difficult to find SFOPT in a large parameter space without either

a large parameter scan or some guiding principle.

SM Plus Real $\mathbb{Z}_2$-Charged Singlet – $\mathbb{Z}_2$xSM

As a final example, we turn out attention to the $\mathbb{Z}_2$xSM, which extends the SM by a real scalar singlet s such that the scalar potential becomes (117; 118)

$$U(h,s) = \frac{\lambda}{4}h^4 - \frac{\mu^2}{2}h^2 + \frac{b_4}{4}s^4 + \frac{b_2}{2}s^2 + \frac{a_2}{4}\,s^2h^2\,. \tag{5.15}$$

The singlet is charged under a $\mathbb{Z}_2$, which restricts the allowed operators, but extends the possible patterns of symmetry breaking, because now $\langle s\rangle = 0$ is radiatively stable. We will focus on a particular parameter region in which there is transitional $\mathbb{Z}_2$ symmetry breaking: at temperature $T > T_a$ both $\mathbb{Z}_2$ and the EW symmetry are restored, at $T = T_a$ the singlet obtains a vev breaking $\mathbb{Z}_2$, and at $T = T_b < T_a$ the Higgs field obtains a vev and the singlet's vev returns to zero, thereby breaking the EW symmetry and restoring the $\mathbb{Z}_2$ (i.e., $\text{EW}\times\mathbb{Z}_2 \to \text{EW}\times\cancel{\mathbb{Z}_2} \to \cancel{\text{EW}}\times\mathbb{Z}_2$). In the context of this pattern of symmetry breaking, the enhanced discrete symmetry point admits an $\mathbb{S}_2$ symmetry,

$$\text{EDSP}: \quad b_4 = \lambda \quad \text{and} \quad b_2 = -\mu^2 \qquad\qquad \mathbb{S}_2 \;:\; h \leftrightarrow s \tag{5.16}$$

where we will also take $a_2 > 2\lambda$ to ensure that the discrete symmetry interchanges vacua. Note that this $\mathbb{S}_2$ symmetry is more restrictive than the $\mathbb{Z}_2$ symmetries we considered in the previous examples. To illuminate the role of the EDSP in locating SFOPT, we will reparametrize $b_4 = \lambda + \Delta b_4$ and $b_2 = -\mu^2 + \Delta b_2$ to write the potential as

$$U(h,s) = \left[\frac{\lambda}{4}\left(h^4 + s^4\right) - \frac{\lambda v^2}{2}\left(h^2 + s^2\right) + \frac{a_2}{4}h^2s^2\right] + \left[\frac{\Delta b_4}{4}s^4 + \frac{\Delta b_2}{2}s^2\right] \tag{5.17}$$

where we have also used $\mu^2 = \lambda v^2$. In this parameterization, we expect to find SFOPT nearby to the EDSP at $\Delta b_4 = \Delta b_2 = 0$.

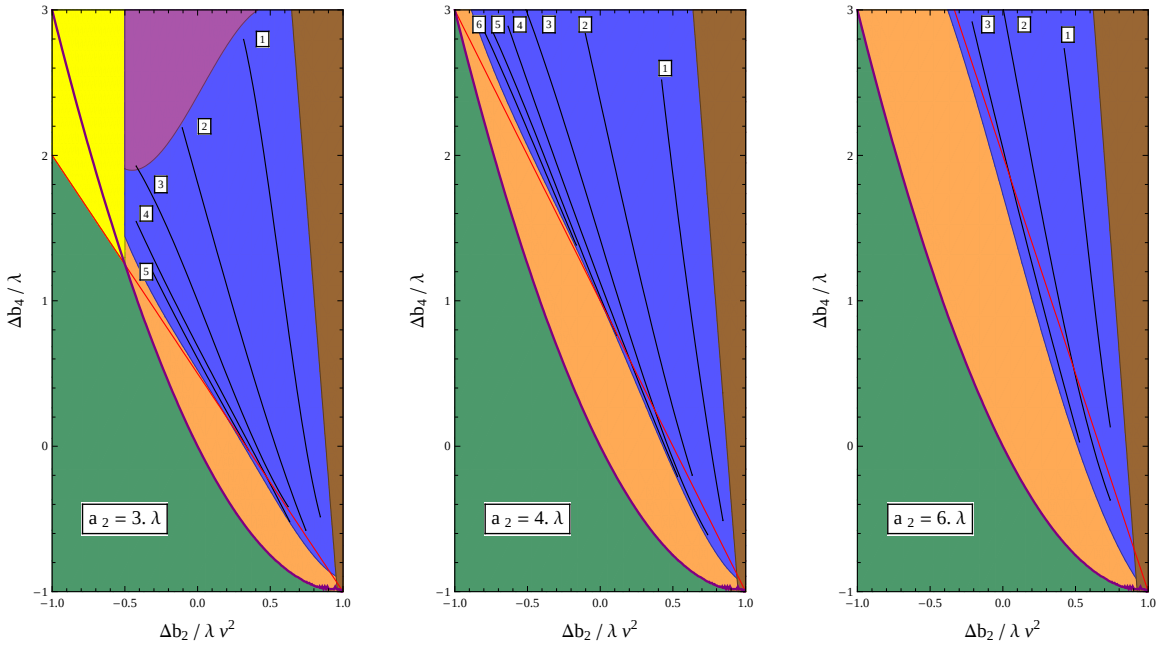

Figure 5.4: Three slices of the $\mathbb{Z}_2$xSM parameter space for fixed $\lambda \approx 0.12$. The origin $\Delta b_2 = \Delta b_4 = 0$ is an EDSP at which the theory has an $\mathbb{S}_2$ discrete symmetry.

We present the results of our numerical analysis in Fig. 5.4, where we have fixed $\lambda \approx 0.12$ to give a Higgs mass[6] of $m_h = \sqrt{2\lambda v^2} = 120$ GeV. As in the previous examples, the phase transition strength decreases monotonically with distance from the enhanced symmetry axis. Significantly far from the EDSP, the phase transition proceeds with a different pattern of symmetry breaking. In the brown region, the EW symmetry breaks without transitional $\mathbb{Z}_2$ violation ($\text{EW} \times \mathbb{Z}_2 \to \cancel{\text{EW}} \times \mathbb{Z}_2$), in the yellow region the $\mathbb{Z}_2$ remains broken in the low temperature vacuum ($\text{EW} \times \mathbb{Z}_2 \to \text{EW} \times \cancel{\mathbb{Z}_2} \to \cancel{\text{EW}} \times \cancel{\mathbb{Z}_2}$), and in the purple region there exists an intermediate phase in

[6]Since the axes of Fig. 5.4 depend only on the ratios $\Delta b_4/\lambda$ and $\Delta b_2/\lambda v^2$, a change in the Higgs mass (via λ) could be absorbed by Δb_4 and Δb_2, such that the qualitative features of Fig. 5.4 would remain unchanged.

which both $\mathbb{Z}_2$ and the electroweak symmetry are broken (EW $\times \mathbb{Z}_2 \to$ EW $\times \cancel{\mathbb{Z}_2} \to$ $\cancel{\text{EW}} \times \cancel{\mathbb{Z}_2} \to \cancel{\text{EW}} \times \mathbb{Z}_2$).

The region of parameter space nearby to the EDSP displays an interesting phenomenology. Since the singlet mass is given by

$$m_s = m_h \left[\frac{a_2/\lambda}{4} - \frac{1 - \Delta b_2/\lambda v^2}{2} \right]^{1/2} \tag{5.18}$$

one typically finds $m_s \lesssim m_h$ nearby to the enhanced symmetry point. The unbroken $\mathbb{Z}_2$ symmetry ensures that the singlet is stable, and thus it is a dark matter candidate which annihilates to Higgses with a cross section proportional to a_2^2. A number of analyses (108; 186–193) have considered this scenario and found that a_2 and the singlet mass m_s can be strongly constrained by assuming that the s particle composes all of the dark matter. Collider experiments, such as the LHC, may also be able to constrain the Higgs-singlet coupling. For $\Delta b_2/\lambda v^2 < (3 - a_2/\lambda)/2$, the singlet mass is less than half of the Higgs mass and the invisible decay channel $h \to ss$ becomes kinematically accessible. Then, a measurement of the invisible decay width may constrain the Higgs-singlet coupling a_2 (185; 193–196). On the other hand, the singlet self-coupling b_4 remains unconstrained. This is because unlike in other limits of this model and similar models (107; 115; 194; 195), the unbroken $\mathbb{Z}_2$ symmetry prevents the Higgs and singlet from mixing. Consequently, the singlet self-coupling b_4 is practically impossible to constrain at colliders, and contributions to the anomalous Higgs trilinear coupling (197) are loop suppressed. Finally, let us point out that the transitional $\mathbb{Z}_2$ violation limit may not suffer from the domain wall problem that generally accompanies models with spontaneously broken discrete symmetries. When the $\mathbb{Z}_2$ breaks in the first step of the PT, domain walls will be generated. However, once the EW symmetry is broken and the $\mathbb{Z}_2$ symmetry is restored, the domain walls should be "wiped out" by the $\mathbb{Z}_2$-symmetric vacuum field configuration. This may

lead to a unique gravitational wave spectrum.

5.4 Summary of the Chapter

Strongly first order phase transitions (SFOPTs) are required for electroweak baryogenesis and may have other interesting implications for early universe relics. In this article we have discussed a general analytic guideline, based on symmetry principles, which is useful in identifying a region of parameter space favorable for SFOPT: an arbitrarily strong PT can be found for parameters near an enhanced discrete symmetry point (EDSP) if the condition for spontaneous symmetry breaking is met and if the discrete symmetry relates the electroweak symmetry preserving vacuum to one in which it is broken. Group theoretically, this means that the coset representation of the broken discrete symmetry contains an electroweak singlet and the discrete group does not commute with the electroweak group. Because of phenomenological requirement of completing the PT at a nonzero temperature, the symmetry must be broken by parametric deformations away from the EDSP. As the deformation decreases, the strength of the PT tends to increase. We applied this guideline to study the electroweak PT in three specific models. In each of the models considered, SFOPTs occur in close proximity to the EDSP, as expected. In this way, the enhanced symmetry point acts like a lamppost in the parameter space, signaling the location of SFOPTs. It would be interesting to apply a similar EDSP-motivated analysis of the electroweak phase transition to models with larger scalar sectors and greater parametric freedom, such as singlet extensions of the Minimal Supersymmetric Standard Model.

It is not unnatural to expect SFOPT to be localized in the vicinity of an EDSP. Strongly first order phase transitions almost always require some fine-tuning of the parameters in the theory. From an UV completion point of view, such fine-tuning

could be more natural if it is close to a point of the parameter space with enhanced symmetry. It is also clear that degenerate vacua may be found even without discrete symmetry, and thus our guideline provides a sufficient, though not necessary, condition for locating SFOPT. Nonetheless, such parametric regions form a large class of possibilities which can most likely always occur in practice.

We also observe (as did (118; 177)) that the PT tends not to proceed at all unless the barrier separating the EW-broken and EW-unbroken vacua is very small or not present at all (along the red curve), because otherwise the tunneling rate is too strongly suppressed. Hence, the deformations away from the EDSP required for phenomenologically viable SFOPTs are not vanishingly small and are model dependent. Although such phenomenologically viable parametric regions can be arrived at by deforming away from enhanced continuous symmetry points rather than EDSPs, the EDSP starting point guarantees the existence of potential barriers required for a first order PT. In that sense, our proposal here is advantageous over the enhanced continuous symmetry point perspective.

Proximity to an EDSP implies interesting relations between parameters in the extended Higgs sector, which is responsible for the dynamics of the electroweak symmetry breaking. Such relations will manifest themselves in both the spectrum of the states in the Higgs sector and their couplings. Probing this sector is the central scientific focus of the LHC. We might have already seen the discovery of the Higgs boson on the horizon (198; 199). Discovering the additional states in the extended Higgs sector and measuring the parameters in the Higgs potential are expected to be very challenging tasks. At the same time, confirming the structure of the Higgs sector to be consistent with a SFOPT would establish a striking link to the generation of the baryonic asymmetry in the universe.

5.A Appendix A. Details of Phase Transition Calculation

For the phase transition analyses in this paper, we have calculated the thermal effective potential $V_{\rm eff}(\vec{\phi}, T)$ through one-loop order using the standard techniques (61; 124; 126). We numerically minimize[7] $V_{\rm eff}$ with respect to $\vec{\phi}$ to obtain the scalar field expectation values in the symmetric and broken phases, $\vec{v}_{\rm sym}(T)$ and $\vec{v}_{\rm brk}(T)$, respectively. The latter quantity is sometimes referred to in the text as simply $v(T)$. The critical temperature T_c is defined as

$$V_{\rm eff}(\vec{v}_{\rm sym}(T_c), T_c) = V_{\rm eff}(\vec{v}_{\rm brk}(T_c), T_c)\,. \tag{5.19}$$

We use $V_{\rm eff}(\vec{\phi}, T)$ to calculate the action[8] $S_3(T)$ of the bubble field configuration that mediates the vacuum transition (202–205). We determine the bubble nucleation temperature T_n by requiring the bubble nucleation rate per Hubble volume to exceed the Hubble expansion rate. This condition may be resolved to

$$S_3(T_n)/T_n = 140 \tag{5.20}$$

where the value on the right hand side depends only logarithmically on the model parameters (98; 206). Finally, we calculate the temperature T_r of the plasma after the phase transition ends and the plasma has been reheated. This is obtained by assuming that the universe does not expand significantly during the phase transition and then by imposing energy conservation (119)

$$\rho_{\rm sym}(T_n) = \rho_{\rm brk}(T_r) \tag{5.21}$$

[7]This definition of $v(T)$ implies that T_c, T_n, and T_r will be dependent upon the choice of gauge (200; 201). Though this may affect the numerical accuracy of our results, we expect that the qualitative parametric dependence of the EW order parameter nearby to an EDSP, which is our primary interest, will remain unchanged.

[8]For the models of Secs. 5.3 and 5.3 which have more than one scalar field participating the phase transition, we calculate the bounce using the approximation described in (119).

where

$$\rho(T) = V_{\text{eff}}(v(T), T) - T\frac{d}{dT}V_{\text{eff}}(v(T), T) \tag{5.22}$$

is the energy density in the symmetric or broken phase, respectively.

Chapter 6

The 125 GeV Higgs and EWPT Model Classes

Recently, the ATLAS and CMS detectors have discovered a scalar particle which, to a reasonable degree of statistical uncertainty, fits the profile of the Standard Model Higgs. One obvious implication is that models which predict a significant departure from SM phenomenology, such as large invisible decay or mixing with a hidden sector scalar, are already ruled out. This observation threatens the viability of electroweak baryogenesis, which favors, for example, a lighter Higgs and a Higgs coupled to or mixed with light scalars. To assess the broad impact of these constraints, we propose a scheme for classifying models of the electroweak phase transition, and we impose constraints on a class-by-class basis. We find that models, such as the MSSM, which rely on thermal loop effects are severely constrained by the measurement of a 125 GeV Higgs. Models which rely on tree-level effects from a light singlet are also restricted by invisible decay and mixing constraints. Moreover, we find that the parametric region favored by EWBG often coincides with an enhanced symmetry point with a distinctive phenomenological character. We also comment on the excess

of diphoton events observed by ATLAS and CMS. We note that although Higgs portal models can accommodate both enhanced diphoton decay and strongly first order phase transiition, the former favors a negative Higgs portal coupling whereas the latter favors a negative one, and therefore these two constraints are at tension with one another.

This work was performed in collaboration with Daniel Chung and Lian-Tao Wang. It has not yet been published.

6.1 Introduction to the Chapter

A number of baryogenesis mechanisms are known to successfully account for the baryon asymmetry of the universe, but many of these operate at a high scale, inaccessible to independent confirmation by direct laboratory tests. The primary motivation for studying electroweak baryogenesis is that the baryon asymmetry is generated by electroweak scale physics, which is tested by experiments aimed at understanding the nature of electroweak symmetry breaking. These include Higgs searches at LEP, the Tevatron, and LHC colliders. Thus, models of the electroweak sector may be constrained from two sides: by the requirement that electroweak baryogenesis is viable and by the requirement that Higgs search constraints are satisfied. Indeed, the ATLAS and CMS collaborations recently announced the discovery of a particle in the mass range $125 - 126$ GeV which matches the profile of the Higgs boson (207; 208). Even at this early stage, without precise knowledge of the alleged Higgs' couplings to SM fields, we have gained a partial picture of the origin of the electroweak symmetry breaking. In this paper, we would like to understand what is the main implications of a 125 GeV SM-like Higgs for electroweak baryogenesis.

Studies of the viability of electroweak baryogenesis and the impact of collider con-

straints are usually performed on a model-by-model basis. However, many individual models can accommodate a partial picture of the electroweak symmetry breaking sector. Thus, as the LHC begins to expose the Higgs sector, revealing only glimpses of the full picture, one would like to understand what classes of models may be consistent with or at tension with the data. To this end, we propose a scheme for classifying models of the electroweak sector based upon the nature of the electroweak phase transition, and we study the implications of the recent Higgs discovery at the LHC on a class-by-class basis. We find, the LHC's detection of a 125 GeV Higgs in conjunction with constraints on invisible decay and hidden sector mixing, provide strong constraints on certain EWPT model classes.

We identify the phase transition model classes in the following way. The success of EWBG relies upon the electroweak phase transition being of the first order (62). In the context of the phase transition calculation, this translates into the requirement that the thermal effective potential, $V_{\rm eff}(h,T)$, possesses a pair of minima *separated by a barrier* for some range of temperatures (209). Thus, we can classify models of the EW sector based on what physics is responsible for providing the requisite barrier in $V_{\rm eff}(h,T)$. When calculated perturbatively, $V_{\rm eff}(h,T)$ is given by a sum of tree-level, quantum (loop), and thermal contributions. Thus, three model classes can be identified[1] (see also Figure 6.1):

I. Thermally Driven. A barrier arises due to thermal loop effects associated with bosonic zero modes. The effective potential acquires a term of the form $-T(h^2)^{3/2}$ where h is the Higgs condensate. This term competes with the h^2 and h^4 terms in the scalar potential to generate a barrier.

II. Tree-Level Driven. A barrier arises due to a competition between terms in the

[1]We do not claim that this classification scheme is exhaustive. For instance, models which rely on non-pertubative effects cannot be classified in this way (see, e.g., (210)). However, this classification does cover most perturbative models in the literature known to us.

effective potential which are already present at tree-level. This model class can be further subdivided.

IIA. Renormalizable Operators. The barrier arises from the competition between renormalizable operators. Since the operator h^3 violates gauge invariance, the models in this class rely upon an additional scalar field (or fields) getting vevs during the EWPT.

IIB. Non-Renormalizable Operators. If higher order operators involving the Higgs field, such as h^6, are added to the scalar potential, a barrier can arises as a result of their competition with the renormalizable terms.

III. Loop Driven. Large loop corrections may generate the term $h^4 \ln h^2$, which can compete with the h^4 term to generate a barrier.

In addition to a barrier in V_{eff}, successful EWBG require the EW sphaleron process to be out of equilibrium in the broken phase to ensure that the baryon asymmetry is not washed out. This condition may be expressed as a bound on the EWPT order parameter (88)

$$\frac{v(T_c)}{T_c} \gtrsim 1 \tag{6.1}$$

where $\langle H \rangle_T = \left(0\,,\, v(T)/\sqrt{2}\right)^{\mathrm{T}}$ is the expectation value (EV) of the Higgs at temperature T and T_c is the temperature at which the phase transition takes place. We say that phase transitions which satisfy Eq. (6.1) are "strongly" first order.

Thus, we will study the EWPT in the context of each model class by writing down an approximate expression for V_{eff} – which captures the physics relevant to the PT (i.e., the source of the barrier), but otherwise doesn't explicitly depend on the underlying model – and then investigating what parametric limit will yield $v(T_c)/T_c \gg 1$. We can then ask what underlying physics would give rise to such an "optimal limit," what does the associated phenomenology look like, and what is the impact of collider

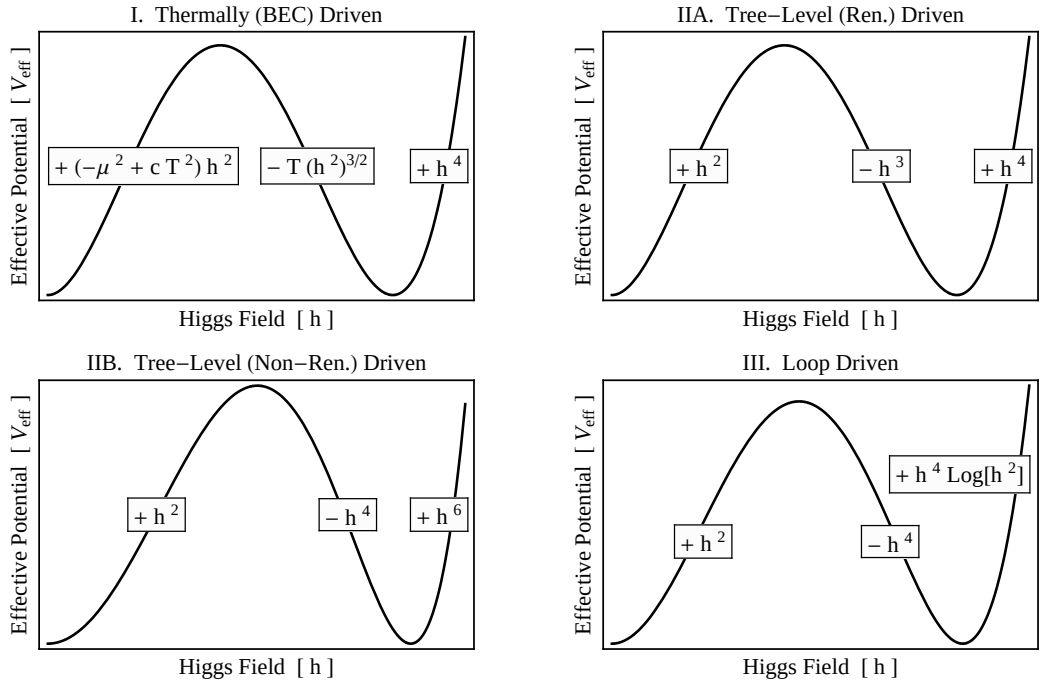

Figure 6.1: The four methods of obtaining a strongly first order phase transition by inducing a barrier in the thermal effective potential, which are discussed in this paper.

constraints. One of the central points of our paper is to note that the optimal limits frequently correspond to enhanced symmetry points in the theory space. This makes the optimal limits straightforward to identify, and moreover associates them with a distinctive phenomenology which is constrained by recent LHC data.

6.2 Collider Data and Interpretation

With certainty, the Tevatron signal and ATLAS/CMS discovery confirm the existence of a scalar boson with an approximate mass of 125 GeV (207; 208) The available statistics suggest that the decays of this boson are consistent with the SM predictions in the channel $b\bar{b}$ (50; 51) as well as $ZZ \to 4\ell$ and $WW \to \ell\nu\ell\nu$ (207; 208). In the diphoton decay channel, both ATLAS and CMS observe approximately twice as

many events as the SM prediction (211) The discovery of a Higgs-like boson strongly constrains or rules out models which predict appreciable (order one) enhancement or reduction of Higgs production and decay channels with respect to the SM predictions. Since models of the EW sector with strongly first order EW phase transitions tend to rely on a large coupling between the Higgs and light scalar fields, it is important to review the relevant constraints here.

Spectrum: It is well known that in models such as the SM and the MSSM, even the LEP Higgs mass bound imposes strong constraints on the viability of EWBG. Of course, these constraints have already ruled out EWBG in the SM (89). The measurement of a Higgs mass of 125 GeV further severely restricts the allowed MSSM parameter space and threatens to rule out EWBG in that model as well (91).

Invisible Decay: If the Higgs had a large branching fraction to invisibles, $\mathrm{BR}_{\mathrm{inv}} = \mathrm{BR}(h \to \mathrm{inv})$, this would suppress the branching fraction in all visible channels, and it would have been more difficult to find the Higgs at the LHC[2] (113). Conversely, the discovery of a SM-like Higgs at the LHC is at tension with a large $\mathrm{BR}_{\mathrm{inv}}$. A number of analyses have investigated this possibility by assuming that the production cross section is the same as for a 125 GeV SM Higgs, but allowing for $\mathrm{BR}_{\mathrm{inv}}$ to vary in fitting the data. They obtain upper bounds on the branching fraction to invisibles in the range $\mathrm{BR}_{\mathrm{inv}} < 0.30 - 0.75$ at 95% CL (211; 213–217). Although this may not seem overly restrictive, we will see that in the phase transition model classes which allow invisible decay, this is naturally the dominant decay channel. Furthermore, the LHC expects to resolve the issue of invisible decay with increased data. It is estimated that with at $20\,\mathrm{fb}^{-1}$ integrated luminosity, the LHC should detect or exclude invisible decay for $\mathrm{BR}_{\mathrm{inv}} > 0.4$ at 95% CL (218), and at $30\,\mathrm{fb}^{-1}$, ATLAS

[2]Assuming that the new physics does not enhance the Higgs production cross section, i.e., we assume $\sigma(pp \to h) = \sigma^{\mathrm{SM}}(pp \to h)$. However, even in the MSSM where new physics both allows invisible decay and enhances the Higgs production cross section, one finds that invisible decay is at tension with the data (212).

should detect or exclude invisible decay for $\mathrm{BR}_{\mathrm{inv}} > 0.24$ at 5σ (113).

Mixing with Hidden Sector: Just as with the case of invisible decay, the ATLAS / CMS data strongly constraints the scenario in which the Higgs is allowed to mix with a hidden sector scalar field or fields, which are singlets under the SM gauge group. For the sake of discussion, we will suppose that only one singlet scalar field is mixing with the SM Higgs. The impact of this mixing on the phenomenology depends on the relative mass scales, of the Higgs-like scalar at $m_H \approx 125$ GeV and the singlet-like scalar with mass m_{hid}. Let θ be the angle between the Higgs-like mass eigenstate and the Higgs gauge eigenstate. The relevant constraints are:

1. **Light Higgs search at LEP.** The existence of a light singlet-like resonance (i.e., $m_{\mathrm{hid}} \ll m_H = 125$ GeV) is constrained by Higgs searches at LEP. In order for the singlet-like particle to have evaded detection, its coupling to the SM must be suppressed. This places an upper bound on θ, which which becomes more stringent as m_{hid} is deceased below the LEP Higgs search bound of 114.4 GeV. For instance, for $m_{\mathrm{hid}} = 20$ GeV one needs $\cos^2\theta > 0.99$ at 95% CL (48).
2. **Heavy Higgs search at LHC.** Similarly, if the singlet-like resonance is heavier (i.e., $m_{\mathrm{hid}} \gg m_H = 125$ GeV), there is an upper bound on θ coming from the requirement that the heavy singlet-like scalar evades detection at the LHC. Again, this is a function of the singlet-like scalar's mass. For instance, if $m_{\mathrm{hid}} = 200$ GeV one needs $\cos^2\theta > 0.60$ at 95% CL to avoid detection (219; 220).
3. **LHC Higgs Detection.** The LHC's signal at 125 GeV places an upper bound on θ, because if there were more mixing the diphoton channel would have been suppressed and there would not have been a detection. Assuming that the Higgs-like resonance is lighter (i.e., $m_H = 125$ GeV $\ll m_{\mathrm{hid}}$), then the consequence of mixing is a universal suppression of all Higgs production processes by a factor of $\cos^2\theta$. Thus, large mixing

is at tension with the LHC's Higgs signal, and one obtains a bound $\cos^2\theta > 0.77$ at 90% CL (221). (See also (213; 219; 222; 223)).

Taken together, these constraints imply that the large mixing scenario (i.e., $\cos^2\theta = 0.5$) is strongly disfavored, independent of the mass of the hidden sector scalar field.

6.3 Electroweak Phase Transition Model Classes

In this section, we will enumerate the phase transition model classes, identify the parametric limits which are optimal for SFOPT by maximizing the washout criterion Eq. (6.1), and discuss phenomenological constraints that arise in those limits. As we discuss further below, the optimal limits for SFOPT often correspond to enhanced symmetry points of the theory at which the symmetry group is extended to include an additional continuous or discrete symmetry. For the sake of brevity, we will not dwell on the details of the phase transition calculation. We refer the interested reader to the review: (209).

Thermally (BEC) Driven

In models such as the SM and the MSSM, the barrier in the thermal effective potential arises from thermal loop effects, which emerge in the following way. The Higgs condensate $\langle H \rangle = \left(0\,, h/\sqrt{2}\right)^T$ modifies the dispersion relation of particles in the plasma causing them to acquire an effective temperature and field-dependent mass $m^2_{\text{eff}}(h,T) = \tilde{m}^2(h) + \Pi(T)$. Here, Π is a temperature-dependent self-energy correction (known as "daisy resummation," see e.g., (175)) and $\tilde{m}^2(h)$ can be obtained by replacing the zero temperature VEVv with h in the standard expression for the field's mass (209). Bosonic fields induce a contribution to the thermal effective poten-

tial of the form[3] $V_{\text{eff}} \ni (-T/12\pi)\big(m^2_{\text{eff}}(h,T)\big)^{3/2}$ in the high-temperature limit. The non-analyticity of this term at $m^2_{\text{eff}} = 0$ can be traced to the non-analyticity of the Bose-Einstein distribution function at zero energy. Hence, we will refer to this term as the "BEC term."

Near the phase transition temperature T_c, we want $(m^2_{\text{eff}}(T_c))^{3/2} \sim h^3$ such that competition between this term and the h^2 and h^4 terms will generate a barrier in V_{eff}. Supposing that $\tilde{m}^2(h)$ can be written as $\tilde{m}^2(h) = \alpha h^2 + \beta$, the effective mass will have the desired scaling if we tune $\beta - \Pi(T_c) \ll \alpha v(T_c)^2$. A general phenomenological consequence of this tuning is that the scalar bosons today will be light, since their mass squared $\tilde{m}^2(v) = \alpha v^2 - \Pi(T_c)$ is given by the difference of two $O\left(v^2\right)$ numbers. The need for this tuning is well-established in the MSSM (92), where light stops are required. Phenomenologically, the light stops tend to enhanced Higgs production by gluon fusion and reduce Higgs diphoton decay. The LHC has already placed strong constraints on EWBG in the MSSM (91).

Near the temperature of the phase transition, the effective potential may be approximated as

$$V_{\text{eff}}(h,T) \approx \frac{1}{2}\left(\mu^2 + c\,T^2\right)h^2 - \frac{e\,T}{12\pi}(h^2)^{3/2} + \frac{\lambda}{4}h^4 \tag{6.2}$$

A potential of this form is illustrated in Figure 6.1. The parameters $\mu^2 = -m_H^2/2$ and $\lambda = m_H^2/(2v^2)$ are related to the Higgs mass m_H and VEVv. The dimensionless parameters c and e quantify the coupling between the Higgs condensate and the relativistic particles in the plasma. In particular, c depends on couplings between H and light ($m < T$) bosons and fermions, whereas e only depends upon couplings between H and light bosons. The contribution from heavy fields ($m > T$) are Boltzmann

[3]In a gauge theory, this term is not gauge-invariant (61). Consequently, this model class suffers from an ambiguity in how to calculate the phase transition parameters reliably and accurately (200; 224).

Model	$\Delta\mathcal{L}$	$\boldsymbol{c}$	$\boldsymbol{e}$
SM (98)		$\frac{6m_t^2+6m_W^2+3m_Z^2+\frac{3}{2}m_H^2}{12v^2}$	$\frac{6m_W^3+3m_Z^3}{v^3}$
MSSM[5] (92)		$c_{\rm SM}+\frac{6m_t^2}{12v^2}\left(1-\frac{\tilde{A}_t^2}{m_Q^2}\right)$	$e_{\rm SM}+\frac{6m_t^3}{v^3}\left(1-\frac{\tilde{A}_t^2}{m_Q^2}\right)^{3/2}$
Colored Scalar[5] (225)	$M_X^2\left\|X\right\|^2+\frac{K}{6}\left\|X\right\|^4+Q\left\|H\right\|^2\left\|X\right\|^2$	$c_{\rm SM}+\frac{6}{24}\frac{Q}{2}$	$e_{\rm SM}+6\left(\frac{Q}{2}\right)^{3/2}$
Singlet Scalar (98)	$M^2\left\|S\right\|^2+\lambda_S\left\|S\right\|^4+2\zeta^2\left\|H\right\|^2\left\|S\right\|^2$	$c_{\rm SM}+\frac{g_S}{24}\zeta^2$	$e_{\rm SM}+g_S\zeta^3$
Singlet Majoron (114)	$\mu_s^2\left\|S\right\|^2+\lambda_s\left\|S\right\|^4+\lambda_{hs}\left\|H\right\|^2\left\|S\right\|^2+\frac{1}{2}y_iS\nu_i\nu_i+$ h.c.	$c_{\rm SM}+\frac{2}{24}\frac{\lambda_{hs}}{2}$	$e_{\rm SM}+2\left(\frac{\lambda_{hs}}{2}\right)^{3/2}$

Table 6.1: Examples of *Thermally (BEC) Driven* SFOPT models.

suppressed, and the $O(T^4\exp\left[-m/T\right])$ terms are dropped. Some examples of models that fall into this class are shown in Table 6.1.

A familiar calculation (see, e.g., (209)), yields the EW order parameter

$$\frac{v(T_c)}{T_c}\approx\frac{e}{6\pi\lambda}\,. \tag{6.3}$$

There are two "optimal" limits in which we can obtain $v(T_c)/T_c\gg 1$.

$e\gg\lambda$ To reach the limit of large e, the Higgs must have a large coupling with many light bosonic degrees of freedom. There are various phenomenological constraints on this limit. First, since e is a sum of dimensionless coupling constants (see, e.g., Table 6.1), it is bounded from above by the perturbative unitarity constraint. Second, heavy bosonic fields will become Boltzmann suppressed and cannot contribute to e. However, the same interactions which allow

[5]In these models, the light scalars that provide the BEC term are colored (e.g., stops in the MSSM). Higher order contributions, which scale like $-g_s^2(N_c^2-1)T^2m_{\tilde{t}}^2\log m_{\tilde{t}}/T$, tend to lower the PT temperature and strengthen the PT (93).

light bosonic fields to contribute to e also provide a mass to those fields after EWSB. Thus, increasing the coupling constants that enter e, will eventually cause the bosons become heavy and their contributions to e become Boltzmann suppressed. Finally, as e is increased, interactions between the Higgs and other bosonic fields are made stronger. Thus, there may be loop-suppressed, but nevertheless significant, modifications to Higgs production and / or decay. For example, if the bosons carry color, then they can significantly enhance Higgs production by gluon fusion (225; 226). We will revisit this constraint in the context of Higgs diphoton decay in Sec. 6.4.

$\boldsymbol{\lambda \to 0}$ In the context of the SM, this limit is obviously forbidden in light of the relationship $\lambda = m_H^2/2v^2$ and the fact that m_H is now a measured quantity. However, in an effort to keep our model classification scheme as general as possible, we will consider the scenario in which the field h that appears in Eq. (6.2) is not the SM Higgs condensate. Instead, it may represent a parametrization of some non-trivial trajectory through an extended scalar field space connecting the EW-preserving vacuum $h = 0$ with the EW-broken vacuum $h = v$. Such situations arise in minimal singlet extensions of the SM (111). Then, the limit $\lambda \to 0$ implies the spectrum contains a light scalar. If the scalar carries SM quantum numbers, it is already excluded by . If the scalar is a SM singlet and if it has a large coupling to the Higgs, then this limit is at tension with constrains on Higgs invisible decay or hidden sector mixing. Moreover, vacuum stability considerations limit the range of the EFT.

To illustrate how these limits and constraints arise in a concrete model, we extend the SM by a color triplet scalar field X (see (225)):

$$\mathcal{L} = \mathcal{L}_{\rm SM} + \left(\partial_\mu X\right)^* \left(\partial^\mu X\right) - \left[M_X^2 X^* X + \frac{K}{6}\left(X^* X\right)^2 + Q H^\dagger H X^* X\right] . \qquad (6.4)$$

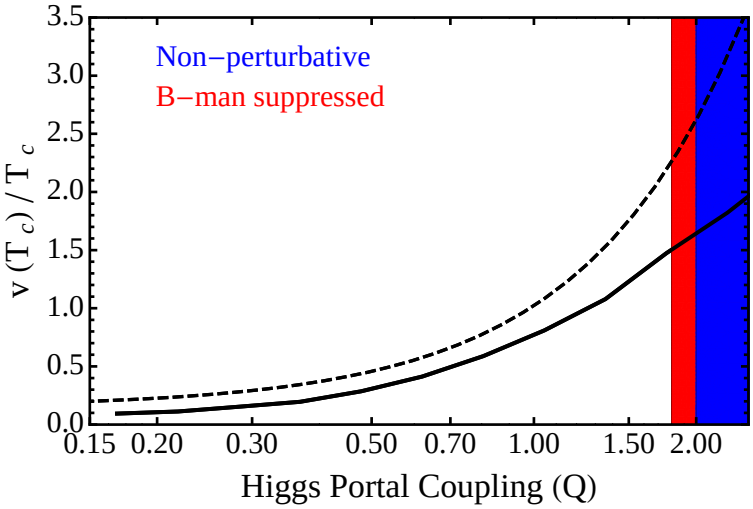

Figure 6.2: The EW order parameter $v(T_c)/T_c$ calculated numerically (solid line) and using the analytic approximation Eq. (6.3) (dashed line).

The effective mass of the scalar X is given by $m_X^2(h,T) = M_X^2 + (Q/2)h^2 + \Pi_X(T)$ where $\Pi_X(T) = (K+Q)T^2/24$. Thus, the BEC term is given by

$$\Delta V_{\text{eff}}(h,T) = -6\frac{T}{12\pi}\left(M_X^2 + \frac{Q}{2}h^2 + \Pi_X(T)\right)^{3/2}, \tag{6.5}$$

where the factor 6 is the number of internal degrees of freedom for the complex, colored X field. As discussed above, we must tune $M_X^2 \approx -\Pi_X(T_c)$. Doing so, Eq. (6.5) takes the form of Eq. (6.2) with $e = e_{\text{SM}} + 6(Q/2)^{3/2}$.

We would like to understand what constraints arise as we go to the SFOPT limit $e \gg \lambda$. This limit is reached by taking $Q \gg \lambda^{2/3}$. First, we verify that the phase transition is strongly first order by calculating $v(T_c)/T_c$ as a function of Q for fixed $m_H = 125$ GeV. The numerical calculation is performed in the standard way (see, e.g., (209)) using the full one-loop thermal effective potential. As shown in Figure 6.2, the EW phase transition becomes strongly first order for sufficiently large values of $Q \gtrsim 1.3$. Second, we note that perturbativity up to 100 TeV requires $Q < 2$ at the weak scale (225). Third, as we discussed above, Boltzmann suppression

of heavy X bosons prevents us from obtaining SFOPT for arbitrarily large Q. We can estimate an upper bound on Q by requiring the X bosons to be light at the temperature of the phase transition. That is, we require $m_X(v(T_c), T_c) < T_c$ where $m_X(v(T_c), T_c) \approx \sqrt{Q/2}v(T_c)$. This becomes the bound $Q \lesssim 2(T_c/v(T_c))^2 \approx 2$, since for a strongly first order phase transition $v(T_c)/T_c \gtrsim 1$. This estimate is confirmed by the numerical calculation, which reveals that for $Q \gtrsim 1.8$, the fractional error between the numeric and analytic expressions becomes greater than 50%. The perturbativity and Boltzmann suppression constraints are also shown on the figure.

Tree-Level (Renormalizable Operators) Driven

As we saw in the previous section, models such as the MSSM which rely upon the BEC term to provide a strongly first order phase transition have become very constrained by the discovery of a 125 GeV SM-like Higgs. The available parameter space opens up if we allow the Higgs sector to be extended by one or more scalar fields which participate in the electroweak phase transition. The phase transition can be made strongly first order if the new scalar fields participate in the EWPT, i.e their expectation value changes during EWBS. The barrier in V_{eff} thereby arises from (renormalizable) tree-level interactions between the Higgs and the new scalars fields.

We can parametrize the additional scalar field(s) as S. The number of degrees of freedom associated with S, its quantum numbers, and its interactions will be model-dependent. The information that is pertinent to our generic phase transition analysis is that there exists a one-dimensional trajectory through the configuration space which interpolates between the EW-symmetric and EW-broken phases[4]. The

[4]We can parametrize the one-dimensional trajectory with a field φ, as $h = \bar{h}(\varphi, T)$ and $S =$

Model	$\Delta\mathcal{L}$
xSM (111; 118)	$\frac{1}{2}\left(\partial S\right)^2 - \left[\frac{b_2}{2}S^2 + \frac{b_3}{3}S^3 + \frac{b_4}{4}S^4 + \frac{a_1}{2}H^\dagger H S^2 + \frac{a_2}{2}H^\dagger H S^2\right]$
$\mathbb{Z}_2$xSM (176)	$\frac{1}{2}\left(\partial S\right)^2 - \left[\frac{b_2}{2}S^2 + \frac{b_4}{4}S^4 + \frac{a_2}{2}H^\dagger H S^2\right]$
Model	ΔW
NMSSM (96)	$\lambda H_1 H_2 N - \frac{\kappa}{3}N^3$
nMSSM (94)	$\lambda H_1 H_2 S + \frac{m_{12}^2}{\lambda}S$
$\mu\nu$MSSM (97)	$-\lambda_i H_1 H_2 \nu_i^c + \frac{\kappa_{ijk}}{3}\nu_i^c\nu_j^c\nu_k^c + Y_\nu^{ij} H_2 L_i \nu_j^c$

Table 6.2: Examples of *Classically Driven* SFOPT models. For the SUSY models, only the superpotential is specified.

effective potential along this trajectory may be approximated as

$$V_{\text{eff}}(\varphi, T) \approx \frac{1}{2}\left(m^2 + c\,T^2\right)\varphi^2 - \mathcal{E}\,\varphi^3 + \frac{\lambda}{4}\varphi^4\,, \tag{6.6}$$

where we have only included the leading temperature dependence, since, as we will see, the $O(T\varphi^3)$ term is not necessary for SFOPT, because the $O(\varphi^3)$ term arises from tree-level interactions. Generally the parameters $m^2, \mathcal{E}$, and λ will also depend on temperature implicitly via the one-dimensional trajectory. This makes it difficult to connect the parameters of Eq. (6.6) to Lagrangian parameters in general. However, we will see that in the optimal limit for SFOPT, the PT temperature approaches zero. In this limit, the parameters of V_{eff} are directly related to the Lagrangian parameters along a particular trajectory. Some examples of models that fall into this class are shown in Table 6.2.

This model class has the significant advantage that thermal loop effects are not necessary to generate a barrier in V_{eff}. As we discussed in Sec. 6.3, the BEC term $eT/(12\pi)(h^2)^{3/2}$ is suppressed by a factor of 12π, and consequently a SFOPT requires a hierarchy of coupling constants (see Eq. (6.3)). However, in the present model class, the barrier is provided by the tree-level potential, and therefore one naturally expects

$\bar{S}(\varphi, T)$. In principle, the functions $\bar{h}$ and $\bar{S}$ can be determined by solving for the multi-field bounce solution.

$v(T_c) \approx v$, such that enhancements of $v(T_c)/T_c$ will be primarily driven by a desire to reduce T_c. The phase transition temperature is calculated from Eq. (6.6) to be

$$T_c \approx \sqrt{\frac{m^2}{c}} \sqrt{\frac{2\mathcal{E}^2}{\lambda m^2} - 1}\,, \tag{6.7}$$

and the EW order parameter is found to be

$$\frac{v(T_c)}{T_c} \approx \sqrt{\frac{2c}{\lambda}} \frac{1}{\sqrt{1 - \frac{\lambda m^2}{2\mathcal{E}^2}}} \cos\alpha\,. \tag{6.8}$$

Here, we have introduced a projection factor of $\cos\alpha$, since in general φ will not correspond to the Higgs field, however this factor will be irrelevant to our discussion, sincne we will focus on scenarios which reduce T_c. The optimal limits for enhancing $v(T_c)/T_c$ are given by:

$c \gg \lambda$ Since c represents a sum of coupling constants controlling interactions between the Higgs and light particle in the plasma, one might try to take the limit $c \gg \lambda$ by increasing the size of these couplings or by increasing the number of degrees of freedom in the plasma. However, the Higgs self-coupling λ is also renormalized by these same couplings. Generally, it is not obvious that the limit used to increase c will not also increase λ and thereby prevent one from reaching the $c \gg \lambda$ limit. For example, we can consider the contributions to c and λ that arise from the Yukawa interaction with the top quark. The contributions scale with the Yukawa coupling h_t and number of colors N_c like $c\tilde{N}_c h_t^2$ and $\lambda \sim -N_c h_t^4$ yielding $c/\lambda \sim -1/h_t^2$. In this example, increasing the value of the Yukawa coupling will tend to decrease the ratio of c/λ. One way to get around this result is to note that contributions to c are non-negative whereas contributions to λ are positive for bosonic fields and negative for fermionic fields. If the underlying model possesses a symmetry relating bosonic and fermionic fields (such as SUSY) then it may be possible to take c large while keeping λ

small. If the light fields do not carry any SM quantum numbers, and if they are sufficiently light ($m < m_H/2$) then $c \gg \lambda$ is at tension with constraints on Higgs invisible decay.

$\boldsymbol{\lambda m^2/2\mathcal{E}^2 \to 1}$ This is the limit in which T_c vanishes and the EW-symmetric and EW-broken vacua are degenerate. As noted in (176), this degeneracy may arise as the result of a discrete symmetry relating the Higgs field with the other field(s) participating in the phase transition. We will refer to this limit as an enhanced (discrete) symmetry point (EdSP), which is also illustrated in Figure 6.3. As one approaches the EdSP, the EW-symmetric vacuum becomes metastable and increasingly degenerate with EW-broken vacuum. Without sufficient degeneracy breaking, tunneling out of the EW-symmetric vacuum may become suppressed to the point that tunneling occurs on a time scale that exceeds the age of the universe. That is, as one approaches the EdSP, it may be the case that the EWPT never occurs, even if the EW-broken vacuum is energetically favored. Otherwise, it is difficult to make any model-independent statements about the phenomenology near the EdSP.

$\boldsymbol{\lambda \to 0}$ We would like to take this limit while fixing $\lambda m^2/2\mathcal{E}^2$ such that Eq. (6.8) just scales like $1/\sqrt{\lambda}$. Moreover, if we also want to fix the VEV of the φ field

$$v_\varphi = \frac{3\mathcal{E}}{2\lambda}\left(1 + \sqrt{1 - \frac{8}{9}\frac{\lambda m^2}{2\mathcal{E}^2}}\right) \tag{6.9}$$

then we see that we must let $m^2 \sim \mathcal{E} \sim \lambda \to 0$. In this limit, the mass of the φ field

$$m_\varphi^2 = \frac{9\mathcal{E}^2}{2\lambda}\left(1 - \frac{8}{9}\frac{\lambda m^2}{2\mathcal{E}^2} + \sqrt{1 - \frac{8}{9}\frac{\lambda m^2}{2\mathcal{E}^2}}\right) \tag{6.10}$$

also scales like λ and goes to zero. Thus, there there will be a light scalar field associated with the φ field direction. The light scalar runs into two phenomenological constraints. If φ represents a mixture of the Higgs with a hidden sector

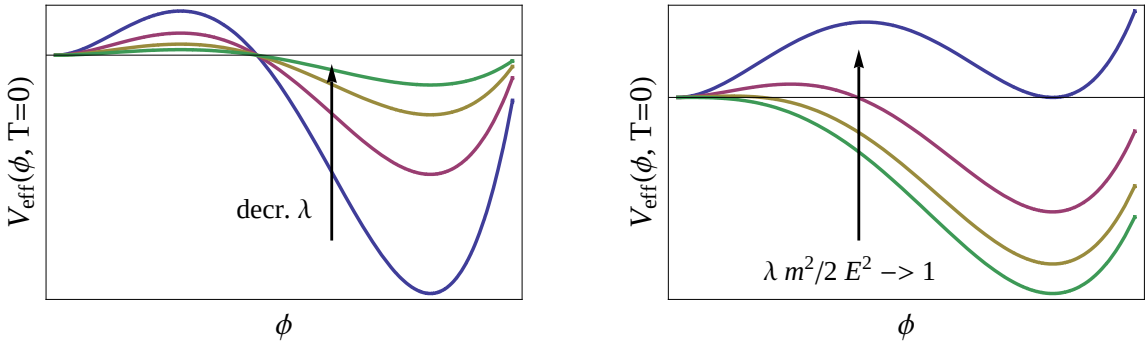

Figure 6.3: An illustration of the behavior of V_{eff} as the limits $\lambda \to 0$ and $\lambda\mu^2/2\mathcal{E}^2 \to 1$ are taken. The former leads to an EcSP whereas the latter leads to an EdSP.

scalar field, then a light Higgs is excluded by searches at LEP and at tension with the LHC Higgs discovery. On the other hand, even if there is no mixing, provided that the light scalar is mostly a SM singlet, then this limit runs into constraints on Higgs invisible decay imposed by the LHC Higgs discovery. We will discuss this scenario further in an example below.

It is important to note that as we take this limit in which $m^2 \sim \mathcal{E} \sim \lambda \to 0$, the effective potential develops a shift symmetry. Thus, we can identify the $\lambda \to 0$ limit with a enhanced symmetry point of the theory at which a continuous symmetry emerges. We will refer to this parametric limit as a enhanced (continuous) symmetry point (EcSP), which is also illustrated in Figure 6.3.

In order to illustrate how these limits and constraints may be realized in a concrete model, we consider the $\mathbb{Z}_2$xSM (176). This model extends the SM by a real scalar field S which is a singlet under the SM gauge group, but which respects a $\mathbb{Z}_2$ discrete symmetry that takes $S \to -S$. The most general, renormalizable Lagrangian

consistent with the SM gauge group and $\mathbb{Z}_2$ is given by[5]

$$\mathcal{L}_{\mathbb{Z}_2\text{xSM}} = \mathcal{L}_{\text{SM}} + \frac{1}{2}\left(\partial_\mu S\right)\left(\partial^\mu S\right) - \left[-\frac{b_2}{2}S^2 + \frac{b_4}{4}S^4 + \frac{a_2}{2}H^\dagger H S^2\right], \tag{6.11}$$

where $\mathcal{L}_{\text{SM}}$ is the Lagrangian of the SM. We assume that S does not acquire a VEV. Thus the $\mathbb{Z}_2$ is unbroken, thereby ensuring stability of S if it is lighter than $2m_H$ and preventing mixing with the Higgs. Although S does not have a VEV, we will allow it to obtain a non-zero EV at finite temperature so that it may participate in the EWPT and render it strongly first order.

With this Lagrangian, we can calculate the effective potential as a function of both the Higgs condensate $\langle H\rangle = \left(0\,,\, h/\sqrt{2}\right)^T$ and singlet condensate $\langle S\rangle = s$. Working to the same level of approximation as in Eq. (6.6), we neglect the loop-suppressed contributions and include only the leading thermal contributions to obtain[6]

$$V_{\text{eff}}(h, s, T) = \frac{-\mu^2 + c_h\, T^2}{2}h^2 + \frac{\lambda}{4}h^4 + \frac{-b_2 + c_s\, T^2}{2}s^2 + \frac{b_4}{4}s^4 + \frac{a_2}{4}h^2 s^2\,. \tag{6.12}$$

The thermal mass terms $c_h\, T^2$ and $c_s\, T^2$ ensure symmetry restoration at sufficiently high temperature.

In light of the general analysis of the preceding subsections, we are motivated to seek out enhanced symmetry points. In the following discussion, we will identify the EcSP, justify the claim that SFOPT are found in its vicinity, determine the phenomenology in this limit, and assess the impact of collider constraints. We will then repeat the analysis for a neighborhood of the EdSP.

The parameters of the $\mathbb{Z}_2$xSM are the SM gauge (g_i) and Yukawa couplings (y_i), the Higgs sector parameters (μ^2 and λ), the singlet sector parameters (b_2 and b_4), and the "Higgs portal" coupling (a_2). The symmetry group of the $\mathbb{Z}_2$xSM Lagrangian

[5]Since the one-loop phase transition analysis does not depend upon the quantum numbers of S, the analysis here will also apply to the more general case of a non-singlet S coupled via the "Higgs portal" operator $H^\dagger H S^* S$.

[6]Note that we now use the convention $\mathcal{L}_{SM} \supset +\mu^2 H^\dagger H$ where $\mu^2 > 0$ triggers SSB.

is $G_{\rm SM} \times \mathbb{Z}_2$ where $G_{\rm SM}$ is the gauge group of the SM. For a particular choice of parameters, an additional continuous symmetry arises. We find this EcSP by requiring the parameters to satisfy

$$\text{EcSP}: \qquad \left\{b_2 = \mu^2 \quad , \quad b_4 = \lambda \quad , \quad a_2 = 2\lambda\right\} \quad \text{and} \quad \left\{g_i = 0 \quad , \quad y_i = 0\right\} , \tag{6.13}$$

where $\lambda = m_H^2/(2v^2)$ and $\mu^2 = m_H^2/2$ are not constrained by the symmetry, but are restricted by measurements of the Higgs mass and VEV. At the EcSP, the Lagrangian can be written as

$$\begin{aligned} \mathcal{L}_{\mathbb{Z}_2 \text{xSM}}\Big|_{\text{EcSP}} \supset & \left(\partial_\mu H\right)^\dagger \left(\partial^\mu H\right) + \frac{1}{2}\left(\partial_\mu S\right)\left(\partial^\mu S\right) \\ & - \left[-\mu^2\left(H^\dagger H + S^2/2\right) + \lambda\left(H^\dagger H + S^2/2\right)^2\right] \end{aligned} \tag{6.14}$$

up to kinetic terms for the other SM fields. This Lagrangian is invariant under the continuous symmetry transformation

$$\text{SO}(2): \qquad \begin{pmatrix} \sqrt{2}\,H \\ S \end{pmatrix} \to \begin{pmatrix} \cos\theta & \sin\theta \\ -\sin\theta & \cos\theta \end{pmatrix} \begin{pmatrix} \sqrt{2}\,H \\ S \end{pmatrix} . \tag{6.15}$$

The symmetry ensures that $c_s = c_h = c_0$ and the effective potential may be written as

$$V_{\text{eff}}(h, s, T)\Big|_{\text{EcSP}} = \frac{1}{2}\left(-\mu^2 + c_0\,T^2\right)\left(h^2 + s^2\right) + \frac{\lambda}{4}\left(h^2 + s^2\right)^2 . \tag{6.16}$$

However, the restriction to vanishing gauge and Yukawa couplings is unphysical, and once these couplings are turned on, radiative corrections to V_{eff} will break the symmetry Eq. (6.15). However, the symmetry breaking terms will carry a loop suppression factor of $1/16\pi^2$ and can be neglected at this level of approximation. On the other hand, contributions to the thermal masses are not loop-suppressed and will generically induce $c_h \neq c_s$. Therefore, in the following discussion we will neglect loop suppressed corrections to V_{eff}, but we will treat c_h and c_s as independent parameters.

We will see that there are SFOPT in a neighborhood of Eq. (6.13), but first it is interesting to remark that the pattern of symmetry breaking is controlled by the symmetry that arises at this EcSP. Provided that $\mu^2 > 0$, the SO(2) will be spontaneously broken. The resulting Goldstone boson is associated with a flat direction in the potential connecting $|H| = v/\sqrt{2}$ with $S = v$. Thus, we anticipate that we will find phase transitions that occur in two steps: first S acquires an EV breaking the $\mathbb{Z}_2$, and second the EV of S returns to zero as H acquires an EV breaking the EW symmetry.

We can proceed to perturb away from the EcSP by writing the parameters as

$$\left\{ b_2 = \mu^2 \left(1 + \epsilon_{b_2}\right) \quad , \quad b_4 = \lambda \left(1 + \epsilon_{b_4}\right) \quad , \quad a_2 = 2\lambda \left(1 + \epsilon_{a_2}\right) \right\} . \tag{6.17}$$

What sort of perturbations will yield SFOPT? At the EcSP, the EW-broken and EW-symmetric vacua are degenerate, and if $c_h = c_s$ then the thermal corrections will maintain that degeneracy. As we perturb away from the EcSP looking for SFOPT, we will need to ensure that degeneracy breaking causes the EW-broken vacuum to be energetically favored and also ensure that the breaking of $c_h \neq c_s$ causes the EW-symmetric vacuum (in which $\mathbb{Z}_2$ is broken) to become (free-)energetically favored above some temperature. Keeping this picture in mind, we can proceed to calculate the phase transition parameters. In this neighborhood of the EcSP, the phase transition temperature and EW order parameter are given by

$$T_c = \frac{m_H}{2\sqrt{c_h - c_s}} \sqrt{\epsilon_{b_4} - 2\epsilon_{b_2}} \Big(1 + O(\epsilon_{b_2}, \epsilon_{b_4}) \Big) \tag{6.18}$$

$$\frac{v(T_c)}{T_c} = 2\sqrt{c_h - c_s} \frac{v}{m_H} \frac{1}{\sqrt{\epsilon_{b_4} - 2\epsilon_{b_2}}} \Big(1 + O(\epsilon_{b_2}, \epsilon_{b_4}) \Big) . \tag{6.19}$$

See also Figure 6.4. As we anticipated, T_c is arbitrarily small and $v(T_c)/T_c$ is arbitrarily large for arbitrarily small perturbations away from the EcSP ($\epsilon_{b_4} - 2\epsilon_{b_2} \ll 1$). The particular combination of parameters $\epsilon_{b_4} - 2\epsilon_{b_2}$ appears, because it controls the

degree of degeneracy breaking between the EW-symmetric and EW-broken vacua. We can verify this by calculating

$$\begin{aligned} &V_{\text{eff}}\left(0, v_s, T\right) - V_{\text{eff}}\left(v, 0, T\right) \\ &\quad = \left[\frac{\mu^4}{4\lambda}\left(\epsilon_{b_4} - 2\epsilon_{b_2}\right) - \frac{\mu^2}{2\lambda}\left(c_h - c_s\right)T^2\right]\left(1 + O(\epsilon_{b_2} \sim \epsilon_{b_4} \sim T^2)\right), \end{aligned} \tag{6.20}$$

where $v_s = \sqrt{b_2/b_4}$ is the expectation value of s in the EW-symmetric vacuum and $v = \sqrt{\mu^2/\lambda} = 246$ GeV is the Higgs VEV. Thus if $\epsilon_{b_4} - 2\epsilon_{b_2} = 0$, the two vacua are degenerate at $T = 0$. If $\epsilon_{b_4} - 2\epsilon_{b_2} > 0$, the broken vacuum is energetically favored and the PT occurs at the temperature T_c given by Eq. (6.18), but if $\epsilon_{b_4} - 2\epsilon_{b_2} < 0$, the symmetric vacuum is energetically favored and the PT does not occur. From this discussion, and particularly Eq. (6.19), we conclude that SFOPT are found in the neighborhood of the EcSP, but additionally the EcSP demarcates a boundary between physical models ($\epsilon_{b_4} - 2\epsilon_{b_2} > 0$) in which EWSB occurs and unphysical models ($\epsilon_{b_4} - 2\epsilon_{b_2} < 0$) in which EWSB does not take place. The singular factor of $1/\sqrt{c_h - c_s}$ in Eq. (6.18) can also be understood in light of Eq. (6.20). If $c_h = c_s$, then thermal corrections lift the EW-broken and EW-symmetric phases together maintaining their degeneracy. One needs $c_h > c_s$ to ensure that V_{eff} at the EW-broken phase (free energy density) is lifted more greatly with increasing temperature than the EW-symmetric phase. Conversely, if $c_h < c_s$ then the EW-symmetric phase in which the $\mathbb{Z}_2$ is broken never becomes (free-)energetically favored.

We can begin to investigate the phenomenology near the EcSP by calculating the mass of the singlet scalar field. The tree-level relationship can be read off of the Lagrangian Eq. (6.14), which gives

$$m_S^2 = -b_2 + \frac{a_2}{2}v^2 \xrightarrow{\text{EcSP}} \frac{m_H^2}{2}\left(\epsilon_{a_2} - \epsilon_{b_2}\right). \tag{6.21}$$

Since this scalar field corresponds to the Goldstone boson of the spontaneously broken symmetry Eq. (6.15), we are not surprised to find that it is light when deviations away

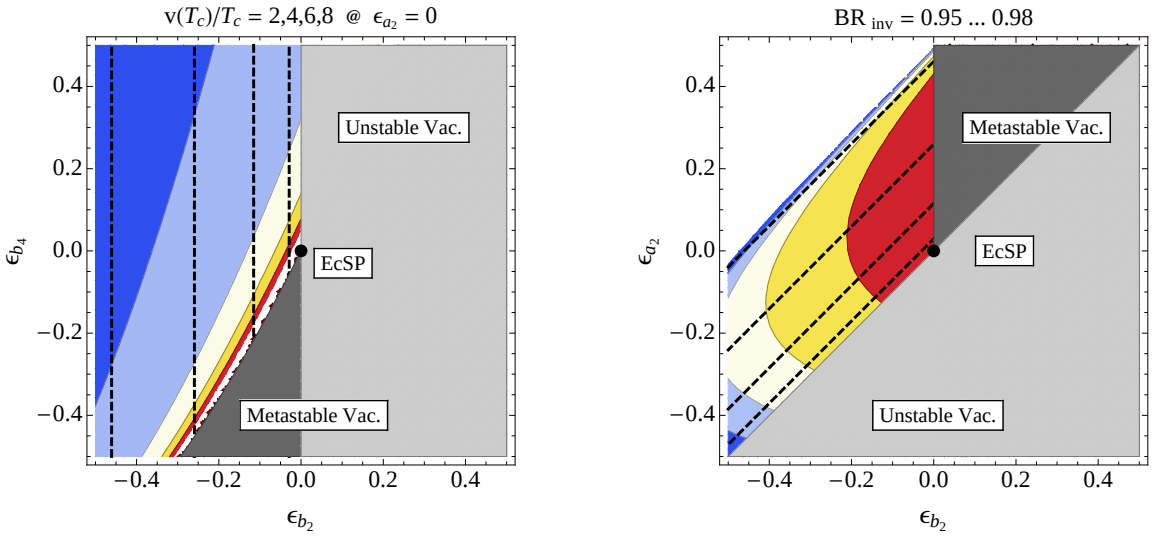

Figure 6.4: A neighborhood of the EcSP. In both panels, the dashed lines corresponds to $m_S = 60, 45, 30$, and 15 GeV as ϵ_{b_2} is increased. *Left.* The EW order parameter, for which Eq. (6.19) is the leading order expression, grows as ϵ_{b_2} increases and ϵ_{b_4} decreases. *Right.* The branching fraction of Higgs to an invisible S-pair, calculated from the width Eq. (6.22). The BR grows with increasing ϵ_{b_2}.

from the EcSP are small $\epsilon_{a_2} - \epsilon_{b_2} \ll 1$. Since the Higgs is coupled to this light singlet, there will generically be a large Higgs invisible decay width. The expression is given by (113)

$$\Gamma(H \to SS) = \frac{a_2^2 v^2}{32\pi m_H}\sqrt{1 - \frac{4m_S^2}{m_H^2}} \xrightarrow{\text{EcSP}} \frac{m_H^3}{32\pi v^2}\Big(1 + (\epsilon_{a_2} + \epsilon_{b_2}) + O(\epsilon_{a_2}^2, \epsilon_{b_2}^2)\Big)\,. \tag{6.22}$$

See also Figure 6.4. Since S only couples to the SM via the Higgs, the width for Higgs decay into SM fields, $\Gamma(H \to \text{SM})$, is only affected by its coupling to S at the multi-loop level. Thus, we can approximate $\Gamma(H \to \text{SM})$ by the SM Higgs total width, which is $\Gamma_{\text{tot}}^{\text{SM}} \approx 5$ MeV for $m_H \approx 125$ GeV (227). We find that the invisible branching ratio is

$$\text{BR}_{\text{inv}} = \frac{\Gamma(H \to SS)}{\Gamma(H \to \text{SM}) + \Gamma(H \to SS)} \approx 0.985\,, \tag{6.23}$$

where we also neglect kinematically suppressed 3-body (and greater) final states. Such a large invisible decay greatly exceeds the 95% CL limits set by analyses of the LHC and Tevatron Higgs data, which were discussed in Sec. 6.2. Thus, the tension which we had discussed between the EcSP limit and invisible decay is illustrated in a concrete setting.

We can attempt to evade the collider constraints on Higgs invisible decay by suppressing the channel $H \to SS$. This can be accomplished by either lifting the singlet mass above the kinematic threshold $m_S > m_H/2$ or by reducing the coupling of the Higgs to the singlet $a_2 \to 0$. Either of these approaches requires us to depart from the EcSP limit which guarantees us SFOPT, but also brings in the dangerous light scalar. In the following, we will discuss two ways of evading the invisible decay constraint by deviating away from the EcSP in a particular way to maintain SFOPT.

It was discussed in the preceding subsection that SFOPT may also be found in the neighborhood of an EdSP. We can perturb away from the EcSP such that the continuous symmetry is broken to its discrete subgroup $\mathbb{S}_2$ which exchanges $\sqrt{2}H \leftrightarrow S$. The EdSP is given by

$$\text{EdSP}: \qquad \left\{b_2 = \mu^2 \quad , \quad b_4 = \lambda\right\} \quad \text{and} \quad \left\{g_i = 0 \quad , \quad y_i = 0\right\} . \tag{6.24}$$

Now μ^2, λ, and a_2 are free to vary, and therefore the EdSP represents a 3-dimensional submanifold of the full $\mathbb{Z}_2$xSM theory space. As before we can consider perturbations away from the EdSP,

$$\left\{b_2 = \mu^2\left(1+\epsilon_{b_2}\right) \quad , \quad b_4 = \lambda\left(1+\epsilon_{b_4}\right)\right\} . \tag{6.25}$$

The singlet is no longer the Goldstone boson of the spontaneously broken SO(2) symmetry, so its mass need not be small

$$m_S^2 = -b_2 + \frac{a_2}{2}v^2 \xrightarrow{\text{EdSP}} \frac{m_H^2}{4\lambda}\left(a_2 - 2\lambda\right)\left(1 - \frac{2\lambda}{a_2 - 2\lambda}\epsilon_{b_2}\right) . \tag{6.26}$$

From this expression we can see how the variation of a_2 affects the vacuum structure. For $a_2 = 2\lambda$ we return to the EcSP and the singlet is the massless Goldstone boson. For $a_2 < 2\lambda$, the singlet becomes tachyonic, signaling that the true vacuum of the theory is one in which the $\mathbb{Z}_2$ is spontaneously broken. This is an undesirable limit, because without the $\mathbb{Z}_2$ preventing the Higgs and singlet from mixing, we run into the collider Higgs mixing constraints, which were discussed in Sec. 6.2. For $a_2 > 2\lambda$, the vacuum preserves the $\mathbb{Z}_2$ and the singlet is massive. Provided that $a_2 > 3\lambda$, the singlet mass $m_S > m_H/2$ will exceed the kinematic threshold and block the invisible decay $H \to SS$. Using $m_H \approx 125$ GeV and $\lambda = m_H^2/(2v^2)$, this bound is approximately $a_2 \gtrsim 0.39$. Moreover, since the expressions for the phase transition temperature and EW order parameter, Eq. (6.18) and Eq. (6.19), were independent of a_2, we still expect to find SFOPT in this corner of parameter space near the EdSP. Thus a departure from the EcSP along the EdSP allows for SFOPT while avoiding Higgs invisible decay by kinematically blocking the $H \to SS$ channel.

A second approach toward avoiding Higgs invisible decay is to reduce the Higgs portal coupling a_2 and thereby suppress $\Gamma(H \to SS)$. In the previous discussion we saw that if we moved away from the EcSP along the direction of the EdSP, then taking $a_2 < 2\lambda$ would change the vacuum structure such that the $\mathbb{Z}_2$ is spontaneously broken and allow the Higgs and singlet to mix. Thus, we must find a different path that continuously connects the EcSP with $a_2 = 0$ but maintains the vacuum structure. This is accomplished with the following parameter choice,

$$\overline{\text{EcSP}}: \qquad \left\{ b_2 = \frac{a_2}{2\lambda}\mu^2 \quad , \quad b_4 = \left(\frac{a_2}{2\lambda}\right)^2 \lambda \right\} . \tag{6.27}$$

At the parameter point Eq. (6.27), the scalar sector Lagrangian can be written as

$$\begin{aligned} \mathcal{L}_{\mathbb{Z}_2\text{xSM}}\Big|_{\overline{\text{EcSP}}} \supset & \left(\partial_\mu H\right)^\dagger \left(\partial^\mu H\right) + \frac{1}{2}\left(\partial_\mu S\right)\left(\partial^\mu S\right) \\ & - \left[-\mu^2 \left(H^\dagger H + \frac{a_2}{2\lambda} S^2/2 \right) + \lambda \left(H^\dagger H + \frac{a_2}{2\lambda} S^2/2 \right)^2 \right] . \end{aligned} \tag{6.28}$$

From this expression we see that the scalar *potential* is invariant under a continuous symmetry transformation which rotates and dilates the fields H and S,

$$\begin{pmatrix} \sqrt{2}\,H \\ \sqrt{\frac{a_2}{2\lambda}}S \end{pmatrix} \to \begin{pmatrix} \cos\theta & \sin\theta \\ -\sin\theta & \cos\theta \end{pmatrix} \begin{pmatrix} \sqrt{2}\,H \\ \sqrt{\frac{a_2}{2\lambda}}S \end{pmatrix} . \tag{6.29}$$

However, the scalar *kinetic terms* are not invariant under this transformation (unless $a_2 = 2\lambda$), and thus Eq. (6.27) is not a true enhanced symmetry point of the $\mathbb{Z}_2$xSM. That is, radiative corrections will spoil the symmetry Eq. (6.29), and therefore we do not expect the effective potential to respect this symmetry (even if we were to also set $g_i = y_i = 0$). Nevertheless, since in this class of models, the phase transition parameters are dominantly controlled by the structure of the tree-level scalar potential, we expect that SFOPT may still be found in the vicinity of Eq. (6.27). However, it turns out that the loop corrections which break Eq. (6.29) and split the degeneracy of the EW-symmetric and EW-broken vacua tend to render the EW-broken vacuum metastable. In this case, the universe becomes trapped in the energetically favored EW-symmetric phase and the electroweak phase transition does not occur. To avoid this outcome, we must allow for a finite perturbation away from the $\overline{\text{EcSP}}$ parameter point. We consider instead

$$\left\{ b_2 = \frac{a_2}{2\lambda}\mu^2\left(1+\epsilon_{b_2}\right) \quad , \quad b_4 = \left(\frac{a_2}{2\lambda}\right)^2 \lambda\left(1+\epsilon_{b_4}\right) \right\} , \tag{6.30}$$

where we will allow α to vary and keep $\epsilon_{b_2} = \epsilon_{b_4} = -1/2$.

Along the trajectory Eq. (6.30) we can take $a_2 \to 0$. The singlet remains light $m_S^2 = -b_2 + a_2 v^2/2 = a_2 v^2 \epsilon_{b_2}$ and the invisible width is approximately given by

$$\Gamma(H \to SS) = \frac{a_2^2 v^2}{32\pi m_H}\sqrt{1-\frac{4m_S^2}{m_H^2}} \xrightarrow{\overline{\text{EcSP}}} \frac{m_H^3}{32\pi v^2}\left(\frac{a_2}{2\lambda}\right)^2 . \tag{6.31}$$

To bring the invisible branching fraction below $\text{BR}_{\text{inv}} < 0.64$ (the weakest 95% CL limit (215)) we need $a_2 < 0.043$. Furthermore, since the expression for the EW order

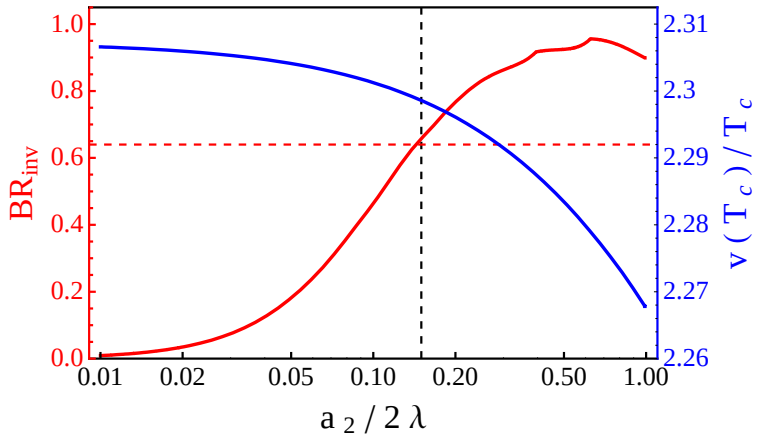

Figure 6.5: The EW order parameter $v(T_c)/T_c$ and invisible branching fraction $\mathrm{BR}_{\mathrm{inv}}$ in the $\mathbb{Z}_2$xSM at the $\overline{\mathrm{EcSP}}$ parameter point Eq. (6.27). As $a_2/2\lambda$ is decreased below about 0.15, Higgs invisible decay becomes sufficiently suppressed to evade collider constraints which impose $\mathrm{BR}_{\mathrm{inv}} \lesssim 0.64$. This threshold corresponds to $a_2 \approx 0.04$. At the same time, the electroweak phase transition remains strongly first order $v(T_c)/T_c > 1$.

parameter Eq. (6.19) is independent of a_2, we still expect to finds SFOPT in this limit. This can be verified by calculating the EW order parameter numerically, and the result is shown in Figure 6.5.

Tree-Level (Non-Renormalizable Operators) Driven

The second way of obtaining a SFOPT using only tree-level operators is to employ higher order, non-renormalizable terms in the potential. If the scale of new physics Λ is not much larger than the EW scale, then the leading correction to the scalar potential, $(H^\dagger H)^3$, may dramatically change the nature of the EWPT. In this scenario, the effective potential may be written as

$$V_{\mathrm{eff}}(h,T) \approx \frac{1}{2}\left(\mu^2 + c\,T^2\right)h^2 + \frac{\lambda}{4}h^4 + \frac{1}{8\Lambda^2}h^6 \tag{6.32}$$

up to terms which are $O(h^8/\Lambda^4)$. By minimizing the potential, the parameters μ^2 and λ may be exchanged for the Higgs VEVv and mass m_H as

$$\lambda = \frac{m_H^2}{2v^2} - \frac{3v^2}{2\Lambda^2} = \frac{m_H^2}{2v^2}\left(1 - \frac{\Lambda_{\max}^2}{\Lambda^2}\right) \tag{6.33}$$

$$\mu^2 = -\frac{m_H^2}{2} + \frac{3v^4}{4\Lambda^2} = \frac{m_H^2}{2}\left(\frac{\Lambda_{\max}^2}{2\Lambda^2} - 1\right). \tag{6.34}$$

In the second equality we have introduced $\Lambda_{\max} \equiv \sqrt{3}v^2/m_H$, this meaning of which will become clear presently. Since we are interested in the limit that will yield a barrier in the effective potential, we will focus on the case of a low-scale cutoff such that $\mu^2 > 0$ stabilizes the EW-symmetric vacuum, $\lambda < 0$ causes the potential to turn over, and the $O(h^6)$ term stabilizes the EW-broken vacuum. In order to obtain $\lambda < 0$, we must have $\Lambda < \Lambda_{\max}$, where the upper bound evaluates to $\Lambda_{\max} \approx 800$ GeV for $m_H \approx 125$ GeV. A potential of this form is illustrated in Figure 6.1. The electroweak phase transition in this effective theory was studied by (183; 184; 228).

As in the *Tree-Level (Renorm. Op.) Driven* Model Class, the presence of the tree level barrier allows $v(T_c) \approx v$ and therefore $v(T_c)/T_c$ may be enhanced by reducing T_c. Once again using standard techniques, we calculate the phase transition temperature and the EW order parameter to be

$$T_c = \sqrt{\frac{\mu^2}{c}}\sqrt{\frac{\lambda^2\Lambda^2}{4\mu^2} - 1} \tag{6.35}$$

$$\frac{v(T_c)}{T_c} = \sqrt{\frac{c}{-\lambda}}\frac{2}{\sqrt{1 - \frac{4\mu^2}{\lambda^2\Lambda^2}}}. \tag{6.36}$$

The optimal limits for enhancing $v(T_c)/T_c$ are given by:

$\boldsymbol{c \gg \lambda}$ This limit was discussed previously in the context of the *Tree-Level (Renorm. Ops.) Driven* Model Class.

$\boldsymbol{4\mu^2/\lambda^2\Lambda^2 \to 1}$ Using the relationships Eqs. (6.33) & (6.34), this combination

of parameters can be expressed as

$$\frac{4\mu^2}{\lambda^2\Lambda^2} = \frac{4}{3}\frac{1-2\Lambda^2/\Lambda^2_{\rm max}}{(1-\Lambda^2/\Lambda^2_{\rm max})^2}\,. \tag{6.37}$$

Then, the limit is obtained when $\Lambda \to \Lambda_{\rm min}$ where $\Lambda_{\rm min} \equiv \Lambda_{\rm max}/\sqrt{3} = v^2/m_H$. For $m_H \approx 125$ GeV this evaluates to $\Lambda_{\rm min} \approx 480$ GeV. As we approach this limit, the phase transition temperature, given by Eq. (6.35), goes to zero. We found a similar behavior in the *Tree-Level (Renorm. Op.) Driven* Model Class, and once again we can identify this degeneracy limit with an EdSP (176).

The $(H^\dagger H)^3$ operator is able to evade the standard phenomenological constraints. Since it preserves the custodial SU(2), there is no anomalous contribution to the ρ parameter, even for a low cutoff (183). However, if other dimension six operators are not forbidden, they may be constrained by electroweak precision tests. The Higgs cubic self-coupling, given by

$$\frac{m_H^2}{v}\left(1 + 2\frac{\Lambda^2_{\rm min}}{\Lambda^2}\right)\,, \tag{6.38}$$

receives $O\,(1)$ corrections in this limit. However, it is unlikely that the LHC will be able to measure the Higgs self-coupling.

$\boldsymbol{\lambda \to 0}$ We would like to take this limit $\lambda \to 0$ while fixing $4\mu^2/(\lambda^2\Lambda^2)$ such that Eq. (6.36) just scales like $1/\sqrt{\lambda}$. Using the relationship Eq. (6.37), this implies that we must let $\Lambda/\Lambda_{\rm max} = $ const.. Then, Eq. (6.33) reveals that in order to take λ to zero we would have to take $m_H \sim \sqrt{\lambda}$ to zero. Obviously, this limit is not viable. However, it is interesting to note that this limit corresponds to an EcSP. Since both λ, μ^2, and $1/\Lambda^2$ all vanish, the potential becomes flat.

This extension of the SM by an $O\left[(H^\dagger H)^3\right]$ term has been studied by (183; 184) in the context of the electroweak phase transition and phenomenology. We have calculated $v(T_c)/T_c$ in the two limits discussed above. First, we allow λ to vary while fixing $4\mu^2/\lambda^2\Lambda^2 = 0.2$. The results, shown in Figure 6.6 (left panel), indicate

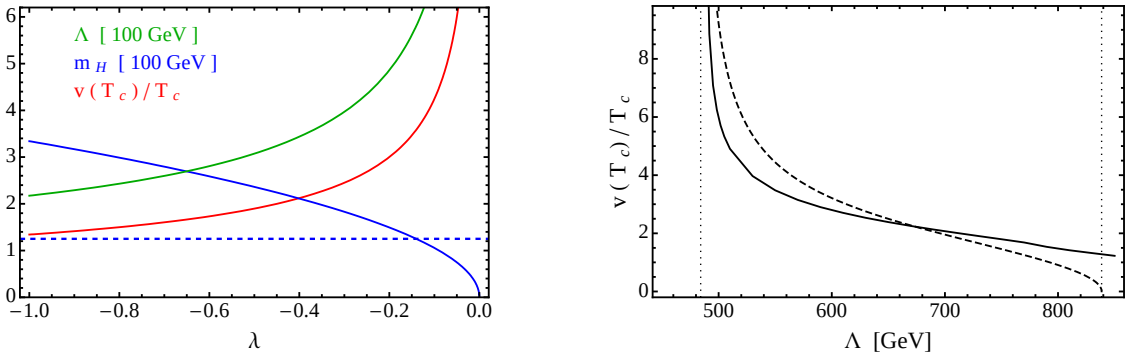

Figure 6.6: *Left:* The EWPT order parameter Eq. (6.36) (red), Higgs mass m_H (blue), and UV cutoff Λ (green) in the vicinity of the EcSP $\lambda = 0$. *Right:* The EWPT order parameter with $m_H = 125$ GeV in the vicinity of the EdSP $\Lambda = \Lambda_{\rm min} \approx 480$ GeV. The solid line shows the result of a calculation using the full one-loop thermal effective potential whereas the dashed line shows the approximation Eq. (6.36).

that $v(T_c)/T_c$ grows like $1/\sqrt{-\lambda}$ as λ approaches zero. For $\lambda \approx -0.15$ the Higgs mass is consistent with the LHC signal at $m_H \approx 125$ GeV, the phase transition is strongly first order, and the cutoff is low $\Lambda \approx 500$ GeV. The behavior of $v(T_c)/T_c$ nearby to the EdSP is shown in Figure 6.6 (right panel) where we have fixed $m_H = 125$ GeV and varied Λ. This figure illustrates that $v(T_c)/T_c$ grows as Λ decreases toward the EdSP where $\Lambda_{\rm min} \approx 480$ GeV and T_c vanishes. For smaller values of Λ, electroweak symmetry breaking does not occur. For large values of the cutoff, the Higgs self-coupling λ becomes positive and the PT proceeds as in the SM without any enhancement.

Loop Driven

In the presence of large quantum corrections, a competition between the terms h^4 and $h^4 \ln h^2$ can generate a barrier in the effective potential. Alternatively, we can say that λ is positive at high scales and runs negative at the electroweak scale. In

this model class, the effective potential may be written as

$$V_{\text{eff}}(h,T) \approx \frac{1}{2}\left(\mu^2 + c\,T^2\right)h^2 + \frac{\lambda}{4}h^4 + \frac{\kappa}{4}\,h^4 \ln\frac{h^2}{M^2}\,. \tag{6.39}$$

Unlike in the previous model classes, the loop-suppressed quantum corrections will play an important role here, and they are not dropped. The parameters μ^2 and λ may be exchanged for the Higgs VEVv and mass[7] $m_H = \sqrt{V''_{\text{eff}}(v, T=0)}$ using

$$\lambda = \frac{m_H^2}{2v^2} - \kappa\left(\ln\frac{v^2}{M^2} + \frac{3}{2}\right) \tag{6.40}$$

$$\mu^2 = -\frac{m_H^2}{2} + \kappa\, v^2\,. \tag{6.41}$$

The dimensionless parameter κ parametrizes loop-suppressed corrections to the effective potential arising from interactions between the Higgs and the other fields. For example, in the SM one finds $\kappa_{\text{SM}} \approx (6M_W^4 + 3M_Z^4 - 12M_t^4)/(16\pi^2 v^4) \approx -0.018$. The loop induced term can help provide a barrier, as shown in Figure 6.1, if $\mu^2 > 0$ stabilizes $h = 0$, $\lambda < 0$ turns the potential over, and $\kappa > 0$ stabilzes $h = v$. To allow $\kappa > 0$, the BSM physics contributions should be dominated by bosonic fields, since fermion loops bring in an additional minus sign. If $\kappa \to \kappa_{\text{SM}} \approx 0$ the SM is regained and the PT will not be Loop Driven. A model which relies on large loop corrections to generate an SFOPT was studied by (110).

From Eq. (6.39) we can calculate the PT temperature and EW order parameter

[7]Since the loop contributions are important in this model class, we must be careful to distinguish the parameter m_H from the Higgs pole mass. They differ by a correction that depends on the renormalization conditions. Since we are primarily interested in the parametric scaling behavior and not numerical precision, we use m_H to characterize the mass scale of fluctuations about $h = v$ and implement LHC Higgs data by setting $m_H \approx 125$ GeV.

to be [8]

$$T_c \approx \frac{m_H}{2\sqrt{c}}\sqrt{1-\kappa v^2/m_H^2} \tag{6.42}$$

$$\frac{v(T_c)}{T_c} \approx \frac{3}{2}\frac{v}{m_H}\frac{\sqrt{c}}{\sqrt{1-\kappa v^2/m_H^2}}\left(1+\frac{1}{3}\frac{\kappa v^2}{m_H^2}\right) \tag{6.43}$$

A comparison of the approximations and the exact values is shown in Figure 6.7. The optimal limits for enhancing $v(T_c)/T_c$ are given by

$\boldsymbol{\kappa v^2/m_H^2 \to 1}$ In this limit, the quantum corrections are large, i.e., $\kappa \to \kappa_{\max} = m_H^2/v^2 \approx 0.26$ for $m_H = 125$ GeV. Since κ contains a suppression factor of $1/16\pi^2$, obtaining $\kappa = O(1)$ requires either many additional (bosonic) degrees of freedom and/or large couplings to the Higgs. This limit is then bounded by perturbativity constraints. Moreover, the large loops which generate κ may also contribute to Higgs production and/or decay processes. We discuss this scenario further in Sec. 6.4 in the context of Higgs diphoton decay. Finally, we can once again identify this limit as an EdSP in which T_c vanishes and the EW-broken and EW-symmetric vacua are degenerate. Above $\kappa = \kappa_{\max}$ electroweak symmetry breaking does not occur.

$\boldsymbol{m_H \ll v}$ This limit is excluded in light of the Higgs discovery.

As an example of a model in the *Loop Driven* class, we will discuss a singlet extension of the SM presented in (110). The SM Lagrangian is extended by

$$\Delta\mathcal{L} = \sum_{i=1}^{N}(\partial S_i)^2 - \zeta^2 H^\dagger H \sum_{i=1}^{N} S_i^2 \tag{6.44}$$

where the N real, scalar fields S_i are singlets under the SM gauge group. We assume that $\zeta^2 > 0$ and the S_i do not acquire VEVs. Instead, they modify the electroweak phase transition by radiatively generating a correction to the effective potential given

[8] In deriving these expressions we have assumed the that PT temperature is low and performed an expansion in cT^2/m_H^2. In the optimal limits $\kappa v^2/m_H^2 \to 1$ and $m_H \ll v$, the PT temperature is low and this expansion is a good approximation.

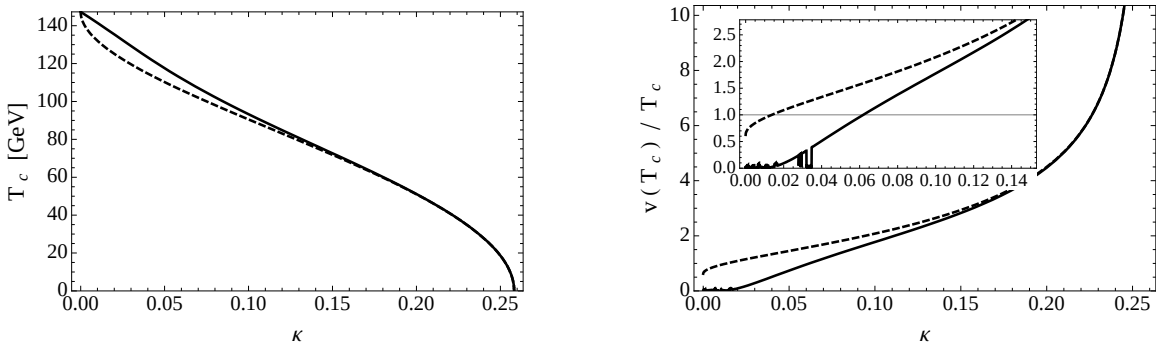

Figure 6.7: A comparison of the approximations Eqs. (6.42) & (6.43) (dashed lines) with the full toy-model potential Eq. (6.39).

by

$$\Delta V_{\rm eff}(h,T) = \frac{N\zeta^4 h^4}{64\pi^2}\left[\ln\frac{\zeta^2 h^2}{Q^2} - \frac{3}{2}\right], \tag{6.45}$$

which is calculated in the $\overline{\rm MS}$ scheme with a renormalization scale Q. This term can be matched onto the $O(h^4 \ln h^2)$ term in the generic potential Eq. (6.39) to find $\kappa = N\zeta^4/16\pi^2$ and $M^2 = Q^2\zeta^{-2}\exp\big[3/2\big]$. With this identification, the optimal limit $\kappa v^2/m_H^2 \to 1$ corresponds to $\zeta \to \zeta_{\rm max} = 2\sqrt{\pi m_H/(\sqrt{N}v)}$, which evaluates to $\zeta_{\rm max} \approx 2.5N^{-1/4}$ for $m_H = 125$ GeV.

Choosing $m_H = 125$ GeV, $N = 12$, and $Q = m_t = 172$ GeV, we calculate $v(T_c)/T_c$ and present the results in Figure 6.8. As expected, $v(T_c)/T_c$ grows upon approaching the EdSP $\zeta_{\rm max} \approx 1.36$. For larger values of ζ, electroweak symmetry breaking does not occur. Comparing the analytic approximation Eq. (6.43) with the full one-loop numerical calculation, we find qualitative agreement. However, they disagree at small ζ where the low T_c expansion used in deriving Eq. (6.43) breaks down, and they disagree at large $\zeta \lesssim \zeta_{\rm max}$ where T_c is low and the high-temperature expansion, implicit in Eq. (6.39), begins to break down.

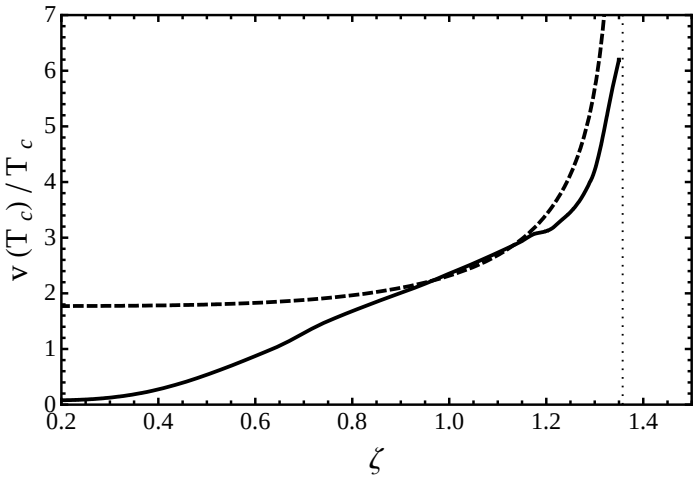

Figure 6.8: The EW order parameter evaluated numerically (solid) with the approximation Eq. (6.43) (dashed) in the vicinity of the EdSP $\zeta = \zeta_{\max} \approx 1.32$.

6.4 Diphoton Excess and SFOPT in the Higgs Portal

One of the most exciting revelations to come out of the recent LHC announcement is the appreciable excess of events the final states with two photons. The $\gamma\gamma$ final state, which is associated with Higgs production by gluon fusion, is observed at a rate that exceeds the SM prediction by a factor of approximately 1.5, while the $\gamma\gamma jj$ final state is enhanced by a factor of approximately three (211) . Consequently, fits to the entire data set favor an enhancement of the diphoton decay rate $\Gamma(h \to \gamma\gamma)$ by a factor of approximately $2-3$ with respect to the SM prediction, as well as a suppression of the rate of Higgs production by $\sigma(gg \to h)$ by a factor of approximately $0.5-0.6$ (see, e.g., (211; 226) and references therein). Since $gg \to h$ and $h \to \gamma\gamma$ are both loop-induced processes in the SM these channels are particularly sensitive to new physics. For instance, the appropriate enhancement and suppression can be achieved by letting the Higgs couple to a new charged scalar or scalars S via the Higgs portal (229–231).

Then, graphs containing an S loop will contribute to the amplitudes for $gg \to h$ and $h \to \gamma\gamma$, and they will interfere with the $t-$ and $W-$loops that dominant the SM contributions to those processes. Generally, *a negative value of the Higgs portal coupling is favored* by the data. This choice of sign ensures that the interference in the $h \to \gamma\gamma$ process is constructive and that it is destructive for $gg \to h$. As we have seen, the Higgs portal operator also provides a means of rendering the electroweak phase transition strongly first order. It is then interesting to ask whether or not the region of parameter space that can accommodate a SFOPT can also allow for enhanced diphoton decay. We will see that generically, *the SFOPT condition favors a positive value of the Higgs portal coupling* and, therefore, is at tension with the diphoton enhancement.

In order to demonstrate that SFOPT favors a positive Higgs portal coupling, let us consider a Higgs portal coupling between the Higgs and a scalar field S, which is given by the Lagrangian

$$-\mathcal{L} \supset \mu_S^2 S^* S + 2\lambda H^\dagger H S^* S \,. \tag{6.46}$$

The phase transition calculation is independent of the quantum numbers of S at the one-loop order, but instead only depends upon the coupling of S to the Higgs[9]. However, in order to obtain an enhanced diphoton decay rate, we need S to carry an electric charge. Consequently, we must ensure that S does not acquire a VEV[10]. In that case, the field-dependent squared mass of the S field is given by

$$m^2_{\text{eff},S}(h,T) = \mu_S^2 + \lambda h^2 + \Pi_S(T) \,, \tag{6.47}$$

[9]If S is colored, then the two-loop contribution from gluons can have an appreciable impact on the order of the phase transition. This is, for example, the case in the MSSM (92).

[10]This discussion presumes that S is a singlet under weak isospin. More generally, the electrically neutral component of S may acquire a VEVwithout breaking $\mathrm{U}(1)_{\mathrm{em}}$. However, unless this VEVis much less than v, it will induce unphysical corrections to electroweak precision observables. Thus, we will restrict ourselves to the case of vanishing VEV.

where $\Pi_S(T)$ is the thermal self-energy correction. In the appropriate limits, this simple extension of the SM Lagrangian can yield any one of the phase transition models classes discussed above. These are as follows:

I. Thermally (BEC) Driven. The BEC term receives a contribution $(\mu_S^2 + \lambda h^2 + \Pi_S(T))^{3/2}$. As discussed in Sec. 6.3, we must tune $\mu_S^2 \approx -\Pi_S(T_c)$. However, in this limit the zero-temperature squared mass of the S field is $-\Pi_S(T_c) + \lambda v^2$. We cannot let $\lambda < 0$, because this would cause S to acquire a VEV.

IIA. Tree-Level (Ren. Ops.) Driven. Since S cannot acquire a VEV, the only way in which tree-level terms can enhance the strength of the phase transition are if S had a VEVin the early universe and its VEVreturned to zero during the electroweak phase transition. This scenario is realized by letting $\mu_S^2 < 0$ such that S obtains a VEVin the early universe, but ensuring $\lambda v^2 > -\mu_S^2 > 0$ such that S has a vanishing VEVtoday. Once again, we find that $\lambda > 0$ is required for a SFOPT in this model class as well.

IIB. Tree-Level (Non-Ren. Ops.) Driven. The non-renormalizable operator $(H^\dagger H)^3/\Lambda^2$ may be generated by integrating out the field S. The leading order contribution to this operator is then given by λ^3/M_S^2. Since this model class relies upon $(H^\dagger H)^3$ having a positive coefficient in order to stabilize the potential against a runaway direction, we must take $\lambda > 0$.

III. Loop Driven. This model class relies upon the addition of a term to the effective potential that goes like $h^4 \ln h^2$ and its competition with the h^4 term to generate a barrier in the effective potential. The Higgs portal operators Eq. (6.46) will instead generate a term of the form $h^4 \ln(\mu_S^2 + \lambda h^2)$. Unless $|\mu_S^2| \ll |\lambda v^2|$, this term will simply scale like h^4 and there will be no competition between terms and no barrier. However, if $\lambda < 0$, then in this limit the S field

develops a tachyonic instability and acquires a VEV.

This analysis may seem to suggest that $\lambda > 0$ is generally favored by SFOPT. However, this is not the case. If we were not interested in enhancing Higgs diphoton decay, then we could achieve a SFOPT by coupling the Higgs to a singlet scalar field using the operators Eq. (6.46). Since there are no restrictions on the VEVof a singlet field, we could have found SFOPT in the *IIA. Tree-Level (Ren. Ops.) Driven* model class (see, e.g., (111)).

6.5 Summary of the Chapter

In this paper we have proposed a scheme for classifying models of the electroweak sector which may yield a strongly first order phase transition – a necessary ingredient for electroweak baryogenesis. For each model class, we investigated the impact of the data that is currently available from the LHC: 1) the discovery of a 125 GeV Higgs-like scalar, 2) the absence of a large invisible width, and 3) the absence of a universal suppression, which would indicate mixing between the Higgs and a hidden sector scalar field. We find that the mass measurement severely constraints models (such as the MSSM (91)) which drive a strongly first order phase transition with thermal loop effects[11]. The invisible decay and mixing constraints are at tension with models which rely on light singlets coupled to the Higgs.

One recurring theme of our analysis is the ubiquity of enhanced symmetry points. We find that the "optimal" limit for SFOPT often corresponds to a parameter point at which the symmetry group of the theory is extended. In the case that the group is enlarged by a continuous symmetry, either the Higgs mass constraint or the invisible decay and mixing constraints will come into play. The case of a discrete symmetry is

[11]However, it may be possible to weaken the tension between the Higgs mass measurement and the baryon asymmetry washout condition in non-standard cosmologies (232).

less restricted (176).

We have also discussed the possibility of employing the Higgs portal operator to both render the EWPT strongly first order and to account for the diphoton excess observed by ATLAS and CMS. We find that these two goals are at odds with one another: the phase transition favors a positive Higgs portal coupling whereas the diphoton enhancement favors a negative coupling. A model which can accommodate EWBG as well as fit the LHC data will most likely require two distinct new physics operators. However, it is worth noting that the diphoton excess does not have a great statistical significance, and the data remains consistent with the SM at the 75 % CL (216) or approximately 2σ (211; 217). It remains entirely possible that the particle recently discovered by ATLAS and CMS is the SM Higgs (233).

Part II

Dark Matter, Cosmological Constant, and the Electroweak Phase Transition

Chapter 7

Introduction to the Dark Side

As we have already discussed in the previous part of this manuscript, the Standard Model of particle physics fails to explain the asymmetry between matter and anti-matter in our universe. The observed baryon asymmetry of the universe, therefore provided a strong motivation for studying physics beyond the Standard Model. However, the BAU is not the only situation in which the SMcannot describe Nature in its entirety. A cosmology constructed with ingredients drawn from the SMalone is incapable of accounting for the two dominant components of our universe: dark matter and dark energy. In this chapter, we will discuss the physics of the dark side of the universe. In the subsequent chapters, we will bring our discussion back to the topic of the Higgs boson and investigate connections between dark matter, dark energy, and the electroweak phase transition.

7.1 Dark Matter

Throughout the 20^{th} century, mounting evidence suggested that the universe contains much more matter than that which can be seen in stars and galaxies. This missing,

non-luminous matter was given the name *dark matter*. Today it is known that dark matter constitutes approximately 22 % of the total energy density of the universe, roughly five times more than the fraction allotted to baryonic matter (14). Despite years of searching, dark matter particles have not been observed directly, and therefore the properties of dark matter – such as its mass and couplings to visible matter – remain undetermined, although constrainted. This uncertainty has allowed for the proliferation of dark matter models. Variants include Cold Dark Matter (234), Warm Dark Matter (235), Hot Dark Matter (236; 237), WIMPs, WIMPzillas (238), Unified Dark Matter (239), Inelastic Dark Matter (240), Quirky Dark Matter (241), Atomic Dark Matter (242), Millicharged Atomic Dark Matter (243), Bound Dark Matter (244), Asymmetric Dark Matter (245), and Dynamical Dark Matter (246; 247) – just to name a few.

We will restrict ourselves to the minimal cold dark matter (CDM) model featured in the ΛCDM concordance model of cosmology. That is, we will suppose that dark matter is a particle, which we represent by χ, that 1) interacts only weakly with visible matter (*i.e.*, it does not carry electromagnetic charge), 2) is not baryonic, 3) is stable, and 4) has mass $m_\chi \neq 0$. On cosmological scales, we can treat dark matter as a pressureless "fluid" with number density n_χ and energy density $\rho_\chi = m_\chi n_\chi$. It will be useful to quantify the amount of dark matter in the universe using the dark matter *relic abundance* defined as

$$\Omega_\chi h^2 = \frac{\rho_\chi}{\rho'_{\rm cr}} \tag{7.1}$$

where $\rho'_{\rm cr} \equiv (8\pi G_N/3)^{-1}(100\ {\rm km\,s^{-1}\,Mpc^{-1}})^2$ and G_N is Newton's gravitational constant. In the remainder of this section, we will discuss the evidence for dark matter and the freeze out process which took place in the early universe and thereby determined the cosmological dark matter relic abundance that we observe today.

Evidence for Dark Matter

There is a multitude of evidence in astrophysical and cosmological systems to support the hypothesized presence and predicted abundance of dark matter in our universe. Thus, it commonly accepted that particle dark matter exists. In the spirit of full disclosure, however, it is worth mentioning that this is only *indirect* evidence, which could perhaps be explained by some other physics, such as a modification of gravity. Moreover, there has not been a convincing signal from dark matter direct detection experiments. Nevertheless, nearly a century of evidence points toward a model of particle dark matter. Therefore, having made this disclaimer, we will speak no further of alternate scenarios.

Galactic Rotation Curves

The existence of dark matter was famously postulated by Fritz Zwicky in 1933 (248). Zwicky had applied the virial theorem to infer the total mass of the Coma galaxy cluster. Upon comparing this value with the observed amount of luminous matter in the galaxies composing the cluster, Zwicky noted the "somewhat unexpected" result: that the luminous mass was on the order of one-hundred times too small (249). He dubbed the non-luminous matter "dark matter."

Decades later, similar techniques were used to "weigh" individual galaxies as well (see, *e.g.*, (250)). The *rotation curve* of a galaxy represents the rotational velocity $V(R)$ of the matter in the galaxy as a function of distance R from the galactic center. For small R, the velocity can be inferred from the Doppler shift of starlight, whereas for larger R, where there are no stars, the velocity may instead be inferred from the 21 cm emission line (hyperfine transition) of neutral hydrogen gas (HI regions). The measured rotation curve $V(R)$ allows for a determination of the mass of the galaxy. The back-of-the-envelope calculation is performed by equating the gravitational force

on a mass m at radius R with the centripetal force,

$$\frac{GM(R)m}{R^2} = m\frac{V^2(R)}{R}\,, \tag{7.2}$$

and solving to obtain $M(R) = RV^2/G$, the mass contained within a radius R. If most of the mass of the galaxy were collected near the core, then $M(R)$ would approach a constant at large R and $V(R) \sim 1/\sqrt{R}$. However, observations of over one-thousand galaxies (251) revealed that in actuality $V(R)$ does not drop like $1/\sqrt{R}$ but remains nearly constant at large R. Since the calculation only relies upon elementary kinematics, gravitation, and electromagnetism, this observation provides strong evidence for the presence of a large *dark matter halo* surrounding the visible galaxy.

Gravitational Lensing

General relativity predicts that light passing by a massive body will be deflected, in analogy to the passage of light through an optical lens. The phenomenon was the central topic of Einstein's 1936 paper in the journal *Science* (252). The first gravitational lens, dubbed "Twin QSO," was not discovered until 1979 (253). Since the lensing is a purely gravitational effect, it provides the opportunity to measure the matter distribution directly.

Strong lensing occurs when a massive galaxy cluster in the foreground – the lens – greatly distorts the image of a background galaxy or galaxies. Just as with an optical lens, the gravitational lens may produce multiple images, which are arranged on a ring. The radius of the ring is related to the mass of the lens M by $R \propto \sqrt{M}$. This relationship allows for the measurement of mass and distribution of dark matter in the galaxy cluster. For example, in 2004 the observation of a set of four multiple images in the cluster lens Abell 2218 yielded a constraint on the cosmic matter fraction (dark plus baryonic) $\Omega_m < 0.33$ (254) However, strongly lensed systems with multiple

images are rare. Moreover, when they do occur, the lensing may be due to the dense baryonic core instead of the sparse dark matter, as in the case of the famous Einstein cross system (255).

Weak lensing, on the other hand, provides a means of probing the spatial distribution of diffuse dark matter in a galaxy cluster. In this scenario, a field of galaxies in the background becomes lensed by the inhomogenous distribution of dark matter in a foreground object, such as a galaxy cluster. In order to infer the distribution of dark matter, a sky survey must measure the ellipticities and magnitudes of millions of galaxies over a small patch of sky. The lensing introduces correlations between the orientation and brightness of nearby galaxies in the field. A statistical analysis allows one to extract the distribution of matter. Weak lensing is typically employed in conjunction with a measurement of the visible matter in order to ascertain the deficit associated with dark matter.

Bullet Cluster

Perhaps the most striking evidence for dark matter, as well as a brilliant demonstration of the utility of weak lensing, is the *Bullet Cluster*. In 2003, the group (256) reported the high-velocity merger of two galaxy clusters, dubbed the *Bullet Cluster*. Imaging the bullet cluster reveals a spatial separation between the sources of galactic starlight in the visible and the regions of hot gas in the X-ray. This is consistent with a two-component model of the system, in which the stellar component is treated as pressureless and the X-ray emitting component is treated as a fluid-like. Moreover, the gas displays a distinct bow shock, suggestive of the recent collision. Using weak lensing, the distribution of matter may be inferred directly. A 2006 analysis (257), revealed that the matter distribution more closely follows the distribution of galaxies than the distribution of X-ray emission, and they identified the spatial offset as an 8σ

effect. This is consistent with the hypothesis that the two clusters contained a large amount of non-luminous, pressureless matter. For most cosmologists (but not all (258)), the Bullet Cluster constitutes sufficient evidence for the existence of particle dark matter.

CMB Power Spectrum

As we have discussed in the context of the BAU, the CMB power spectrum provides the best probe of the composition of the universe on cosmological scales. During the formation of the baryon acoustic oscillations, dark matter acted like a driving force by sourcing the gravitational potential wells in which the baryon-photon plasma would oscillate. Thus, the CMB power spectrum that we see today holds information about the amount of dark matter present in the universe. Precise measurements of the CMB by the WMAP satellite (71) allow us to determine $\Omega_c = 0.222 \pm 0.026$.

Dark Matter Freeze Out

In the ΛCDM cosmological model, it is assumed that the dark matter present in the universe today is a *thermal relic* which underwent the process of *freeze out* in the early universe.

The freeze out calculation allows us to relate the relic abundance of dark matter $\Omega_\chi h^2$, which may be inferred from the astrophysical and cosmological systems discussed above, with properties of the dark matter particle, which can vary significantly from model to model. In this way, even without a direct detection of the dark matter particle, it is possible to strongly constrain models of dark matter. In this section, we will discuss the dark matter freeze out calculation (see, e.g., (72)).

We suppose that the dark matter is weakly coupled to visible matter. This assumption ensures that at a sufficiently high temperature T in the early universe, the

dark matter was in thermal equilibrium with the plasma and the number density of dark matter particles $n_\chi(T)$ remained very nearly equal to the equilbrium number density $n_\chi^{(\mathrm{eq})}$. We further assume that the dark mater was non-relativistic (cold) at the time of freeze out. This lets us write the dark matter equilibrium number density as

$$n_\chi^{(\mathrm{eq})}(T) = \frac{g}{2\pi}(m_\chi T)^{3/2}\, \exp\big[-m_\chi/T\big] \tag{7.3}$$

where g is the number of dynamical degrees of freedom, which depends on the spin and quantum numbers of χ. As the universe expands and its temperature decreases, n_χ must fall exponentially quickly in order to remain equal to $n_\chi^{(\mathrm{eq})}$. The reduction in the number density of dark matter is primarily accomplished by the annihilation of dark matter into SM particles

$$\chi + \chi \to \mathrm{SM} + \mathrm{SM}\,. \tag{7.4}$$

Since two DM particles must find one other in order to annihilate, the rate at which this process occurs should scale like $(n_\chi)^2$. This rate falls exponentially rapidly, and eventually it become smaller than the rate of expansion of the universe, given by the Hubble parameter H. At this point, DM annihilations must cease and we say that the dark matter has frozen out. Since we have also assumed that the DM particles are stable, the number of DM particles in the universe just after freeze out is the same as the number today.

We calculate the relic abundance of dark matter by solving the thermally averaged Boltzman equation in the presence of an expanding universe. Working in the homogenous, isotropic Friedmann-Robertson-Walker (FRW) metric, this equation may be written as

$$a^{-3}\frac{d(n_\chi a^3)}{dt} = -\left\langle \sigma v \right\rangle \left[(n_\chi)^2 - \left(n_\chi^{(\mathrm{eq})}\right)^2\right] \tag{7.5}$$

where a is the FRW scale factor and $\langle \sigma v \rangle$ is the thermally averaged dark matter annihilation cross section. To proceed, we make a series of variable changes. First define $Y_\chi \equiv n_\chi / s$ where $s = (2\pi^2/45) g_{*S}(T) T^3$ is the entropy density and $g_{*S}(T)$ counts the number of relativistic species at temperature T. In general, $g_{*S}(T)$ varies with temperature from a value of approximately 106.75 in the early universe to approximately 3 today. However, assuming that freeze out occurs rapidly compared to the time scale on which other species are becoming non-relativistic, we can approximate g_{*S} as a constant. Next, we eliminate t in favor of a using $da/dt = aH$ where H is the Hubble parameter that represents the expansion rate of the universe. Provided that freeze out occurs during the radiation dominated era of the universe, H is given by $H = \sqrt{(8\pi G_N/3)(\pi^2/30) g_*(T) T^4}$ where $g_* \approx g_{*S}$. We eliminate a in favor of T using the fact that the entropy per comoving volume $S = sa^3$ is conserved. Finally we introduce the dimensionless variable $x = m_\chi / T$. After the dust settles, we find

$$\frac{dY_\chi}{dx} = -\frac{\lambda}{x^2} \left[(Y_\chi)^2 - \left(Y_\chi^{(\mathrm{eq})} \right)^2 \right] \tag{7.6}$$

where

$$\lambda(x) \equiv \frac{\langle \sigma v \rangle \, s(x) x}{H(x)} \, . \tag{7.7}$$

In general, $\langle \sigma v \rangle$ will depend on temperature, but assuming that the dominant annihilation channel is through the s-wave, we can approximate $\langle \sigma v \rangle \sim x^0$ as a constant. Since we also have the scaling relations $H \sim x^{-2}$ and $s \sim x^{-3}$, we see that $\lambda \sim x^0$ is approximately constant.

We solve for the relic abundance long after freeze out by integrating Eq. (7.6). We suppose that freeze out takes place "abruptly" at $x = x_f$, and that after freeze out the equilbrium term is exponentially suppressed and negligible. Dropping this term,

we obtain the solution by integrating from x_f to $x = \infty$

$$\frac{1}{Y_\chi(x=\infty)} - \frac{1}{Y_\chi(x=x_f)} = \frac{\lambda_f}{x_f}\,, \tag{7.8}$$

where $\lambda_f = \lambda(x_f)$. After freeze out occurs, residual annihilations cause Y_χ to decrease further. This allows us to neglect the $Y_\chi^{-1}(x_f)$ term. Moreover, we have assumed that various quantitites are constant or scale in a particular way, but these assumptions break down long after freeze out. Thus, $Y_\chi(x = \infty)$ does not represent the relic abundance today, but instead the abundance long after freezeout but still early enough that our assumptions are valid. Thus, we have

$$Y_\chi(\text{after f.o.}) \approx \frac{x_f}{\lambda} \approx \frac{H(x_f)}{\langle\sigma v\rangle\, s(x_f)}\,. \tag{7.9}$$

We can relate this to the relic abundance Eq. (7.1) as

$$\begin{aligned}
\Omega_\chi h^2 &= \frac{\rho_\chi(\text{today})}{\rho'_{\text{cr}}} \\
&= m_\chi Y_\chi(\text{today}) s(\text{today}) \left(\rho'_{\text{cr}}\right)^{-1} \\
&= m_\chi \frac{\sqrt{\frac{8\pi G}{3}} T_f^2}{\langle\sigma v\rangle} \frac{g_{*S}(\text{today}) T_0^3}{g_{*S}(x_f) T_f^3} \left(\rho'_{\text{cr}}\right)^{-1} \\
\Omega_\chi h^2 &= x_f T_0^3 \langle\sigma v\rangle^{-1} \frac{g_{*S}(\text{today})}{g_{*S}(x_f)} \sqrt{\frac{8\pi G}{3}} \left(\rho'_{\text{cr}}\right)^{-1}\,.
\end{aligned} \tag{7.10}$$

Finally our work has paid off; Eq. (7.10) is a very revealing equation. We can see that the relic abundance is inversely related to the annihilation cross section. This means that dark matter which interacts more strongly with the SM will remain coupled to the plasma longer and will consequently have a smaller relic abundance. Conversely, models which predict too small of a coupling between the dark matter and SM particles will generate too great a relic abundance. We also see that $\Omega_\chi h^2$ is only indirectly dependent on m_χ the dark matter mass. One can show that $x_f \approx 1/10$ is only logarithmically sensitive to m_χ (72). In this way, the freeze out calculation provides a

robust prediction of the relic abundance for a given model. In the subsequent chapters, we will explore how the various assumed used in this derivation break down if freeze out occurs during the electroweak phase transition, and we will investigate the resulting relationships between parameters of the EWPT and the dark matter relic abundance.

7.2 Dark Energy & the Cosmological Constant

We have already seen that our universe is full of surprises and challenges – the perplexing baryon asymmetry, the interesting origin of mass and electroweak symmetry breaking, and the mysterious abundance of dark matter. But, perhaps the most remarkable surprise of all is that for the past few billion years, the rate of expansion of the universe has been accelerating. This is quite astounding, in light of the prediction that if the dominant source of energy in the universe were dark matter, then the induced gravitational attraction would cause the expansion to decelerate. The cosmic acceleration tells us that the dominant source of energy in the universe is, in fact, something else all together. The term *dark energy* was introduced as a "catch all" to refer to whatever the origin of cosmic acceleration may be. The extent of our knowledge about dark energy is incredibly limited, and can be summarized as follows: most of the energy density of the universe arises from a "substance" with an energy density $\rho_\Lambda \approx \frac{3}{4}\rho_{\rm cr}$ and an equation of state $w \approx -1$ that are, as best as we can tell, homogenous and static. Needless to say, dark energy is very poorly understood.

Evidence for Accelerated Expansion

The expansion of the universe was discovered long before it was known that the expansion is accelerating. In 1929, Hubble used distance and velocity data for 24

nearby galaxies (out to 2 Mpc) to infer that their their recession velocity grew linearly with distance from the Earth (259). This is formulated as Hubble's law $v = H_0\ell$ where H_0 is the recession rate (Hubble's constant) and ℓ is the distance between the Earth and the galaxy. With the available data, Hubble estimated $H_0 \approx (50-60)\,\mathrm{km/s/Mpc}$. Today, Hubble's constant is measured directly via the magnitude-redshift relation of 240 low-redshift ($z < 0.1$) SNe Ia $H_0 = (74.2 \pm 3.6)\,\mathrm{km/s/Mpc}$ (260) and improved to $H_0 \approx (70.4 \pm 1.3)\,\mathrm{km/s/Mpc}$ (71) with CMB data.

The first evidence for accelerated expansion (and thereby for dark energy) began to appear in the early 1990's. At that point, the matter abundance was estimated to be $\Omega_m \sim 0.15 - 0.4$ through galaxy clustering surveys (261), but inflationary models predicted (and the homogeneity of the CMB later confirmed) that $\Omega_{\mathrm{tot}} \sim 1$ (i.e., flat universe). There needed to be an undiscovered energy component to make up the difference. As early as 1990 (262–264), cosmologists began to suggest that the missing energy may be in the form of a cosmological constant. The breakthrough came in 1998 when Riess (265) & Perlmutter (266), et. al., measured the distance to high redshift ($z \approx 0.5$) Type Ia supernovae and used this observation to infer that the expansion of the universe was accelerated. Today, a combination of supernovae data as well as measurements of the cosmic microwave background, baryon acoustic oscillations, and measurements of H_0 provide good measurements of the parameters of dark energy: $\rho_\Lambda = (0.728 \pm 0.015)\rho_{\mathrm{cr}}$ and $w = (-1.10 \pm 0.14)$ (71). Note that this energy density corresponds to $\rho_\Lambda \approx 10\mathrm{meV}^4$. For a historical review of the evidence for accelerated expansion, see (267).

The Cosmological Constant

In the two decades since the discovery of dark energy, theorists have remained very active. Many models have been proposed which attempt to model the dark energy

as the energy density of a scalar field (e.g., (268; 269)) analogous to inflationary models. Other models seek to unify dark matter and dark energy in a single framework (270; 271) or to implement dark energy as a modification to gravity (272). However, the oldest and most minimal model of dark energy is still the *cosmological constant* (CC). In 1917, Einstein attempted to create a theory of a static universe by adding a term to the gravitational action of the form

$$S_\Lambda = -\frac{1}{16\pi G_N}\int d^4x\sqrt{-g}(2\Lambda) \tag{7.11}$$

where Λ is the cosmological constant. Although Hubble's observation of the expansion of the universe obviated the need for a cosmological constant, it has been revived to model the accelerated expansion of the universe. The action S_Λ may arise from the energy-momentum tensor

$$(T_\Lambda)_{\mu\nu} = \rho_\Lambda \delta_{\mu\nu} \tag{7.12}$$

where $\rho_\Lambda = \Lambda/(8\pi G_N)$. As a phenomenological model, Λ is a free parameter, and may be chosen appropriately to reproduced the observed value of $\rho_\Lambda \approx 10\text{meV}^4$. Moreover, since $T_{\mu\nu}$ is proportional to $\delta_{\mu\nu}$, the equation of state of the cosmological constant is precisely $w = -1$. In this way, the CC model of dark energy has been able to fit all available data.

A negative equation of state is very unusual since it implies that the pressure $p_\Lambda = w\rho_\Lambda$ is negative. As the universe expands, instead of doing work and loosing energy, the dark energy exerts a negative work and thereby gains energy. In fact for $w = -1$, it gains just enough energy to compensate for the expansion such that the energy density remains fixed. To understand the behavior of a DE dominated universe, by solving Friedmann's equation

$$H^2 = \frac{8\pi G_N}{3}\rho_\Lambda \tag{7.13}$$

to find

$$a(t) = a_0 \exp\left[t\sqrt{\frac{8\pi G_N}{3}\rho_\Lambda}\right]. \tag{7.14}$$

We see now that not only is the expansion accelerated, but it is growing exponentially. This reveals the fate of our own universe: the exponential expansion phase has already begun, and if DE truly is a cosmological constant, the expansion will continue indefinitely.

CC Problem and Fine Tuning

Although the CC model of dark energy provides an excellent fit to all available data, it suffers from a major theoretical shortcoming. From the phenomenological perspective, we think of the CC as a homogenous, static, energy density with equation of state $w = -1$. However, we would also like to have an understanding of the physical origin of the cosmological constant as well. In the context of quantum field theory, we can understand the CC as the energy density of the vacuum state, and, moreover, we can even predict the value of the cosmological constant. In fact, we have already encountered this calculation. The vacuum energy is just the non-thermal part of the effective potential, which we evaluated in Chapter 3 by summing the "vacuum bubble graphs" shown in Figure 3.6. The non-thermal contribution to these graphs (which we did not write down explicitly earlier) is given by

$$\rho_{\text{vac}} \sim \int \frac{d^4q}{(2\pi)^4} \ln\left(q^2 + M^2\right) \tag{7.15}$$

where M is the mass of the particle in the loop. The divergence of this integral is problematic but not all together unexpected. We had no reason to think that our QFT would be an accurate model of the physics at very high energies, because it does not – for instance – incorporate gravity, which we anticipate to be relevant at

energies above the Planck scale M_P. Thus, cutoff the integration at $q < M_P$, and find that the integral evaluates to $\rho_{\text{vac}} \sim M_P^4 \approx 10^{73}$ GeV^4. Comparing this with the measured value, $\rho_\Lambda \approx 10$ meV$^4 \approx 10^{-47}$ GeV^4, we find that they disagree by 120 order of magnitude. This enormous discrepancy between theory and observation is known as the *cosmological constant problem*. The history of the problem was discussed by Weinberg in 1988 (273), even before the CC was fully revived in the 1990's.

Resolving the CC problem is not an easy task. One proposed solution is that a cancellation occurs between the enormous ρ_{vac} predicted by QFT and another enormous number ρ_{tune} which is *finely tuned* to leave behind the tiny value of $\rho_\Lambda = \rho_{\text{vac}} - \rho_{\text{tune}}$ that we measure. Such a cancellation seems astronomically unlikely (for most definitions of unlikely) and marginally unphysical. However, it is very fortunate that our cosmological constant is finely tuned, because if its value were much larger or smaller, we would not find ourselves in a universe with conditions hospitable to life. This has lead some to invoke the *anthropic principle*, that is, we find ourselves in this unimaginably rare universe, because in any other universe, we would not be around to talk about it. At face value, the anthropic principle is somewhat unpalatable and seems like a "cheat." However, in order to justify the anthropic principle, some people have turned to an idea known as the *string landscape* (274). In the type IIB limit of string theories, each compactification of the internal space is associated with a different vacuum state of the theory, and there are on the order of 10^{500} such vacua. Although the physical parameters of each of the vacua are not known, it is reasonable that with such a large number of possible vacuum state, one of them may have conditions similar to our own universe. Moreover, if our universe entered a phase of *eternal inflation* (275; 276), then it is reasonable that each of the vacua will have been populated at some point. In this way, a combination of the anthropic principle, string landscape, and eternal inflation may be able to explain why the cosmological

constant is so finely tuned.

Chapter 8

Probing the Cosmological Constant and Phase Transitions with Dark Matter

The Standard Model and its extensions predict multiple phase transitions in the early universe. In addition to the electroweak phase transition, one or several of these could occur at energies close to the weak scale. Such phase transitions can leave their imprint on the relic abundance of TeV-scale dark matter. In this paper, we enumerate several physical features of a generic phase transition and parameterize the effect of each on the relic abundance. In particular, we include among these effects the presence of the scalar field vacuum energy and the cosmological constant, which is sensitive to UV physics. Within the context of the Standard Model Higgs sector, we find that the relic abundance of generic TeV-scale dark matter is affected by the vacuum energy at the order of a fraction of a percent. For scalar field sectors with strong first order phase transitions, an order one percent apparent tuning of coupling constants may allow corrections induced by the vacuum energy to be of order unity.

This work was performed in collaboration with Daniel Chung and Lian-Tao Wang. It was published in the journal Physical Review **D** in August of 2011 (177).

8.1 Introduction to the Chapter

Phase transitions (PTs) are expected to be generic in the early universe (277). The high temperature environment gives rise to significant corrections to the vacuum structure, and symmetries which are broken in the universe today can be restored at earlier times (59–61). The Standard Model (SM) predicts early universe phase transitions in both the electroweak and QCD sectors. Beyond the SM, it is well-known that additional degrees of freedom can modify the dynamics of the electroweak phase transition significantly (92; 94–97; 103; 106; 109–111; 139; 278–285). Furthermore, because almost all scenarios beyond the SM have extended symmetries, an even richer thermal history is expected in general (e.g., (60; 180; 286–296)).

Most phenomenologically viable, cosmological PTs do not leave significant observable signals today. The successful and precisely measured theories of big bang nucleosynthesis, cosmic microwave background, and large scale structure formation strongly constrain late time PTs. At earlier stages of the cosmic evolution, thermal equilibrium erases most of the traces of PTs. Therefore, particle species which decouple early offer us perhaps the best probe PTs in the early universe. Among candidate particles, possibly the most obvious is the TeV-scale dark matter (DM), which is expected to freeze out of thermal equilibrium around $O(10-100)$ GeV. The successful prediction of its relic abundance, sometimes referred to as the WIMP miracle, is considered to be one the most important hints of new physics at the TeV-scale. Such a scenario is expected to be thoroughly probed at the LHC.

In this paper, we assess the sensitivity with which DM may probe the physics of

PTs by exploring how PTs occurring nearly coincident with freeze out can modify the relic abundance calculation and alter the predicted relic density. In PTs for which supercooling is non-negligible, we find that several competing effects contribute to an overall shift in the DM relic abundance (as compared to the usual calculation without a PT). Two of these effects, the decoupling of non-relativistic species and the vacuum energy contribution to the Hubble expansion rate, tend to increase the relic abundance, while the entropy produced by the PT tends to decrease it. The principal result of this paper is summarized in Eq. (9.47), and the central discussion will emphasize the role of vacuum energy during the PT (297), since that is the most novel aspect of this letter as compared to previous studies. We find that a parametric tuning of order one percent can lead to an order unity dark matter abundance shift due to the presence of vacuum energy, assuming that a tuning of the cosmological constant sets the vacuum energy today. In such situations, it may be possible to use DM as a probe of vacuum energy during the early universe by measuring the DM properties at terrestrial experiments and making mild assumptions about cosmology and UV completions of the effective field theory.

This work is related to past papers which discuss moduli dilution, such as (298) (and hundreds of inflationary papers), in that we calculate how the PT effects (including the vacuum energy) alter the relic abundance.[1] However, unlike the present work, most of these papers do not consider the case of a PT which nearly coincides with freeze out, nor do they consider the case of a low scale (e.g., electroweak scale) PT with electroweak scale vacuum expectation values. As in (179; 302), our calculation incorporates the possibility that the dark matter annihilation cross section may change after the freeze out, and as in (178), we estimate the dilution of dark matter

[1]It is also related to papers such as (299–301) and many others which consider the change in the relic density due to a change in the equation of state during the freeze out process. Instead of listing all papers, interested readers can consider finding citations to and references within these papers.

due to a release of entropy at the PT. However, we also include additional features of the PT such as the changing vacuum energy.

This paper is organized as follows. In Sec. 8.2, we derive a generic parameterization with which one can discuss the effects of a PT on the DM relic abundance. In Sec. 8.3, we use this parameterization to estimate the correction to the relic abundance in two toy models in which a real scalar field experiences a phase transition. In Sec. 9.5 we summarize and briefly discuss which aspects of a generic model could be favorable for enhancing the effect of vacuum energy on the relic abundance. Being a letter, we restrict ourselves to the highlights.

Throughout the paper, we work in the FLRW spacetime $ds^2 = dt^2 - a^2(t)|d\mathbf{x}|^2$ in which $a(t)$ is a monotonically increasing function of t.

8.2 General Framework

In this section, we discuss the various ways in which phase transitions can affect the relic density, and we provide a general parameterization which is useful for analyzing specific models.

Integrating the thermally averaged Boltzmann equation, we obtain the number density of dark matter today ($a = a_0$ and $t = t_0$)

$$n_X(t_0) = x_0^{-3}\left(\int_0^{\ln x_0} \frac{d\ln(x)}{H}\,\langle\sigma v\rangle\right)^{-1}, \qquad x = \frac{a}{a_f}, \quad x_0 = \frac{a_0}{a_f} \tag{8.1}$$

where a_f corresponds to the scale factor at the time of the freeze out. We define the fractional deviation of the relic abundance as

$$\delta n_X(t_0) = \frac{n_X(t_0)}{n_X^{(U)}(t_0)} - 1 \tag{8.2}$$

where $n_X^{(U)}(t_0)$ is the "usual" relic density that one finds assuming that the PT does not occur. In Eq. (9.9), the quantities that will be affected by the PT are the Hubble

expansion rate $H(a)$, the thermally averaged cross section $\langle \sigma v \rangle$ (also a function of a), and the dilution factor $x_0^{-3} = (a_f/a_0)^3 \ll 1$, which accounts for the expansion of the universe from freeze out until today (related to $T(a)$).

Suppose that a PT occurs after the time of the freeze out. This PT can affect $H(a)$ (though the energy density) in three ways: exotic energy, reheating, and decoupling. First, the PT is a change in the vacuum state and is typically accompanied by a decrease in the vacuum energy. For all (cosmological) intents and purposes, this vacuum energy behaves as a cosmological constant (CC). Speaking more generally, we can collectively refer to the vacuum energy, cosmological constant, and any other non-thermal sources of energy (e.g., quintessence) as "exotic energy." We assume that the exotic energy density can be written as $\rho(x) = \rho_{\rm ex}\kappa(x)$ with

$$\kappa(x) \approx \Theta((1+\delta) - x) + \Theta(x - (1+\delta)) \left(1 - \frac{\Delta\rho_{\rm ex}}{\rho_{\rm ex}}\right) \kappa_2(x)\,, \tag{8.3}$$

where $\Theta(z)$ is a step function and $\delta \equiv \frac{a_{PT}}{a_f} - 1 \lesssim 1$ quantifies the delay between freeze out and the phase transition. During the phase transition, the exotic energy decreases by $\Delta\rho_{\rm ex} > 0$, and the step function approximation corresponds to restricting ourselves to only phase transitions that occur on a time scale much shorter than $1/H$. Such short time scale phase transitions are expected to be generic for models in which the thermal bounce action has a strong temperature dependence.[2] In the case that the exotic energy is simply composed of vacuum energy plus a tuned cosmological constant,[3] we have $\Delta\rho_{\rm ex} \approx 0$ if the phase transition is of the second order or a smooth cross over and $\Delta\rho_{\rm ex} \approx \rho_{\rm ex}$ if the phase transition is first order with large supercooling. In the case $\Delta\rho_{\rm ex} \neq \rho_{\rm ex}$, the behavior of $\kappa_2(x)$ can parameterize quintessence dynamics which we assume decreases approximately as $(x\, a_f/a_{PT})^{-n_d}$ where n_d is a computable

[2] For a recent discussion of situations with a longer time scale transitions, see for example (303).

[3] This has been considered as an acceptable possibility (39; 304), and it is a consequence of recently proposed string landscape scenario (305).

model dependent parameter. We focus on phase transitions that can be parameterized by a weakly coupled scalar field description.

The remaining ways in which a PT can affect $H(a)$ are via the radiation energy density. From energy conservation, the change in exotic energy $\Delta\rho_{\rm ex}$ must be compensated by a release of radiation energy, or equivalently, a reheating with entropy release Δs. In addition, generically particle masses may depend upon the scalar field vacuum expectation value (VEV) and may increase during the phase transition (e.g., this is the case in the SM electroweak phase transition). The heavier degrees of freedom can become non-relativistic and decouple. Consequently, the remaining relativistic species have a relatively lower energy density. We can parameterize this decoupling effect by writing the effective number of degrees of freedom for radiation energy g_E and entropy g_S as

$$g_{E/S}\,(x) = g_{E/S}(1) - h(x) \tag{8.4}$$

$$h(x) = \frac{7}{8} N_{PT}\,\Theta(x-(1+\delta)) + \frac{7}{8} N f(x)\,, \tag{8.5}$$

where (N_{PT}) N represents the number of fermionic degrees of freedom which have (non-) adiabatically decoupled, and $f(x)$, which rises from 0 to 1, is given by Eq. (9.125).

Treating all of the aforementioned effects as small perturbations and using $T(a)$ from Eq. (9.121), the modification to $H(a)$ can be expressed as

$$H \approx H_R^{(U)}(x)\left[1 + \frac{\epsilon_1}{2} x^4\,\kappa(x) + \frac{2}{3}\epsilon_2\Theta(x-(1+\delta)) + \frac{\epsilon_{31}\Theta(x-(1+\delta)) + \epsilon_{32} f\,(x)}{6}\right] \tag{8.6}$$

where

$$H_R^{(U)}(x) \equiv \frac{T_f^2}{3\,M_p\,x^2}\sqrt{\frac{\pi^2}{10}\,g_E(T_f)} \tag{8.7}$$

is the "usual" Hubble parameter in the absence of a PT, T_f is the temperature at freeze out, and

$$\epsilon_1 \equiv \frac{\rho_{\rm ex}}{\frac{\pi^2}{30} g_E(T_f)\, T_f^4} = \text{fractional energy of the exotic during freeze out} \tag{8.8a}$$

$$\epsilon_2 \equiv (1+3\,\delta)\,\frac{\Delta s}{\frac{2\pi^2}{45} g_S(T_f)\, T_f^3} = \text{fractional entropy increase during PT} \tag{8.8b}$$

$$\epsilon_{31} \equiv \frac{\frac{7}{8} N_{PT}}{g_E(T_f)} = \text{ fractional decoupling degrees of freedom during PT} \tag{8.8c}$$

$$\epsilon_{32} \equiv \frac{\frac{7}{8} N}{g_E(T_f)} = \text{ fractional decoupling degrees of freedom} \tag{8.8d}$$

are small, dimensionless quantities.

Furthermore, if the dark matter is coupled to the scalar sector directly, a PT in the scalar sector may alter the annihilation cross section $\langle \sigma v \rangle$. This effect can be parameterized by

$$\langle \sigma v \rangle = \langle \sigma v \rangle^{(U)} \Big(1 - \epsilon_4\, \Theta(x - (1+\delta)) \Big) \qquad \text{with} \qquad \epsilon_4 \equiv -\frac{\Delta_\sigma}{\langle \sigma v \rangle^{(U)}}\,. \tag{8.9}$$

Since the derivation of Eq. (9.9) assumes that the dark matter is decoupled after T_f, we will assume that $\epsilon_4 \gtrsim 0$ in order to prevent re-thermalization due to an increase $\langle \sigma v \rangle$.

Finally, we turn our attention to the dilution factor x_0^{-3}. Phase transitions occurring close to the freeze out can change the Hubble expansion rate, which in turn can cause dark matter to freeze out earlier or later. We can parameterize this effect by approximating the freeze out temperature as

$$T_f \approx \frac{m_X}{\ln A} \left[1 + \frac{\epsilon_1}{2} \left(\frac{1}{\ln A} + O\left((\ln A)^{-2} \right) \right) \right] \tag{8.10}$$

where

$$A \equiv \frac{N_{DM} 3\sqrt{5} M_p \sqrt{m_X T_f} \langle \sigma v \rangle}{4\pi^{5/2} \sqrt{g_E(T_f)}} \sim \exp\big[[]20\big]\,, \tag{8.11}$$

m_X is the dark matter mass, and N_{DM} counts the real dynamical degrees of freedom of the dark matter. By also taking into account the effect of a late time entropy release associated with the PT, we obtain

$$x_0 = \left.\frac{a_0}{a_f}\right|_{\rm usual} \times \left[1 + \frac{\epsilon_1}{2}\frac{1}{\ln A} + \frac{\epsilon_2}{3}\right] \tag{8.12}$$

where

$$\left.\frac{a_0}{a_f}\right|_{\rm usual} \equiv \left(\frac{g_S(T_f)}{g_S(T_0)}\right)^{1/3} \frac{m_X}{T_0}\frac{1}{\ln A} \tag{8.13}$$

is the "usual" dilution factor in the absence of a PT, and T_0 is the temperature today. In this paper we assume that the PT described by Eq. (9.19) is the last PT that generates appreciable entropy, but one can easily generalize Eq. (8.13) to accommodate later PTs that generate more entropy.[4]

Putting everything together, we obtain a general parameterization of the changes to the dark matter relic abundance which are induced by a PT:

$$\delta n_X(t_0) = c_1\,\epsilon_1 + c_2\,\epsilon_2 + c_{31}\,\epsilon_{31} + c_{32}\,\epsilon_{32} + c_4\,\epsilon_4 \tag{8.14}$$

where the coefficients

$$c_1 \equiv \frac{1}{2}\left(\delta + \frac{(1+3\delta)}{n_d - 3}\left(1 - \frac{\Delta\rho_{\rm ex}}{\rho_{\rm ex}}\right)\right) - \frac{3}{2}\frac{1}{\ln A} \tag{8.15a}$$

$$c_2 \equiv -\frac{1}{3}(1+2\delta) \tag{8.15b}$$

$$c_{31} \equiv \frac{1}{6}(1-\delta) \tag{8.15c}$$

$$c_{32} \equiv \frac{1}{6}\int_1^{a_0/a_f|_{\rm usual}} \frac{dx}{x^2} f\,(x) \tag{8.15d}$$

$$c_4 \equiv 1 - \delta \tag{8.15e}$$

are order one numbers that account for the delay between freeze out and the PT (recall $\delta = a_{PT}/a_f - 1 \gtrsim 0$). Note that c_{32} receives most of contributions from

[4] In particular, we assume that QCD phase transition is not a significant source of entropy (306).

near the freeze out temperature. The usefulness of this parameterization is that it is general enough to classify most phase transitions that can affect the DM relic abundance. This is one of the main results of this paper.

8.3 Phase transition effects as a function of Lagrangian parameters

In the section, we discuss how the parameters of a scalar field theory map to the freeze out modifying effects discussed in the previous section. In particular, we focus on a generic real scalar field for which the one-loop thermal effective potential is well-approximated by

$$V_{\rm eff}(\phi, T) \approx \rho_{\rm ex} + \frac{1}{2}M^2\phi^2 - \mathcal{E}\,\phi^3 + \frac{\lambda}{4}\phi^4 + c\,T^2\phi^2 \tag{8.16}$$

where $M^2, \mathcal{E}, \lambda$, and c are free parameters.[5] This can be viewed as the effective description of the dynamics of a large class of PTs with a tuned cosmological constant. This simple description contains all the information that is necessary to discuss the vacuum energy contribution ($c_1\epsilon_1$) and reheating contribution ($c_2\epsilon_2$) to $\delta n_X(t_0)$. The contributions from the decoupling ($c_{31}\epsilon_{31}$ and $c_{32}\epsilon_{32}$) depend on additional details of the model and, as we will see, they have the dominant effect on the DM abundance. Therefore, as far as we are concerned with the mapping of Lagrangian parameters to $c_i\epsilon_i$, we will focus our discussion on just $c_1\epsilon_1$ and $c_2\epsilon_2$. Here, we also follow the traditional abuse of language in classifying the cosmological phase transitions as first

[5] In order to treat c as a free parameter, we must suppose that the ϕ-sector is coupled to another sector, call it sector X, which is not strongly constrained phenomenologically. The interaction between ϕ and sector X can then be considered a nearly a free parameter and generates the thermal mass cT^2. For instance, suppose a Yukawa coupling $\mathcal{L} \ni y\phi\bar{\psi}\psi$ where ψ is a spin-1/2 X-sector field with N dynamical degrees of freedom, and then $c \approx Ny^2/48$. E.g., to obtain $c \approx 0.1$ one needs $y \approx 1.1$ if $N = 4$ (Dirac fermion) and $y \approx 0.6$ if $N = 12$. Moreover, the X-sector particles must be lighter than the PT temperature. Otherwise, Boltzmann suppression drives $c \to 0$.

order or second order dependent on whether or not (transient) bubbles are involved during changes in the vacuum determining the 1-particle state.

$\mathcal{E} = 0$, "second order" phase transition

We first restrict our analysis to the case of $\mathcal{E} = 0$. In this limit there is a $\mathbb{Z}_2$ symmetry, and the finite temperature effective potential can be written as

$$V_{\text{eff}}(\phi, T) \approx \frac{\lambda}{4}\left(\phi^2 - v_\phi^2\right)^2 + c\,T^2\phi^2, \tag{8.17}$$

where $v_\phi = \sqrt{-M^2/\lambda}$ is the VEV in the $\mathbb{Z}_2$ broken phase at $T = 0$. Because there is no cubic term, no sub-horizon bubbles are involved as the vacuum changes from $\phi = 0$ to $\phi = v_\phi$ at the PT.[6] The temperature at the beginning of the PT can be approximately mapped to the Lagrangian parameters as $(T_{PT}^-)^2 = \frac{\lambda}{2c}v_\phi^2$. By requiring that the exotic energy be zero today when $T = 0$, we find the exotic energy at the time of the phase transition to be

$$\rho_{\text{ex}} = V_{\text{eff}}(0, 0) = \frac{\lambda}{4}v_\phi^4 = \frac{c^2}{\lambda}(T_{PT}^-)^4. \tag{8.18}$$

Therefore using Eqs. (9.26a) and (9.48a) the exotic energy contribution is given by (for $\delta < 1$)

$$c_1\epsilon_1 \approx \frac{\delta}{2g_E}\frac{c^2}{\lambda} \sim \frac{1}{10}\frac{1}{g_E}c^2\frac{v_\phi^2}{m_\phi^2} \tag{8.19}$$

where $m_\phi^2 = 2\lambda v_\phi^2$ is the approximate scalar mass in the $\phi = v_\phi$ vacuum, and typically $g_E \gtrsim 100$.

In the minimal scenario of the SM supplemented by a DM sector, one finds $c_{\text{SM}}^2/\lambda_{\text{SM}} \approx 0.28$ where c_{SM} is dominated by the top Yukawa and does not take into account the coupling of DM to the Higgs sector. If electroweak symmetry breaking

[6] Horizon sized domain walls do form, however (180).

occurs soon after the dark matter freeze out, Eq. (8.19) allows us to estimate that the DM relic abundance will experience a fractional change at the order of 10^{-3} due to each of the CC effect. Moreover, soon after the electroweak phase transition, the heavy quarks decouple and $N \sim 20$ fermionic degrees of freedom are lost from the tally of relativistic species. Consequently, the ratio

$$\frac{c_1\epsilon_1}{c_{32}\epsilon_{32}} \sim -\frac{c^2}{\lambda}\frac{1}{N} \lesssim 1 \tag{8.20}$$

is small, and we expect that the shift in the relic abundance is dominated by the decoupling of these heavy degrees of freedom.

In the SM, the exotic energy effect is subdominant, but Eq. (8.19) provides a guide to constructing models with enhanced $c_1\epsilon_1$. This term can be made larger if $v_\phi^2/m_\phi^2 \gg 1$, which could be realized by invoking fine tuning or some additional symmetry to generate a flat potential. Alternatively, one could contrive a model in which $\rho_{\rm ex} \gg T_f^4 \geq (T_{PT}^-)^4$ and thereby enhance ϵ_1 directly. Such a scenario can be naturally realized if supercooling occurs, as in the case of a "first order" PT. We now turn our attention to this scenario.

$\mathcal{E} \neq 0$, supercooling and "first order" phase transition

At $T = 0$, the general potential in Eq. (9.68) has extrema at

$$\phi = 0 \quad \text{and} \quad \phi = v_\phi = \frac{3\mathcal{E}}{2\lambda}\left(1 + \sqrt{1 - \frac{8}{9}\alpha_0}\right), \tag{8.21}$$

where we have introduced the dimensionless quantity $\alpha_0 \equiv \lambda M^2/2\mathcal{E}^2$, which controls the vacuum structure. For $\alpha_0 > 1$, $\phi = 0$ is the true vacuum; for $0 < \alpha_0 < 1$, $\phi = v_\phi$ is the true vacuum while $\phi = 0$ is metastable; and for $\alpha_0 < 0$, $\phi = 0$ becomes unstable. The barrier separating the metastable and true vacua has a height (for $0 < \alpha_0 < 1$)

$$V_{\rm barrier} = \frac{4\mathcal{E}^4\alpha_0^3}{27\lambda^3}\Big(1 + O\left(\alpha_0\right)\Big) \tag{8.22}$$

which vanishes rapidly as $\alpha_0 \to 0$. As in Eq. (8.18), by requiring the exotic energy to vanish today, we calculate the exotic energy prior to the PT to be

$$\rho_{\rm ex} = \frac{\mathcal{E}^4}{8\lambda^3}\left[27 - 36\,\alpha_0 + 8\,\alpha_0^2 + 27\left(1 - \frac{8}{9}\alpha_0\right)^{3/2}\right] \tag{8.23}$$

and note that all of this energy is converted into radiation at the phase transition (i.e., $\Delta\rho_{\rm ex} = \rho_{\rm ex}$).

In order to compute the CC's effect on the relic abundance, we need to know the PT temperature T_{PT}^-, or equivalently the amount of supercooling, which has an interesting dependence on α_0. We require $\alpha_0 < 1$ such that there exists a temperature

$$T_c = \mathcal{E}\sqrt{\frac{1-\alpha_0}{\lambda\, c}} \tag{8.24}$$

below which the symmetric phase $\phi = 0$ becomes metastable. The PT begins at a temperature $T_{PT}^- < T_c$ when the bubble nucleation rate per Hubble volume $\Gamma\, H^{-3} \sim T^4 e^{-S^{(3)}/T}\, H^{-3}$ is comparable to Hubble expansion rate $H \sim T^2/M_p$. Here $S^{(3)}$ is the action of the O(3) symmetric bounce. For an electroweak scale phase transition this condition is satisfied when $S^{(3)}/T$ drops below approximately 140 (209). Provided that the potential can be expressed in the form of Eq. (9.68), then the action is well-approximated by the empirical formula (307)

$$\frac{S^{(3)}}{T} \approx 13.7\,\frac{\mathcal{E}}{T}\left(\frac{\alpha}{\lambda}\right)^{3/2} f(\alpha) \tag{8.25}$$

$$f(\alpha) \equiv 1 + \frac{\alpha}{4}\left(1 + \frac{2.4}{1-\alpha} + \frac{0.26}{(1-\alpha)^2}\right) \tag{8.26}$$

where the temperature dependence is parameterized by $\alpha(T) = \alpha_0(1 - T^2/T_0^2)$, and $T_0^2 = -M^2/(2c)$ can be positive or negative.

The PT temperature is constrained by $\mathrm{Max}\,[T_0^2, 0] < (T_{PT}^-)^2 < T_c^2$ where the lower bound depends on the sign of α_0. We will discuss the two cases separately. For $\alpha_0 > 0$ (or $T_0^2 < 0$), the vacuum $\phi = 0$ remains metastable as $T \to 0$. This

suggests that the PT temperature can be arbitrarily low, and in this limit of large supercooling the CC effect may be arbitrarily large. Unfortunately, if the barrier persists as $T \to 0$, it is possible that the PT does not occur at any temperature – a obviously unphysical scenario in the case of the electroweak phase transition. This follows from the observation that for $\alpha_0 > 0$, $S^{(3)}/T$ has a minimum at $T \neq 0$: at low temperatures $S^{(3)}/T$ grows due to the explicit factor of T in the denominator, and at high temperatures $f(\alpha)$ diverges as $\alpha \to 1$. Over some of the parameter space, the inequality $S^{(3)}/T \lesssim 140$ is not satisfied at any temperature, and the PT does not occur. In particular, if α_0 is close to one, then $\alpha > \alpha_0 \approx 1$ at all temperatures, and it is very difficult for the PT to proceed. Therefore, if we require that the PT must occur via thermal bubble nucleation, we obtain an upper bound on α_0. For the case $\alpha_0 < 0$, the PT necessarily occurs at a temperature $T_{PT}^- > T_0 > 0$, since the $\phi = 0$ vacuum becomes perturbatively unstable below T_0. This case has the drawback that supercooling cannot last an arbitrarily long time, but on the other hand, one is guaranteed that the PT proceeds.

Provided that the PT does occur, we define

$$\delta_{\rm SC} = 1 - \frac{T_{PT}^-}{T_c} \tag{8.27}$$

which ranges from 0 to 1 and quantifies the amount of supercooling. Using $\delta_{\rm SC}$ to parameterize the temperature dependence, we can rewrite Eq. (9.71) in the form

$$\left.\frac{S^{(3)}}{T}\right|_{T_{PT}^-} \approx \left(\frac{\lambda}{\sqrt{c}}\right)^{-1} \frac{1}{\sqrt{1-\alpha_0}} \left[\frac{a_{-2}}{\delta_{SC}^2} + \frac{a_{-1}}{\delta_{SC}} + a_0 + a_1\delta_{SC} + O\left(\delta_{SC}^2\right)\right], \tag{8.28}$$

where the a_i are functions of α_0. We require $S^{(3)}/T\big|_{T_{PT}^-} = 140$ and solve for $\delta_{\rm SC}$, which we have plotted in Figure 9.5. The supercooling grows with increasing α_0 and decreasing $\lambda/\sqrt{c}$ as the barrier and bounce action are made larger. In the shaded region the lower bound on $T_{PT}^- > T_0$ is not satisfied. The amount of supercooling is

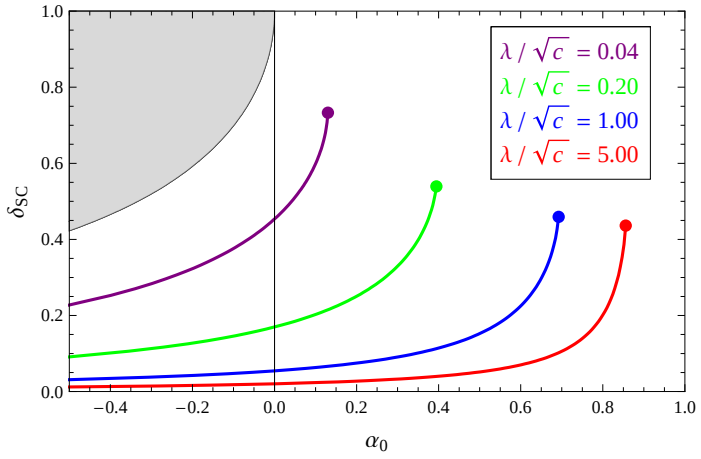

Figure 8.1: We have plotted the amount by which the phase transition temperature drops below the critical temperature, quantified by $\delta_{\rm SC}$, against the parameter α_0 which controls the height of the barrier. These curves only depend on the parametric combination $\lambda/\sqrt{c}$. The amount of supercooling grows as α_0 is made larger, but reaches a finite maximum $\delta_{\rm SC}^{(max)} \lesssim O(1)$ at a value of α_0 that depends on the ratio $\lambda/\sqrt{c}$.

typically of the order $\delta_{\rm SC} \lesssim 0.5$ which implies $T_{PT}^{-} \gtrsim T_c/2$. Above a finite value of α_0 (indicated by a dot) the barrier becomes insurmountably large, and the universe becomes trapped in the metastable vacuum. The existence of this upper bound on α_0 does not allow a phenomenologically viable, arbitrarily large supercooling, contrary to naive expectations. The largest amount of supercooling is achieved for $\lambda/\sqrt{c} \ll 1$ and $\alpha_0 \gtrsim 0$. In this parameter regime the exotic energy is large (see Eq. (9.66)), and the metastable vacuum is separated from the true vacuum by a small barrier (see Eq. (9.67)).

We have calculated the exotic energy and reheating contributions to the relic abundance shift by using Eq. (9.47), and we present the results in Figure 8.2. In generating these plots, we have fixed $c = 0.1$, $\mathcal{E} = 5$ GeV, and $g_{E/S} = 106.75$ (SM degrees of freedom[7]) while allowing α_0 to vary. We select two values for the dark

[7]We choose this value as a fiducial reference. Realistically, for these parameters the PT occurs at $T_{PT}^{-} \approx 1 - 100$ GeV, which could be later than the electroweak phase transition. In that case,

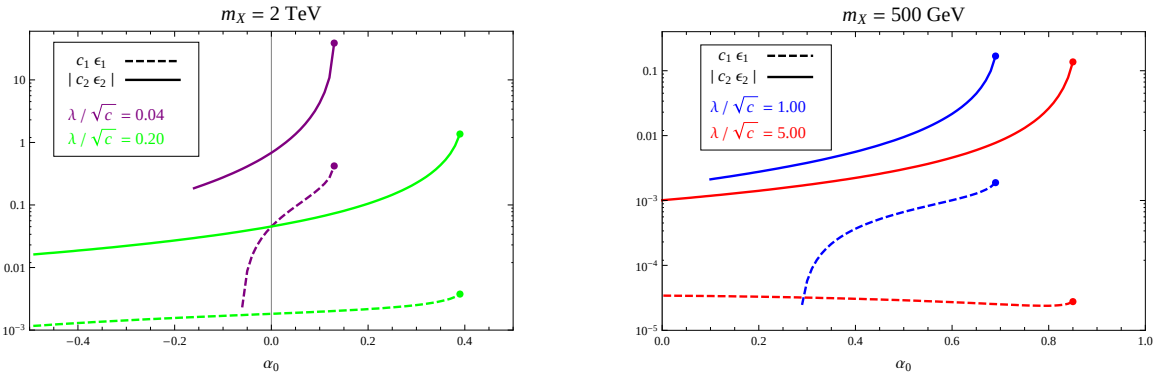

Figure 8.2: The fractional shift in the dark matter relic abundance due to the exotic energy (dashed, $c_1\epsilon_1$) and the reheating (solid, $c_2\epsilon_2$). Note that the two figures have different scales, and that we have plotted $|c_2\epsilon_2|$ since this quantity is negative. When $\lambda/\sqrt{c}$ is smaller than 0.04, then one may enter a regime of large supercooling for tuned values of α_0. The reheating effect dominates by an order of magnitude or more. The contours extend over a finite range of α_0 because for larger α_0 the PT does not occur, and for smaller α_0 the PT occurs before freeze out. Since our analytical approximation breaks down when $c_i\epsilon_i \sim O(1)$, the extrapolation into this region should only be treated as an indication of possible size of the effect.

matter mass, which in turn fixes the freeze out temperature via Eq. (9.34). For the heavier case $m_X = 2$ TeV, the freeze out occurs quite early, and if $\lambda/\sqrt{c} = 1.00, 5.00$ (which are not shown) the PT would occur much later, in the limit where our analytic approximations break down (i.e., $\delta > 1$). Some of the curves are truncated at small α_0, because we require that the PT occur after the freeze out (i.e., $\delta > 0$), and the phase transition temperature increases with decreasing α_0 (see Figure 9.5). It is also for this reason that, the $\lambda/\sqrt{c} = 0.04$ and 0.2 curves are entirely absent from the $m_X = 500$ GeV plot.

These figures indicate that the exotic energy effect on the relic abundance is typically on the order of 10^{-3} and is subdominant to the reheating effect by an order of magnitude. Both contributions become larger in the limit of large supercooling where

some of the SM degrees of freedom would have decoupled, $g_{E/S}$ would be smaller, and the ϵ_i would be relatively larger.

$\lambda/\sqrt{c}$ is small and α_0 approaches its maximal value. For smaller values of $\lambda/\sqrt{c}$ a brief period of inflation might even be possible. The curves $\{\lambda/\sqrt{c} = 0.04, m_X = 2 \text{ TeV}\}$ and $\{\lambda/\sqrt{c} = 1.00, m_X = 500 \text{ GeV}\}$ illustrate the parametric tuning of α_0 that is required to achieve a large correction to the relic abundance. If α_0 is made too large, the PT does not occur, and if α_0 is made too small, the PT occurs before freeze out. Comparing the $m_X = 2$ TeV and $m_X = 500$ GeV plots reveals the parametric tuning that must occur between the DM and scalar sectors. If the DM mass is small, for example, then the parameters of the scalar sector must conspire to generate a low scale PT, otherwise the PT occurs too early and decouples from the physics of the freeze out.

8.4 Summary of the Chapter

If the properties of dark matter can be measured accurately in laboratories, the information that these experiments yield can be used to probe the properties of early universe phase transitions. This is a particularly exciting prospect given that phase transition physics incorporates the energy densities of the false vacuum and the cosmological constant, and thereby it provides an empirical method to directly probe the tuning of the cosmological constant. With this in mind, we have developed a general parameterization to characterize the effects of a single field phase transition on the thermal dark matter relic abundance in a freeze out scenario.

In the context of the SM (supplemented by a DM candidate) and assuming a tuned cosmological constant, we find that the exotic energy (i.e. the Higgs field vacuum energy plus the cosmological constant energy) leads to a fractional increase in the dark matter abundance by $O(10^{-3})$. The dominant change in the dark matter abundance comes from a decoupling of relativistic degrees of freedom near the time of the freeze

out, which leads to a fractional increase in the relic abundance of order 10^{-2}. Without extreme tuning, we expect that most second order PTs share the characteristics of the SM case.

In the case of a second order phase transition, models with a very flat potential (i.e., $m_\phi^2 \lesssim H_{PT}$) generally give a large dark matter abundance shift via the exotic energy contribution. In this limit, Hubble friction can enhance the supercooling as in the case of slow-roll inflation (as signaled by the enhancement attendant with large v_ϕ/m_ϕ in Eq. (8.19)). Although pseudo-Nambu-Goldstone boson models may be useful for producing such flat potentials, the required hierarchies can be somewhat unnatural during the electroweak phase transition since $H_{PT} \sim 10^{-14}$ GeV.

In first order phase transitions with supercooling, there is a somewhat surprising theoretical upper limit on the duration of supercooling which follows from the fact that the bubble nucleation rate is not a monotonically decreasing function of time. In certain parametric regimes, the phase transition never occurs. Close to this failed phase transition case, the maximum fractional increase in the relic abundance due to the exotic energy effect can become $O(0.1)$ and due to the reheating effect can become $O(1)$. However, reaching these large magnitudes requires some degree of parametric tuning. As the parameters deviate from their tuned values, either the PT will not occur at all, or it will occur before the freeze out.

In order for dark matter freeze out to act as a probe of the phase transition, as we have considered, it must be the case that freeze out occurs soon before or concurrently with the phase transition. Since phase transitions typically occur at electroweak scale temperatures or higher and since the mass of weakly interacting dark matter is typically 20 times larger than the freeze out temperature, these DM particles must be heavy, and they may be difficult to discover at the LHC.

It is nonetheless an exciting prospect that LHC and other experiments sensitive

to dark matter's non-gravitational interaction properties may unveil a new probe of dark energy. This is particularly interesting given that there is almost no other way to probe the conjecture of a tuned cosmological constant.[8]

[8]There are generic theoretical limitations on empirical reconstruction of the phase transition scenario. This study will be presented elsewhere (308).

8.A Appendix A. Derivation of PT induced change in the degree of freedom

We begin with the well-known formula for the energy density of a gas of fermions at temperature T with N dynamical degrees of freedom:

$$\rho(T) = N \int \frac{d^3p}{(2\pi)^3} \frac{E_p}{1 + e^{E_p/T}} \,. \tag{8.29}$$

The gas has an effective number of degrees of freedom g_E given implicitly by $\rho(T) = \frac{\pi^2}{30}\, g_E(T)\, T^4$. We can parameterize the decrease in g_E due to the decoupling of the fermionic gas by writing

$$g_E(T) = g_E(T_f) - \frac{7}{8}\, N f\, (a/a_f) \tag{8.30}$$

where

$$f\,(x = a/a_f) = \left(\frac{7}{8}\frac{\pi^2}{30}\right)^{-1} \int \frac{d^3p}{(2\pi)^3} E_p \left[\frac{1}{T_f^4} \frac{1}{e^{\frac{E_p}{T_f}} + 1} - \frac{1}{T^4(a_f x)} \frac{1}{e^{\frac{E_p}{T(a_f x)}} + 1}\right] . \tag{8.31}$$

The temperature $T = T(a)$ is given by Eq. (9.121) to leading order in the perturbations ϵ_i. Since f already multiplies a small term in Eq. (9.22), we need only keep the leading factor in Eq. (9.121) which is $T = T_f\, a_f/a = T_f/x$. This lets us write Eq. (9.124) as

$$f\,(x) = \frac{8}{7}\left(\frac{30}{\pi^2}\right) \int \frac{d^3p}{(2\pi)^3} \frac{E_p}{T_f^4} \left[\frac{1}{e^{\frac{E_p}{T_f}} + 1} - \frac{x^4}{e^{\frac{xE_p}{T_f}} + 1}\right] . \tag{8.32}$$

Note that $f(x)$ increases from $f(1) = 0$ to $f(\infty) \approx 1$. Due to the exponential temperature dependence, the transition to $f \approx 1$ occurs at $T \approx m_N$ and is smoothly steplike over a time scale $\Delta t \approx 1/H$. In this discussion we have assumed $E_p = \sqrt{\mathbf{p}^2 + m_N^2}$ with m_N constant, that is, we neglect any change in the mass of the particle as a function of time. This assumption is valid sufficiently far after the PT such that the scalar VEV and field-dependent masses have approximately stopped varying.

8.B Appendix B. Derivation of T_{PT}^{+}, Δs, and $T(a)$

In this appendix, we calculate the temperature after the phase transition T_{PT}^{+} by imposing energy conservation at the PT. This allows us to calculate Δs and ϵ_2 in terms of $\Delta\rho_{\rm ex}$. Provided that there is a negligible change in $a \approx a_{PT}$ during reheating, energy conservation can be written as

$$\frac{\pi^2}{30}\, g_E(T_{PT}^{-}) \left(T_{PT}^{-}\right)^4 + \Delta\rho_{\rm ex} = \frac{\pi^2}{30}\, g_E(T_{PT}^{+}) \left(T_{PT}^{+}\right)^4 . \tag{8.33}$$

Using the perturbative expansions introduced in Section 8.2, Eq. (9.110) can be solved for T_{PT}^{+} at leading order to obtain

$$T_{PT}^{+} \approx T_{PT}^{-} \left[1 + \frac{1}{4}\,\epsilon_{31} + \frac{1}{4}\frac{\Delta\rho_{\rm ex}}{\frac{\pi^2}{30}\, g_E(T_f)\,(T_{PT}^{-})^4}\right] \tag{8.34}$$

where ϵ_{31} is given by Eq. (9.26c). As expected, the amount of exotic energy released $\Delta\rho_{\rm ex} > 0$ controls the reheating from T_{PT}^{-} to T_{PT}^{+}. Additionally, the reheating is larger when more species non-adiabatically decouple (larger ϵ_{31}), because there are fewer degrees of freedom after the PT to distribute $\Delta\rho_{\rm ex}$ over, which makes them comparatively hotter.

Similarly, we can calculate the entropy density increase at the PT. Writing the entropy density as $s(T) = \frac{2\pi^2}{45} g_S(T) T^3$, we can calculate Δs as

$$\Delta s = \frac{2\pi^2}{45}\Big\{ g_S(T_{PT}^{+})(T_{PT}^{+})^3 - g_S(T_{PT}^{-})(T_{PT}^{-})^3 \Big\} \tag{8.35}$$

$$\approx \frac{2\pi^2}{45}\left\{ -\frac{g_E(T_f)}{g_S(T_f)}\epsilon_{31} + \frac{3}{4}\left[\epsilon_{31} + \frac{\Delta\rho_{\rm ex}}{\frac{\pi^2}{30} g_E(T_f)(T_{PT}^{-})^4}\right]\right\} g_S(T_f)\left(T_{PT}^{-}\right)^3 \tag{8.36}$$

where we have used Eq. (9.112) and linearized in perturbations. We can calculate ϵ_2, given by Eq. (9.26b), by noting $T_{PT}^{-}\, a_{PT} \approx T_f\, a_f$ and $g_S(T_f) \approx g_E(T_f)$ up to higher order terms. Doing so yields

$$\epsilon_2 \approx -\frac{1}{4}\,\epsilon_{31} + \frac{3}{4}\frac{\Delta\rho_{\rm ex}}{\frac{\pi^2}{30} g_E(T_f)(T_{PT}^{-})^4}\,. \tag{8.37}$$

These expressions for Δs and ϵ_2 illustrate that the entropy increase at the PT is controlled by the amount of latent heat released and the number of particles that non-adiabatically decouple.

Lastly, we will solve the equation of entropy conservation for $T(a)$. The entropy per comoving volume $S = s\,a^3$ is conserved except for the entropy injection at re-heating, which is assumed to occur rapidly at a_{PT}. Entropy conservation may be expressed as

$$g_S(T)\,T^3a^3 = g_S(T_f)\,T_f^3a_f^3 + \Theta(a - a_{PT})\,a_{PT}^3\left(\frac{2\pi^2}{45}\right)^{-1}\Delta s \tag{8.38}$$

and implicitly defines $T(a)$. To solve for T we use Eq. (9.21) to expand $g_S(T)$ then linearize in h and Δs to obtain

$$T(a) \approx T_f\frac{a_f}{a}\left[1 + \frac{1}{3}\frac{h(a/a_f)}{g_S(T_f)} + \Theta\left(a - a_{PT}\right)\frac{1}{3}\left(\frac{a_{PT}}{a_f}\right)^3\frac{\Delta s}{\frac{2\pi^2}{45}g_S(T_f)\,T_f^3}\right]. \tag{8.39}$$

Further expanding h using Eq. (9.22), approximating $g_S(T_f) \approx g_E(T_f)$, and applying Eq. (9.26b) we obtain the final expression,

$$T(a) \approx T_f\frac{a_f}{a}\left[1 + \frac{1}{3}\epsilon_{32}\,f(a/a_f) + \Theta\left(a - a_{PT}\right)\frac{1}{3}\left(\epsilon_{31} + \epsilon_2\right)\right]. \tag{8.40}$$

After the PT, the exotic energy component behaves approximately adiabatically.

Chapter 9

Cosmological Constant, Dark Matter, and Electroweak Phase Transition

Accepting the fine tuned cosmological constant hypothesis, we have recently proposed that this hypothesis can be tested if the dark matter freeze out occurs at the electroweak scale and if one were to measure an anomalous shift in the dark matter relic abundance. In this paper, we numerically compute this relic abundance shift in the context of explicit singlet extensions of the Standard Model and explore the properties of the phase transition which would lead to the observationally most favorable scenario. Through the numerical exploration, we explicitly identify a parameter space in a singlet extension of the standard model which gives order unity observable effects. We also clarify the notion of a temperature dependence in the vacuum energy.

This work was performed in collaboration with Daniel Chung. It was published in the journal Physical Review **D** in November of 2011 (119).

9.1 Introduction to the Chapter

The hypothesis that the cosmological constant (CC) energy density today is a result of a tuning between UV and IR contributions (39; 304) is favored according to some versions of the string landscape proposal (see e.g. (305)). Furthermore, this hypothesis has always been the default assumption in particle physics model building (see e.g. (273; 309)). Unfortunately, this conjecture is notoriously difficult to test with lab experiments, such as those at colliders.

One of the predictions of the tuning hypothesis is that there can be an electroweak scale effective CC in the early universe if there was a phase transition (PT) at that scale. A well-known reason to suspect that there was an electroweak scale PT in the early universe is the thermally supported electroweak symmetry restoration phenomenon in the context of the Standard Model (SM) of particle physics (58; 59). Hence, if lab experiments, such as particle colliders, can eventually measure the field content and couplings of the scalar sector at the electroweak scale with sufficient accuracy, then one may be able to predict the CC energy density existing at around the time of the PT. Such an energy density would interact with gravity to modify the expansion history of the universe. Indeed, Kolb and Wolfram (297) were one of the first to state that this computable energy density arising from the Standard Model Higgs condensate may have an observationally acceptable yet significant effect in cosmology.

In a recent paper (177), we proposed that dark matter freeze out can be used to probe PTs, including the properties of such a computable CC, through its effect on the expansion rate of the universe during freeze out. Such an idea is abstractly very similar to the well known big bang nucleosynthesis idea, as well as generic particle probes of cosmology (see e.g. (277; 299; 310–312)). In particular, if a weakly

interacting massive particle (WIMP) dark matter candidate is discovered with a mass of the order of TeV, then its freeze out dynamics would be sensitive to the value of the CC during the electroweak scale PT at a temperature of the order of 100 GeV. Therefore accurate measurements of the dark matter and scalar sector properties will, in principle, make possible a lab test of the tuning of the CC. More accurately, what is being tested is the absence of self-tuning mechanisms and/or modified gravitational theories (313–325) that would eliminate or significantly change the effects of vacuum energy during a PT.

For non-first order PTs, it was found that the shift in the relic abundance due to the CC energy density effects is suppressed by $\Delta n_X/n_X = O\left(g_E^{-1}\right)$ where g_E is the number of of relativistic degrees of freedom contributing to the energy density. For first order PTs, it was found that this fractional shift can be generically enhanced by supercooling such that the CC effects can be $O(1)$ with a 1% parameteric tuning. In all cases, the sought after CC "signal" is buried in the dominant "background" coming from the adiabatic change in the number of degrees of freedom and possibly the entropy release near the time of the dark matter freeze out. The adiabatic change in the number of degrees of freedom and the vacuum energy effect tend to increase the relic density today while the entropy production effect decreases the relic density.

The purpose of this paper is to complement the previous short paper (177) in several ways:

1. Present an explicit singlet extension of the Standard Model (SM) that gives a large supercooling with a first order PT at the electroweak scale.
2. Clarify the notion of how an effective vacuum energy (which is Lorentz invariant in the flat space limit) can depend on temperature (which manifestly breaks Lorentz invariance).
3. Compare numerical results with analytic results presented in (177).

4. Provide relevant technical details that were left out in (177) to aid future research efforts in this direction.

In addition to giving a generic singlet scalar model coupled to a Dirac fermion that gives a significant supercooling, we analyze xSM, i.e. a real singlet coupled to the SM, and identify a parametric region in which significant supercooling occurs. As anticipated in (177), an $O(10^{-2})$ tuning is sufficient to induce an $O(1)$ supercooling effect on the relic abundance.

The order of presentation is as follows. In Section 9.2 we review the physics of PTs and focus on the myriad ways in which a PT may impact dark matter freeze out. We clarify the notion of a temperature dependence of vacuum energy density in this section. In Section 9.3 we analytically compute the fractional shift of the relic abundance $\delta n_X(t_0)$ due to an electroweak scale PT in the limit in which the PT represents a small perturbation to the usual freeze out. In Section 9.4 we compute the relic abundance deviation in the SM and minimal singlet extensions (both supplemented by a generic dark matter which is assumed to play a negligible role in determining the properties of the PT). In Section 9.5 we conclude with a summary and suggestions for future work. An extensive set of appendices detail technicalities useful for the material presented in the body of the paper.

Throughout the paper, we assume a flat Friedmann-Robertson-Walker (FRW) metric, $ds^2 = dt^2 - a^2(t)|d\mathbf{x}|^2$, and use the reduced Planck mass $M_p \approx 2.4 \times 10^{18}$ GeV.

9.2 A Brief Review of the Physics of Phase Transitions

In this section, we review the physical features that accompany a cosmological PT. Each of these features modifies one of the relationships, $\rho \sim T^4$, $T \sim a^{-1}$, or $\langle \sigma v \rangle = \langle \sigma v \rangle (T)$, which are assumed in the usual freeze out calculation. One of the topics discussed in this section is how to understand the thermal dependence of vacuum energy, which a priori is an oxymoron. Readers interested in mostly the phenomenology can skip to the next section.

The standard cosmological model assumes an expanding FRW universe which leads to the temperature of the relativistic species in the universe decreasing as a function of time except during the time periods when entropy is generated. As the temperature decreases, there may exist critical temperatures at which the thermodynamic quantities are not analytic as a function of temperature and/or the symmetries of the effective Lagrangian governing the dynamical degrees of freedom changes. Following the typical convention in the literature, we refer to the passages through these critical temperatures as PTs.

In order to calculate thermodynamic quantities in the system described above, we will use the thermal effective potential (see (209) for a review). The thermal effective potential $V_{\text{eff}}(\phi_c, T)$, derived from Legendre transforming the partition function coupled to external sources, represents the free energy density of the plasma at temperature T dynamically interacting with a homogeneous scalar field background ϕ_c which may affect the masses and interactions of particles in the plasma. A local minimum $\phi_c = v(T)$ is called the thermal vacuum, and PTs occur near critical temperatures T_c which will be defined more precisely below.[1]

[1]We will leave out the adjective "thermal" in "thermal vacuum" whenever no confusion should

The critical temperature T_c in the case of what is conventionally referred to as a first order PT is defined by the existence of two or more degenerate minima $\phi = v(T_c)$ existing for the thermal effective potential $V_{\rm eff}(\phi, T_c)$. In such cases, we refer to the vacuum of the universe just prior to the PT as $v^{(s)}(T)$ (where the "s" superscript denotes "symmetric" vacuum) whether or not there is a symmetry in the thermal effective potential prior to the PT. The vacuum solution after the first order PT is referred to as $v^{(b)}(T)$ where "b" denotes "broken." A non-first order PT (sometimes loosely referred to as a second order PT) is characterized by a single continuous function $v(T)$ before and after the PT: i.e. $v^{(b)}(T_c) = v^{(s)}(T_c)$. Even in such situations, it is sometimes useful to define $v^{(s)}(T)$ to be the vacuum before the PT whenever there is a restored symmetry prior to the PT. The quantity $v^{(s)}(T)$ can then be taken as an order parameter associated with spontaneous symmetry breaking.

The thermal vacua $v^{(s/b)}(T)$ can be obtained from summing up thermal tadpole corrections obtained from expanding perturbatively about the zero temperature vacua $v^{(s/b)}(0)$. Despite the suggestive notation of the thermally shifted vacuum $v^{(s/b)}(T)$, the resummation of tadpoles is nothing more than a reorganization of perturbation theory, and the vacuum energy represented by the Lorentz-invariant part of the energy-momentum tensor, is not shifted by the manifestly Lorentz-noninvariant thermal tadpoles. Note that symmetry restoration cannot be inferred from the thermal tadpole resummation alone since the thermal perturbation theory breaks down when the perturbations are expanded about the inflection points of the effective potential.

Let us now establish some more notation for the quantities introduced above. The thermal effective potential and $v^{(s/b)}(T)$ can be used to construct the thermodynamic

---

arise.

quantities

$$\mathcal{F}^{(s/b)}(T) = V_{\text{eff}}(v^{(s/b)}(T), T) \tag{9.1a}$$

$$s^{(s/b)}(T) = -\frac{d}{dT}\mathcal{F}^{(s/b)} \tag{9.1b}$$

$$\rho^{(s/b)}(T) = \mathcal{F}^{(s/b)} + T\, s^{(s/b)} \tag{9.1c}$$

representing the free energy density $\mathcal{F}$, entropy density s, and energy density ρ in the symmetric and broken phases. A typical PT occurs as the universe cools, and the free energy of the broken phase, in which the entropy and energy densities are high, drops below the free energy of the symmetric phase, in which the entropy and energy densities are low. It will be useful to define the critical temperature of the PT T_c by

$$\mathcal{F}^{(s)}(T_c) = \mathcal{F}^{(b)}(T_c)\,, \tag{9.2}$$

but note that the PT may not actually occur until a much lower temperature if the symmetric phase experiences supercooling. The PT is accompanied by a number of physical features, which we will outline in the remainder of this section and which each have an impact on dark matter freeze out.

The first feature that we would like to discuss is the vacuum energy associated with the PT. We assume that the energy density $\rho^{(s/b)}(T)$ can be partitioned into the energy associated with the plasma and the energy associated with the condensate (i.e. the vacuum energy with an effective equation of state of -1), and we define the latter as

$$\rho_{cc}^{(s/b)}(T) \equiv V_{\text{eff}}(v^{(s/b)}(T), 0) \tag{9.3}$$

which has an observable consequence when coupled to gravity. This equation is artificial because the vacuum energy cannot be rigorously separated from the particle energy with which it is associated for most of the states populating the density matrix.

Nonetheless, it is useful because it captures the CC type of contribution (i.e. negative equation of state contribution) to the energy-momentum tensor.

Note that flat space thermal corrections to the zero temperature effective potential cannot generate Lorentz invariant contributions to the energy-momentum tensor because temperature T dependent quantities are not Lorentz invariant. Since the CC contribution to the energy-momentum tensor in the flat space limit is Lorentz invariant, one may wonder whether Eq. (9.3) is valid since it implies that thermal tadpoles are contributing to the vacuum energy. Furthermore, the fact that the effective vacuum energy takes on a continuum of values while the only non-perturbatively stable vacuum state is at $v^{(b)}(0)$ (which we will assume to be associated with negligible vacuum energy) also leads one to be suspicious of Eq. (9.3).

To semi-quantitatively resolve this puzzle, one notes that near the time of the PT, there are $A \leftrightarrow B$ processes in equilibrium where A and B schematically correspond to states of the form $|\text{particles} + \text{vacuum energy}\rangle$ and $|\text{particles}\rangle$, respectively. These transitions are mediated by non-perturbative processes since they are vacuum changing processes. Classically, the plasma (when these transitions are efficient) is approximately described by inhomogeneous solutions in Minkowski space. This can easily be characterized by computing for example the thermal two-point function.

The equation of state for such a plasma in the classical approximation corresponds to neither that of quantum expectation values with respect to states A nor B, but is a mixture which from the quantum perspective depends on the non-perturbative transition operators as well as the relative statistical and/or coherent weighting of A and B type of states. The incoherent aspect of this mixture is what the T dependence of Eq. (9.3) reflects.[2] To corroborate this picture, one can easily solve classical equations

[2]Note also unlike in flat spacetime, there are IR cutoffs associated with the expansion rate H for a single causal domain during the PT and H_0 associated with the presently observable universe. The former scale H is also associated with one of the scales at wich quasi-equilibrium assumption

of motion in models with spontaneous symmetry breaking to obtain *inhomogeneous background* field solutions which have an inhomogeneous equation of state. Since the Friedmann equation (which is the only gravitational probe we will be concerned in this paper) approximately describes the gravitational response to the spatial average of the energy-momentum tensor, one can spatially average the energy density and the pressure. This leads to an effectively homogeneous energy density and pressure which is approximately the same as that due to particles plus a vacuum condensate energy density. The resulting effective vacuum condensate energy density is somewhere between $V_{\rm eff}(v^{(s)}(0),0)$ and $V_{\rm eff}(v^{(b)}(0),0)$, justifying the diagnostic quantity defined by Eq. (9.3).

To renormalize the CC, we impose the tuning condition

$$\rho_{cc}^{(b)}(T=0)=0\,, \tag{9.4}$$

which states that the vacuum energy density today is on the order of the meV^4 dark energy density (71; 326) and negligible as compared to the PT scale. Hence, we will refer to $\rho_{cc}^{(s/b)}(T)$ as the "effective CC energy density." With this normalization, the CC energy density before a PT at scale M will typically be

$$\rho_{cc}^{(s)}(T\gtrsim M)\sim M^4, \tag{9.5}$$

which can be measured, in principle, by gravitational probes such as the Hubble expansion rate and its impact on dark matter freeze out.[3] Any self-tuning/modified-gravity mechanism which decouples the vacuum energy or significantly modifies the vacuum energy effect on gravity on a time scale shorter than that of the expansion scale will have an effective $\rho_{cc}^{(s)}$ significantly different from Eq. (9.5). It would be

breaks down.

[3]Although an in depth discussion of UV sensitivity of the CC is beyond the scope of this paper, one should keep in mind that using Eq. (9.4) as a quantum renormalization condition leads to Eq. (9.5) as a prediction only if assumptions about analyticity of the effective potential as well as Lorentz invariance structure of the UV cutoff is assumed.

interesting in future studies to compare various self-tuning/modified gravity models which may have non-trivial time dependence in the effective vacuum energy different from that in this paper.

The second PT feature is the decoupling of heavy degrees of freedom which become non-relativistic after the PT and cause the number of relativistic species, denoted here as g, to decrease. This has two consequences for the dark matter freeze out calculation. First, the energy density of the plasma $\rho \sim g\,T^4$ and Hubble expansion rate $H \sim \sqrt{\rho}$ decrease more rapidly than usual after the PT. Second, since temperature is related to the FRW scale factor by entropy conservation, which gives $T \sim g^{-1/3}a^{-1}$, the temperature decreases less rapidly than usual after the PT. To estimate the magnitude of the effect on dark matter freeze out, consider the SM electroweak PT at $T \sim 100$ GeV and suppose that freeze out occurs at the same temperature. Then during the residual annihilation stage of freezeout, which lasts until $T \sim 10$ GeV, g will decrease by approximately 20% corresponding to the decoupling of the top, Higgs, and massive gauge bosons. In the usual freeze out calculation, changes in g are neglected, because freeze out occurs much later than the electroweak PT when g is insensitive to T. When we arrange for the two events to occur at the same scale, g decreases significantly and can have a large effect on the relic abundance.

The third feature is related to the coupling between the PT sector and the rest of the particle physics model. As the phase changes at the PT, in general the masses and interactions of particles in the plasma can change as well. In particular, it is possible for the scalar field to couple to dark matter in such a way that the dark matter's mass and/or annihilation cross section is different in the symmetric and broken phases. This scenario, studied by (179; 302), may allow dark matter to rethermalize and can have a significant effect on the relic abundance.

If the PT is of the first order, then it possesses a number of additional features

(see e.g. (303) for a more detailed discussion). A first order PT can be divided into two stages. The first stage, known as supercooling, occurs while the universe remains in the symmetric phase after it has become metastable at $T \approx T_c$. As the temperature decreases and the CC energy density remains approximately constant, the total energy density can deviate from the standard $\rho \sim T^4$ scaling (i.e., first feature above). Supercooling ends when it becomes energetically favorable for bubbles of the broken phase to nucleate. Determining the temperature T_{PT}^- at which bubble nucleation begins requires one to solve for the non-perturbative bounce solution and evaluate the decay rate of the metastable phase (203). During the second stage, known as reheating, the expanding bubbles release an energy density

$$\Delta\rho_{\rm ex} = \rho_{cc}^{(s)}(T_{PT}^-) - \rho_{cc}^{(b)}(T_{PT}^+) \tag{9.6}$$

which is converted into radiation and heats the gas from T_{PT}^- before the PT to $T_{PT}^+ > T_{PT}^-$ after the PT. We assume that reheating occurs rapidly as compared with the expansion rate of the universe[4], which allows us to treat reheating as an abrupt process at time t_{PT} when $a = a_{PT}$. Reheating is accompanied by a non-adiabatic entropy increase. This entropy growth modifies the relationship between temperature and the FRW scale factor in such a way that the universe is relatively larger for a given temperature. As a result, the dark matter number density undergoes a longer period of dilution and the relic abundance can be significantly smaller (178). Finally, just as massive species can adiabatically decouple after the electroweak PT occurs, heavy particles can undergo a non-adiabatic decoupling at the time of a first order PT if they abruptly acquire a mass $m \gtrsim T_{PT}$.

[4] A third stage, known as phase coexistence, can occur if a large latent heat is released by the expanding bubbles and the plasma is reheated to the point where the pressure gradient across the bubble wall vanishes (144). Subsequently, the bubbles expand only insofar as the universe expands, and the PT completes on a time scale $t \sim H^{-1}$. Typically, this stage does not occur during an electroweak-scale PT because the number of relativistic species $O\,(100)$ is too many to allow for sufficient reheating.

9.3 An Analytic Estimate of the Change in the Dark Matter Abundance

In this section, we estimate the change in the dark matter relic abundance due to the presence of a PT, and the CC energy density in particular, during freeze out. Our final result is the fractional deviation of the relic abundance, denoted $\delta n_X(t_0)$ and given by Eq. (9.47), in which we have linearized in the various effects of the PT on freeze out. Although most of the results in this section have already been presented in (177), we repeat some of the results for self-containedness as well as serving as introduction for more complete results such as Eqs. (9.49) and (9.50). The main point of this section is to present a formalism to understand analytically the effects outlined in Sec. 9.3.

Throughout the calculation, we will take a as the independent variable and rewrite functions of temperature using $T = T(a)$ given by Eq. (9.121). In particular, we will assume that freeze out occurs at a temperature $T_f = T(a_f)$ before the PT at $a = a_{PT}$. Since all of the thermodynamic quantities depend on the phase of the system which changes at $a = a_{PT}$, the formulas in this section would become unnecessarily obscure if we persisted in writing all the (s/b) superscripts and distinguishing the $a < a_{PT}$ and $a > a_{PT}$ cases. Therefore, we introduce the following shorthand. Whenever a temperature-dependent function $F^{(s/b)}(T)$ appears without the (s/b) superscript, the intended meaning is

$$F(a) = \begin{cases} F^{(s)}(T(a)) & a < a_{PT} \\ F^{(b)}(T(a)) & a > a_{PT} \end{cases} . \tag{9.7}$$

In particular, one always has $F(a_f) = F^{(s)}(T_f)$ since $a_f < a_{PT}$ by assumption.

We calculate the thermal relic abundance of dark matter by integrating the ther-

mally averaged Boltzmann equation,

$$\frac{1}{a^3}\frac{d}{dt}\left(a^3 n_X\right) = -\langle\sigma v\rangle\left(n_X^2 - n_X^{\mathrm{eq}\,2}\right), \tag{9.8}$$

over the era of residual annihilations from freeze out at $a = a_f$ until today. Subject to general assumptions (see Appendix 9.B for more details), we obtain

$$n_X(t_0) = \left(\int_0^{\ln a_0/a_f} \frac{d\ln(a/a_f)}{H}\,\langle\sigma v\rangle\,\frac{a_0^3}{a^3}\right)^{-1} \tag{9.9}$$

for the number density of dark matter today at $a = a_0$ and $t = t_0$. In this expression, the quantities that will be affected by the PT are the Hubble expansion rate $H(a)$, the thermally averaged cross section $\langle\sigma v\rangle\,(a)$, and the dilution number since the time of the freeze out to today a_0/a_f, which is related to $T(a)$. As a fiducial reference value, we also calculate the "usual" relic abundance $n_X^{(U)}(t_0)$ by assuming that the PT does not occur, but instead that the universe remains radiation dominated and has the standard scaling relations

$$H^{(U)} \sim a^{-2}, \qquad \langle\sigma v\rangle^{(U)} = \langle\sigma v\rangle\,(T(a)), \qquad \text{and} \qquad T^{(U)} \sim a^{-1} \tag{9.10}$$

throughout freeze out. We define the relic abundance fractional deviation as

$$\delta n_X(t_0) = \frac{n_X(t_0)}{n_X^{(U)}(t_0)} - 1 \tag{9.11}$$

and expect this quantity to depend on the way in which H, $\langle\sigma v\rangle$, and a_0/a_f deviate from the usual freeze out scenario. We will consider each effect in turn.

Before addressing each of the factors in Eq. (9.9), let us discuss the partitioning of energy. The Hubble expansion rate, which appears in Eq. (9.9), is related to the total energy density $\rho^{(s/b)}(T)$. However, we are particularly interested in determining the impact of the effective CC on the calculation of dark matter freeze out. Therefore we will assume that the energy can be partitioned as

$$\rho \approx (\text{particle degrees of freedom} + \text{exotic energy component})\,. \tag{9.12}$$

In general, the exotic energy component can arise from physics other than the effective CC, such as quintessence (e.g. (299; 312; 327–331)) or late-decaying massive particles (e.g. (332–339)). To maintain a minimal degree of generality throughout our analytic estimates (without accumulating distasteful notational complication), we will parametrize the exotic energy component as $\rho_{\rm ex}\,\kappa(a)$. However, since our primary interest is in the case that the exotic energy component represents an effective CC, we will write

$$\rho_{\rm ex}\,\kappa(a) = \rho_{cc}(a) \tag{9.13}$$

where $\rho_{cc}^{(s/b)}(T)$ is defined by Eq. (9.3), and we have used the shorthand Eq. (9.7). The remaining energy density can be attributed to relativistic particles in the plasma, which we will denote by[5]

$$\rho_R^{(s/b)}(T) = \rho^{(s/b)}(T) - \rho_{cc}^{(s/b)}(T)\,. \tag{9.14}$$

To connect with a familiar and intuitive notation, we let the functions g_E and g_S be defined implicitly by

$$\rho_R^{(s/b)}(T) = \frac{\pi^2}{30}\,g_E^{(s/b)}(T)\,T^4 \tag{9.15}$$

$$s^{(s/b)}(T) = \frac{2\pi^2}{45}\,g_S^{(s/b)}(T)\,T^3 \tag{9.16}$$

such that they represent the number of relativistic degrees of freedom at temperature T in either the symmetric or broken phase. As shown in Appendix 9.C, one must have $g_S(T) \neq g_E(T)$ if entropy and energy are to be conserved during the time when a species adiabatically decouples.

[5] Contributions from non-relativistic species are Boltzmann suppressed. Defined in this way, $\rho_R^{(s/b)}$ includes a term proportional to $dv^{(s/b)}/dT$ which arises from the derivative in Eq. (9.1b). This term represents kinetic energy in the scalar field and, strictly speaking, should not be included in ρ_R. Nevertheless, we do not separate out the kinetic term, because it is typically negligible.

Now, we will begin our investigation of the quantities in Eq. (9.9). First, consider the effect on the Hubble expansion rate $H(a)$ which is obtained by solving the Friedmann equation. To do so, we partition the energy as described above and assume that $\rho_{\rm ex} \ll \rho_R(a_f)$ such that we can treat the CC energy density as a perturbation. With these assumptions, we obtain

$$H(a) = \frac{1}{\sqrt{3}M_p}\sqrt{\rho(a)} \tag{9.17}$$

$$\approx \frac{T^2}{3M_p}\sqrt{\frac{\pi^2}{10}\,g_E(a)}\left[1+\frac{1}{2}\frac{\rho_{\rm ex}\,\kappa(a)}{\frac{\pi^2}{30}\,g_E(a)\,T(a)^4}\right]. \tag{9.18}$$

where we have used the shorthand Eq. (9.7). During the PT, we can approximate $\kappa(a)$ as

$$\kappa(a) \approx \Theta(a_{PT}-a) + \Theta(a-a_{PT})\left(1-\frac{\Delta\rho_{\rm ex}}{\rho_{\rm ex}}\right)\kappa_2(a) \tag{9.19}$$

where $\Theta(z)$ is a step function, $\Delta\rho_{\rm ex} > 0$ is given by Eq. (9.6), and $\kappa_2(a)$ is a function which starts from $\kappa_2(a_{PT}) = 1$ and decreases as fast as

$$\left(\frac{a}{a_{PT}}\right)^{-n_d} \tag{9.20}$$

with $n_d \gtrsim 4$. If $\Delta\rho_{\rm ex} = 0$, we have a continuous second order transition or a crossover. If $\Delta\rho_{\rm ex} = \rho_{\rm ex}$, then the supercooling is sufficiently strong as to end up with no CC energy just after the PT. The step functions represent the fact that the PT occurs with negligible change in the scale factor. With this assumption, Δs and the corresponding change in the temperature become functions of $\Delta\rho_{\rm ex}$ according to Eq. (9.117) in Appendix 9.D. Finally, the $\Theta(a_{PT}-a)$ term in Eq. (9.19) should, in general, be multiplied by another smooth function unless there is some symmetry fixing $v^{(s)}(T)$, and consequently $\rho_{cc}^{(s)}(T)$, to a particular value in the high energy limit. However, we will neglect this detail in favor of cleaner notation, since the final result will be approximately unchanged.

As discussed in Section 9.2, particle species start becoming non-relativistic after the (electroweak) PT which causes $g_{E/S}(a)$ to decrease. We will parametrize this decrease by focusing on the (non-)adiabatic decoupling of (N_{PT}) N fermionic dynamical degrees of freedom and write

$$g_{E/S}(a) = g_{E/S}(a_f) - h(a) \tag{9.21}$$

$$h(a) = \frac{7}{8} N_{PT}\, \Theta(a - a_{PT}) + \frac{7}{8} N\, f(a) \tag{9.22}$$

where $f(a)$, which rises from 0 to 1, is given by Eq. (9.125). Note that in reality, $h(a)$ is a smooth complicated function (particularly $Nf(a)$), but here we are accounting for the change in the number of degrees of freedom in a physically suggestive approximation. As we will see below, this effect will be one of the dominant "backgrounds" to the "signal" of measuring the effects of the cosmological constant. We treat this effect as a perturbation to linear order, and we estimate the Hubble expansion rate to be

$$H(a) \approx \frac{T(a)^2}{3M_p} \sqrt{\frac{\pi^2}{10} g_E(a_f)} \left[1 - \frac{1}{2} \frac{h(a)}{g_E(a_f)} + \frac{1}{2} \frac{\rho_{\rm ex}\, \kappa(a)}{\frac{\pi^2}{30} g_E(a_f) T(a)^4} \right] . \tag{9.23}$$

Writing $T(a)$ using Eq. (9.121) and linearizing further with respect to small quantities, we have

$$H(a) \approx H^{(U)}(a) \Bigg[1 + \frac{\epsilon_1}{2} \left(\frac{a}{a_f} \right)^4 \kappa(a) + \frac{2}{3} \epsilon_2 \Theta(a - a_{PT}) + \frac{1}{6} \epsilon_{31} \Theta(a - a_{PT}) + \frac{1}{6} \epsilon_{32} f\,(a) \Bigg] \tag{9.24}$$

where

$$H^{(U)}(a) \equiv \frac{T_f^2}{3\, M_p \left(\frac{a}{a_f} \right)^2} \sqrt{\frac{\pi^2}{10}\, g_E(a_f)} \tag{9.25}$$

and

$$\epsilon_1 \equiv \frac{\rho_{\rm ex}}{\frac{\pi^2}{30} g_E(a_f)\, T_f^4} = \text{fractional energy of the exotic during freeze out} \tag{9.26a}$$

$$\epsilon_2 \equiv \left(\frac{a_{PT}}{a_f}\right)^3 \frac{\Delta s}{\frac{2\pi^2}{45} g_S(a_f)\, T_f^3} = \text{fractional entropy increase during PT} \tag{9.26b}$$

$$\epsilon_{31} \equiv \frac{\frac{7}{8} N_{PT}}{g_E(a_f)} = \text{ fractional decoupling degrees of freedom during PT} \tag{9.26c}$$

$$\epsilon_{32} \equiv \frac{\frac{7}{8} N}{g_E(a_f)} = \text{ fractional decoupling degrees of freedom near freeze out} \tag{9.26d}$$

where Δs, denoting the entropy density change at the time of the PT, is given by Eq. (9.117). Although $H(a)$ appears to vary discontinuously at $a = a_{PT}$, its continuity is ensured by the conservation of energy. At the PT, the CC energy converts into radiation, which generates an entropy but leaves the total energy density fixed (i.e., ϵ_2 compensates for the discontinuity of the ϵ_1 term) because the volume remains approximately constant through the duration of the PT. The fact that H is boosted by ϵ_{31} and ϵ_{32} is intuitive for the following reason. When a particle species becomes non-relativistic, the effective equation of state becomes smaller, such that the energy dilutes less, which in turn leads to a larger expansion rate for the same scale factor. The term ϵ_{31} accounts for the non-adiabatic change in the number of degrees of freedom during the PT, while the term ϵ_{32} accounts for the adiabatic change in the number of degrees of freedom.

Next, consider the change in the cross section due to the PT. We parametrize this effect as

$$\langle \sigma v \rangle = \langle \sigma v \rangle^{(U)} \Big(1 - \epsilon_4\, \Theta(a - a_{PT})\Big) \tag{9.27}$$

where

$$\epsilon_4 \equiv -\frac{\Delta_\sigma}{\langle \sigma v \rangle^{(U)}} \tag{9.28}$$

and Δ_σ is the change in $\langle\sigma v\rangle$ due to the PT. Since the derivation of Eq. (9.9) assumes that the dark matter is decoupled after T_f, we will assume that $\epsilon_4 \gtrsim 0$ in order to prevent re-thermalization due to an increase in the cross section. Hence, we can evaluate Eq. (9.9) by linearizing in the ϵ's to obtain

$$n_X(t_0) \approx \left(\frac{a_f}{a_0}\right)^3 \left(\int_0^{\ln a_0/a_f} \frac{d\ln a/a_f}{H^{(U)}(a)} \frac{\langle\sigma v\rangle^{(U)}}{(a/a_f)^3} \left[1 + \sum_n \theta_n(a)\epsilon_n\right]\right)^{-1} \tag{9.29}$$

where

$$\begin{aligned}\sum_n \theta_n(a)\,\epsilon_n = &-\frac{\epsilon_1}{2}\left(\frac{a}{a_f}\right)^4 \kappa(a) - \Theta(a-a_{PT})\frac{2}{3}\epsilon_2 \\ &- \frac{1}{6}\left[\epsilon_{31}\,\Theta(a-a_{PT}) + \epsilon_{32}\,f\,(a)\right] - \epsilon_4\,\Theta(a-a_{PT})\end{aligned} \tag{9.30}$$

implicitly defines the θ_n. Note that the integral is dominated by contributions around $\ln a/a_f = 0$. On the other hand, the $(a_f/a_0)^3$ prefactor should be evaluated with all the g_S changes accounted for, not just the effects around $\ln x = 0$.

Next, let's consider the effects on the a_f/a_0 factor determined by the freeze out condition itself. The freeze out temperature T_f can be solved using (297)

$$\langle\sigma v\rangle\, n_X^{\rm eq}(T_f) = C\frac{m_X}{T_f}H(T_f) \tag{9.31}$$

$$n_X^{\rm eq}(T) \equiv g_X\left(\frac{m_X T}{2\pi}\right)^{3/2}\exp\big[-\frac{m_X}{T}\big] \tag{9.32}$$

where C is an order unity number whose optimum value to reproduce numerical integration is cross section dependent (e.g., $C \approx 2$), g_X counts the real dynamical degrees of freedom of the dark matter, and m_X is the dark matter mass. Evaluating $H(T_f)$ with Eq. (9.24) and assuming freeze out occurs before the PT, Eq. (9.31) becomes

$$\begin{aligned}&\langle\sigma v\rangle\, g_X\left(\frac{m_X T_f}{2\pi}\right)^{3/2}\exp\big[-\frac{m_X}{T_f}\big] \\ &\qquad\approx \frac{C\,m_X\,T_f}{3M_p}\sqrt{\frac{\pi^2}{10}g_E(a_f)}\Big[1+\frac{\epsilon_1}{2}\Big]\,.\end{aligned} \tag{9.33}$$

Although not solvable in closed form, one can linearize in the perturbation again to obtain

$$T_f \approx \frac{m_X}{\ln A}\left[1+\frac{\epsilon_1}{2}\left(\frac{1}{\ln A}+O\left((\ln A)^{-2}\right)\right)\right] \tag{9.34}$$

where

$$A \equiv \frac{g_X 3\sqrt{5} M_p \sqrt{m_X T_f}\langle\sigma v\rangle}{2C\pi^{5/2}\sqrt{g_E(a_f)}} \sim \exp\big[20\big] \tag{9.35}$$

for electroweak mass scales. If we assume that there is only one period of entropy production between freeze out and today, and that it occurs at the PT temperature T_{PT}, we can use entropy conservation in the form of Eq. (9.119) to write

$$\frac{a_0}{a_f} = \left(\frac{g_S(a_f)}{g_S(a_0)}\right)^{1/3}\frac{T_f}{T_0}\left[1+\frac{1}{3}\epsilon_2\right] \tag{9.36}$$

where T_0 is the temperature today. Combining this with Eq. (9.34), we find

$$\frac{a_0}{a_f} = \left(\frac{a_0}{a_f}\bigg|^{(U)}\right)\left[1+\frac{\epsilon_1}{2}\frac{1}{\ln A}+\frac{1}{3}\epsilon_2\right] \tag{9.37}$$

where

$$\left(\frac{a_0}{a_f}\bigg|^{(U)}\right) \equiv \left(\frac{g_S(a_f)}{g_S(a_0)}\right)^{1/3}\frac{m_X}{T_0}\frac{1}{\ln A}\,. \tag{9.38}$$

Putting Eq. (9.37) into Eq. (9.29) results in

$$\begin{aligned} n_X(t_0) \approx{}& \left(\frac{a_0}{a_f}\bigg|^{(U)}\right)^{-3}\left[1-\frac{3\epsilon_1}{2}\frac{1}{\ln A}-\epsilon_2\right] \\ &\times\left(E_1+\int_0^{\ln(a_0/a_f|^{(U)})}\frac{d\ln a/a_f}{H^{(U)}(a)}\frac{\langle\sigma v\rangle^{(U)}}{(a/a_f)^3}\left[1+\sum_n\theta_n(a)\epsilon_n\right]\right)^{-1} \end{aligned} \tag{9.39}$$

where the endpoint contribution to the integral has been written as

$$E_1 \equiv \frac{\frac{\epsilon_1}{2}\frac{1}{\ln A}+\frac{\epsilon_2}{3}}{H^{(U)}(a_0)}\frac{\langle\sigma v\rangle^{(U)}}{(a_0/a_f|^{(U)})^3}\,. \tag{9.40}$$

The term E_1 is negligible because of the volume dilution factor in its denominator. Linearizing the small factors gives

$$n_X(t_0) \approx n_X^{(U)}(t_0)\left[1 - \frac{3\epsilon_1}{2}\frac{1}{\ln A} - \epsilon_2 - F_u^{-1}\sum_n \tilde{\theta}_n \epsilon_n\right] \tag{9.41}$$

where

$$F_u \equiv \int_0^{\ln(a_0/a_f|^{(U)})} \frac{d\ln a/a_f}{H^{(U)}(a)}\frac{\langle\sigma v\rangle^{(U)}}{(a/a_f)^3} \tag{9.42}$$

$$n_X^{(U)}(t_0) \equiv \left(\frac{a_0}{a_f}\bigg|^{(U)}\right)^{-3} F_u^{-1} = \text{usual computation of relic abundance} \tag{9.43}$$

$$\tilde{\theta}_n \equiv \int_0^{\ln(a_0/a_f|^{(U)})} \frac{d\ln a/a_f}{H^{(U)}(a)}\frac{\langle\sigma v\rangle^{(U)}}{(a/a_f)^3}\theta_n(a)\,. \tag{9.44}$$

In particular, if we assume an s-wave cross section (i.e., constant $\langle\sigma v\rangle$), we can express $\tilde{\theta}_1$ explicitly as

$$F_u^{-1}\tilde{\theta}_1 \approx -\frac{1}{2}\left[\delta + \frac{(1+3\delta)}{n_d - 3}\left(1 - \frac{\Delta\rho_{\rm ex}}{\rho_{\rm ex}}\right)\right] \tag{9.45}$$

where we have expanded in $\delta \equiv a_{PT}/a_f - 1 \gtrsim 0$ which represents the delay between freeze out and the PT. The first term in square brackets comes from integrating the CC energy density from a_f to a_{PT}, and the second term comes from integrating the decreasing CC energy density after the PT. This equation shows that if $\frac{\Delta\rho_{\rm ex}}{\rho_{\rm ex}} \approx 1$ (large supercooling) there is a suppression of the ϵ_1 effect by a factor of order δ. Although we have linearized in δ along with ϵ_i, terms of the form $\epsilon_i\,\delta$ are not higher order. The expansion in ϵ_i reflects the fact that we treat the PT as a perturbation, whereas the expansion in δ is performed merely to simplify the expressions. With the same assumptions, we can evaluate the other $F_u^{-1}\tilde{\theta}_n$ terms:

$$\begin{aligned} F_u^{-1}\tilde{\theta}_2 &\approx -\frac{2}{3}(1-\delta)\,, & F_u^{-1}\tilde{\theta}_{31} &\approx -\frac{1}{6}(1-\delta)\,, \\ F_u^{-1}\tilde{\theta}_4 &\approx -(1-\delta)\,, & F_u^{-1}\tilde{\theta}_{32} &\approx -\frac{1}{6}\int_0^{\ln(a_0/a_f|^{(U)})}\frac{d\ln a/a_f}{(a/a_f)^2}f(a)\,. \end{aligned} \tag{9.46}$$

Hence, for s-wave cross sections, the change in the relic abundance due to small changes made by the PT can be expressed as

$$\delta n_X(t_0) = c_1\,\epsilon_1 + c_2\,\epsilon_2 + c_{31}\,\epsilon_{31} + c_{32}\,\epsilon_{32} + c_4\,\epsilon_4 \tag{9.47}$$

where

$$c_1 \equiv \frac{1}{2}\left(\delta + \frac{(1+3\delta)}{n-3}\left(1 - \frac{\Delta\rho_{\rm ex}}{\rho_{\rm ex}}\right)\right) - \frac{3}{2}\frac{1}{\ln A} \tag{9.48a}$$

$$c_2 \equiv -\frac{1}{3}(1+2\delta) \tag{9.48b}$$

$$c_{31} \equiv \frac{1}{6}(1-\delta) \tag{9.48c}$$

$$c_{32} \equiv \frac{1}{6}\int_0^{\ln(a_0/a_f|^{(U)})} \frac{d\ln a/a_f}{(a/a_f)^2}\,f\,(a) \tag{9.48d}$$

$$c_4 \equiv 1-\delta\,. \tag{9.48e}$$

The key point of Eq. (9.47) is that despite the "background" represented by $\epsilon_{n\neq 1}$, the "signal" contained in ϵ_1 can be "measured" and represents a prediction of the hypothesis of a tuned CC. It is a tuned but striking statement, nonetheless. Since this term is central to the rest of our calculation, we have reproduced the so called "CC effect" term here as

$$\begin{aligned} c_1\,\epsilon_1 = &\left(\frac{\rho_{\rm ex}}{\frac{\pi^2}{30}g_E(a_f)T_{PT}^4}\right)\frac{1}{(1+\delta)^4} \\ &\times\left\{\frac{1}{2}\left[\frac{(1+\delta)^3-1}{3} + \frac{(1+\delta)^3}{n_d-3}\left(1-\frac{\Delta\rho_{\rm ex}}{\rho_{\rm ex}}\right)\right] - \frac{3}{2}\frac{1}{\ln A}\right\} \end{aligned} \tag{9.49}$$

without linearizing in δ. We also write the so called "entropy effect" as

$$c_2\,\epsilon_2 = -\frac{\delta+\frac{1}{3}}{\delta+1}\frac{\Delta s}{\frac{2\pi^2}{45}g_S(a_{PT})\,T_{PT}^3}\,. \tag{9.50}$$

Note finally that we can obtain a smooth non-first order PT by taking the limit $\Delta\rho_{\rm ex} = \epsilon_2 = \epsilon_{31} = \epsilon_4 = 0$.

One should remember that all of the analysis has assumed that the entropy released from the PT (in the case of a first order PT) did not reheat the system to the point that the dark matter rethermalized after freeze out, i.e., $T_{PT}^{+} \lesssim T_f$. This provides a lower bound on δ for a given $\Delta\rho_{\rm ex}$, which can be expressed as

$$\frac{1}{4}\epsilon_{31} + \frac{1}{4}\frac{\Delta\rho_{\rm ex}}{\frac{\pi^2}{30}\, g_E(a_f)\,(T_{PT}^{-})^4} \lesssim \delta \tag{9.51}$$

by using Eq. (9.112) and assuming that $f(a_{PT})$ is negligible.

Note also that the range and independence of $\{\epsilon_i, \delta\}$ that is achievable by choosing a beyond the SM Lagrangian is not easy to compute nor to generalize. For example, suppose we want to increase δ while keeping ϵ_1 fixed. To increase δ, we increase a_{PT} more than a_f. Since a_f is mostly determined by the mass of the dark matter m_X while a_{PT} is determined in part by the competition between the thermal mass support and scalar field mass at the field origin, we can keep a_f fixed and increase a_{PT} by decreasing the scalar field mass competing with the thermal support. This, however, typically changes the fractional entropy increase ϵ_2 during the PT. Furthermore, this will change the index n_d (defined in Eq. (9.20)) which depends partly on the flatness of the non-thermal part of the scalar potential. Indeed, we see that if this n_d can be engineered to be as close to 3 as possible (i.e. a flat potential with no thermal particles decoupling), then the ϵ_1 signal can be enhanced. One also sees that in the case of a first order PT, the prediction for the effect of the cosmological constant (i.e., the ϵ_1 piece) depends on $\Delta\rho_{\rm ex}$ and δ, both of which depend on knowing exactly when the PT occurs. As described in Sec. 9.2, an accurate computation of this will require a non-perturbative numerical treatment. Hence, the first order PT situation, which can give a larger CC dependent signal, presents an interesting computational challenge of its own.

9.4 Illustrative Models

In this section, we present numerical calculations of $\delta n_X(t_0)$ for various models. This section represents one of the key features of the paper that distinguish it from (177), as discussed in the introduction. For each model we specify the parameters of the scalar sector, which appear in the thermal effective potential $V_{\text{eff}}(\phi_c, T)$, and the parameters of the dark matter sector, m_X, g_X, and $\langle \sigma v \rangle$. We then calculate the relic abundance shift using the methods of Section 9.3. Most of the numerical results have not been reported previously, and the model dependent analysis of a real singlet extension of the standard model is entirely new.

Standard Model with Dark Matter

We calculate here the relic abundance deviation due to the SM electroweak PT. The qualitative results were already given in (177). The numerical details that we discuss in this section can be summarized as $\delta n_X(t_0) = O\left(10^{-3} - 10^{-2}\right)$ with the CC contributing $c_1\epsilon_1 = O\left(10^{-4} - 10^{-3}\right)$. With $m_h = 115$ GeV, the largest CC effect occurs for $m_X \approx 4.2$ TeV where $c_1\epsilon_1 \approx 9.5 \times 10^{-4}$. Our results are summarized in Figure 9.2. In this section, we first discuss this figure and then extend the analytic estimate of Section 9.3, now in the context of a concrete model, to obtain Eq. (9.57), which lets us motivate extensions of the SM that achieve larger $\delta n_X(t_0)$. Some of the qualitative discussion of (177) is reproduced for completeness.

In Appendix 9.F we compute the SM thermal effective potential $V_{\text{eff}}(h_c, T)$ through one-loop order[6], where $h(x) = \sqrt{2}\left|H^\dagger H\right|^{1/2}$ is the radial component of the Higgs

[6]It is well known that the one-loop approximation breaks down at the temperature of the SM electroweak PT (340), and that accurate results require lattice calculations (89; 341; 342). However, since the CC contribution already represents perturbative correction to dark matter freeze out, we will neglect higher-order corrections to the PT physics and simply apply the mean field approximation described in Section 9.2.

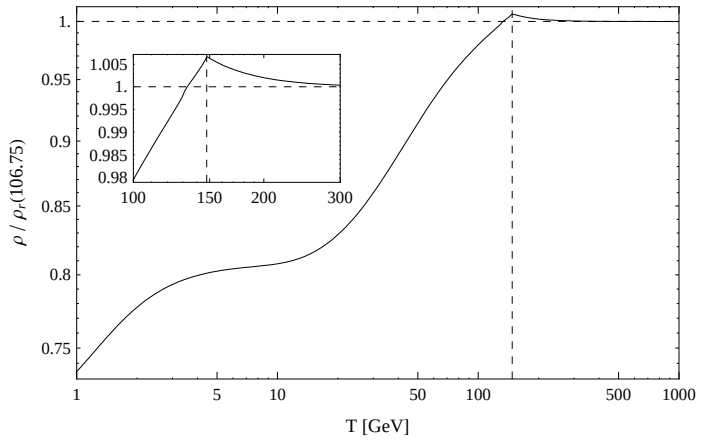

Figure 9.1: The energy density at the SM PT, $\rho(T) = \rho_{cc}(T) + \rho_R(T)$, relative to the energy density when the entire SM is relativistic, $\rho_r(106.75) \equiv \frac{\pi^2}{30} 106.75\, T^4$. Just before the PT at $T \gtrsim 150$ GeV, the energy density grows relative to ρ_r due to the temperature independent CC contribution, $\rho_{cc}(T > T_{PT}) \approx$ const. After the PT, the top, bottom, Higgs, and massive gauge boson adiabatically decouple causing ρ/ρ_r to drop below one. This adiabatic decoupling is the dominant feature of the SM PT that is relevant for freeze out.

field and $h_c = \langle h(x) \rangle$. It is important to point out that the renormalization conditions, given by Eq. (9.130), are chosen such that $V_{\text{eff}}(h_c, 0)$ has a minimum at $v = 246$ GeV where the curvature is m_h^2 and, most importantly the CC is tuned by requiring $V_{\text{eff}}(v, 0) = 0$.

Before discussing the numerical results, it is useful to recall from Section 9.3 that for a non-first order PT, freeze out is only affected by modifications to the relations $H(T) \propto \sqrt{\rho(T)} \propto T^2$ and $T^3 \propto g_S^{-1}\, a^{-3} \sim a^{-3}$. These modifications arise when the energy partitioning deviates from radiation domination and the number of relativistic degrees of freedom deviates from a constant value. These deviations can be visualized in Figure 9.1, where we plot $\rho(T)$ normalized by $\rho_r(106.75) \equiv (\pi^2/30)(106.75)\, T^4$, the energy density of the SM as if all particles were relativistic. We have taken $m_h = 115$ GeV which gives a PT at $T_{PT} \approx 148$ GeV. As the temperature decreases toward T_{PT} from above, ρ/ρ_r grows to approximately 1.006 due to the presence

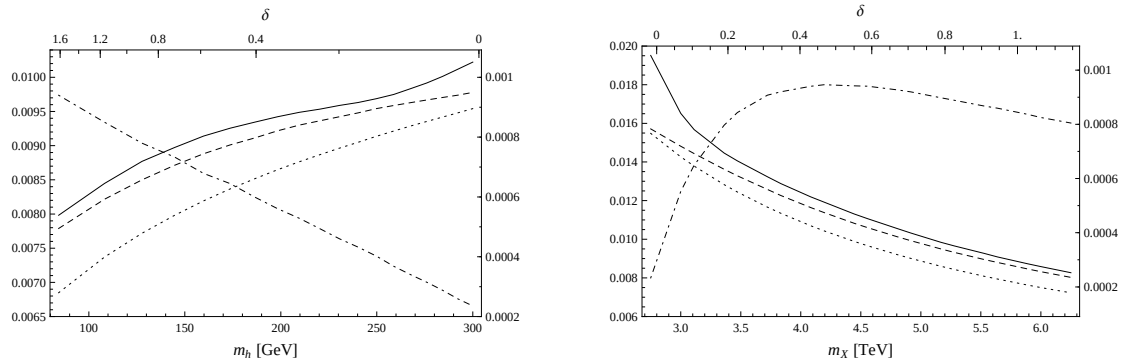

Figure 9.2: Fractional deviation of the relic abundance and due to the SM electroweak PT plotted against m_h (left) and m_X (right). The numerical calculation is represented by the solid curve, the analytic estimate Eq. (9.47) by the dashed curve, the CC effect ($c_1\epsilon_1$ term) by the dot-dashed curve, and the adiabatic decoupling effect ($c_{32}\epsilon_{32}$ term) by the dotted curve. The right axis shows the values of the $c_1\epsilon_1$ curve only, and the left axis shows the values of the three other curves.

of the additional CC energy density (i.e., $\lambda v^4/(106.75\, T_{PT}^4) \approx 10^{-3}$). Below T_{PT} the massive species decouple, the plasma loses about twenty relativistic degrees of freedom, and ρ/ρ_r decreases to approximately 0.8. This figure illustrates that the adiabatic decoupling has an effect on ρ which is two orders of magnitude larger than that from the CC. Therefore, we expect that the Standard Model electroweak effective CC will have a subdominant effect on the relic abundance as well.

The fractional shift $\delta n_X(t_0)$ is calculated using the perturbative, analytic expressions in Section 9.3 as well as by solving the Boltzmann equation numerically. In the left panel of Figure 9.2 we have plotted $\delta n_X(t_0)$ by varying m_h and fixing $m_X = 6$ TeV, $g_X = 2$, and $\langle \sigma v \rangle = 2.33 \times 10^{-39}\,\mathrm{cm}^2$. As seen in the figure, the PT causes an $O\left(10^{-3} - 10^{-2}\right)$ fractional increase in the relic abundance. We have chosen the DM mass to be 6 TeV such that freeze out and the PT coincide at $T \approx 303$ GeV for $m_h = 300$ GeV. For smaller m_h, the PT is delayed with respect to freezeout. The analytic estimate, given by Eq. (9.47), only receives contributions from the CC effect ($c_1\epsilon_1$ term) and the adiabatic decoupling effect ($c_{32}\epsilon_{32}$ term), because the PT

is not first order. As we anticipated in the discussion of the preceeding paragraph, the ϵ_{32} term dominates. The analytic formula consistently underestimates the numerical calculation by $2-3\%$, and moreover, in the large m_h limit where $\delta \approx 0$, the deviation grows to approximately 4.5%. Both of these features can be traced back to approximations we have made in the analytic estimate. The first is associated with the approximation Eq. (9.96), which assumes the number density per comoving volume decreases significantly due to residual annihilations and introduces an $O\left(T_f/m_X\right) \lesssim 5\%$ error at all m_h. The second is associated with neglecting the equlilibrium term $n_X^{\rm eq}$ in Eq. (9.8), which is not negligible at the start of the residual annihilation era. The scaling with m_h also has a simple, intuitive explanation. One can understand why $\delta n_X(t_0)$ is small at small m_h, because in this limit the PT occurs too late and becomes decoupled from freeze out. Considering the opposite limit, one may wonder if $\delta n_X(t_0)$ continues to increase for $m_h \gtrsim 300$ GeV where $\delta < 0$. For $\delta < 0$ the PT occurs before freeze out, as in the usual cosmology, and one would naively expect $\delta n_X(t_0) = 0$. Nevertheless, $\delta n_X(t_0)$ does continue to grow because of the way we have defined $n_X^{(U)}$. To calculate the usual relic abundance $n_X^{(U)}$ we assume that there are 106.75 relativistic species at freeze out. If the PT occurs much earlier, the number of relativistic species at freeze out will be significantly less than 106.75 and $\delta n_X(t_0)$ will be non-zero. The CC contribution grows monotonically with decreasing m_h, since in this limit the PT temperature decreases and $c_1\epsilon_1 \sim \rho_{\rm ex}/T_{PT}^4$.

On the right panel of Figure 9.2 we plot the relic abundance shift by fixing $m_h = 115$ GeV and varying m_X. At large m_X, freeze out occurs well before the PT, the two events decouple, and the relic abundance shift is small. At small $m_X \lesssim 2.8$ TeV, freeze out occurs after the PT, and the analytic estimate fails. The CC effect $c_1\epsilon_1$ has a maximum of approximately 10^{-3} at $\delta_{max} \approx 0.5$. For $\delta > \delta_{max}$ the factor ϵ_1, given by Eq. (9.26a), is small because T_f in the denominator is large. For $\delta < \delta_{max}$ the

factor c_1, given by Eq. (9.48a), is small because the CC is only present over a short time during WIMP residual annihilations. The presence of this maximum suggests that $c_1\epsilon_1$ will typically be more sensitive to variations in the parameters of the scalar sector (e.g., m_h) than in variations of the DM sector (e.g., m_X). With this in mind, we will focus the remainder of our discussion on determining the conditions that a scalar potential must satisfy to maximize $c_1\epsilon_1$.

We will now extend the estimates of Section 9.3 in order to understand Figure 9.2 through a simple analytic approximation. We focus on the CC contribution to $\delta n_X(t_0)$, given by Eq. (9.49), which is

$$\delta n_X(t_0) \ni c_1\epsilon_1 \sim \frac{1}{10}\frac{\rho_{\rm ex}}{g_E\, T_{PT}^4} \tag{9.52}$$

up to multiplication by an $O(1)$ function of δ. The factor of $g_E \approx 106.75$ represents the SM relativistic degrees of freedom before the PT. If we assume that before the PT, the SM particles are light with respect to the temperature, then we can approximate $V_{\rm eff}$ using the so-called high-temperature approximation

$$V_{\rm eff}(h_c, T) \approx \frac{\lambda_{eff}}{4}\left(h_c^2 - v^2\right)^2 + c\,T^2 h_c^2\,. \tag{9.53}$$

Here we have defined $\lambda_{eff} \equiv \frac{4}{v^4}\left[V_{\rm eff}(0,0) - V_{\rm eff}(v,0)\right]$ to be the one-loop effective self-coupling and $2\,c\,T^2$ is the thermal mass acquired by Higgs particles passing through the plasma. In the SM and subject to our renormalization scheme, these dimensionless numbers are $\lambda_{eff} \approx \lambda_{SM}$ and $c \approx c_{SM}$ where

$$c_{SM} = \frac{1}{24v^2}\left(6m_t^2 + 6m_b^2 + 6m_w^2 + 3m_z^2 + \frac{3}{2}m_h^2\right) \tag{9.54a}$$

$$\lambda_{SM} = \frac{m_h^2}{2v^2} + \frac{48m_t^4 + 48m_b^4 - 24m_w^4 - 12m_z^4 - (15+\log 4)m_h^4}{128\pi^2 v^4}\,, \tag{9.54b}$$

which yield $c_{SM} \approx 0.18$ and $\lambda_{SM} \approx 0.12$ for $m_h \approx 115$ GeV. The PT occurs at a temperature T_{PT} where $\partial_{h_c}^2 V_{\rm eff}(0, T_{PT}) = 0$. Solving for this temperature one obtains

$$c\,T_{PT}^2 = \frac{\lambda_{eff}}{2}v^2\,. \tag{9.55}$$

Before the PT, the CC energy density is

$$\rho_{\rm ex} = V_{\rm eff}(0,0) = \frac{\lambda_{eff}}{4} v^4 \tag{9.56}$$

and we can estimate the deviation in the relic abundance using Eq. (9.52) to be

$$c_1 \epsilon_1 \sim \frac{1}{10} \frac{1}{g_E} \frac{c^2}{\lambda_{eff}} \,. \tag{9.57}$$

For natural couplings one expects $c^2/\lambda_{eff} \sim O\,(1)$ (e.g., $c_{SM}^2/\lambda_{SM} \approx 0.28$) and finds $c_1\epsilon_1 \sim 1/(10 g_E) \sim 10^{-3}$. Recalling also that $\lambda_{eff} \sim m_h^2$, one sees that this estimate agrees well with both the magnitude and scaling shown in Figure 9.2. Note that in the $\lambda_{eff} \to 0$ limit, we find that both $\rho_{\rm ex}$ and T_{PT} approach zero, but the ratio $\rho_{\rm ex}/T_{PT}^4$ becomes large. This simple approximation suggests that the region of parameter space that maximizes the CC contribution to $\delta n_X(t_0)$ will have low temperature PTs. This is evident in Figure 9.2 because the CC effect grows at low m_h where the PT temperature is low. Hence we will next consider a model in which a scalar singlet coupled to the Higgs is introduced to lower the PT temperature.

SM Singet Extension with $\mathbb{Z}_2$

In this section, we briefly discuss an extension of the Standard Model in which the presence of an additional scalar field modifies the electroweak PT dynamics. However, we show that the dark matter relic abundance is not significantly enhanced, and we argue that we should consider models with first order PTs. Consider an extension of the SM in which a real, singlet, scalar field $s(x)$ is coupled to the Higgs $h(x)$ through interactions which respect the $\mathbb{Z}_2$ symmetry $s \to -s$. The renormalized potential for this theory can be written as

$$U(\{h,s\}) = \frac{m_h^2}{8v^2}\left(h^2 - v^2\right)^2 + \frac{b_4}{4}s^4 + \frac{1}{2}m_s^2 s^2 + \frac{a_2}{2}s^2\left(h^2 - v^2\right) \tag{9.58}$$

such that $\partial_h U(\{v,0\}) = 0$, $\partial_h^2 U(\{v,0\}) = m_h^2$ and $\partial_s^2 U(\{v,0\}) = m_s^2$. We require

$$m_s^2 - a_2\, v^2 > 0 \qquad \text{and} \qquad 2a_2 + b_4 + \frac{m_h^2}{2v^2} > 0 \tag{9.59}$$

to ensure $\langle s \rangle = 0$. This model, known as the $\mathbb{Z}_2$xSM, has been previously studied in order to determine the viability of s as a dark matter candidate (108; 186–191). We will not restrict ourselves to this scenario, but instead treat the dark matter as a separate sector. The role of s is simply to modify the PT dynamics (107; 110; 112; 117; 118)[7].

Since this model possesses a greater parametric freedom than the SM, we can attempt to verify the relationship Eq. (9.57), derived in the previous section, which relates $c_1\epsilon_1 \sim c^2/\lambda_{eff}$. This is accomplished by first mapping the parameters of the $\mathbb{Z}_2$xSM to c and λ_{eff}, and second by performing a parameter scan while calculating $c_1\epsilon_1$. We obtain c and λ_{eff} by calculating the thermal effective potential as described in the previous section (see also Appendix 9.F). If we assume that the quanta of $s(x)$ are light with respect to the temperature, we can then extract c and λ_{eff} by matching the effective potential to Eq. (9.53). Doing so yields the expressions

$$c = c_{SM} + \frac{a_2}{24} \tag{9.60}$$

$$\lambda_{eff} = \lambda_{SM} - \frac{a_2^2}{32\pi^2}\,\psi\left(\frac{a_2 v^2}{m_S^2}\right) \tag{9.61}$$

$$\psi(x) \equiv 3 - \frac{2}{x} - 2\left(1 - \frac{2}{x} + \frac{1}{x^2}\right)\log\left[1 - x\right] \tag{9.62}$$

where the terms containing a_2 arise from 1-loop diagrams with an s-particle in the loop, and the function ψ varies from $\psi(0) = 0$ to $\psi(1) = 1$. As a result of the minus sign in Eq. (9.61), there is an upper bound $a_2 \lesssim 5$ given by the constraint $\lambda_{eff} > 0$. Now we can see the impact of the singlet field on the PT. For $a_2 > 0$,

[7] See also (99–101; 114) for PT studies of the similar singlet Majoron model and (98; 102; 104) for the complex singlet.

the parameter c is slightly larger and λ_{eff} is slightly smaller than in the SM. Recall that the PT temperature, given by Eq. (9.55), scales like $T_{PT}^2 \sim \lambda_{eff}/c$. Hence, the singlet field lowers the PT temperature and makes the CC energy density relatively more significant, which causes the relic abundance shift to be greater.

To verify these analytic arguments, we calculate the PT temperature and $c_1\epsilon_1$ numerically over a region of the theory space. We allow m_h^2 and a_2 to vary in the ranges $m_h^2 \in [(50\text{ GeV})^2, (300\text{ GeV})^2]$ and $a_2 \in [-0.1, 4.0]$, and we fix $b_4 = 0.25$ and $m_s^2 = (500\text{ GeV})^2$. The range for m_h is chosen to prevent the Higgs from becoming unacceptably light[8], while the range for a_2 is chosen to satisfy Eq. (9.59) and to avoid the unitarity bound. We map m_h^2 and a_2 to c and λ_{eff} using Eqs. (9.60) and (9.61). In Figure 9.3, we have plotted the contribution to $\delta n_X(t_0)$ from the CC effect ($c_1\epsilon_1$) over the c^2/λ_{eff}–m_h plane. This figure shows that the CC effect grows with increasing c^2/λ_{eff} and decreasing m_h, as we anticipated in Eq. (9.57). The largest value of $c_1\epsilon_1$ is approximately 1.3×10^{-3}, which is only about 40% larger than in the SM. The insignificant enhancement can be understood by observing that although $a_2 > 0$ tends to decrease c, given by Eq. (9.60), its contribution is suppressed by a factor of 24. Since $c_{SM} \approx 0.18$ we run into the unitarity bound on a_2 before it contributes significantly to c. If we were to add N light singlet fields instead of one, the contribution to c would be $Na_2/24$, which can be order one even for small a_2. We have not take this approach here because the N additional relativistic degrees of freedom would have a larger effect on the relic abundance by increasing the energy density of radiation than through the CC. We have also plotted $c_1\epsilon_1$ for three different values of the WIMP mass from 4 to 8 TeV. This narrow range of viable parameters illustrates the tuning that is required to ensure that the PT and freeze out occur

[8]Mixing with the singlet does not significantly reduce the LEP Higgs search bound (108). Moreover, for small m_h the electroweak breaking minimum may become metastable (117; 186), and the PT becomes first order (90). Nevertheless, we have allowed m_h to be as small as 50 GeV to illustrate the parametric dependence of the CC effect.

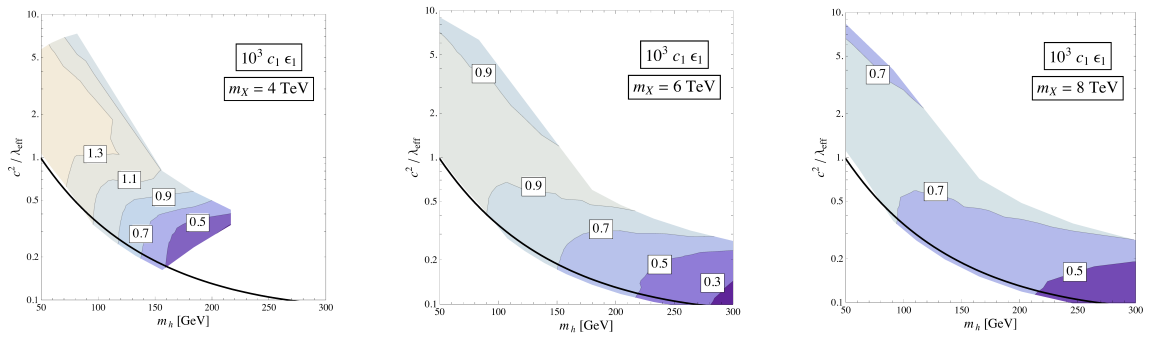

Figure 9.3: The CC contribution to $\delta n_X(t_0)$, given by the $c_1\epsilon_1$ term of Eq. (9.47), plotted over the c^2/λ_{eff}–m_h plane for three values of m_X. The black line represents the SM ($a_2 = 0$).

at the same time. If the WIMP mass is too large, freeze out occurs too long before the PT when the CC energy density was subdominant to the energy density of the plasma. As the WIMP mass is lowered, the delay between freeze out and the PT decreases and $c_1\epsilon_1$ grows. If the WIMP mass is too small, freeze out occurs after the PT when the CC energy density has been converted into radiation. This is the case in the $m_h \gtrsim 200$ region of the $m_X = 4$ TeV plot.

The examples of the SM and the $\mathbb{Z}_2$xSM demonstrate that it is challenging to obtain $c_1\epsilon_1$ larger than $O\left(10^{-3}\right)$. Our discussion at the end of Section 9.4 and simple dimensional analysis illustrate why this is the case. In that calculation we obtained Eq. (9.57) which can be written schematically as $c_1\epsilon_1 \sim \rho_{\rm ex}/T_{PT}^4 \sim c^2/\lambda_{eff}$. Note that the mass scale v, which controls both $\rho_{\rm ex}$ and T_{PT}, cancels out in the ratio $\rho_{\rm ex}/T_{PT}^4$. In light of Eq. (9.57) we propose that the CC effect can be enhanced by working in a model that has multiple mass scales if there exists a hierarchy between them. We will explore different applications in the remainder of this section.

Generic Single Scalar Model

In this section we calculate the CC contribution to the relic abundance shift in a generic single scalar model. Although extensions of the Standard Model typically contain multiple scalar degrees of freedom related by symmetries, the thermal dynamics (supercooling and reheating) of a symmetry breaking PT can often be modeled by a single scalar degree of freedom which does not display the symmetries of the full theory (111; 177). With this motivation in mind, we consider the theory of a real scalar field $\varphi(x)$ coupled to N Dirac fields $\psi_i(x)$. The scalar field will experience a first order PT during which dark matter freezes out, and the light fermions will compose the hot thermal bath. Using this construction, we will be able to calculate the CC effect, which is related to the non-thermal energy density and the amount of supercooling, but we cannot estimate the entropy and decoupling effects since these depends on how φ is coupled to the full theory. Therefore, in this section we assume no decoupling occurs near the time of the PT and that the number of relativistic species is fixed to $g_{E/S} \approx 106.75$, the relativistic SM background. Let the action be given by

$$S[\varphi] = \int d^4x \left\{ \frac{1}{2}(\partial\varphi)^2 - U(\varphi) - \sum_{i=1}^{N} \bar{\psi}_i \left(i\partial\!\!\!/ - m_i - h_i\varphi \right) \psi_i + \mathcal{L}_{\rm ct} \right\} \tag{9.63}$$

where

$$U(\varphi) = \rho_{\rm ex} + \frac{1}{2}M^2\varphi^2 - \mathcal{E}\varphi^3 + \frac{\lambda}{4}\varphi^4 \tag{9.64}$$

is the renormalized potential and $\mathcal{L}_{\rm ct}$ is the counterterm Lagrangian. Note that we have eliminated the tadpole term in $U(\varphi)$ by defining the origin in field space appropriately, but there is still a counterterm for the tadpole in $\mathcal{L}_{\rm ct}$. As discussed in Section 9.4, we expect that there will be a greater impact on the dark matter relic abundance if freeze out occurs during a first order PT with large supercooling. Hence,

we would like to understand what region of parameter space yields a PT of this kind. In particular, we expect that large supercooling can be obtained if the theory $S[\varphi]$ possesses two vacua, which will correspond to the low- and high-temperature phases, and that the vacua are separated by a barrier (106; 115; 118).

We can determine the vacuum structure by identifying the minima of the effective potential, which is calculated in Appendix 9.F. Provided that the non-thermal radiative corrections are negligible, the effective potential can be approximated as $V_{\rm eff}(\varphi_c, T = 0) \approx U(\varphi_c)$. It is convenient to eliminate M^2 for the dimensionless quantity $\alpha_0 \equiv \lambda M^2/2\mathcal{E}^2$ while assuming $\lambda\mathcal{E} \neq 0$. We now see that the parameter α_0 controls the shape of the potential $U(\varphi)$: for $\alpha_0 = 1$, the potential has two degenerate minima at $\varphi_c = 0$ and $\varphi_c = v|_{\alpha_0=1}$ where

$$v = \frac{3\mathcal{E}}{2\lambda}\left(1 + \sqrt{1 - \frac{8}{9}\alpha_0}\right) ; \tag{9.65}$$

for $\alpha_0 > 1$, $\varphi_c = 0$ is the global minimum; for $0 < \alpha_0 < 1$, $\varphi_c = v$ is the global minimum; and for $\alpha_0 < 0$, $\varphi_c = 0$ becomes a maximum (see also Figure 9.4). Therefore, provided that we take $0 \lesssim \alpha_0 \lesssim 1$, the theory possesses a metastable vacuum in which $\varphi_c \approx 0$ and a stable vacuum in which $\varphi_c \approx v$. In the stable vacuum, we impose the tuning condition $V_{\rm eff}(v, 0) = 0$ to solve for

$$\rho_{\rm ex} \approx \frac{\mathcal{E}^4}{8\lambda^3}\left[27 - 36\,\alpha_0 + 8\,\alpha_0^2 + 27\left(1 - \frac{8}{9}\alpha_0\right)^{3/2}\right] + O\left(\hbar\right) , \tag{9.66}$$

which represents the CC energy density prior to the PT. Finally, the barrier separating the two vacua has a "height"

$$V_{\rm barrier} = U(\text{barrier}) - U(0) \approx \frac{4\mathcal{E}^4\alpha_0^3}{27\lambda^3}\Big[1 + O\left(\alpha_0\right)\Big] \tag{9.67}$$

relative to the metastable vacuum. Due to the factor of α_0^3, the barrier vanishes rapidly as α_0 approaches zero. This is illustrated by the $\alpha_0 = 0.5$ curve of Figure 9.4 in which the barrier is already almost imperceptible to the eye.

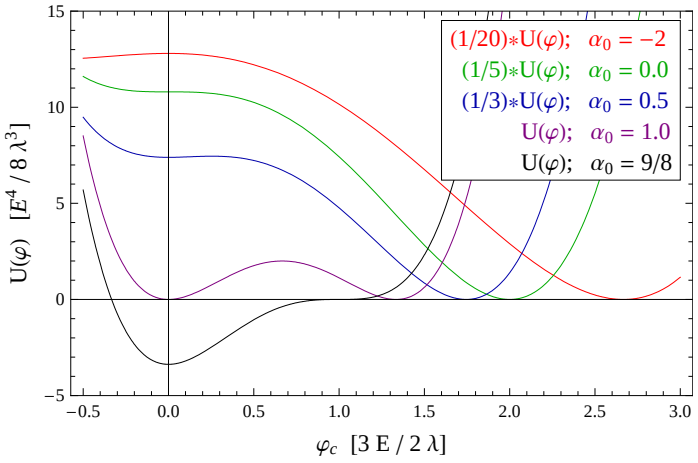

Figure 9.4: An illustration of the α_0 dependance of the potential given by Eq. (9.64). The curves represent $\alpha_0 = -2$ (red), $\alpha_0 = 0$ (green), $\alpha_0 = 0.5$ (blue), $\alpha_0 = 1$ (purple), and $\alpha_0 = 9/8$ (black).

Having established that this theory admits two vacua, we will study the PT using the thermal effective potential. Although the numerical calculations use the full effective potential, we can gain some intuition by making the high temperature approximation. We assume that the ψ_i-particles are light with respect to the temperature of the thermal bath, $m_i^2 \ll T^2$, and that the φ-particles are heavy. In this limit, then the one-loop thermal effective potential may be approximated by the high temperature expansion

$$V_{\text{eff}}(\varphi_c, T) \approx U(\varphi_c) + c\,T^2\varphi_c^2 + O\left(m_i^2/T^2\right) + O\left(\hbar\right) \tag{9.68}$$

where $c \approx \sum_{i=1}^{N} h_i^2/12$ is related to the couplings between φ and ψ_i. Just as we introduced α_0 to reparametrize $V_{\text{eff}}(\varphi_c, 0)$, we can now introduce

$$\alpha(T) = \alpha_0\left(1 + \frac{\lambda c}{\mathcal{E}^2\alpha_0}T^2\right) \geq \alpha_0 \tag{9.69}$$

to parameterize $V_{\text{eff}}(\varphi_c, T)$. This definition is particularly convenient, because now Figure 9.4 also illustrates the temperature dependence of $V_{\text{eff}}(\varphi_c, T)$ (up to φ_c-independent terms) if one replaces α_0 with $\alpha(T)$. We obtain the expectation values of φ in the

"symmetric" and "broken" phases, $v^{(s)}(T)$ and $v^{(b)}(T)$, by solving $(\partial/\partial\varphi_c)V_{\rm eff}(\varphi_c, T) = 0$ subject to the boundary conditions $v^{(b)}(0) = v$ and $v^{(s)}(0) = 0$. We use the terms "symmetric" and "broken," eventhough $S[\varphi]$ does not display a symmetry in order to connect with the notation of Section 9.2.

Provided that this model experiences a first order PT, the CC's effect on the relic abundance will depend sensitively on the amount of supercooling at the PT (112). This is seen by the factor of $(T_f)^4 \approx (T_{PT}^-)^4$ in Eq. (9.26a). Therefore, we will begin by investigating the parametric dependence of the amount of supercooling, and we will see that it has an interesting dependance on the parameter α_0. The supercooling stage begins when the temperature drops below

$$T_c \approx \mathcal{E}\sqrt{\frac{1-\alpha_0}{\lambda\, c}}\,, \tag{9.70}$$

defined by Eq. (9.2), or equivalently when $\alpha(T_c) = 1$. During supercooling, the universe remains in the metastable, symmetric phase until bubbles of the broken phase begin to nucleate. Bubble nucleation is a non-perturbative process (343), and it occurs at a rate per unit volume which carries the standard exponential suppression $\Gamma \sim T^4 \exp\left[-S^{(3)}/T\right]$, where $S^{(3)}(T)$ is the action of the O(3) symmetric bounce (202; 204; 205). Provided that $V_{\rm eff}(\varphi_c, T)$ can be expressed in the form of Eq. (9.68), then $S^{(3)}$ is well approximated by the empirical formula (307)

$$\frac{S^{(3)}}{T} \approx 13.7\,\frac{\mathcal{E}}{T}\left(\frac{\alpha}{\lambda}\right)^{3/2} f(\alpha) \tag{9.71}$$

$$f(\alpha) \equiv 1 + \frac{\alpha}{4}\left(1 + \frac{2.4}{1-\alpha} + \frac{0.26}{(1-\alpha)^2}\right) \tag{9.72}$$

with $\alpha = \alpha(T)$. Bubbles form rapidly once the bubble nucleation rate averaged over a Hubble volume $\Gamma\, H^{-3}$ is comparable to the Hubble expansion rate $H \sim T^2/M_p$. For an electroweak scale PT, this equality occurs when $S^{(3)}/T$ drops below approximately 140 (98; 206). Therefore, we can determine the amount of supercooling by solving $S^{(3)}/T \approx 140$ for $T = T_{PT}^-$ and comparing this temperature with T_c.

Considerations of the equation $S^{(3)}/T \approx 140$ demonstrate that the nature of the PT is strongly dependent upon the vacuum structure of the theory, as parametrized by α_0. We will discuss the two cases $\alpha_0 > 0$ and $\alpha_0 < 0$ separately. For $\alpha_0 > 0$, the vacuum with $\varphi_c = 0$ remains metastable as $T \to 0$. This implies that T_{PT}^{-} can be arbitrarily low, and in this limit of large supercooling the CC effect may be arbitrarily large. However, in this case the barrier in $V_{\rm eff}(\varphi_c, T)$ persists as $T \to 0$, and it is possible that the PT does not occur at any temperature, but instead that the universe becomes trapped in the metastable vacuum. This follows from the observation that for $\alpha_0 > 0$, $S^{(3)}/T$ has a minimum at finite T: at low temperatures $S^{(3)}/T$ grows due to the explicit factor of T in the denominator, and at high temperatures $f(\alpha)$ diverges as T approaches T_c and $\alpha \to 1$. For $\alpha_0 \lesssim 1$ the inequality $S^{(3)}/T \lesssim 140$ is not satisfied at any temperature, and the PT does not occur[9]. Therefore, if we require that the PT must occur via thermal bubble nucleation, we obtain an upper bound on α_0. On the other hand, for the case $\alpha_0 < 0$, the PT necessarily occurs at a temperature $T_{PT}^{-} > 0$, since the symmetric phase becomes perturbatively unstable at low temperatures. This latter case has the drawback that supercooling cannot last an arbitrarily long time.

Assuming that the PT does occur, we can quantify the amount of supercooling using

$$\delta_{SC} = 1 - \frac{T_{PT}^{-}}{T_c}\,, \tag{9.73}$$

which takes values between 0 and 1. Parametrizing the temperature dependance with

[9] At least, the PT does not occur as a thermal process, although it may still occur as a quantum tunneling process (204). However, since quantum tunneling typically proceeds on a longer time scale, the universe could enter an inflationary phase, which leads to a cosmological history that deviates significantly from the perturbations we consider in Section 9.3.

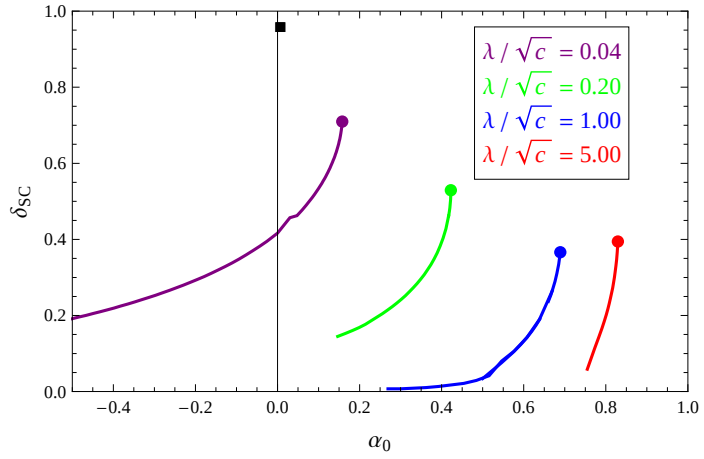

Figure 9.5: The amount by which the PT temperature drops below the critical temperature, quantified by δ_{SC}, is plotted against the parameter α_0 which controls the height of the barrier. The curves represent $\lambda/\sqrt{c} = 0.04$ (purple), 0.20 (green), 1.00 (blue), and 5.00 (red). The square indicates the especially tuned parameter set given by Eq. (9.78).

δ_{SC}, we can rewrite Eq. (9.71) as

$$\left.\frac{S^{(3)}}{T}\right|_{T_{PT}^-} \approx 13.7 \left(\frac{\lambda}{\sqrt{c}}\right)^{-1} \frac{\alpha^{3/2}}{\sqrt{1-\alpha_0}} \frac{f(\alpha)}{1-\delta_{SC}} \tag{9.74}$$

$$\alpha = \alpha_0 + (1-\alpha_0)(1-\delta_{SC})^2\,, \tag{9.75}$$

which is now only a function of $\alpha_0, \lambda/\sqrt{c}$, and δ_{SC}. Of course, this expression is approximate, since we assumed $V_{\rm eff}$ took the form of Eq. (9.68), but it suggests that the amount of supercooling will depend most sensitively on α_0 and $\lambda/\sqrt{c}$. Now using the full thermal effective potential, we impose $S^{(3)}/T\big|_{T_{PT}^-} = 140$ and solve for δ_{SC}, which we have plotted in Figure 9.5 for various parameter sets:

$$\mathcal{E} = 5 \text{ GeV} \qquad \lambda = \{0.004,\ 0.02,\ 0.10,\ 0.50\}$$
$$N = 1 \qquad m = 10 \text{ GeV} \qquad h = 0.346 \qquad c \approx 0.01\,. \tag{9.76}$$

The supercooling grows with increasing α_0 and decreasing $\lambda/\sqrt{c}$ as the barrier height and bounce action are made larger. The amount of supercooling is typically $\delta_{SC} =$

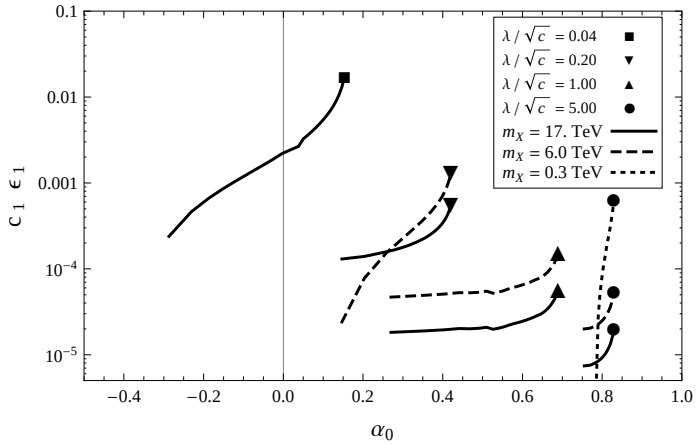

Figure 9.6: The CC effect on the relic abundance $c_1\epsilon_1$ plotted against α_0 for $m_X = 17$ TeV (solid), 6 TeV (dashed), and 0.3 TeV (dotted), and for four values of $\lambda/\sqrt{c}$ as indicated by the shape used to denote the endpoint. For the contours which are absent, freeze out occurs after the PT when the CC is not EW-scale.

$O\,(0.5)$ which implies $T_{PT}^{-} = O\,(T_c/2)$. Above a finite value of α_0 (indicated by a dot) the barrier becomes insurmountably large, and the universe becomes trapped in the metastable vaccum. The largest amount of supercooling is achieved for $\lambda/\sqrt{c} \ll 1$ and $0 < \alpha_0 \ll 1$. In this parameter regime the CC is large (see Eq. (9.66)), and the metastable vacuum is separated from the true vacuum by small barrier (see Eq. (9.67)).

Having come to understand the parametric dependance of the amount of supercooling as φ experiences a first order PT, we turn our attention back to calculating the impact of such a PT on dark matter freeze out. Using Eq. (9.49) we calculate the effect of the CC on the relic abundance shift and present the results in Figure 9.6. We have chosen the same parameters as indicated in Eq. (9.76) and have taken

$$m_X = \{0.3,\ 6.0,\ 17\}\ \text{TeV} \qquad g_X = 2 \qquad \langle\sigma v\rangle = 2.33 \times 10^{-39}\text{cm}^{-2} \tag{9.77}$$

as well. The figure illustrates that is possible to achieve $c_1\epsilon_1 = O\,(0.01)$ in the tuned parametric regime where $\lambda/\sqrt{c}$ is small and α_0 approaches its maximally allowed

value. Some of the curves are absent for the smaller WIMP masses. This occurs because as m_X is lowered, the temperature of freeze out decreases as well. In the case that $\lambda/\sqrt{c}$ is small and the PT temperature is high (see Eq. (9.70)), freeze out will occur after the PT for small m_X. This statement about the relative times of freeze out and the PT also explains why $c_1\epsilon_1$ is insensitive to α_0 for certain parameter sets (e.g., $\lambda/\sqrt{c} = 1$, $m_X = 17$ TeV) and very sensitive for others (e.g., $\lambda/\sqrt{c} = 5$, $m_X = 0.3$ TeV). In the first case, freeze out occurs long before the PT while in the latter case, freeze out occurs just before and during the PT and there is a large impact on the relic abundance.

To conclude this section, we present a particular tuned parameter set which yields $c_1\epsilon_1 = O(1)$. Suppose that we have only one fermion ψ and the parameters of $S[\varphi]$ are given by

$$\begin{gathered} \lambda = 5.4 \times 10^{-4} \qquad\qquad h = 0.1 \\ \mathcal{E} = 0.27 \text{ GeV} \qquad M^2 = (1.89 \text{ GeV})^2 \qquad m = 10 \text{ GeV} \end{gathered} \tag{9.78}$$

which leads to

$$\begin{aligned} v &\approx 1497 \text{ GeV} & \alpha_0 &\approx 0.007 \\ c &\approx 8.3 \times 10^{-4} & \frac{\lambda}{\sqrt{c}} &\approx 0.018 \end{aligned} \tag{9.79}$$

and PT temperatures

$$T_c \approx 374 \text{ GeV} \qquad T_{PT}^{-} \approx 16 \text{ GeV} \qquad \delta_{SC} \approx 0.96\,. \tag{9.80}$$

This parameter set is represented on Figure 9.5 by a square marker. In the dark matter sector we take

$$m_X = 600 \text{ GeV} \qquad g_X = 2 \qquad \langle \sigma v \rangle = 2.33 \times 10^{-39} \text{cm}^{-2} \tag{9.81}$$

such that

$$T_f \approx 34 \text{ GeV} \qquad \text{and} \qquad \delta \approx 1.12\,. \tag{9.82}$$

Using these values we can estimate the CC effect as

$$c_1\epsilon_1 \approx 6.1 \tag{9.83}$$

Note that the potential obtained with these parameters has a very shallow metastable vacuum at $\varphi_c \approx 0$, separated from the global vacuum at $\varphi_c \approx v$ by a very small barrier.

Singlet Extension with First Order PT

In this section, we consider a generalization of the SM extension studied in Section 9.4, in which we do not impose a $\mathbb{Z}_2$ symmetry on the singlet field $s(x)$. This leads to model known as the xSM (108; 186). The xSM admits a first order electroweak PT (103; 105–107; 109; 111; 115; 116; 118), and we seek to compute the effect on the relic abundance due to the effective CC at the PT. As discussed in Section 9.4, the CC effect grows with the duration of supercooling. With this in mind, we will focus on a region of parameter space in which we expect to have first order PTs with large supercooling. Supercooling is an example of the hierarchy of mass scales which we argued in Section 9.4 helps to obtain a larger CC effect.

We generalize the $\mathbb{Z}_2$xSM potential Eq. (9.58) by relaxing the $\mathbb{Z}_2$ symmetry. This allows us to write down the three additional operators sh^2, s^3, and s, but we eliminate the tadpole by an appropriate shift in the field space. We are left with the xSM renormalized potential

$$\begin{aligned} U(\{h,s\}) =& \frac{m_h^2}{8v^2}\left(h^2-v^2\right)^2 + \frac{b_4}{4}s^4 + \frac{1}{2}m_s^2 s^2 \\ &+ \frac{b_3}{3}s^3 + \frac{1}{2}s\left(h^2-v^2\right)(a_1+a_2 s)\,. \end{aligned} \tag{9.84}$$

The thermal effective potential $V_{\rm eff}$ is calculated in Appendix 9.F. With this parametrization, $V_{\rm eff}(\{h_c, s_c\}, T = 0)$ has a minimum at $\{h_c, s_c\} = \{v, 0\}$ where $V_{\rm eff}(\{v, 0\}, T = 0) = 0$ and the curvatures in the h and s directions are m_h^2 and m_s^2 respectively. The Higgs vacuum expectation value is fixed by electroweak constraints, but the six real numbers $\{m_h^2, m_s^2, b_4, b_3, a_1, a_2\}$ are free parameters.

As in the previous section, we compute the bounce action $S^{(3)}$ in order to estimate the PT temperature T_{PT}^- by solving $S^{(3)}/T \approx 140$. This calculation is made more challenging by the presence of the additional field direction. To obtain $S^{(3)}$ we make the approximation that the PT occurs along the trajectory $\bar{s}(h_c)$ satisfying

$$\left.\frac{dU(\{h_c, s_c\}, 0)}{ds}\right|_{\bar{s}_c} = 0 \qquad \text{and} \qquad \bar{s}_c(v) = 0\,, \tag{9.85}$$

which reduces the problem back to solving for the bounce in one dimension. In the region of parameter space on which we are focused, this approximation gives T_{PT}^- to within a few percent (see Appendix 9.G for details). Note that the empirical formula Eq. (9.71) cannot be applied here, because the effective potential is not well approximated by the form Eq. (9.68).

We have performed a parameter space scan and searched for a region with large corrections to the relic abundance from the CC. In the scan we fix the parameters $b_3 = -20$ GeV, $b_4 = 0.2$, $a_1 = -25$ GeV, and $a_2 = 0.2$, and we vary $m_h^2 \in [(65\text{ GeV})^2, (170\text{ GeV})^2]$ and $m_S^2 \in [(40\text{ GeV})^2, (140\text{ GeV})^2]$. In order to connect with the intuition garnered from the single field model of Section 9.4, we have mapped the xSM parameter space to a single parameter M^2. This is accomplished by restricting to the trajectory given by Eq. (9.85) and defining

$$M^2 \equiv \frac{d}{dx^2} V_{\rm eff}\left(\{h_c(x), \bar{s}_c(h_c(x))\}, T = 0\right)\Big|_{x=0} \tag{9.86}$$

where x parametrizes the position along the curve $\bar{s}_c(h)$. The parameter M^2 controls the stability of the electroweak preserving vacuum: if $M^2 > 0$ the symmetric phase

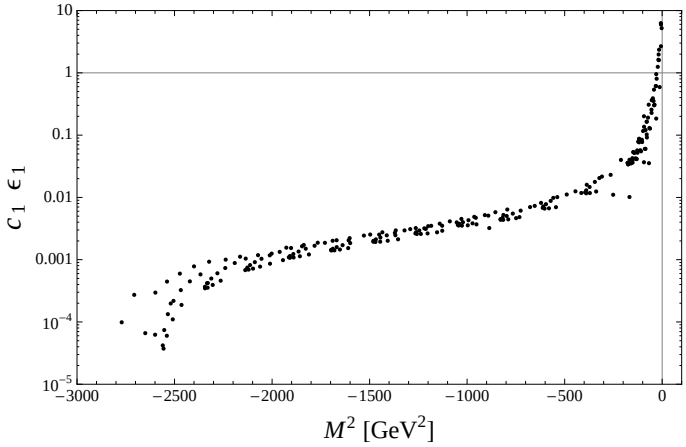

Figure 9.7: The fractional deviation in the relic abundance of a 2 TeV WIMP due to the CC at the xSM electroweak PT. The parameter M^2 controls the curvature of the zero temperature effective potential along the PT trajectory. For $M^2 \lesssim 0$ large supercooling enhances the CC's effect. For $M^2 \gtrsim 0$ the PT does not occur, and for $M^2 \lesssim -2500$ GeV^2 the PT occurs before freeze out leading to a suppression of the relic abundance shift.

remains metastable as $T \to 0$, whereas if $M^2 < 0$ the symmetric phase becomes perturbatively unstable at some finite temperature $T_0 > 0$. In this way, the potential depends on the parameter M^2 in the same way as the parameter α_0 from Section 9.4. We cannot map the xSM parameter space to α_0 directly because the effective potential along the trajectory Eq. (9.85) cannot be expressed in the form of Eq. (9.68).

In Figure 9.7, we have plotted $c_1\epsilon_1$, given by Eq. (9.49), by projecting onto the M^2 axis and choosing $m_X = 2$ TeV. For $M^2 \lesssim 0$ the CC has an $O(1)$ impact on the relic abundance. In this region, the supercooling is maximal[10] and $T_{PT}^- \gtrsim T_0 = O(\text{few GeV})$. For smaller values of M^2, the CC effect rapidly decreases and drops below 1% for $M^2 \lesssim 500$ GeV^2. Therefore, in order for the CC to have a significant impact on the relic abundance, the parameters of the scalar sector must be tuned into a narrow band where supercooling is large. In Figure 9.8, we have allowed the WIMP

[10] A recent phase transition analysis of this model (118) also concluded that the order parameter is enhanced in the limit in which the potential possesses a flat direction.

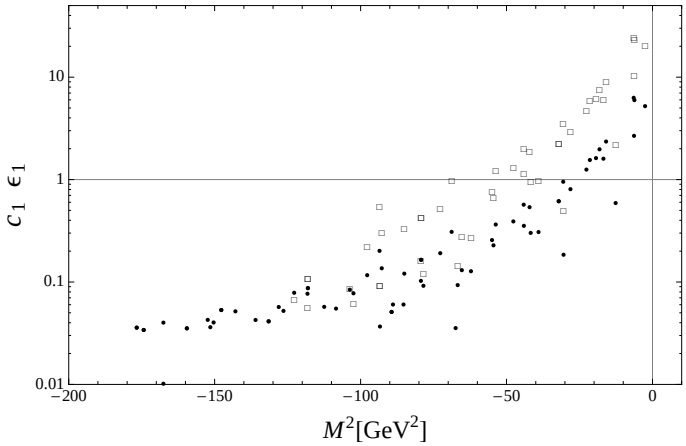

Figure 9.8: This figure shows a subset of Figure 9.7 as well as the CC effect for a 500 GeV WIMP represented by squares. As the WIMP mass is reduced, freeze out occurs at a lower temperature. This increases $c_1\epsilon_1$ for $M^2 \lesssim 0$ where the PT temperature is low, but excludes points $M^2 \lesssim -100$ GeV^2 where freeze out occurs after the PT.

mass to decrease to 500 GeV. This change lowers the freeze out temperature, reduces the delay δ between freeze out and the PT, and therefore increases the CC effect. However, this increase is small compared with the amount by which $c_1\epsilon_1$ varies with M^2 in the $M^2 \lesssim 0$ region. For smaller values of M^2, the PT temperature is higher and for the 500 GeV WIMP, freeze out occurs after the PT causing the CC effect to be suppressed. These calculations lead us to the conclusion that the optimal region of parameter space is one in which the symmetric phase becomes perturbatively unstable at a low temperature and the effective potential is concave at zero temperature. We were unable to find any points with $M^2 > 0$ in which the PT completes.

The following is a benchmark parameter point:

$$\begin{aligned}
\{a_1, b_3, m_h, m_s, m_X\} &= \{-25, -20, 128, 91.1, 2000\}\ \text{GeV}, \\
\{a_2, b_4\} &= \{0.2, 0.2\}\,, \\
M^2 &= -47.7\ \text{GeV}^2, \\
\left\{T_f, T_c, T_{PT}^+, T_{PT}^-, T_0\right\} &= \{107, 70.7, 30.0, 13.7, 12.7\}\ \ \text{GeV}, \\
c_1\epsilon_1 &= 0.390, \\
\rho_{\text{ex}} &= (69.7\ \text{GeV})^4\ . \qquad (9.87)
\end{aligned}$$

The scalar masses are given by the eigenvalues of Eq. (9.141) which are

$$\begin{aligned}
M_H &= 141\ \text{GeV}\,, \quad \{0.78, 0.22\} \\
M_S &= 70.7\ \text{GeV}\,, \quad \{0.22, 0.78\} \qquad (9.88)
\end{aligned}$$

with the respective squared eigenvectors indicated to the right.

9.5 Summary of the Chapter

We have considered a way to probe the hypothesis that the present-day, minute CC energy density is the result of a tuning between UV contributions of unspecified origin and IR contributions that arise from cosmological PTs. Prior to the electroweak scale PT, the UV contribution would have been partially uncancelled leaving an $O\left(M_W^4\right)$ energy density. It is possible to probe this energy density with the physics of dark matter freeze out provided that the dark matter mass is greater than a few hundred GeV. The dark matter relic abundance is increased due to the effective CC's contribution to the Hubble expansion rate during freeze out.

The notion of how an effective vacuum energy (which is Lorentz invariant in the flat space limit) can depend on temperature (which manifestly breaks Lorentz

invariance) has been clarified. The temperature is an approximation to the mixed vacua, inhomogeneous states whose occupation is very probable near the time of the PT. This leads to a spatially averaged equation of state that is expressed in terms of an effective vacuum energy density that is somewhere between the false and true vacuum energy densities. The true inhomogeneous field configurations may also lead to additional dark matter freeze out effects that have not been investigated in this paper. This would be an interesting avenue for future investigations.

To provide a generic prediction associated with the established physics and to provide the computational details missing in (177), we have analyzed the Standard Model with a 115 GeV Higgs and a single WIMP dark matter degree of freedom, assuming that the WIMP interaction effects on the dynamics of the PT is negligible. We have found that the CC causes an $O\left(10^{-3}\right)$ fractional increase in the relic abundance of a 4 TeV WIMPs. This is typical of non-first order PTs.

We have also investigated minimal singlet extensions of the SM and searched for parametric regimes in which the CC effect on the relic abundance is enhanced. We find that a low temperature, first order PT with large supercooling is the optimal scenario for maximizing the CC effect. In this limit, the effective CC energy density's contribution to the Hubble expansion rate can be comparable to the radiation energy density, and the CC effect can become order one. In the context of a generic single field model, we find that reaching this limit requires a tuning of the scalar sector parameters and the WIMP mass. Without appropriate tuning, either 1) the PT will not occur at all by thermal bubble nucleation, 2) the PT will occur before freeze out (when the dark matter is still in equilibrium and the CC effect is suppressed), or 3) the CC effect will not be large.

As a specific example, we have considered the xSM, an extension of the SM that adds a real scalar singlet. In that model, we find that the CC may increase the

relic abundance by as much as a factor of order few. To maximize the CC effect, the scalar parameters must be tuned into a narrow band where fluctuations around the symmetric "vacuum" are slightly tachyonic, which allow for a long period of supercooling. The magnitude of the CC effect is relatively insensitive to the WIMP mass provided that the latter is sufficiently large such that freeze out begins before the PT occurs.

The tests of CC fine tuning hypothesis are notoriously rare. In the context of a dark matter probe, it is encouraging that parametric possibilities do exist within simple extensions of the SM. It would be interesting to further advance this exploration by computing the dark matter implications of modified gravity/self-tuning models and comparing the results with those of this paper. Furthermore, it would be interesting to cross correlate other astrophysical tests of those modified gravity/self-tuning models with the dark matter predictions made within those models. Note also that there are other probes of the cosmological constant during a PT such as gravity wave probes (167) that will need more development as the gravity wave spectrum calculational technology improves (159; 161; 164).

9.A Appendix A. Renormalization Scale

Any measurable quantity is independent of the renormalization scale. Hence, one should not expect that the running of the cosmological constant parameter should affect any physical observable. Indeed, the running of the other parameters in the Lagrangian will compensate the running of the CC parameter to yield the same T_{00} governing the expansion rate H which can be measured for example by a test photon redshift. The renormalization scheme and scale does however determine the manner in which radiative corrections play a role. Furthermore, in any practical computations involving finite order truncation in $\hbar$ expansion, there is a renormalization scale dependence to next order in the perturbation power unless one is able to explicitly keep exactly the terms of the relevant order in $\hbar$.

Given that we are computing homogeneous quantities, one might also naively worry that there is a coarse graining requirement down to length scales of H^{-1}. To see why this is not the case and to see what renormalization scales would minimize the radiative correction dependence, consider the effective action generating the gravitational equation of motion for the metric g:

$$e^{iS_{\rm eff}[g]} = e^{iS_{EH}[g]} \int D_\Lambda\phi \, e^{iS_M[g,\phi]} \tag{9.89}$$

where S_{EH} is the Einstein-Hilbert action, the matter field schematically written as ϕ satisfies the appropriate boundary conditions relevant for the matter distribution, and we assume a renormalization scale at Λ. Since we are going to resolve the one-particle thermal states with masses of order the freeze out temperature T_f, we should have $\Lambda \gtrsim T_f$. Semiclassically expanding about the classical path ϕ_0 on the right hand side of Eq. (9.89), we have

$$e^{iS_{\rm eff}[g]} = e^{i(S_{EH}[g]+S_M[g,\phi_0])}\mathcal{N} \int D_\Lambda \, \delta\phi \, e^{i\int d^4x \frac{\delta\phi^2(x)}{2} \frac{\delta^2 S_M[g,\phi]}{\delta\phi^2(x)}|_{\phi=\phi_0}+\ldots} \tag{9.90}$$

where the path integral will have the usual perturbative renormalization. Hence, one can consider the physical observables to be defined through

$$T_{\mu\nu}(y) = \frac{2}{\sqrt{g(y)}} \frac{\delta}{\delta g^{\mu\nu}(y)} \Bigg(S_M[g, \phi_0] \\ - i \ln \left\{ \mathcal{N} \int D_\Lambda \, \delta\phi \exp\big[i \int d^4x \frac{\delta\phi^2(x)}{2} \frac{\delta^2 S_M[g,\phi]}{\delta\phi^2(x)} |_{\phi=\phi_0} + \ldots \big] \right\} \Bigg). \tag{9.91}$$

Note that in practice, we are expanding $g_{\mu\nu}$ perturbatively about a homogeneous and isotropic FRW background before doing the path integral. Hence, the inhomogeneities can be computed using classical perturbation theory and the renormalization scale need not be at $\Lambda = H_{PT}$ even though it is at length scales longer than H_{PT}^{-1} for which homogeneity and isotropy are typically a good assumptions.

9.B Appendix B. Derivation of Eq. (9.9)

Start with the thermally averaged Boltzmann equation for $n_X(t)$

$$\frac{1}{a^3} \frac{d}{dt} \left(n_X a^3 \right) = -\langle \sigma v \rangle \left(n_X^2 - n_X^{\mathrm{eq}\,2} \right) \tag{9.92}$$

which says that n_X tracks the equilibrium number density n_X^{eq} until freeze out occurs at $t = t_f$. Long after freeze out, the equilibrium term can be neglected, and the equation asymptotically approaches

$$\frac{d}{dt} \left(n_X a^3 \right) = -\langle \sigma v \rangle \left(n_X a^3 \right)^2 \frac{1}{a^3} \, . \tag{9.93}$$

One can solve for $n_X(t_0)$ by integrating

$$n_X(t_0) = \frac{n_X(t_f) \left(\frac{a_f}{a_0} \right)^3}{1 + n_X(t_f) \left(\frac{a_f}{a_0} \right)^3 \int_{t_f}^{t_0} dt \, \langle \sigma v \rangle \, \frac{a_0^3}{a^3}} \, . \tag{9.94}$$

The integral in the denominator accounts for residual annihilations of dark matter particles after freeze out. The freeze out time t_f is not fundamental but instead an artifact of defining when the solution deviates "significantly" from the equilibrium distribution. For temperatures away from resonances and thresholds, one can typically parameterize $\langle \sigma v \rangle$ as

$$\langle \sigma v \rangle = \tilde{a} + \tilde{b} \frac{T}{m_X}, \tag{9.95}$$

where T is the temperature and m_X is the mass of the dark matter. To further reduce Eq. (9.94) we apply Eq. (9.31), which implicitly defines t_f, and approximate $n_X(t_f) \approx n_X^{\rm eq}(t_f)$. Then, the denominator of Eq. (9.94) satisfies

$$n_X(t_f) \left(\frac{a_f}{a_0} \right)^3 \int_{t_f}^{t_0} dt \, \langle \sigma v \rangle \, \frac{a_0^3}{a^3} \approx \frac{m_X}{T_f} \left(\frac{\tilde{a} + \frac{\tilde{b}}{2} \frac{T_f}{m_X}}{\tilde{a} + \tilde{b} \frac{T}{m_X}} \right) \gg 1 \tag{9.96}$$

for $T_f \approx m_X/20$ the freeze out temperature. Using this approximation we can express the relic abundance as

$$n_X(t_0) = \left(\int_0^{\ln a_0/a_f} \frac{d \ln(a/a_f)}{H} \langle \sigma v \rangle \frac{a_0^3}{a^3} \right)^{-1} \tag{9.97}$$

after also applying $dt = H^{-1} \, d \ln a$.

9.C Appendix C. Difference Between Entropy and Energy Degrees of Freedom

In this appendix, we show that as the universe expands adiabatically during radiation domination, the relationship $g_E(T) = g_S(T)$ hold iff

$$\frac{d \ln g_E}{d \ln T} = \frac{d \ln g_S}{d \ln T} = 0 \tag{9.98}$$

where g_E is the effective number of degrees of freedom for the thermal energy density and g_S is the effective number of degrees of freedom for the entropy density. We also justify an ansatz that can be used to relate g_E and g_S.

Assume that the CC energy density is negligible so that $\rho \approx \rho_R$, which is the case sufficiently far before or after the PT. The entropy and energy densities of a gas are related by Eq. (9.1c), which can be written as

$$\rho + P - T\,s = 0 \tag{9.99}$$

where the pressure P of the gas is given by $P(T) = -\mathcal{F}(T)$. The functions g_E and g_S representing the number of relativistic degrees of freedom were defined by Eq. (9.15) and Eq. (9.16) and are reproduced here for convenience:

$$\rho = \frac{\pi^2}{30}\, g_E(T)\, T^4 \qquad \text{and} \qquad s = \frac{2\pi^2}{45}\, g_S(T)\, T^3\,. \tag{9.100}$$

As the universe expands, energy conservation is enforced by

$$d\left(\rho a^3\right) + P\, da^3 = 0\,. \tag{9.101}$$

Using Eq. (9.99) and Eq. (9.100) this becomes

$$\frac{d\ln g_E(T)}{d\ln a} + 4\frac{d\ln T}{d\ln a} + 4\frac{g_S}{g_E} = 0\,, \tag{9.102}$$

which can be resolved as

$$\frac{d\ln T}{d\ln a} = -\,\frac{g_S}{g_E}\,\left[1 + \frac{1}{4}\frac{d\ln g_E(T)}{d\ln T}\right]^{-1}. \tag{9.103}$$

Next, impose adiabaticity $d(sa^3)/da = 0$ by first using Eq. (9.100) to write

$$\frac{d\ln(s\,a^3)}{d\ln a} = -\left[\frac{d\ln g_S}{d\ln T} + 3\right]\frac{g_S}{g_E}\left[1 + \frac{1}{4}\frac{d\ln g_E(T)}{d\ln T}\right]^{-1} + 3\,, \tag{9.104}$$

and then setting this to zero and solving to find

$$\frac{g_S}{g_E} = 1 + \frac{1}{4}\frac{d\ln g_E}{d\ln T} - \frac{1}{3}\frac{d\ln g_S}{d\ln T}\,. \tag{9.105}$$

This equation implies $g_E = g_S$ iff

$$\frac{d\ln g_E}{d\ln T} = \frac{d\ln g_S}{d\ln T} = 0 \tag{9.106}$$

as claimed.

To obtain some intuition for this theorem consider the SM electroweak PT. Before the PT, the entire spectrum is massless and Eq. (9.106) is satisfied exactly so $g_E(T) = g_S(T) = \text{const}$ for $T > T_{PT}$. After the PT, we can estimate how much difference between g_S and g_E is required for self-consistency and to justify an intuitive parameterization, by considering a hypothetical situation in which one can approximate

$$g_{E/S}(T) = g_{E/S}(T_i)\,[T/T_i]^{-12K} \tag{9.107}$$

where K is a constant and T_i is an initial condition temperature. Then, one can solve Eq. (9.105) as

$$\frac{g_S(T)}{g_E(T)} = \frac{1-3K}{1-4K}. \tag{9.108}$$

Hence, if $0 < K \ll 1$, we have a situation in which $g_E(T)$ decreases slowly as a function of time while satisfying both entropy conservation and $g_S(T) \approx g_E(T)$. Presumably, K can be viewed as a leading term in a Taylor expansion regarding g_S/g_E. Hence, we will approximate

$$g_S(T) \approx (1+K)\,g_E(T) \tag{9.109}$$

even though we are not necessarily making the assumption of Eq. (9.107) throughout the paper.

9.D Appendix D. Derivation of T_{PT}^{+}, Δs, and $T(a)$

To find $T(a)$, we start with the temperature before the PT T_{PT}^{-} and impose energy conservation to solve for the temperature after the PT T_{PT}^{+}. This allows us to calculate

Δs and ϵ_2 in terms of $\Delta\rho_{\rm ex}$. Then, we require the entropy per comoving volume $S = s\,a^3$ to be conserved before and after the PT to find $T(a)$.

Assuming that there is a negligible change in a during reheating, we can impose energy conservation at a_{PT}. Using Eqs. (9.6), (9.14), and (9.15), energy conservation can be written as

$$\frac{\pi^2}{30}\,g_E^{(s)}\left(T_{PT}^-\right)\left(T_{PT}^-\right)^4 + \Delta\rho_{\rm ex} = \frac{\pi^2}{30}\,g_E^{(b)}\left(T_{PT}^+\right)\left(T_{PT}^+\right)^4\,, \tag{9.110}$$

which implicitly defines T_{PT}^+. This equation can be solved analytically by expanding $T_{PT}^+ = T_{PT}^-\,(1+\Delta\tau)$ and linearizing in $\Delta\tau$ along with other small quantities. Using Eq. (9.21) to expand $g_E^{(s)}(T)$ around $g_E^{(s)}(T_f)$, Eq. (9.110) becomes

$$\begin{aligned}\frac{\pi^2}{30}\left[\lim_{\epsilon\to 0} h(a_{PT}+\epsilon) - h(a_{PT}-\epsilon)\right]\left(T_{PT}^-\right)^4 + \Delta\rho_{\rm ex}& \\ \approx 4\frac{\pi^2}{30} g_E^{(s)}(T_f)\left(T_{PT}^-\right)^4\Delta\tau\,.&\end{aligned} \tag{9.111}$$

where we have dropped higher order terms. Using Eq. (9.22), the term in brackets is $(7/8)N_{PT}$. Finally, the equation can be solved for $\Delta\tau = T_{PT}^+/T_{PT}^- - 1$ to obtain

$$T_{PT}^+ \approx T_{PT}^-\left[1 + \frac{1}{4}\,\epsilon_{31} + \frac{1}{4}\frac{\Delta\rho_{\rm ex}}{\frac{\pi^2}{30}\,g_E^{(s)}(T_f)\,(T_{PT}^-)^4}\right] \tag{9.112}$$

where ϵ_{31} is given by Eq. (9.26c). As expected, the energy released $\Delta\rho_{\rm ex} > 0$ controls the reheating from T_{PT}^- to T_{PT}^+. Additionally, the reheating is larger when more particles non-adiabatically decouple (larger ϵ_{31}), because the latent heat is distributed over fewer degrees of freedom after the PT.

Next we can calculate the entropy density increase at the PT given by

$$\Delta s \equiv s^{(b)}(T_{PT}^+) - s^{(s)}(T_{PT}^-) \tag{9.113}$$

$$= \frac{2\pi^2}{45}\left\{g_S^{(b)}(T_{PT}^+)(T_{PT}^+)^3 - g_S^{(s)}(T_{PT}^-)(T_{PT}^-)^3\right\}\,. \tag{9.114}$$

Once again we will linearize in the perturbation by expanding g_S using Eq. (9.21) and writing T_{PT}^{+} using Eq. (9.112). This gives

$$\Delta s \approx \frac{2\pi^2}{45}\left\{-\frac{1}{g_S^{(s)}(T_f)}\left[\lim_{\epsilon\to 0} h(a_{PT}+\epsilon) - h(a_{PT}-\epsilon)\right] + 3\Delta\tau\right\} g_S^{(s)}(T_f)\left(T_{PT}^{-}\right)^3 \tag{9.115}$$

$$\approx \frac{2\pi^2}{45}\left\{-\frac{g_E^{(s)}(T_f)}{g_S^{(s)}(T_f)}\epsilon_{31} + 3\left[\frac{1}{4}\,\epsilon_{31} + \frac{1}{4}\frac{\Delta\rho_{\rm ex}}{\frac{\pi^2}{30}g_E^{(s)}(T_f)(T_{PT}^{-})^4}\right]\right\} g_S^{(s)}(T_f)\left(T_{PT}^{-}\right)^3 \tag{9.116}$$

As discussed in Section 9.C, we can approximate $g_S^{(s)}(T_f) \approx g_E^{(s)}(T_f)$. Then finally Δs becomes

$$\Delta s \approx \frac{2\pi^2}{45} g_S^{(s)}(T_f)\left(T_{PT}^{-}\right)^3\left[-\frac{1}{4}\,\epsilon_{31} + \frac{1}{4}\frac{\Delta\rho_{\rm ex}}{\frac{\pi^2}{30}g_E^{(s)}(T_f)(T_{PT}^{-})^4}\right]. \tag{9.117}$$

Using Eq. (9.26b) and noting $T_{PT}^{-}\,a_{PT} = T_f\,a_f$ up to higher order terms, we also obtain

$$\epsilon_2 \approx -\frac{1}{4}\,\epsilon_{31} + \frac{1}{4}\frac{\Delta\rho_{\rm ex}}{\frac{\pi^2}{30}g_E^{(s)}(T_f)(T_{PT}^{-})^4}\,. \tag{9.118}$$

Both of these equations illustrate that the entropy increase at the PT is controlled by the amount of latent heat released and the number of particles that non-adiabatically decouple.

Finally we will solve the equation of entropy conservation for $T(a)$. The entropy per comoving volume $S = s\,a^3$ is conserved excepting the entropy injection at reheating which is assumed to occur rapidly at a_{PT}. Entropy conservation may be expressed as

$$g_S(a)\,T(a)^3 a^3 = g_S^{(s)}(T_f)\,T_f^3 a_f^3 + \Theta(a-a_{PT})\,a_{PT}^3\left(\frac{2\pi^2}{45}\right)^{-1}\Delta s\,, \tag{9.119}$$

which implicitly defines $T(a)$. To solve for T we use Eq. (9.21) to expand $g_S(a)$ then

linearize in h and Δs to obtain

$$T(a) \approx T_f \frac{a_f}{a}\left[1+\frac{1}{3}\frac{h(a)}{g_S^{(s)}(T_f)} + \Theta\left(a-a_{PT}\right)\frac{1}{3}\left(\frac{a_{PT}}{a_f}\right)^3 \frac{\Delta s}{\frac{2\pi^2}{45}g_S^{(s)}(T_f)\,T_f^3}\right]. \tag{9.120}$$

Further expanding h using Eq. (9.22), approximating $g_S(T_f) \approx g_E(T_f)$, and applying Eq. (9.26b) we obtain the final expression,

$$T(a) \approx T_f \frac{a_f}{a}\left[1+\frac{1}{3}\epsilon_{32}\, f(a) + \Theta\left(a-a_{PT}\right)\frac{1}{3}\left(\epsilon_{31}+\epsilon_2\right)\right] \tag{9.121}$$

After the PT, the exotic energy component behaves approximately adiabatically.

9.E Appendix E. Derivation of PT induced change in the degree of freedom

We begin with the well-known formula for the energy density of a gas of fermions at temperature T with N dynamical degrees of freedom:

$$\rho(T) = N\int \frac{d^3p}{(2\pi)^3}\frac{E_p}{1+e^{E_p/T}}\,. \tag{9.122}$$

The gas has an effective number of degrees of freedom g_E given implicitly by $\rho(T) = \frac{\pi^2}{30}\,g_E(T)\,T^4$. We can parameterize the decrease in g_E due to the decoupling of the fermionic gas by writing

$$g_E(T) = g_E(T_f) - \frac{7}{8}\,N f\left(a/a_f\right) \tag{9.123}$$

where

$$f\left(a\right) = \left(\frac{7}{8}\frac{\pi^2}{30}\right)^{-1}\int \frac{d^3p}{(2\pi)^3}E_p\left[\frac{1}{T_f^4}\frac{1}{e^{\frac{E_p}{T_f}}+1} - \frac{1}{T^4(a)}\frac{1}{e^{\frac{E_p}{T(a)}}+1}\right]. \tag{9.124}$$

The temperature $T = T(a)$ is given by Eq. (9.121) to leading order in the perturbations ϵ_i. Since f already multiplies a small term in Eq. (9.22), we need only keep the leading factor in Eq. (9.121) which is $T = T_f\, a_f/a$. This lets us write Eq. (9.124) as

$$f\,(a) = \frac{8}{7}\left(\frac{30}{\pi^2}\right)\int \frac{d^3p}{(2\pi)^3}\frac{E_p}{T_f^4}\left[\frac{1}{e^{\frac{E_p}{T_f}}+1} - \frac{(a/a_f)^4}{e^{\frac{aE_p}{a_f T_f}}+1}\right]. \tag{9.125}$$

Note that $f(a)$ increases from $f(a_f) = 0$ to $f(\infty) \approx 1$. Due to the exponential temperature dependence, the transition to $f \approx 1$ occurs at $T \approx m_N$ and is smoothly steplike over a time scale $\Delta t \approx 1/H$. In this discussion we have assumed $E_p = \sqrt{\mathbf{p}^2 + m_N^2}$ with m_N constant, that is, we neglect any change in the mass of the particle as a function of time. This assumption is valid sufficiently far after the PT such that the scalar field expectation value and field-dependent masses have approximately stopped varying.

9.F Appendix F. Thermal Effective Potential Details

We have calculated the thermal effective potential through one-loop order for each of the models in Section 9.4. Our calculation employs the standard techniques (61; 124; 126), and the case of the Standard Model is particularly well documented (175; 340; 344). As such, we do not feel the need to reproduce the entire calculation here. However, we have chosen to use renormalization schemes which are convenient for our calculation, but not standardly employed. Hence, we will use this appendix to write down the thermal effective potentials for each of the models in Section 9.4 and to spell out our renormalization conditions.

In calculating thermal corrections to the scalar effective potential, we do not include contributions from the dark matter sector. This is an excellent approximation

provided that freeze out occurs prior to the phase transition (as we have assumed), such that the dark matter is decoupled from the plasma during the phase transition.

Thermal Effective Potential: Standard Model

Let $h(x) = \sqrt{2}\left|H^\dagger H\right|^{1/2}$ be the radial component of the SM Higgs field and let $h_c = \langle h \rangle$. In calculating the radiative corrections, we need not include the contributions from every field in the Standard Model. With regards to the non-thermal corrections, light particles which couple weakly to the Higgs can be neglected, and with regards to the thermal corrections, particles which are light and do not decouple during freeze out can be treated as massless. Since we expect that freeze out will coincide with the PT at a mass scale of about 100 GeV and that residual annihilations will occur down to a mass scale of about 10 GeV, we can neglect particles with a mass below that of the bottom quark (i.e., 4.2 GeV). We retain the top quark, bottom quark, physical Higgs, and massive gauge bosons[11] which have field dependent masses

$$M^2_{t/b/Z/W}(h_c) = \left(\frac{m_{t/b/Z/W}}{v}\right)^2 h_c^2 \tag{9.126a}$$

$$M^2_h(h_c) = \frac{m_h^2}{2v^2}\left(3h_c^2 - v^2\right) \tag{9.126b}$$

where $m_t = 172.6$ GeV, $m_b = 4.2$ GeV, $m_Z = 91.2$ GeV, and $m_W = 80.4$ GeV (14). The non-thermal corrections can be expressed as functions of the Coleman-Weinberg potential (124). Regulating in ($d = 4 - 2\epsilon$) spacetime dimensions, the unrenormalized potential is given by

$$V_{\text{cw}}(M^2) = \frac{M^4}{64\pi^2}\left(\log\frac{M^2}{\mu^2} - \frac{3}{2} - C_{\text{uv}}\right) \tag{9.127}$$

[11] We work in the Landau gauge ($\xi = 0$) for which the scalar polarization mode and ghost propagators are independent of h_c (124).

where $C_{\rm uv} = \epsilon^{-1} - \gamma_E + \ln 4\pi$ and μ is the t'Hooft scale. The thermal corrections can be expressed in terms of the bosonic and fermionic thermal functions (61; 182)

$$J_B\left(y\right) \equiv \int_0^\infty dx\, x^2 \log\left(1 - e^{-\sqrt{x^2+y}}\right) = -\sum_{n=1}^{\infty} \frac{1}{n^2} y\, K_2\left(n\sqrt{y}\right) \tag{9.128a}$$

$$J_F\left(y\right) \equiv \int_0^\infty dx\, x^2 \log\left(1 + e^{-\sqrt{x^2+y}}\right) = -\sum_{n=1}^{\infty} \frac{(-1)^n}{n^2} y\, K_2\left(n\sqrt{y}\right) \tag{9.128b}$$

where $K_2(z)$ is the modified Bessel function of the second kind. Putting the pieces together, the Standard Model thermal effective potential (through one-loop order and before renormalization) is given by

$$\begin{aligned} V_{\rm eff}^{\rm (SM)}(h_c, T) \approx \frac{m_h^2}{8v^2}\left(h_c^2 - v^2\right)^2 + \Bigg\{ & \delta\Omega + \frac{1}{2}\delta m^2\, h_c^2 + \frac{\delta\lambda}{4}\, h_c^4 \\ & - 12\, V_{\rm cw}\left(M_t^2(h_c)\right) - 12\, V_{\rm cw}\left(M_b^2(h_c)\right) + 3\, V_{\rm cw}\left(M_Z^2(h_c)\right) \\ & + 6\, V_{\rm cw}\left(M_W^2(h_c)\right) + V_{\rm cw}\left(M_h^2(h_c)\right) \Bigg\} \\ & + \Bigg\{ -\frac{\pi^2}{90} 75.75\, T^4 + \frac{T^4}{2\pi^2}\Big[-12\, J_F\left(M_t^2(h_c)\, T^{-2}\right) \\ & - 12\, J_F\left(M_b^2(h_c)\, T^{-2}\right) + 3\, J_B\left(M_Z^2(h_c)\, T^{-2}\right) \\ & + 6\, J_B\left(M_W^2(h_c)\, T^{-2}\right) + J_B\left(M_h^2(h_c)\, T^{-2}\right) \Big] \Bigg\} \end{aligned} \tag{9.129}$$

where $\delta\Omega$, δm^2, and $\delta\lambda$ are counterterms. We have also included the term $(-\frac{\pi^2}{90} 75.75\, T^4)$, which represents the thermal radiative contribution from light quarks, leptons, and massless gauge bosons which are relativistic at temperatures $T \gtrsim 10$ GeV. The renormalization conditions,

$$\left.\frac{\partial}{\partial h_c} V_{\rm eff}^{\rm (SM)}(h_c, 0)\right|_{h_c = v} = 0 \tag{9.130a}$$

$$\left.\frac{\partial^2}{\partial h_c^2} V_{\rm eff}^{\rm (SM)}(h_c, 0)\right|_{h_c = v} = m_h^2 \tag{9.130b}$$

$$V_{\rm eff}^{\rm (SM)}(v, 0) = 0\,, \tag{9.130c}$$

are chosen such that tadpole graphs vanish and $V_{\rm eff}^{(\rm SM)}(h_c, 0)$ has a minimum at $h_c = v$, self-energy graphs vanish and the Higgs mass[12] is m_h, and the CC is tuned against the vacuum energy density to zero.

Thermal Effective Potential: $\mathbb{Z}_2$xSM

The $\mathbb{Z}_2$xSM potential was specified by Eq. (9.58). Since we focus on the case $\langle s \rangle = 0$, we need only calculate the effective potential as a function of h_c and not $s_c = \langle s \rangle$. That is, the presence of the singlet in this model simply add an additional degree of freedom, with field dependent mass

$$M_s^2(h_c) = \left(m_s^2 - a_2 v^2\right) + a_2 h_c^2 \,, \tag{9.131}$$

to the radiative corrections. We can construct the effective potential from the SM effective potential Eq. (9.129) as

$$V_{\rm eff}^{(\mathbb{Z}_2{\rm xSM})}(h_c, T) = V_{\rm eff}^{(\rm SM)}(h_c, T) + V_{\rm cw}\left(M_s^2(h_c)\right) + \frac{T^4}{2\pi^2} J_B\left(M_s^2(h_c) T^{-2}\right) \,. \tag{9.132}$$

An additional UV divergence arises from the term $V_{\rm cw}(M_s^2)$, and is cancelled by solving the renormalization conditions Eq. (9.130) once again for the counterterms.

Thermal Effective Potential: Generic Singlet

For the theory specified by the action Eq. (9.63), we have the field dependent masses

$$M_\varphi^2(\varphi_c) = M^2 - 6\mathcal{E}\varphi_c + 3\lambda\varphi_c \tag{9.133}$$

$$M_{\psi_i}^2(\varphi_c) = \left(m_i + h_i \varphi_c\right)^2 \,. \tag{9.134}$$

[12] Since the effective potential is computed from diagrams with zero external momentum, the mass $\partial_{h_c}^2 V_{\rm eff}(h_c = v, 0) = m_h^2$ differs from the Higgs pole mass by logarithmic corrections (345), which we verify are O(few %). As such, we will neglect this distinction and continue to refer to m_h as the "Higgs mass."

We construct the thermal effective potential as

$$\begin{aligned} V_{\text{eff}}^{(\text{GS})}(\varphi_c, T) =& \rho_{\text{ex}} + \frac{1}{2}M^2\varphi_c^2 - \mathcal{E}\varphi_c^3 + \frac{\lambda}{4}\varphi_c^4 \\ &+ \frac{T^4}{2\pi^2}\left[J_B\left(M_\varphi^2(\varphi_c)\right) - 4\sum_{i=1}^{N} J_F\left(M_{\psi_i}^2(\varphi_c)\right)\right] \\ &+ \left\{\delta\Omega + \delta t\,\varphi_c + \frac{1}{2}\delta M^2\varphi_c^2 - \delta\mathcal{E}\,\varphi_c^3 + \frac{\delta\lambda}{4}\varphi_c^4\right. \\ &\left. + V_{\text{cw}}\left(M_\varphi^2(\varphi_c)\right) - 4\sum_{i=1}^{N} V_{\text{cw}}\left(M_{\psi_i}^2(\varphi_c)\right)\right\} \end{aligned} \tag{9.135}$$

where $\delta\Omega$, δt, δM^2, $\delta\mathcal{E}$, and $\delta\lambda$ are counterterms. We do not renormalize using the same renormalization conditions as we did for the SM. To simply the discussions of Section 9.4, we have attempted to choose the renormalization conditions such that the effective potential preserves certain features of the renormalized tree-level potential. For example, the renormalization conditions that we applied to the SM, Eq. (9.130), ensured that the effective potential and the tree-level potential agreed to order h_c^2 as an expansion around $h_c = v$. In our analysis of Section 9.4, we found it convenient to define the parameter α_0 which controls the shape of the effective potential. This parameter is defined using the tree-level potential $U(\varphi)$, but we claim that it also describes the shape of the one-loop effective potential provided that the radiative corrections do not significantly distort the shape of the potential. For the tuned limit $0 \lesssim \alpha_0 \ll 1$, this parameter is particularly sensitive to the shape of the potential near the origin $\varphi_c = 0$ since the barrier is very small. The radiative corrections grow as $\varphi_c \to 0$, because the fermions ψ_i become light, but these logarithmic corrections remain subdominant. However, with a renormalization scheme of the form of Eq. (9.130), the counterterms pick up a finite piece, which depends on derivatives of logarithms at the renormalization point $\varphi_c \approx v$, and which contributes non-negligibly near $\varphi_c \approx 0$. If we were to use such a renormalization scheme in the limit where $U(\varphi_c)$ has a small barrier so $0 \lesssim \alpha_0 \ll 1$, then the radiative

corrections may lift the minimum at $\varphi_c \approx 0$ and eliminate the barrier. Of course, there is nothing incorrect with using such a renormalization scheme except that it is inconvenient since we would not be able to characterize the shape of the potential using α_0 derived from $U(\varphi_c)$.

In light of this discussion, we will use a renormalization scheme which preserves the location of the minimum at $\varphi_c = v$ and also preserves the shape of the potential near $\varphi_c = 0$. This is accomplished by first writing Eq. (9.135) for $T = 0$ as

$$V_{\text{eff}}^{(\text{GS})}(\varphi_c, 0) = \bar{\Omega}(\varphi_c) + \bar{t}(\varphi_c)\varphi_c + \frac{1}{2}\bar{M}^2(\varphi_c)\varphi_c^2 - \bar{\mathcal{E}}(\varphi_c)\varphi_c^3 + \frac{\bar{\lambda}(\varphi_c)}{4}\varphi_c^4 \qquad (9.136)$$

where

$$\bar{\Omega}(\varphi_c) = \rho_{\rm ex} + \delta\Omega + \frac{\hbar}{4\pi^2}\Big[\frac{1}{16}M^4 f_\varphi(\varphi_c) - \frac{1}{4}\sum_{i=1}^{N} m_i^4 f_{\psi_i}(\varphi_c)\Big] \tag{9.137a}$$

$$\bar{t}(\varphi_c) = \delta t + \frac{\hbar}{4\pi^2}\Big[-\frac{3}{4}\mathcal{E}M^2 f_\varphi(\varphi_c) - \sum_{i=1}^{N} m_i^3 h_i f_{\psi_i}(\varphi_c)\Big] \tag{9.137b}$$

$$\bar{M}^2(\varphi_c) = M^2 + \delta M^2 + \frac{\hbar}{4\pi^2}\Big[\frac{3}{4}M^2\lambda f_\varphi(\varphi_c) + \frac{9}{2}\mathcal{E}^2 f_\varphi(\varphi_c) - 3\sum_{i=1}^{N} m_i^2 h_i^2 f_{\psi_i}(\varphi_c)\Big] \tag{9.137c}$$

$$\bar{\mathcal{E}}(\varphi_c) = \mathcal{E} + \delta\mathcal{E} + \frac{\hbar}{4\pi^2}\Big[\frac{9}{4}\mathcal{E}\lambda f_\varphi(\varphi_c) + \sum_{i=1}^{N} m_i h_i^3 f_{\psi_i}(\varphi_c)\Big] \tag{9.137d}$$

$$\bar{\lambda}(\varphi_c) = \lambda + \delta\lambda + \frac{\hbar}{4\pi^2}\Big[\frac{9}{4}\lambda^2 f_\varphi(\varphi_c) - \sum_{i=1}^{N} h_i^4 f_{\psi_i}(\varphi_c)\Big] \tag{9.137e}$$

and

$$f_\varphi(\varphi_c) = \left(\ln\frac{M_\varphi^2(\varphi_c)}{\mu^2} - \frac{3}{2} - C_{\rm uv}\right) \tag{9.138}$$

$$f_{\psi_i}(\varphi_c) = \left(\ln\frac{M_{\psi_i}^2(\varphi_c)}{\mu^2} - \frac{3}{2} - C_{\rm uv}\right). \tag{9.139}$$

Then the renormalization conditions can be expressed as

$$\bar{\Omega}(v) = \rho_{\rm ex} \tag{9.140a}$$

$$\bar{t}(v) = 0 \tag{9.140b}$$

$$\bar{M}^2(v) = M^2 \tag{9.140c}$$

$$\bar{\mathcal{E}}(v) = \mathcal{E} \tag{9.140d}$$

$$\bar{\lambda}(v) = \lambda\,. \tag{9.140e}$$

Near $\varphi_c \approx 0$, the radiative corrections are at most logarithmic.

Thermal Effective Potential: xSM

In Section 9.4 we wrote down the xSM renormalized potential in Eq. (9.84). For general h_c and s_c, the Higgs and singlet fields mix. In order to calculate the radia-

tive corrections, we must generalize the field-dependent Higgs mass M_h^2, given by Eq. (9.126b), to the Higgs-singlet mass matrix M_{hs}^2, which has components

$$\left[M_{hs}^2(\{h_c, s_c\})\right]_{11} = m_h^2/(2v^2)\left(3h_c^2 - v^2\right) + s_c\left(a_1 + a_2\, s_c\right) \tag{9.141a}$$

$$\left[M_{hs}^2(\{h_c, s_c\})\right]_{12} = \left[M_{hs}^2(\{h_c, s_c\})\right]_{21} = h_c\left(a_1 + 2\, a_2\, s_c\right) \tag{9.141b}$$

$$\left[M_{hs}^2(\{h_c, s_c\})\right]_{22} = m_s^2 + a_2\left(h_c^2 - v^2\right) + 2b_3\, s_c + 3b_4\, s_c^2\,. \tag{9.141c}$$

Now we can write down the thermal effective potential in terms of $V_{\text{eff}}^{(\text{SM})}$ by subtracting the contribution from the SM Higgs and adding the contribution from the mixed Higgs and singlet. Doing so we obtain

$$\begin{aligned} V_{\text{eff}}^{(\text{xSM})}(\{h_c, s_c\}, T) = {} & V_{\text{eff}}^{(\text{SM})}(h_c, T) + \frac{b_4}{4}s_c^4 + \frac{1}{2}m_s^2 s_c^2 + \frac{b_3}{3}s_c^3 \\ & + \frac{1}{2}s_c\left(h_c^2 - v^2\right)(a_1 + a_2 s_c) \\ & + \left\{ \frac{\delta b_4}{4}s_c^4 + \frac{\delta b_3}{3}s_c^3 + \frac{1}{2}\delta b_2 s_c^2 + \delta b_1 s_c + \frac{1}{2}\delta a_2 s_c^2 h_c^2 \right. \\ & \left. + \frac{1}{2}\delta a_1 s_c h_c^2 + \delta\Omega - V_{\text{cw}}\left(M_h^2(h_c)\right) + \operatorname{Tr} V_{\text{cw}}\left(M_{hs}^2(\{h_c, s_c\})\right) \right\} \\ & + \frac{T^4}{2\pi^2}\left[-J_B\left(M_h^2(h_c)T^{-2}\right) + \operatorname{Tr} J_B\left(M_{hs}^2(\{h_c, s_c\})T^{-2}\right)\right] \end{aligned} \tag{9.142}$$

where $\delta\Omega$, δb_i, and δa_i are counterterms. The trace is interpreted to mean evaluating V_{cw} or J_B with the eigenvalues of M_{hs}^2. We generalize the SM renormalization conditions Eq. (9.130) to incorporate the additional fields,

$$\begin{aligned} & \left(\frac{\partial}{\partial h_c}\right)^{n_h}\left(\frac{\partial}{\partial s_c}\right)^{n_s} V_{\text{eff}}^{(\text{xSM})}(\{h_c, s_c\})\Big|_{\{v,0\}} \\ & \qquad = \left(\frac{\partial}{\partial h_c}\right)^{n_h}\left(\frac{\partial}{\partial s_c}\right)^{n_s} U(\{h_c, s_c\})|_{\{v,0\}} \\ & \{n_h, n_s\} = \{1,0\}, \{2,0\}, \{0,1\}, \{0,2\}, \{1,1\}, \{1,2\}, \{0,3\}, \{0,4\}, \{0,0\} \end{aligned} \tag{9.143}$$

where $U(\{h_c, s_c\})$ is given by Eq. (9.84). Once again, we require $V_{\text{eff}}^{(\text{xSM})}(\{v, 0\}, 0) = 0$ which tunes the CC.

9.G Appendix G. xSM Bounce Calculation

As discussed in Section 9.4, the xSM electroweak PT is first order in the parametric regime of interest and proceeds through thermal bubble nucleation. In order to determine the bubble nucleation temperature T_{PT}^{-} we estimate the action of the three dimensional bounce $S^{(3)}(T)$ and require $S^{(3)}/T\big|_{T_{PT}^{-}} \sim 140$. The bounce field configuration $\phi_B(r)$ is a saddle point solution of the Euclidean equation of motion with an O(3) symmetry. Let $\vec{\phi} = \{h, s\}$ be the field space coordinate and let $\vec{\phi}_{sym} = v^{(s)}(T)$ and $\vec{\phi}_{brk} = v^{(b)}(T)$ be the location of the symmetric and broken phases at temperature T. In this notation, the field equation and boundary conditions can be written as

$$\frac{d^2\vec{\phi}}{dr^2} + \frac{2}{r}\frac{d\vec{\phi}}{dr} - \vec{\nabla}_{\vec{\phi}} V_{\text{eff}}(\vec{\phi}, T) = 0 \tag{9.144}$$

$$\left.\frac{d\vec{\phi}}{dr}\right|_{r=0} = 0\,, \qquad \lim_{r\to\infty} \vec{\phi}(r) = \vec{\phi}_{sym} \tag{9.145}$$

where r is the radial coordinate and V_{eff} is the thermal effective potential. The bounce solution is a curve $\vec{\phi}_B(r)$ which starts nearby to $\vec{\phi}_{brk}$ at $r = 0$ and approaches $\vec{\phi}_{sym}$ as $r \to \infty$. Once the solution $\vec{\phi}_B(r)$ is obtained, the bounce action is calculated as

$$S^{(3)}(T) = 4\pi \int_0^\infty r^2 dr \left[\frac{1}{2}\left(\frac{d\vec{\phi}_B}{dr}\right)^2 + V_{\text{eff}}(\vec{\phi}_B(r), T)\right]\,. \tag{9.146}$$

It is difficult to solve Eq. (9.144) by brute force numerics, because the solution is unstable to perturbations about the initial point $\vec{\phi}_B(0)$, and the over shoot / under shoot method is non-trivial to apply in two dimensions.

Profumo et. al. (117) have outlined a numerical procedure which reduces the calculation to iteratively solving the one-dimensional analog of Eq. (9.144). They suggest that one should decompose the field equation into a basis with unit vectors parallel and perpendicular to the solution curve $\vec{\phi}(r)$. Suppose that there exists a

curve $\vec{\phi}(x)$ that interpolates between $\vec{\phi}(0) = \vec{\phi}_{sym}$ and $\vec{\phi}(L) = \vec{\phi}_{brk}$. Let

$$x = \int_{\vec{\phi}_{sym}}^{\vec{\phi}(x)} \left| d\vec{\phi} \right| \tag{9.147}$$

be the distance along the curve such that L is the total length and

$$\hat{e}_{\parallel} = \frac{d\vec{\phi}}{dx} \qquad \text{and} \qquad \hat{e}_{\perp} = \begin{pmatrix} 0 & 1 \\ -1 & 0 \end{pmatrix} \frac{d\vec{\phi}}{dx} \tag{9.148}$$

are the unit vectors parallel and perpendicular to the curve at x. In this basis, Eq. (9.144) becomes

$$\left\{ \frac{d^2x}{dr^2} + \frac{2}{r}\frac{dx}{dr} - \frac{dV(\vec{\phi}(x))}{dx} \right\} \hat{e}_{\parallel} = 0 \tag{9.149}$$

$$\left\{ \left| \frac{d^2\vec{\phi}}{dx^2} \right| \left(\frac{dx}{dr} \right)^2 - \left(\vec{\nabla}_{\vec{\phi}} V \right)_{\perp} \right\} \hat{e}_{\perp} = 0 \,. \tag{9.150}$$

The authors of (117) solve these equations numerically using an iterative procedure.

Since we compute T_{PT}^{-} by calculating the bounce at various temperatures in order to solve $S^{(3)}/T \approx 140$, the iterative procedure is too computationally intensive for our purposes. Fortunately, in the parametric regime of interest the bounce solution $\vec{\phi}_B(r)$ can be approximated by $\vec{\phi}_{\rm app}(x) = \{h(x), \bar{s}(h(x))\}$ where $\bar{s}(h)$ satisfies[13]

$$\left. \frac{dU(\{h, s\}, 0)}{ds} \right|_{\bar{s}} = 0 \qquad \text{and} \qquad \bar{s}(v) = 0 \,, \tag{9.151}$$

U is the classical potential, and $\vec{\phi}_{\rm app}(x)$ is parametrized by its length x given by Eq. (9.147). Using $\vec{\phi}_{\rm app}(x)$, we solve Eq. (9.149) for $x(r)$ and calculate $S^{(3)}$ using Eq. (9.146).

To check our approximation, we also compute the PT temperature using the method of (117) for a few parameter sets. In Figure 9.9 we contrast our approximation

[13] In the parametric region described in Section 9.4, the solution of $dU/ds = 0$ is not generally a single-valued function of h. However, the boundary condition $\bar{s}(v) = 0$ selects out a unique trajectory which tends to stay in the "valley" connecting the two minima and passes through the saddle point.

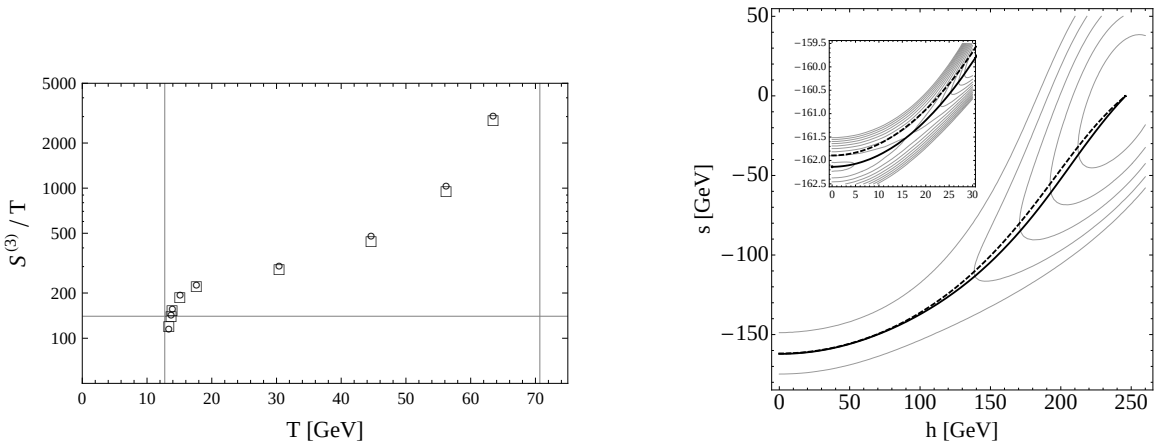

Figure 9.9: Comparisons of bounce calculations for the xSM benchmark point Eq. (9.87). On the left, the bounce action computed at various temperatures between $T_0 = 12.7$ GeV and $T_c = 70.7$ GeV using the method of (117) (squares) and our approximation (circles). On the right, the xSM thermal effective potential at $T_{PT}^- = 13.7$ GeV. The solid curve shows the trajectory $\vec{\phi}_B(x)$ obtained using the method of (117), and the dashed curve shows the approximation $\vec{\phi}_{\rm app}(x)$ given by Eq. (9.151). The curves do not coincide at small h because the minimum along the $h = 0$ axis shifts as the temperature is raised. Nevertheless, the action along the two paths still agrees remarkably well.

with the procedure of (117) for the xSM benchmark point Eq. (9.87). We find that our approximation tends to overestimate $S^{(3)}$ by a few percent generically. However, $S^{(3)}$ is a rapidly increasing function of temperature, and even an $O(5\%)$ deviation in $S^{(3)}$ does not causes T_{PT}^- to deviate appreciably.

Chapter 10

*

Bibliography

[1] C.-N. Yang and R. L. Mills, "Conservation of Isotopic Spin and Isotopic Gauge Invariance," *Phys.Rev.* **96** (1954) 191–195.

[2] D. Gross and F. Wilczek, "Ultraviolet Behavior of Nonabelian Gauge Theories," *Phys.Rev.Lett.* **30** (1973) 1343–1346.

[3] H. D. Politzer, "Reliable Perturbative Results for Strong Interactions?," *Phys.Rev.Lett.* **30** (1973) 1346–1349.

[4] S. Glashow, "Partial Symmetries of Weak Interactions," *Nucl.Phys.* **22** (1961) 579–588.

[5] S. Weinberg, "A Model of Leptons," *Phys.Rev.Lett.* **19** (1967) 1264–1266.

[6] A. Salam, "Weak and Electromagnetic Interactions," *Conf.Proc.* **C680519** (1968) 367–377.

[7] S. Glashow, J. Iliopoulos, and L. Maiani, "Weak Interactions with Lepton-Hadron Symmetry," *Phys.Rev.* **D2** (1970) 1285–1292.

[8] D. Hanneke, S. Fogwell, and G. Gabrielse, "New Measurement of the Electron Magnetic Moment and the Fine Structure Constant," *Phys.Rev.Lett.* **100** (2008) 120801, `0801.1134`.

[9] E. Fermi, "An attempt of a theory of beta radiation. 1.," *Z.Phys.* **88** (1934) 161–177.

[10] F. Wilson, "Fermi's Theory of Beta Decay," *Am.J.Phys.* **36** (1968), no. 12,.

[11] T. Lee and C.-N. Yang, "Question of Parity Conservation in Weak Interactions," *Phys.Rev.* **104** (1956) 254–258.

[12] R. Feynman and M. Gell-Mann, "Theory of Fermi interaction," *Phys.Rev.* **109** (1958) 193–198.

[13] F. Halzen and A. D. Martin, *Quarks and Leptons: An Introductory Course in Modern Particle Physics*. John Wiley and Sons, 1984.

[14] **Particle Data Group** Collaboration, K. Nakamura *et al.*, "Review of particle physics," *J.Phys.G* **G37** (2010) 075021.

[15] G. 't Hooft, "Renormalizable Lagrangians for Massive Yang-Mills Fields," *Nucl.Phys.* **B35** (1971) 167–188.

[16] G. 't Hooft and M. Veltman, "Regularization and Renormalization of Gauge Fields," *Nucl.Phys.* **B44** (1972) 189–213.

[17] J. Goldstone, A. Salam, and S. Weinberg, "Broken Symmetries," *Phys.Rev.* **127** (1962) 965–970.

[18] Y. Nambu, "Quasiparticles and Gauge Invariance in the Theory of Superconductivity," *Phys.Rev.* **117** (1960) 648–663.

[19] J. Goldstone, "Field Theories with Superconductor Solutions," *Nuovo Cim.* **19** (1961) 154–164.

[20] P. W. Higgs, "Broken symmetries, massless particles and gauge fields," *Phys.Lett.* **12** (1964) 132–133.

[21] P. W. Higgs, "Broken Symmetries and the Masses of Gauge Bosons," *Phys.Rev.Lett.* **13** (1964) 508–509.

[22] P. W. Higgs, "Spontaneous Symmetry Breakdown without Massless Bosons," *Phys.Rev.* **145** (1966) 1156–1163.

[23] F. Englert and R. Brout, "Broken Symmetry and the Mass of Gauge Vector Mesons," *Phys.Rev.Lett.* **13** (1964) 321–323.

[24] G. Guralnik, C. Hagen, and T. Kibble, "Global Conservation Laws and Massless Particles," *Phys.Rev.Lett.* **13** (1964) 585–587.

[25] F. Hasert, H. Faissner, W. Krenz, J. Von Krogh, D. Lanske, *et al.*, "Search for Elastic Muon-Neutrino Electron Scattering," *Phys.Lett.* **B46** (1973) 121–124.

[26] **Gargamelle Neutrino Collaboration** Collaboration, F. Hasert *et al.*, "Observation of Neutrino Like Interactions Without Muon Or Electron in the Gargamelle Neutrino Experiment," *Phys.Lett.* **B46** (1973) 138–140.

[27] **UA1 Collaboration** Collaboration, G. Arnison *et al.*, "Experimental Observation of Isolated Large Transverse Energy Electrons with Associated Missing Energy at s**(1/2) = 540-GeV," *Phys.Lett.* **B122** (1983) 103–116.

[28] **UA1 Collaboration** Collaboration, G. Arnison *et al.*, "Experimental Observation of Lepton Pairs of Invariant Mass Around 95-GeV/c**2 at the CERN SPS Collider," *Phys.Lett.* **B126** (1983) 398–410.

[29] J. Ellis, M. K. Gaillard, and D. V. Nanopoulos, "A Historical Profile of the Higgs Boson," `1201.6045`.

[30] P. D. Group, "Archives and Errata for the Review of Particle Physics." http://pdg.lbl.gov/2012/html/rpp_archives.html.

[31] M. Dixit, H. Anderson, C. Hargrove, R. Mckee, D. Kessler, *et al.*, "Experimental test of the theory of muonic atoms," *Phys.Rev.Lett.* **27** (1971) 878–881.

[32] H. Walter, J. Vuilleumier, H. Backe, F. Boehm, R. Engfer, *et al.*, "Test of quantum-electrodynamical corrections in muonic atoms," *Phys.Lett.* **B40** (1972) 197–199.

[33] L. Resnick, M. Sundaresan, and P. Watson, "Is there a light scalar boson?," *Phys.Rev.* **D8** (1973) 172–178.

[34] D. Kohler, B. Watson, and J. Becker, "Experimental Search for a Low-Mass Scalar Boson," *Phys.Rev.Lett.* **33** (1974) 1628–1631.

[35] S. L. Adler, R. F. Dashen, and S. Treiman, "Comments on Proposed Explanations for the mu - Mesic Atom x-Ray Discrepancy," *Phys.Rev.* **D10** (1974) 3728.

[36] R. Barbieri and T. E. O. Ericson, "Evidence Against the Existence of a Low Mass Scalar Boson from Neutron-Nucleus Scattering," *Phys.Lett.* **B57** (1975) 270.

[37] K. Sato and H. Sato, "Primordial Higgs Mesons and Cosmic Background Radiations," *Prog.Theor.Phys.* **54** (1975) 912–913.

[38] K. Sato and H. Sato, "Higgs Meson Emission from a Star and a Constraint on Its Mass," *Prog.Theor.Phys.* **54** (1975) 1564–1565.

[39] J. R. Ellis, M. K. Gaillard, and D. V. Nanopoulos, "A Phenomenological Profile of the Higgs Boson," *Nucl.Phys.* **B106** (1976) 292.

[40] T. Yamazaki, T. Ishikawa, T. Taniguchi, T. Yamanaka, T. Tanimori, *et al.*, "Search for a Neutral Boson in a Two-Body Decay of K+ to pi+ X0," *Phys.Rev.Lett.* **52** (1984) 1089–1091.

[41] M. Atiya, I. Chiang, J. Frank, J. Haggerty, M. Ito, *et al.*, "Search for the Decay K+ to pi+ neutrino anti-neutrino," *Phys.Rev.Lett.* **64** (1990) 21–24.

[42] P. Franzini, D. Son, P. Tuts, S. Youssef, T. Zhao, *et al.*, "Limits on Higgs Boson, Scalar Quarkonia, And Eta (B)'s from Radiative Upsilon Decays," *Phys.Rev.* **D35** (1987) 2883–2886.

[43] J. Lee-Franzini, "Searching for Higgs' Bosons from Upsilon and chi(b)-prime Decays,".

[44] **NA31 Collaboration** Collaboration, G. Barr *et al.*, "Search for a Neutral Higgs Particle in the Decay Sequence K0(L) to pi0 H0 and H0 to e+ e-," *Phys.Lett.* **B235** (1990) 356.

[45] **SINDRUM Collaboration** Collaboration, S. Egli *et al.*, "Measurement of the decay pi+ to e+ electron-neutrino e+ e- and Search for a Light Higgs Boson," *Phys.Lett.* **B222** (1989) 533.

[46] **CLEO Collaboration** Collaboration, M. Alam *et al.*, "Search for a Neutral Higgs Boson in B Meson Decay," *Phys.Rev.* **D40** (1989) 712–720.

[47] **Particle Data Group** Collaboration, R. M. Barnett *et al.*, "Review of particle physics. Particle Data Group," *Phys.Rev.* **D54** (1996) 1–720.

[48] **LEP Working Group for Higgs boson searches, ALEPH Collaboration, DELPHI Collaboration, L3 Collaboration, OPAL Collaboration** Collaboration, R. Barate *et al.*, "Search for the standard model Higgs boson at LEP," *Phys.Lett.* **B565** (2003) 61–75, `hep-ex/0306033`.

[49] **TEVNPH (Tevatron New Phenomina and Higgs Working Group), CDF Collaboration, D0 Collaboration** Collaboration, "Combined CDF and D0 Search for Standard Model Higgs Boson Production with up to 10.0 fb^{-1} of Data," `1203.3774`. Preliminary results prepared for the Winter 2012 Conferences.

[50] **Tevatron New Physics Higgs Working Group, CDF Collaboration, D0 Collaboration** Collaboration, "Updated Combination of CDF and D0 Searches for Standard Model Higgs Boson Production with up to 10.0 fb^{-1} of Data," `1207.0449`.

[51] **D0 Collaboration** Collaboration, V. M. Abazov *et al.*, "Updated Combination of Searches for the Standard Model Higgs Boson at the D0 Experiment in 9.7 fb-1 of Data," `1207.0422`.

[52] **CMS Collaboration** Collaboration, S. Chatrchyan *et al.*, "Combined results of searches for the standard model Higgs boson in pp collisions at sqrt(s) = 7 TeV," `1202.1488`.

[53] **CMS Collaboration** Collaboration, S. Chatrchyan *et al.*, "Search for the standard model Higgs boson decaying into two photons in pp collisions at sqrt(s)=7 TeV," 1202.1487.

[54] **CMS Collaboration** Collaboration, S. Chatrchyan *et al.*, "Search for the standard model Higgs boson in the decay channel H to ZZ to 4 leptons in pp collisions at sqrt(s) = 7 TeV," 1202.1997.

[55] **ATLAS Collaboration** Collaboration, G. Aad *et al.*, "Search for the Standard Model Higgs boson in the diphoton decay channel with 4.9 fb-1 of pp collisions at sqrt(s)=7 TeV with ATLAS," *Phys.Rev.Lett.* **108** (2012) 111803, 1202.1414.

[56] **ATLAS Collaboration** Collaboration, G. Aad *et al.*, "Combined search for the Standard Model Higgs boson using up to 4.9 fb-1 of pp collision data at sqrt(s) = 7 TeV with the ATLAS detector at the LHC," *Phys.Lett.* **B710** (2012) 49–66, 1202.1408.

[57] **ATLAS Collaboration** Collaboration, G. Aad *et al.*, "Search for the Standard Model Higgs boson in the decay channel H to ZZ(*) to 4l with 4.8 fb-1 of pp collision data at sqrt(s) = 7 TeV with ATLAS," *Phys. Lett.* **B710** (2012) 383–402, 1202.1415.

[58] D. A. Kirzhnits, "Weinberg model in the hot universe," *JETP Lett.* **15** (1972) 529–531.

[59] D. A. Kirzhnits and A. D. Linde, "Macroscopic Consequences of the Weinberg Model," *Phys. Lett.* **B42** (1972) 471–474.

[60] S. Weinberg, "Gauge and Global Symmetries at High Temperature," *Phys.Rev.* **D9** (1974) 3357–3378.

[61] L. Dolan and R. Jackiw, "Symmetry Behavior at Finite Temperature," *Phys. Rev.* **D9** (1974) 3320–3341.

[62] V. A. Kuzmin, V. A. Rubakov, and M. E. Shaposhnikov, "On the Anomalous Electroweak Baryon Number Nonconservation in the Early Universe," *Phys. Lett.* **B155** (1985) 36.

[63] A. G. Cohen, D. B. Kaplan, and A. E. Nelson, "Weak Scale Baryogenesis," *Phys.Lett.* **B245** (1990) 561–564.

[64] A. G. Cohen, D. B. Kaplan, and A. E. Nelson, "Baryogenesis at the weak phase transition," *Nucl.Phys.* **B349** (1991) 727–742.

[65] A. Beach, J. Beatty, A. Bhattacharyya, C. Bower, S. Coutu, *et al.*, "Measurement of the cosmic ray anti-proton to proton abundance ratio between 4 and 50 GeV," *Phys.Rev.Lett.* **87** (2001) 271101, astro-ph/0111094.

[66] G. Steigman, "Observational tests of antimatter cosmologies," *Ann.Rev.Astron.Astrophys.* **14** (1976) 339–372.

[67] A. G. Cohen, A. De Rujula, and S. Glashow, "A Matter - antimatter universe?," *Astrophys.J.* **495** (1998) 539–549, `astro-ph/9707087`.

[68] G. Gamow, "Expanding universe and the origin of elements," *Phys. Rev.* **70** (1946) 572–573.

[69] B. Fields and S. Sarkar, "Big-Bang nucleosynthesis (Particle Data Group mini-review)," *J.Phys.G* **G33** (2006) 1, `astro-ph/0601514`. In the Review of Particle Properties, please cite the entire review:J.Phys.G33:1,2006.

[70] W. Hu and N. Sugiyama, "Anisotropies in the cosmic microwave background: An Analytic approach," *Astrophys.J.* **444** (1995) 489–506, `astro-ph/9407093`.

[71] **WMAP Collaboration** Collaboration, E. Komatsu *et al.*, "Seven-Year Wilkinson Microwave Anisotropy Probe (WMAP) Observations: Cosmological Interpretation," *Astrophys.J.Suppl.* **192** (2011) 18, `1001.4538`.

[72] E. W. Kolb and M. S. Turner, *The Early Universe*. Westview Press, 1990.

[73] A. Sakharov, "Violation of CP Invariance, c Asymmetry, and Baryon Asymmetry of the Universe," *Pisma Zh.Eksp.Teor.Fiz.* **5** (1967) 32–35.

[74] J. Bell and R. Jackiw, "A PCAC puzzle: pi to gamma gamma in the sigma model," *Nuovo Cim.* **A60** (1969) 47–61.

[75] S. L. Adler, "Axial vector vertex in spinor electrodynamics," *Phys.Rev.* **177** (1969) 2426–2438.

[76] G. 't Hooft, "Symmetry breaking through Bell-Jackiw anomalies," *Phys. Rev. Lett.* **37** (1976) 8–11.

[77] G. 't Hooft, "Computation of the Quantum Effects Due to a Four-Dimensional Pseudoparticle," *Phys.Rev.* **D14** (1976) 3432–3450.

[78] A. Belavin, A. M. Polyakov, A. Schwartz, and Y. Tyupkin, "Pseudoparticle Solutions of the Yang-Mills Equations," *Phys.Lett.* **B59** (1975) 85–87.

[79] R. Jackiw and C. Rebbi, "Vacuum Periodicity in a Yang-Mills Quantum Theory," *Phys.Rev.Lett.* **37** (1976) 172–175.

[80] J. Callan, Curtis G., R. Dashen, and D. J. Gross, "The Structure of the Gauge Theory Vacuum," *Phys.Lett.* **B63** (1976) 334–340.

[81] M. Shaposhnikov, "Baryon Asymmetry of the Universe in Standard Electroweak Theory," *Nucl.Phys.* **B287** (1987) 757–775.

[82] M. Shaposhnikov, "Possible Appearance of the Baryon Asymmetry of the Universe in an Electroweak Theory," *JETP Lett.* **44** (1986) 465–468.

[83] N. Manton, "Topology in the Weinberg-Salam Theory," *Phys.Rev.* **D28** (1983) 2019.

[84] F. R. Klinkhamer and N. S. Manton, "A Saddle Point Solution in the Weinberg-Salam Theory," *Phys. Rev.* **D30** (1984) 2212.

[85] Y. Brihaye and J. Kunz, "Electroweak bubbles and sphalerons," *Phys. Rev.* **D48** (1993) 3884–3890, `hep-ph/9304256`.

[86] L. Carson, X. Li, L. D. McLerran, and R.-T. Wang, "Exact Computation of the Small Fluctuation Determinant Around a Sphaleron," *Phys.Rev.* **D42** (1990) 2127–2143.

[87] M. Quiros, "Field Theory at Finite Temperature and Phase Transitions," *Acta Phys. Polon.* **B38** (2007) 3661–3703.

[88] M. Shaposhnikov, "Standard model solution of the baryogenesis problem," *Phys.Lett.* **B277** (1992) 324–330.

[89] K. Kajantie, M. Laine, K. Rummukainen, and M. E. Shaposhnikov, "Is there a hot electroweak phase transition at m(H) $>\approx$ m(W)?," *Phys. Rev. Lett.* **77** (1996) 2887–2890, `hep-ph/9605288`.

[90] F. Csikor, Z. Fodor, and J. Heitger, "Endpoint of the hot electroweak phase transition," *Phys. Rev. Lett.* **82** (1999) 21–24, `hep-ph/9809291`.

[91] D. Curtin, P. Jaiswal, and P. Meade, "Excluding Electroweak Baryogenesis in the MSSM," `1203.2932`.

[92] M. S. Carena, M. Quiros, and C. E. M. Wagner, "Opening the Window for Electroweak Baryogenesis," *Phys. Lett.* **B380** (1996) 81–91, `hep-ph/9603420`.

[93] J. Espinosa, "Dominant two loop corrections to the MSSM finite temperature effective potential," *Nucl.Phys.* **B475** (1996) 273–292, `hep-ph/9604320`.

[94] A. Menon, D. E. Morrissey, and C. E. M. Wagner, "Electroweak baryogenesis and dark matter in the nMSSM," *Phys. Rev.* **D70** (2004) 035005, `hep-ph/0404184`.

[95] S. J. Huber and M. G. Schmidt, "Electroweak baryogenesis: Concrete in a SUSY model with a gauge singlet," *Nucl. Phys.* **B606** (2001) 183–230, `hep-ph/0003122`.

[96] M. Pietroni, "The Electroweak phase transition in a nonminimal supersymmetric model," *Nucl. Phys.* **B402** (1993) 27–45, `hep-ph/9207227`.

[97] D. J. H. Chung and A. J. Long, "Electroweak Phase Transition in the munuSSM," *Phys. Rev.* **D81** (2010) 123531, 1004.0942.

[98] G. W. Anderson and L. J. Hall, "The Electroweak phase transition and baryogenesis," *Phys. Rev.* **D45** (1992) 2685–2698.

[99] Y. Kondo, I. Umemura, and K. Yamamoto, "First order phase transition in the singlet Majoron model," *Phys. Lett.* **B263** (1991) 93–96.

[100] K. Enqvist, K. Kainulainen, and I. Vilja, "Phase transitions in the singlet majoron model," *Nucl. Phys.* **B403** (1993) 749–769.

[101] N. Sei, I. Umemura, and K. Yamamoto, "Constraints on the electroweak phase transition in the singlet majoron model," *Phys. Lett.* **B299** (1993) 286–292.

[102] K. E. C. Benson, "Avoiding baryon washout in the extended Standard Model," *Phys. Rev.* **D48** (1993) 2456–2461.

[103] J. Choi and R. R. Volkas, "Real Higgs singlet and the electroweak phase transition in the standard model, (UM-P-93/80, OZ-93/20)," *Phys. Lett.* **B317** (1993) 385–391, hep-ph/9308234.

[104] J. R. Espinosa and M. Quiros, "The Electroweak phase transition with a singlet," *Phys. Lett.* **B305** (1993) 98–105, hep-ph/9301285.

[105] G. C. Branco, D. Delepine, D. Emmanuel-Costa, and F. R. Gonzalez, "Electroweak baryogenesis in the presence of an isosinglet quark," *Phys. Lett.* **B442** (1998) 229–237, hep-ph/9805302.

[106] S. W. Ham, Y. S. Jeong, and S. K. Oh, "Electroweak phase transition in an extension of the standard model with a real Higgs singlet," *J. Phys.* **G31** (2005) 857–872, hep-ph/0411352.

[107] A. Noble and M. Perelstein, "Higgs Self-Coupling as a Probe of Electroweak Phase Transition," *Phys. Rev.* **D78** (2008) 063518, 0711.3018.

[108] V. Barger, P. Langacker, M. McCaskey, M. J. Ramsey-Musolf, and G. Shaughnessy, "LHC Phenomenology of an Extended Standard Model with a Real Scalar Singlet," *Phys. Rev.* **D77** (2008) 035005, 0706.4311.

[109] A. Ahriche, "What is the Criterion for a Strong First Order Electroweak Phase Transition in Singlet Models?," *Phys. Rev.* **D75** (2007) 083522, hep-ph/0701192.

[110] J. R. Espinosa and M. Quiros, "Novel effects in electroweak breaking from a hidden sector," *Phys. Rev.* **D76** (2007) 076004, hep-ph/0701145.

[111] S. Profumo, M. J. Ramsey-Musolf, and G. Shaughnessy, "Singlet Higgs Phenomenology and the Electroweak Phase Transition," *JHEP* **08** (2007) 010, 0705.2425.

[112] J. R. Espinosa, T. Konstandin, J. M. No, and M. Quiros, "Some Cosmological Implications of Hidden Sectors," *Phys. Rev.* **D78** (2008) 123528, 0809.3215.

[113] V. Barger, P. Langacker, M. McCaskey, M. Ramsey-Musolf, and G. Shaughnessy, "Complex Singlet Extension of the Standard Model," *Phys. Rev.* **D79** (2009) 015018, 0811.0393.

[114] J. M. Cline, G. Laporte, H. Yamashita, and S. Kraml, "Electroweak Phase Transition and LHC Signatures in the Singlet Majoron Model," *JHEP* **07** (2009) 040, 0905.2559.

[115] A. Ashoorioon and T. Konstandin, "Strong electroweak phase transitions without collider traces," *JHEP* **0907** (2009) 086, 0904.0353.

[116] S. Das, P. J. Fox, A. Kumar, and N. Weiner, "The Dark Side of the Electroweak Phase Transition," *JHEP* **11** (2010) 108, 0910.1262.

[117] S. Profumo, L. Ubaldi, and C. Wainwright, "Singlet Scalar Dark Matter: Monochromatic Gamma Rays and Metastable Vacua," 1009.5377.

[118] J. R. Espinosa, T. Konstandin, and F. Riva, "Strong Electroweak Phase Transitions in the Standard Model with a Singlet," 1107.5441.

[119] D. J. Chung and A. J. Long, "Cosmological Constant, Dark Matter, and Electroweak Phase Transition," *Phys.Rev.* **D84** (2011) 103513, 1108.5193.

[120] W. Heisenberg and H. Euler, "Consequences of Dirac's theory of positrons," *Z.Phys.* **98** (1936) 714–732, physics/0605038.

[121] J. S. Schwinger, "On the Green's functions of quantized fields. 1.," *Proc.Nat.Acad.Sci.* **37** (1951) 452–455.

[122] J. S. Schwinger, "On the Green's functions of quantized fields. 2.," *Proc.Nat.Acad.Sci.* **37** (1951) 455–459.

[123] G. Jona-Lasinio, "Relativistic field theories with symmetry breaking solutions," *Nuovo Cim.* **34** (1964) 1790–1795.

[124] S. R. Coleman and E. J. Weinberg, "Radiative Corrections as the Origin of Spontaneous Symmetry Breaking," *Phys.Rev.* **D7** (1973) 1888–1910.

[125] S. Weinberg, "Perturbative Calculations of Symmetry Breaking," *Phys.Rev.* **D7** (1973) 2887–2910.

[126] R. Jackiw, "Functional evaluation of the effective potential," *Phys. Rev.* **D9** (1974) 1686.

[127] L. Dolan and R. Jackiw, "Gauge Invariant Signal for Gauge Symmetry Breaking," *Phys.Rev.* **D9** (1974) 2904.

[128] T. Matsubara, "A New approach to quantum statistical mechanics," *Prog. Theor. Phys.* **14** (1955) 351–378.

[129] R. Kubo, "Statistical mechanical theory of irreversible processes. 1. General theory and simple applications in magnetic and conduction problems," *J. Phys. Soc. Jap.* **12** (1957) 570–586.

[130] P. C. Martin and J. S. Schwinger, "Theory of many particle systems. I," *Phys. Rev.* **115** (1959) 1342–1373.

[131] J. S. Schwinger, "Brownian motion of a quantum oscillator," *J. Math. Phys.* **2** (1961) 407–432.

[132] L. V. Keldysh, "Diagram technique for nonequilibrium processes," *Zh. Eksp. Teor. Fiz.* **47** (1964) 1515–1527.

[133] C. W. Bernard, "Feynman Rules for Gauge Theories at Finite Temperature," *Phys.Rev.* **D9** (1974) 3312.

[134] A. Guth, "Particle Physics of the Early Universe,".

[135] D. E. Lopez-Fogliani and C. Munoz, "Proposal for a new minimal supersymmetric standard model," *Phys. Rev. Lett.* **97** (2006) 041801, `hep-ph/0508297`.

[136] J. R. Ellis, J. F. Gunion, H. E. Haber, L. Roszkowski, and F. Zwirner, "Higgs Bosons in a Nonminimal Supersymmetric Model," *Phys. Rev.* **D39** (1989) 844.

[137] A. Bochkarev, S. Kuzmin, and M. Shaposhnikov, "On the Model Dependence of the Cosmological Upper Bound on the Higgs Boson and Top Quark Masses," *Phys.Rev.* **D43** (1991) 369–374.

[138] N. Escudero, D. E. Lopez-Fogliani, C. Munoz, and R. R. de Austri, "Analysis of the parameter space and spectrum of the $\mu\nu$SSM," *JHEP* **12** (2008) 099, `0810.1507`.

[139] A. T. Davies, C. D. Froggatt, and R. G. Moorhouse, "Electroweak Baryogenesis in the Next to Minimal Supersymmetric Model," *Phys. Lett.* **B372** (1996) 88–94, `hep-ph/9603388`.

[140] S. A. Abel, S. Sarkar, and P. L. White, "On the Cosmological Domain Wall Problem for the Minimally Extended Supersymmetric Standard Model," *Nucl. Phys.* **B454** (1995) 663–684, hep-ph/9506359.

[141] D. J. Miller, 2, R. Nevzorov, and P. M. Zerwas, "The Higgs sector of the next-to-minimal supersymmetric standard model," *Nucl. Phys.* **B681** (2004) 3–30, hep-ph/0304049.

[142] A. Masiero and J. W. F. Valle, "A Model for Spontaneous R Parity Breaking," *Phys. Lett.* **B251** (1990) 273–278.

[143] P. J. Steinhardt, "Relativistic Detonation Waves and Bubble Growth in False Vacuum Decay," *Phys. Rev.* **D25** (1982) 2074.

[144] E. Witten, "Cosmic Separation of Phases," *Phys. Rev.* **D30** (1984) 272–285.

[145] A. Kosowsky, M. S. Turner, and R. Watkins, "Gravitational radiation from colliding vacuum bubbles," *Phys. Rev.* **D45** (1992) 4514–4535.

[146] A. Kosowsky, M. S. Turner, and R. Watkins, "Gravitational waves from first order cosmological phase transitions," *Phys. Rev. Lett.* **69** (1992) 2026–2029.

[147] M. Kamionkowski, A. Kosowsky, and M. S. Turner, "Gravitational radiation from first order phase transitions," *Phys. Rev.* **D49** (1994) 2837–2851, astro-ph/9310044.

[148] R. Apreda, M. Maggiore, A. Nicolis, and A. Riotto, "Gravitational waves from electroweak phase transitions," *Nucl. Phys.* **B631** (2002) 342–368, gr-qc/0107033.

[149] A. Kosowsky, A. Mack, and T. Kahniashvili, "Gravitational radiation from cosmological turbulence," *Phys. Rev.* **D66** (2002) 024030, astro-ph/0111483.

[150] A. D. Dolgov, D. Grasso, and A. Nicolis, "Relic backgrounds of gravitational waves from cosmic turbulence," *Phys. Rev.* **D66** (2002) 103505, astro-ph/0206461.

[151] A. Nicolis, "Relic gravitational waves from colliding bubbles and cosmic turbulence," *Class. Quant. Grav.* **21** (2004) L27, gr-qc/0303084.

[152] C. Caprini and R. Durrer, "Gravitational waves from stochastic relativistic sources: Primordial turbulence and magnetic fields," *Phys. Rev.* **D74** (2006) 063521, astro-ph/0603476.

[153] C. Grojean and G. Servant, "Gravitational Waves from Phase Transitions at the Electroweak Scale and Beyond," *Phys. Rev.* **D75** (2007) 043507, hep-ph/0607107.

[154] L. Randall and G. Servant, "Gravitational Waves from Warped Spacetime," *JHEP* **05** (2007) 054, hep-ph/0607158.

[155] G. Gogoberidze, T. Kahniashvili, and A. Kosowsky, "The spectrum of gravitational radiation from primordial turbulence," *Phys. Rev.* **D76** (2007) 083002, 0705.1733.

[156] S. J. Huber and T. Konstandin, "Production of Gravitational Waves in the nMSSM," *JCAP* **0805** (2008) 017, 0709.2091.

[157] C. Caprini, R. Durrer, and G. Servant, "Gravitational wave generation from bubble collisions in first-order phase transitions: an analytic approach," *Phys. Rev.* **D77** (2008) 124015, 0711.2593.

[158] A. Megevand, "Gravitational waves from deflagration bubbles in first- order phase transitions," *Phys. Rev.* **D78** (2008) 084003, 0804.0391.

[159] S. J. Huber and T. Konstandin, "Gravitational Wave Production by Collisions: More Bubbles," *JCAP* **0809** (2008) 022, 0806.1828.

[160] C. Caprini, R. Durrer, T. Konstandin, and G. Servant, "General Properties of the Gravitational Wave Spectrum from Phase Transitions," *Phys. Rev.* **D79** (2009) 083519, 0901.1661.

[161] C. Caprini, R. Durrer, and G. Servant, "The stochastic gravitational wave background from turbulence and magnetic fields generated by a first-order phase transition," *JCAP* **0912** (2009) 024, 0909.0622.

[162] A. Kusenko, A. Mazumdar, and T. Multamaki, "Gravitational waves from the fragmentation of a supersymmetric condensate," *Phys. Rev.* **D79** (2009) 124034, 0902.2197.

[163] A. Megevand and A. D. Sanchez, "Detonations and deflagrations in cosmological phase transitions," *Nucl. Phys.* **B820** (2009) 47–74, 0904.1753.

[164] T. Kahniashvili, L. Kisslinger, and T. Stevens, "Gravitational Radiation Generated by Magnetic Fields in Cosmological Phase Transitions," *Phys. Rev.* **D81** (2010) 023004, 0905.0643.

[165] J. Kehayias and S. Profumo, "Semi-Analytic Calculation of the Gravitational Wave Signal From the Electroweak Phase Transition for General Quartic Scalar Effective Potentials," *JCAP* **1003** (2010) 003, 0911.0687.

[166] R. Durrer, "Gravitational waves from cosmological phase transitions," 1002.1389.

[167] D. J. H. Chung and P. Zhou, "Gravity Waves as a Probe of Hubble Expansion Rate During An Electroweak Scale Phase Transition," 1003.2462.

[168] A. Vilenkin, "Cosmic Strings and Domain Walls," *Phys. Rept.* **121** (1985) 263.

[169] J. R. Ellis *et al.*, "Problems for (2,0) Compactifications," *Phys. Lett.* **B176** (1986) 403.

[170] G. B. Gelmini, M. Gleiser, and E. W. Kolb, "Cosmology of Biased Discrete Symmetry Breaking," *Phys. Rev.* **D39** (1989) 1558.

[171] B. Rai and G. Senjanovic, "Gravity and domain wall problem," *Phys. Rev.* **D49** (1994) 2729–2733, `hep-ph/9301240`.

[172] S. A. Abel and P. L. White, "Baryogenesis from domain walls in the next-to-minimal supersymmetric standard model," *Phys. Rev.* **D52** (1995) 4371–4379, `hep-ph/9505241`.

[173] S. A. Abel, "Destabilising divergences in the NMSSM," *Nucl. Phys.* **B480** (1996) 55–72, `hep-ph/9609323`.

[174] C. Panagiotakopoulos and K. Tamvakis, "Stabilized NMSSM without domain walls," *Phys. Lett.* **B446** (1999) 224–227, `hep-ph/9809475`.

[175] M. E. Carrington, "The Effective potential at finite temperature in the Standard Model," *Phys. Rev.* **D45** (1992) 2933–2944.

[176] V. Barger, D. J. Chung, A. J. Long, and L.-T. Wang, "Strongly First Order Phase Transitions Near an Enhanced Discrete Symmetry Point," *Phys.Lett.* **B710** (2012) 1–7, `1112.5460`.

[177] D. Chung, A. Long, and L.-T. Wang, "Probing the Cosmological Constant and Phase Transitions with Dark Matter," *Phys.Rev.* **D84** (2011) 043523, `1104.5034`.

[178] C. Wainwright and S. Profumo, "The impact of a strongly first-order phase transition on the abundance of thermal relics," *Phys. Rev.* **D80** (2009) 103517, `0909.1317`.

[179] T. Cohen, D. E. Morrissey, and A. Pierce, "Changes in Dark Matter Properties After Freeze-Out," *Phys. Rev.* **D78** (2008) 111701, `0808.3994`.

[180] T. Kibble, "Topology of Cosmic Domains and Strings," *J.Phys.A* **A9** (1976) 1387–1398.

[181] A. Vilenkin and E. Shellard, *Cosmic strings and other topological defects*. Cambridge monographs on mathematical physics. Cambridge University Press, 2000.

[182] J. I. Kapusta, *Finite-Temperature Field Theory*. Cambridge University Press, The Pitt Building, Trumpington Street, Cambridge CB2 1RP, 1989.

[183] C. Grojean, G. Servant, and J. D. Wells, "First-order electroweak phase transition in the standard model with a low cutoff," *Phys.Rev.* **D71** (2005) 036001, hep-ph/0407019.

[184] C. Delaunay, C. Grojean, and J. D. Wells, "Dynamics of Non-renormalizable Electroweak Symmetry Breaking," *JHEP* **04** (2008) 029, 0711.2511.

[185] V. Barger, T. Han, P. Langacker, B. McElrath, and P. Zerwas, "Effects of genuine dimension-six Higgs operators," *Phys.Rev.* **D67** (2003) 115001, hep-ph/0301097.

[186] M. Gonderinger, Y. Li, H. Patel, and M. J. Ramsey-Musolf, "Vacuum Stability, Perturbativity, and Scalar Singlet Dark Matter," *JHEP* **01** (2010) 053, 0910.3167.

[187] J. McDonald, "Gauge Singlet Scalars as Cold Dark Matter," *Phys. Rev.* **D50** (1994) 3637–3649, hep-ph/0702143.

[188] C. P. Burgess, M. Pospelov, and T. ter Veldhuis, "The minimal model of nonbaryonic dark matter: A singlet scalar," *Nucl. Phys.* **B619** (2001) 709–728, hep-ph/0011335.

[189] X.-G. He, T. Li, X.-Q. Li, and H.-C. Tsai, "Scalar dark matter effects in Higgs and top quark decays," *Mod. Phys. Lett.* **A22** (2007) 2121–2129, hep-ph/0701156.

[190] H. Davoudiasl, R. Kitano, T. Li, and H. Murayama, "The new minimal standard model," *Phys. Lett.* **B609** (2005) 117–123, hep-ph/0405097.

[191] A. Bandyopadhyay, S. Chakraborty, A. Ghosal, and D. Majumdar, "Constraining Scalar Singlet Dark Matter with CDMS, XENON and DAMA and Prediction for Direct Detection Rates," *JHEP* **11** (2010) 065, 1003.0809.

[192] T. Cohen, J. Kearney, A. Pierce, and D. Tucker-Smith, "Singlet-Doublet Dark Matter," *Phys.Rev.* **D85** (2012) 075003, 1109.2604.

[193] I. Low, P. Schwaller, G. Shaughnessy, and C. E. Wagner, "The dark side of the Higgs boson," 1110.4405.

[194] C. Englert, T. Plehn, D. Zerwas, and P. M. Zerwas, "Exploring the Higgs portal," *Phys.Lett.* **B703** (2011) 298–305, 1106.3097.

[195] S. Bock, R. Lafaye, T. Plehn, M. Rauch, D. Zerwas, *et al.*, "Measuring Hidden Higgs and Strongly-Interacting Higgs Scenarios," *Phys.Lett.* **B694** (2010) 44–53, 1007.2645.

[196] C. Englert, T. Plehn, M. Rauch, D. Zerwas, and P. M. Zerwas, "LHC: Standard Higgs and Hidden Higgs," 1112.3007.

[197] A. Djouadi, W. Kilian, M. Muhlleitner, and P. Zerwas, "Production of neutral Higgs boson pairs at LHC," *Eur.Phys.J.* **C10** (1999) 45–49, hep-ph/9904287.

[198] *Combination of Higgs Boson Searches with up to 4.9 fb-1 of p p Collision Data Taken at sqrt(s)=7 TeV with the ATLAS Experiment at the LHC,* The ATLAS collaboration, ATLAS–CONF–2011–163.

[199] *Combination of CMS searches for a Standard Model Higgsboson,* The CMS collaboration, CMS PAS HIG–11–032.

[200] H. H. Patel and M. J. Ramsey-Musolf, "Baryon Washout, Electroweak Phase Transition, and Perturbation Theory," 1101.4665.

[201] W. Loinaz and R. S. Willey, "Gauge dependence of lower bounds on the Higgs mass derived from electroweak vacuum stability constraints," *Phys. Rev.* **D56** (1997) 7416–7426, hep-ph/9702321.

[202] A. D. Linde, "On the Vacuum Instability and the Higgs Meson Mass," *Phys. Lett.* **B70** (1977) 306.

[203] A. D. Linde, "Decay of the False Vacuum at Finite Temperature," *Nucl. Phys.* **B216** (1983) 421.

[204] S. R. Coleman, "The Fate of the False Vacuum. 1. Semiclassical Theory," *Phys. Rev.* **D15** (1977) 2929–2936.

[205] C. G. Callan and S. R. Coleman, "The Fate of the False Vacuum. 2. First Quantum Corrections," *Phys. Rev.* **D16** (1977) 1762–1768.

[206] L. D. McLerran, M. E. Shaposhnikov, N. Turok, and M. B. Voloshin, "Why the baryon asymmetry of the universe is approximately 10**-10," *Phys. Lett.* **B256** (1991) 477–483.

[207] F. Gianotti, for the ATLAS Collaboration, "July 4, 2012 CERN Seminar." see also: http://www.atlas.ch/news/2012/latest-results-from-higgs-search.html.

[208] J. Incandela, for the CMS Collaboration, "July 4, 2012 CERN Seminar." see also: http://cms.web.cern.ch/news/observation-new-particle-mass-125-gev.

[209] M. Quiros, "Finite temperature field theory and phase transitions," hep-ph/9901312.

[210] T. Konstandin, G. Nardini, and M. Quiros, "Gravitational Backreaction Effects on the Holographic Phase Transition," *Phys.Rev.* **D82** (2010) 083513, 1007.1468.

[211] P. P. Giardino, K. Kannike, M. Raidal, and A. Strumia, "Is the resonance at 125 GeV the Higgs boson?," 1207.1347.

[212] N. Desai, B. Mukhopadhyaya, and S. Niyogi, "Constraints on invisible Higgs decay in MSSM in the light of diphoton rates from the LHC," 1202.5190.

[213] P. P. Giardino, K. Kannike, M. Raidal, and A. Strumia, "Reconstructing Higgs boson properties from the LHC and Tevatron data," 1203.4254.

[214] C. Englert, "The Higgs Portal from LHC to ILC," 1204.4579.

[215] J. R. Espinosa, M. Muhlleitner, C. Grojean, and M. Trott, "Probing for Invisible Higgs Decays with Global Fits," 1205.6790.

[216] D. Carmi, A. Falkowski, E. Kuflik, T. Volansky, and J. Zupan, "Higgs After the Discovery: A Status Report," 1207.1718.

[217] J. Espinosa, C. Grojean, M. Muhlleitner, and M. Trott, "First Glimpses at Higgs' face," 1207.1717.

[218] Y. Bai, P. Draper, and J. Shelton, "Measuring the Invisible Higgs Width at the 7 TeV LHC," 1112.4496.

[219] A. Azatov, R. Contino, and J. Galloway, "Model-Independent Bounds on a Light Higgs," *JHEP* **1204** (2012) 127, 1202.3415.

[220] Y. Bai, J. Fan, and J. L. Hewett, "Hiding a Heavy Higgs Boson at the 7 TeV LHC," 1112.1964.

[221] D. Carmi, A. Falkowski, E. Kuflik, and T. Volansky, "Interpreting LHC Higgs Results from Natural New Physics Perspective," 1202.3144.

[222] A. Azatov, R. Contino, D. Del Re, J. Galloway, M. Grassi, *et al.*, "Determining Higgs couplings with a model-independent analysis of h to gamma gamma," 1204.4817.

[223] J. Espinosa, C. Grojean, M. Muhlleitner, and M. Trott, "Fingerprinting Higgs Suspects at the LHC," 1202.3697.

[224] M. Garny and T. Konstandin, "On the gauge dependence of vacuum transitions at finite temperature," 1205.3392.

[225] T. Cohen, D. E. Morrissey, and A. Pierce, "Electroweak Baryogenesis and Higgs Signatures," 1203.2924. 21 pages, 4 figures.

[226] M. R. Buckley and D. Hooper, "Are There Hints of Light Stops in Recent Higgs Search Results?," 1207.1445.

[227] A. Djouadi, "The Anatomy of electro-weak symmetry breaking. I: The Higgs boson in the standard model," *Phys. Rept.* **457** (2008) 1–216, hep-ph/0503172.

[228] B. Grinstein and M. Trott, "Electroweak Baryogenesis with a Pseudo-Goldstone Higgs," *Phys.Rev.* **D78** (2008) 075022, 0806.1971.

[229] B. Batell, S. Gori, and L.-T. Wang, "Exploring the Higgs Portal with 10/fb at the LHC," *JHEP* **1206** (2012) 172, 1112.5180.

[230] W.-F. Chang, J. N. Ng, and J. M. Wu, "Constraints on New Scalars from the LHC 125 GeV Higgs Signal," 1206.5047.

[231] H. An, T. Liu, and L.-T. Wang, "125 GeV Higgs Boson, Enhanced Di-photon Rate, and Gauged $U(1)_{PQ}$-Extended MSSM," 1207.2473.

[232] G. Barenboim and J. Rasero, "Electroweak baryogenesis window in non standard cosmologies," 1202.6070.

[233] J. Ellis and T. You, "Global Analysis of the Higgs Candidate with Mass 125 GeV," 1207.1693.

[234] G. R. Blumenthal, S. M. Faber, J. R. Primack, and M. J. Rees, "Formation of galaxies and large-scale structure with cold dark matter," *Nature* **311** (1984) 517–525.

[235] S. Colombi, S. Dodelson, and L. M. Widrow, "Large scale structure tests of warm dark matter," *Astrophys.J.* **458** (1996) 1, astro-ph/9505029.

[236] P. J. E. Peebles, "Primeval Adiabatic Perturbations: Effect of Massive Neutrinos," *Astrophys. J.* **258** (1982) 415–424.

[237] Y. B. Zeldovich, J. Einasto, and S. F. Shandarin, "Giant Voids in the Universe," *Nature* **300** (1982) 407–413.

[238] D. J. H. Chung, E. W. Kolb, and A. Riotto, "Superheavy dark matter," *Phys. Rev.* **D59** (1999) 023501, hep-ph/9802238.

[239] N. Bilic, G. B. Tupper, and R. D. Viollier, "Unification of dark matter and dark energy: The inhomogeneous Chaplygin gas," *Phys. Lett.* **B535** (2002) 17–21, astro-ph/0111325.

[240] D. Tucker-Smith and N. Weiner, "Inelastic dark matter," *Phys.Rev.* **D64** (2001) 043502, hep-ph/0101138.

[241] G. D. Kribs, T. S. Roy, J. Terning, and K. M. Zurek, "Quirky Composite Dark Matter," 0909.2034.

[242] D. E. Kaplan, G. Z. Krnjaic, K. R. Rehermann, and C. M. Wells, "Atomic Dark Matter," *JCAP* **1005** (2010) 021, 0909.0753.

[243] J. M. Cline, Z. Liu, and W. Xue, "Millicharged Atomic Dark Matter," *Phys.Rev.* **D85** (2012) 101302, 1201.4858.

[244] A. de la Macorra, "BDM Dark Matter: CDM with a core profile and a free streaming scale," *Astropart. Phys.* **33** (2010) 195–200, 0908.0571.

[245] D. E. Kaplan, M. A. Luty, and K. M. Zurek, "Asymmetric Dark Matter," *Phys.Rev.* **D79** (2009) 115016, 0901.4117.

[246] K. R. Dienes and B. Thomas, "Dynamical Dark Matter: I. Theoretical Overview," 1106.4546.

[247] K. R. Dienes and B. Thomas, "Dynamical Dark Matter: II. An Explicit Model," 1107.0721.

[248] F. Zwicky, "Spectral displacement of extra galactic nebulae," *Helv. Phys. Acta* **6** (1933) 110–127.

[249] F. Zwicky, "On the Masses of Nebulae and of Clusters of Nebulae," *Astrophys.J.* **86** (1937) 217–246.

[250] S. Faber and J. Gallagher, "Masses and mass-to-light ratios of galaxies," *Ann.Rev.Astron.Astrophys.* **17** (1979) 135–183.

[251] M. Persic, P. Salucci, and F. Stel, "The Universal rotation curve of spiral galaxies: 1. The Dark matter connection," *Mon.Not.Roy.Astron.Soc.* **281** (1996) 27, astro-ph/9506004.

[252] A. Einstein, "Lens-Like Action of a Star by the Deviation of Light in the Gravitational Field," *Science* **84** (1936) 506–507.

[253] D. Walsh, R. Carswell, and R. Weymann, "0957 + 561 A, B - Twin quasistellar objects or gravitational lens," *Nature* **279** (1979) 381–384.

[254] G. Soucail, J.-P. Kneib, and G. Golse, "Multiple - images in the cluster lens Abell 2218: Constraining the geometry of the universe?," *Astron.Astrophys.* **417** (2004) L33–L38, astro-ph/0402658.

[255] G. van de Ven, J. Falcon-Barroso, R. M. McDermid, M. Cappellari, B. W. Miller, *et al.*, "The Einstein Cross: constraint on dark matter from stellar dynamics and gravitational lensing," *Astrophys.J.* **719** (2010) 1481–1496, 0807.4175.

[256] M. Markevitch *et al.*, "Direct constraints on the dark matter self-interaction cross-section from the merging galaxy cluster 1E0657-56," *Astrophys. J.* **606** (2004) 819–824, astro-ph/0309303.

[257] D. Clowe, M. Bradac, A. H. Gonzalez, M. Markevitch, S. W. Randall, *et al.*, "A direct empirical proof of the existence of dark matter," *Astrophys.J.* **648** (2006) L109–L113, astro-ph/0608407.

[258] J. Brownstein and J. Moffat, "The Bullet Cluster 1E0657-558 evidence shows Modified Gravity in the absence of Dark Matter," *Mon.Not.Roy.Astron.Soc.* **382** (2007) 29–47, astro-ph/0702146.

[259] E. Hubble, "A relation between distance and radial velocity among extra-galactic nebulae," *Proc.Nat.Acad.Sci.* **15** (1929) 168–173.

[260] A. G. Riess, L. Macri, S. Casertano, M. Sosey, H. Lampeitl, *et al.*, "A Redetermination of the Hubble Constant with the Hubble Space Telescope from a Differential Distance Ladder," *Astrophys.J.* **699** (2009) 539–563, 0905.0695.

[261] S. Maddox, G. Efstathiou, W. Sutherland, and J. Loveday, "Galaxy correlations on large scales," *Mon.Not.Roy.Astron.Soc.* **242** (1990) 43–49.

[262] G. Efstathiou, W. Sutherland, and S. Maddox, "The cosmological constant and cold dark matter," *Nature* **348** (1990) 705–707.

[263] L. M. Krauss and M. S. Turner, "The Cosmological constant is back," *Gen.Rel.Grav.* **27** (1995) 1137–1144, astro-ph/9504003.

[264] J. Ostriker and P. J. Steinhardt, "The Observational case for a low density universe with a nonzero cosmological constant," *Nature* **377** (1995) 600–602.

[265] **Supernova Search Team** Collaboration, A. G. Riess *et al.*, "Observational evidence from supernovae for an accelerating universe and a cosmological constant," *Astron.J.* **116** (1998) 1009–1038, astro-ph/9805201.

[266] **Supernova Cosmology Project** Collaboration, S. Perlmutter *et al.*, "Measurements of Omega and Lambda from 42 high redshift supernovae," *Astrophys.J.* **517** (1999) 565–586, astro-ph/9812133.

[267] D. H. Weinberg, M. J. Mortonson, D. J. Eisenstein, C. Hirata, A. G. Riess, *et al.*, "Observational Probes of Cosmic Acceleration," 1201.2434.

[268] C. Armendariz-Picon, V. F. Mukhanov, and P. J. Steinhardt, "A Dynamical solution to the problem of a small cosmological constant and late time cosmic acceleration," *Phys.Rev.Lett.* **85** (2000) 4438–4441, astro-ph/0004134.

[269] R. R. Caldwell, M. Kamionkowski, and N. N. Weinberg, "Phantom energy and cosmic doomsday," *Phys.Rev.Lett.* **91** (2003) 071301, astro-ph/0302506.

[270] M. Kunz, "The dark degeneracy: On the number and nature of dark components," astro-ph/0702615.

[271] J.-S. Gagnon and J. Lesgourgues, "Dark goo: Bulk viscosity as an alternative to dark energy," 1107.1503.

[272] A. Nicolis, R. Rattazzi, and E. Trincherini, "The galileon as a local modification of gravity," *Phys. Rev.* **D79** (2009) 064036, 0811.2197.

[273] S. Weinberg, "The Cosmological Constant Problem," *Rev.Mod.Phys.* **61** (1989) 1–23. Morris Loeb Lectures in Physics, Harvard University, May 2, 3, 5, and 10, 1988.

[274] M. R. Douglas and S. Kachru, "Flux compactification," *Rev. Mod. Phys.* **79** (2007) 733–796, hep-th/0610102.

[275] A. Vilenkin, "The Birth of Inflationary Universes," *Phys.Rev.* **D27** (1983) 2848.

[276] A. D. Linde, "Eternally Existing Self-Reproducing Chaotic Inflationary Universe," *Phys. Lett.* **B175** (1986) 395–400.

[277] E. W. Kolb and M. S. Turner, "The Early universe," *Front.Phys.* **69** (1990) 1–547.

[278] J. McDonald, "Electroweak baryogenesis and dark matter via a gauge singlet scalar," *Phys. Lett.* **B323** (1994) 339–346.

[279] J. Kang, P. Langacker, T.-j. Li, and T. Liu, "Electroweak baryogenesis in a supersymmetric U(1) -prime model," *Phys. Rev. Lett.* **94** (2005) 061801, hep-ph/0402086.

[280] S. J. Huber, T. Konstandin, T. Prokopec, and M. G. Schmidt, "Electroweak Phase Transition and Baryogenesis in the nMSSM," *Nucl. Phys.* **B757** (2006) 172–196, hep-ph/0606298.

[281] M. Laine and K. Rummukainen, "The MSSM electroweak phase transition on the lattice," *Nucl. Phys.* **B535** (1998) 423–457, hep-lat/9804019.

[282] J. R. Espinosa, M. Quiros, and F. Zwirner, "On the electroweak phase transition in the minimal supersymmetric Standard Model," *Phys. Lett.* **B307** (1993) 106–115, hep-ph/9303317.

[283] Z. Fodor, J. Hein, K. Jansen, A. Jaster, and I. Montvay, "Simulating the electroweak phase transition in the SU(2) Higgs model," *Nucl. Phys.* **B439** (1995) 147–186, hep-lat/9409017.

[284] J. M. Cline and G. D. Moore, "Supersymmetric electroweak phase transition: Baryogenesis versus experimental constraints," *Phys. Rev. Lett.* **81** (1998) 3315–3318, hep-ph/9806354.

[285] A. Ahriche and S. Nasri, "Electroweak Phase Transition in the U(1)' MSSM," *Phys. Rev.* **D83** (2011) 045032, 1008.3106.

[286] A. H. Guth and E. J. Weinberg, "Cosmological Consequences of a First Order Phase Transition in the SU(5) Grand Unified Model," *Phys.Rev.* **D23** (1981) 876.

[287] A. H. Guth and S. Tye, "Phase Transitions and Magnetic Monopole Production in the Very Early Universe," *Phys.Rev.Lett.* **44** (1980) 631.

[288] M. B. Einhorn, D. Stein, and D. Toussaint, "Are Grand Unified Theories Compatible with Standard Cosmology?," *Phys.Rev.* **D21** (1980) 3295.

[289] T. Kibble, G. Lazarides, and Q. Shafi, "Strings in SO(10)," *Phys.Lett.* **B113** (1982) 237.

[290] A. Kusenko, P. Langacker, and G. Segre, "Phase transitions and vacuum tunneling into charge and color breaking minima in the MSSM," *Phys.Rev.* **D54** (1996) 5824–5834, hep-ph/9602414.

[291] R. H. Brandenberger, B. Carter, A.-C. Davis, and M. Trodden, "Cosmic vortons and particle physics constraints," *Phys.Rev.* **D54** (1996) 6059–6071, hep-ph/9605382.

[292] J. M. Cline, J. Espinosa, G. D. Moore, and A. Riotto, "String mediated electroweak baryogenesis: A Critical analysis," *Phys.Rev.* **D59** (1999) 065014, hep-ph/9810261.

[293] J. M. Cline, G. D. Moore, and G. Servant, "Was the electroweak phase transition preceded by a color broken phase?," *Phys.Rev.* **D60** (1999) 105035, hep-ph/9902220.

[294] J. Shu, T. M. Tait, and C. E. Wagner, "Baryogenesis from an Earlier Phase Transition," *Phys.Rev.* **D75** (2007) 063510, hep-ph/0610375.

[295] Y. Cui, S. P. Martin, D. E. Morrissey, and J. D. Wells, "Cosmic Strings from Supersymmetric Flat Directions," *Phys.Rev.* **D77** (2008) 043528, 0709.0950.

[296] H. Murayama and J. Shu, "Topological Dark Matter," *Phys.Lett.* **B686** (2010) 162–165, 0905.1720.

[297] E. W. Kolb and S. Wolfram, "Spontaneous Symmetry Breaking and the Expansion Rate of the Early Universe," *Astrophys. J.* **239** (1980) 428.

[298] D. H. Lyth and E. D. Stewart, "Thermal inflation and the moduli problem," *Phys.Rev.* **D53** (1996) 1784–1798, hep-ph/9510204.

[299] M. Kamionkowski and M. S. Turner, "Thermal Relics: Do We Know Their Abundances?," *Phys.Rev.* **D42** (1990) 3310–3320.

[300] A. G. Polnarev and M. Y. Khlopov, "The era of superheavy-particle dominance and big bang nucleosynthesis," *Sov. Astron.* **26** (1982) 9–12.

[301] A. G. Doroshkevich and M. Y. Khlopov, "Grand-unification cosmology and the parameters of a neutrino-dominanted universe," *Sov. Astron. Lett.* **9** (1983) 171–173.

[302] J. L. Feng, M. Kaplinghat, H. Tu, and H.-B. Yu, "Hidden Charged Dark Matter," *JCAP* **0907** (2009) 004, 0905.3039.

[303] A. Megevand and A. D. Sanchez, "Supercooling and phase coexistence in cosmological phase transitions," *Phys.Rev.* **D77** (2008) 063519, 0712.1031.

[304] A. D. Linde, "Is the Lee constant a cosmological constant?," *JETP Lett.* **19** (1974) 183.

[305] J. Polchinski, "The cosmological constant and the string landscape," hep-th/0603249.

[306] E. Laermann and O. Philipsen, "The Status of lattice QCD at finite temperature," *Ann.Rev.Nucl.Part.Sci.* **53** (2003) 163–198, hep-ph/0303042.

[307] M. Dine, R. G. Leigh, P. Y. Huet, A. D. Linde, and D. A. Linde, "Towards the theory of the electroweak phase transition," *Phys. Rev.* **D46** (1992) 550–571, hep-ph/9203203.

[308] D. J. H. Chung, A. J. Long, and L. Wang. In preparation.

[309] H. P. Nilles, "Supersymmetry, Supergravity and Particle Physics," *Phys.Rept.* **110** (1984) 1–162.

[310] R. A. Alpher, J. W. Follin, and R. C. Herman, "Physical Conditions in the Initial Stages of the Expanding Universe," *Phys.Rev.* **92** (1953) 1347–1361.

[311] J. D. Barrow, "Massive Particles as a Probe of the Early Universe," *Nucl.Phys.* **B208** (1982) 501–508.

[312] P. Salati, "Quintessence and the relic density of neutralinos," *Phys.Lett.* **B571** (2003) 121–131, astro-ph/0207396.

[313] S. Aslanbeigi, G. Robbers, B. Z. Foster, K. Kohri, and N. Afshordi, "Phenomenology of Gravitational Aether as a solution to the Old Cosmological Constant Problem," *Phys.Rev.* **D84** (2011) 103522, 1106.3955.

[314] N. Agarwal, R. Bean, J. Khoury, and M. Trodden, "Screening bulk curvature in the presence of large brane tension," *Phys.Rev.* **D83** (2011) 124004, 1102.5091.

[315] C. de Rham, G. Gabadadze, L. Heisenberg, and D. Pirtskhalava, "Cosmic Acceleration and the Helicity-0 Graviton," *Phys.Rev.* **D83** (2011) 103516, 1010.1780.

[316] L. Smolin, "The Quantization of unimodular gravity and the cosmological constant problems," *Phys.Rev.* **D80** (2009) 084003, 0904.4841.

[317] C. Wetterich, "Warping with dilatation symmetry and self-tuning of the cosmological constant," *Phys.Rev.* **D81** (2010) 103508, 1003.3809.

[318] J. E. Kim, "Self-tuning of the cosmological constant," *J.Phys.Conf.Ser.* **259** (2010) 012005, 1009.5071.

[319] A. Davidson and S. Rubin, "Zero Cosmological Constant from Normalized General Relativity," *Class.Quant.Grav.* **26** (2009) 235019, 0905.0661.

[320] P. Koroteev and M. Libanov, "On Existence of Self-Tuning Solutions in Static Braneworlds without Singularities," *JHEP* **0802** (2008) 104, 0712.1136.

[321] F. Klinkhamer and G. Volovik, "Self-tuning vacuum variable and cosmological constant," *Phys.Rev.* **D77** (2008) 085015, 0711.3170.

[322] G. Dvali, S. Hofmann, and J. Khoury, "Degravitation of the cosmological constant and graviton width," *Phys.Rev.* **D76** (2007) 084006, hep-th/0703027.

[323] N. Itzhaki, "A Comment on Technical Naturalness and the Cosmological Constant," *JHEP* **0608** (2006) 020, hep-th/0604190.

[324] H. M. Lee, "A Comment on the selftuning of cosmological constant with deficit angle on a sphere," *Phys.Lett.* **B587** (2004) 117–120, hep-th/0309050.

[325] S. Kachru, M. B. Schulz, and E. Silverstein, "Selftuning flat domain walls in 5-D gravity and string theory," *Phys.Rev.* **D62** (2000) 045021, hep-th/0001206.

[326] R. R. Caldwell and M. Kamionkowski, "The Physics of Cosmic Acceleration," *Ann.Rev.Nucl.Part.Sci.* **59** (2009) 397–429, 0903.0866. * Brief entry *.

[327] F. Rosati, "Quintessential enhancement of dark matter abundance," *Phys.Lett.* **B570** (2003) 5–10, hep-ph/0302159.

[328] S. Profumo and P. Ullio, "SUSY dark matter and quintessence," *JCAP* **0311** (2003) 006, hep-ph/0309220.

[329] C. Pallis, "Quintessential kination and cold dark matter abundance," *JCAP* **0510** (2005) 015, hep-ph/0503080.

[330] D. J. Chung, L. L. Everett, K. Kong, and K. T. Matchev, "Connecting LHC, ILC, and Quintessence," *JHEP* **0710** (2007) 016, 0706.2375.

[331] D. J. Chung, L. L. Everett, and K. T. Matchev, "Inflationary cosmology connecting dark energy and dark matter," *Phys.Rev.* **D76** (2007) 103530, 0704.3285.

[332] S. Weinberg, "Cosmological Constraints on the Scale of Supersymmetry Breaking," *Phys.Rev.Lett.* **48** (1982) 1303.

[333] G. Coughlan, W. Fischler, E. W. Kolb, S. Raby, and G. G. Ross, "Cosmological Problems for the Polonyi Potential," *Phys.Lett.* **B131** (1983) 59.

[334] J. McDonald, "WIMP Densities in Decaying-Particle-Dominated Cosmology," *Phys. Rev.* **D43** (1991) 1063–1068.

[335] T. Banks, D. B. Kaplan, and A. E. Nelson, "Cosmological implications of dynamical supersymmetry breaking," *Phys.Rev.* **D49** (1994) 779–787, hep-ph/9308292.

[336] T. Moroi and L. Randall, "Wino cold dark matter from anomaly mediated SUSY breaking," *Nucl.Phys.* **B570** (2000) 455–472, hep-ph/9906527.

[337] M. Berkooz, D. J. Chung, and T. Volansky, "Constraining modular inflation in the MSSM from giant Q-ball formation," *Phys.Rev.* **D73** (2006) 063526, hep-ph/0507218.

[338] M. Dine, R. Kitano, A. Morisse, and Y. Shirman, "Moduli decays and gravitinos," *Phys.Rev.* **D73** (2006) 123518, hep-ph/0604140.

[339] B. S. Acharya, P. Kumar, K. Bobkov, G. Kane, J. Shao, *et al.*, "Non-thermal Dark Matter and the Moduli Problem in String Frameworks," *JHEP* **0806** (2008) 064, 0804.0863.

[340] P. B. Arnold and O. Espinosa, "The Effective potential and first order phase transitions: Beyond leading-order," *Phys.Rev.* **D47** (1993) 3546, hep-ph/9212235.

[341] K. Kajantie, M. Laine, K. Rummukainen, and M. E. Shaposhnikov, "A non-perturbative analysis of the finite T phase transition in SU(2) x U(1) electroweak theory," *Nucl. Phys.* **B493** (1997) 413–438, hep-lat/9612006.

[342] K. Kajantie, M. Laine, K. Rummukainen, and M. E. Shaposhnikov, "The Electroweak Phase Transition: A Non-Perturbative Analysis," *Nucl. Phys.* **B466** (1996) 189–258, `hep-lat/9510020`.

[343] W. H. Miller, "Quantum mechanical transition state theory and a new semiclassical model for reaction rate constants," *J. Chem. Phys.* **61** (1974) 1823.

[344] C. Ford, D. R. T. Jones, P. W. Stephenson, and M. B. Einhorn, "The Effective potential and the renormalization group," *Nucl. Phys.* **B395** (1993) 17–34, `hep-lat/9210033`.

[345] J. A. Casas, J. R. Espinosa, M. Quiros, and A. Riotto, "The Lightest Higgs Boson Mass in the Minimal Supersymmetric Standard Model," *Nucl. Phys.* **B436** (1995) 3–29, `hep-ph/9407389`.